The Pre-Alpine Evolution of the Basement of the Pelagonian Zone and the Vardar Zone, Greece

Dissertation zur Erlangung des Grades

„Doktor der Naturwissenschaften“

am Fachbereich Chemie, Pharmazie und Geowissenschaften
der Johannes Gutenberg-Universität Mainz

Birte Anders

Mainz, Juni 2005

Erklärung:

Hiermit versichere ich, die vorliegende Arbeit selbstständig und nur unter Verwendung der angegebene Quellen und Hilfsmittel verfasst zu haben.

Mainz, Juni 2005

Tag der mündlichen Prüfung: 27.07.2005

Summary

The Hellenides in Greece constitute an integral part of the Alpine-Himalayan mountain chain. They are traditionally divided into several subparallel, *c*. NNW-SSE trending tectono-stratigraphic zones. These zones are grouped into two large units, namely the External Hellenides (Hellenide foreland) in the west and the Internal Hellenides (Hellenide hinterland) in the east. The External Hellenides comprise the Paxon, Ionian and Gavrovo-Tripolis Zones, which are dominated by Mesozoic and Cainozoic cover rocks. The Pelagonian Zone, the Attico-Cycladic Massif, the Vardar Zone, the Serbo-Macedonian Massif and the Rhodope Massif (from west to east) form the Internal Hellenides. They are characterised by abundant occurrences of crystalline basement.

The Pelagonian Zone and the Vardar Zone in Greece represent the western part of the Internal Hellenides. While the Pelagonian Zone comprises predominantly crystalline basement and sedimentary cover rocks, the Vardar Zone has long been regarded as an ophiolite-decorated suture zone separating the Pelagonian Zone from the Serbo-Macedonian Massif to the east. In order to identify the major crust-forming episodes and to improve the understanding of the evolutionary history of this region, felsic basement rocks from both the Pelagonian Zone and the Vardar Zone were dated, with the main focus being on the Pelagonian Zone. Different methods of single-zircon dating were applied, namely the Pb-Pb evaporation method, the conventional U-Pb method and secondary-ionisation mass spectrometry (SIMS) using sensitive high-resolution ion microprobe (SHRIMP). The geochronological results were aided by geochemical investigations.

The majority of the basement rocks from the Pelagonian Zone (variably deformed felsic and intermediate rocks) yielded Permo-Carboniferous intrusion ages, thus underlining the importance of this crust-forming event for the Internal Hellenides of Greece. Importantly, six samples formed a coherent group of Neoproterozoic intrusion ages. Moreover, three samples yielded Triassic ages whereas a single Late Precambrian/Early Cambrian, an Upper Jurassic and a Tertiary age have also been determined. The geochronological results demonstrate that the magmatic episodes during which most of the Pelagonian Zone crystalline basement formed are predominantly pre-Alpine in age. Whole-rock geochemical and Sr- and Nd-isotope composition investigations indicate that variable amounts of older, pre-existing crust contributed to the magma source. Therefore, most of the felsic basement rocks show hybrid characteristics between I-type and S-type granitoids. According to their geochemistry the basement rocks most likely formed in a subduction-related environment, such as an active continental margin. The Triassic rocks possibly originated in an extensional environment, as extension and rifting was generally suggested for the Triassic, indicated by geochemical investigations of Triassic volcanic rocks and their associated sediments.

An important discovery is the identification of a Precambrian crustal unit within the crystalline basement of the Pelagonian Zone. Orthogneisses from the NW Pelagonian Zone yielded Neoproterozoic ages between 699 ± 7 Ma and 713 ± 18 Ma; these rocks are the oldest so far known rocks in Greece. These basement rocks are interpreted as remnants of a terrane, the Florina Terrane. Geochemically, the Florina orthogneisses represent granites formed at an active continental margin. Because of the Late Proterozoic ages, this arc can be correlated to a Pan-African or Cadomian arc derived from the northern margin of Gondwana. Since the gneisses contain inherited zircons of Late to Middle Proterozoic age, the original position of Florina was probably at the northwestern margin of Gondwana.

Similarly to other Gondwana-derived terranes, such as East Avalonia, Florina could have approached the southern margin of Eurasia during the Palaeozoic, where it later became part of an active continental margin above the subducting Palaeotethys. During the Permo-Carboniferous, the Florina Terrane served as the basement for the Pelagonian magmatic arc. The geochronological and geochemical investigations of crystalline basement rocks from the Pelagonian Zone demonstrate that subduction / accretion processes characterised the pre-Alpine evolution of this region.

In the Vardar Zone, several bodies of granites, gneisses, migmatites and felsic volcanic rocks are associated with the ophiolitic rocks and can provide additional constraints on the evolution of the suture. Single-zircon and monazite dating of felsic rocks yield accurate ages for the processes of accretion of the suture. The majority of the igneous formation ages obtained range from 155 to 164 Ma, suggesting an important magmatic phase in the Upper Jurassic. The geochemical and isotopic composition of these rocks is in accord with their formation in a volcanic-arc setting at an active continental margin. Older continental material incorporated in the Vardar Zone is documented by 319 Ma old gneisses and by inherited zircons of mainly Middle Palaeozoic age. The Upper Jurassic magmatic event overprinted such gneisses, as is evident in monazite ages of 158 Ma. The prevalence of Upper Jurassic subduction-related igneous rocks supports the conclusion from the study of basement rocks from the Pelagonian Zone that arc formation and accretion orogeny were the most important processes during the evolution of the westernmost Internal Hellenides.

Zusammenfassung

Die Helleniden Griechenlands sind Teil des Gebirgsgürtels, der von den Alpen über die Dinariden bis in den Himalaya reicht. Sie werden unterteilt in die Externen Helleniden im Westen und die Internen Helleniden im Osten, wobei jede dieser Einheiten aus mehreren subparallelen, ca. NNW-SSE verlaufenden tektono-stratigraphischen Zonen besteht. Die Externen Helleniden (Paxon Zone, Ionische Zone und Gavrovo-Tripolis Zone) sind überwiegen aus mesozoischem und tertiärem Deckgebirge aufgebaut. Die Zonen der Internen Helleniden sind, von Osten nach Westen, das Rhodope Massif, das Serbo-Macedonische Massif, die Vardar Zone, das Attico-Cycladische Massif und die Pelagonische Zone. Sie sind durch verbreitetes Auftreten von kristallinem Grundgebirge charakterisiert.

Die Pelagonische Zone und die sie nach Osten begrenzende Vardar Zone bilden den westlichen Teil der Internen Helleniden. Während die Pelagonische Zone zu großen Teilen aus kristallinem Grundgebirge und sedimentärem Deckgebirge besteht, ist die Vardar Zone durch Ophiolit-Vorkommen geprägt und wurde deshalb auch schon früh als Suturzone angesehen, welche die Pelagonische Zone im Westen vom Serbo-Macedonischen Massif im Osten trennt.

Ziel der Arbeit war es, die Hauptphasen der Krustenbildung in diesen Regionen zu identifizieren und zu einem verbesserten Verständnis der regionalgeologischen Entwicklung beizutragen. Dazu wurden felsische Grundgebirgsgesteine sowohl aus der Pelagonischen als auch aus der Vardar Zone datiert, wobei das Hauptaugenmerk auf der Pelagonischen Zone lag. Für die geochronologischen Untersuchungen wurden verschiedene Methoden der Einzelzirkondatierung angewandt. Dies waren die Pb-Pb Evaporationsmethode, die konventionelle U-Pb Methode und die SIMS Methode mit der SHRIMP. Geochemische Gesteinsanalysen ergänzten die Datierungen.

Für eine deutliche Mehrheit der Grundgebirgsgesteine aus der Pelagonischen Zone (Granite, Gneise, ein Meta-Rhyolit und Mylonite) wurden permo-karbonische Intrusionsalter bestimmt. Zu dieser magmatischen Phase gehört damit das wichtigste Krustenbildungsereignis in der Pelagonischen Zone. Andere Altersgruppen treten nur untergeordnet auf. So zeigen nur einige wenige Gesteine triassische Zirkonalter, und bei je einer einzigen Probe wurde ein spät-präkambrisches/früh-kambrisches, ein jurassisches und ein tertiäres Alter bestimmt. Eine etwas größere Altersgruppe (6 Proben) bilden Gneise mit neoproterozoischen Intrusionsaltern. Die geochronologischen Untersuchungen zeigen sehr deutlich, dass der weitaus größte Teil des Pelagonischen Grundgebirges während prä-alpiner magmatischer Phasen entstand. Geochemische und isotopengeochemische Untersuchungen am Gesamtgestein zeigen einen variablen, aber in der Regel sehr deutlichen Einfluss einer älteren Krustenkomponente bei der Magmengenese. Die meisten Gesteine lassen sich als vulkanischer Bogen- oder aktiver Kontinentalrand-Granitoide klassifizieren. Die triassischen Gesteine entstanden wahrscheinlich während einer Extensionsphase, da bisher generell aus geochemische Untersuchungen triassischer Vulkanite und den mit ihnen vorkommenden Sedimenten auf ein Extensionsregime während der Untere Trias geschlossen wurde.

Das wichtigste Ergebnis dieser Arbeit ist der Nachweis präkambrischen Grundgebirges in der nordwestlichen Pelagonischen Zone. Hier wurden für einige Gneise Intrusionsalter zwischen 699 ± 7 Ma und 713 ± 18 Ma bestimmt. Die Intrusionsalter dieser Gesteine sind damit die ältesten bislang bekannten Intrusionsalter in Griechenland. Aufgrund ihres einheitlichen Alters und dessen deutlicher Abweichung von Intrusionsaltern aus benachbarten Gebieten der Helleniden wurden diese

Gneise als Reste eines Terranes (Florina Terran) interpretiert. Die Orthogneise des Florina Terrans haben die geochemische Charakteristik von Granitoiden, die in einem subduktions-bezogenen Umfeld, so z.B. dem magmatischen Bogen eines aktiven Kontinentalrands, entstanden sind. Durch das spät-proterozoische Alter wird eine Beziehung dieses Bogens zu dem panafrikanischen oder cadomischen Bogen vom Nordrand Gondwanas nahegelegt. Da die Orthogneise des Florina Terrans ererbte Zirkonkomponenten mit mittel- bis spät-proterozoischen $^{207}Pb/^{206}Pb$-Altern enthalten, stammt das Florina Terran wahrscheinlich vom nordwestlichen Kontinentalrand Gondwanas oder aus dessen unmittelbarer Nähe. Ähnlich wie andere Terrane, die vom Nordrand Gondwanas stammen, wie z.B. Ost-Avalonien, könnte das Florina Terran den Südrand Eurasiens während des Paläozoikums erreicht haben und dort Teil des aktiven Kontinentalrands oberhalb der subduzierenden Paläotethys geworden sein. Im Permo-Karbon war das Florina Terran dann Teil des Grundgebirges, auf dem sich der pelagonische magmatische Bogen bildete.

In der Vardar Zone treten neben den ophiolitischen Gesteinen auch einige Granitkörper, Gneise, Migmatite und felsische vulkanische Gesteine auf, die zusätzliche Informationen zur Entwicklungsgeschichte der Sutur liefern. Für (meta-) vulkanische Gesteine sowie den Fanos Granit wurden Intrusionsalter zwischen 164 und 155 Ma bestimmt, die belegen, dass in dieser Region eine wichtige magmatische Phase im Oberen Jura war. Die geochemische Zusammensetzung und die Sr- und Nd-Isotopie dieser Gesteine weist auf ihre Entstehung entlang eines vulkanischen Bogens oder aktiven Kontinentalrands hin. In der Vardar Zone sind auch vereinzelt Reste älteren Grundgebirges aufgeschlossen. Für einen Orthogneis in der östlichen Vardar Zone nahe der Ortschaft Pigi wurde ein karbonisches Intrusionsalter von ca. 319 Ma bestimmt. Dieses Alter legen eine Affinität des hier aufgeschlossenen Grundgebirges zu dem der Pelagonischen Zone nahe. Die Alter von Zirkonen eines Granites nahe der Ortschaft Platania streuten zu stark, als dass ein Intrusionsalter abgeleitet werden konnte, sie gehören aber überwiegend dem mittleren Paläozoikum an. Datierte Monazite des Pigi-Orthogneises ergaben ein Alter von ca. 158 Ma und zeigen damit, dass die älteren paläozoischen Gesteine im Oberen Jura metamorph überprägt wurden.

Die geochronologische und geochemische Untersuchung des Grundgebirges der westlichen Internen Helleniden machte deutlich, dass Subduktions- und Akkretionsprozesse die prä-alpine Entwicklung dieser Region entscheidend geprägt haben. Krustenbildung fand ganz überwiegend vor der alpinene Orogenese statt.

Zusammenfassung für Fachfremde

Die Helleniden Griechenlands sind Teil eines Gebirgsgürtels, der sich von den Alpen über den östlichen Mittelmeerraum bis in die Himalaya-Region erstreckt. Diese Gebirge enstanden im späten Mesozoikum (Erdmittelalter, ca. 245-65 Millionen Jahre) durch die Kollision von Afrika mit Europa. Bei der Kollision wurden Gesteinseinheiten übereinandergestapelt, die sich vorher nebeneinander befanden. Gesteinseinheiten im tieferen Bereich des Stapels wurden dadurch erhöhten Temperaturen und Drücken ausgesetzt, Änderungen im Mineralbestand und im Gefüge waren die Folge (Metamorphose). Solche tektonischen und metamorphen Ereignisse, vor allem wenn sie noch von weiteren jüngeren Ereignissen unter veränderten Rahmenbedingungen (Änderung des Spannungsfeldes, z.B. Wechsel von Kollision zu Extension) begleitet sind, verdunkeln die frühe Entwicklungsgeschichte einer Region. Für das Gebiet des östlichen Mittelmeerraumes wird seit geraumer Zeit versucht, diese vor-alpine Geschichte zu entschlüsseln, einzelne Gesteinseinheiten (Mikrokontinente, Terrane) voneinander abzugrenzen und die Zeitabfolge ihrer relativen Position zueinander aufzudecken (paläogeographische Rekonstruktion).

Ziel der vorliegenden Studie ist, durch Altersbestimmung und geochemische Untersuchungen Aussagen über die vor-alpine Entwicklungsgeschichte eines kleinen Teils dieser Region zu treffen und dadurch ein Puzzleteilchen zu dieser Rekonstruktion beizutragen. Dabei stellte sich die Frage, ob diese vor-alpine Entwicklungsgeschichte ähnlich der alpinen Gebirgsbildung verlief (Kollision zweier Kontinente) oder vielleicht eher durch Magmatismus entlang eines aktiven Kontinentalrands geprägt wurde, bei dem Ozeanboden unter einen Kontinent abtaucht wie z.B. in den Anden Südamerikas.

Das Forschungsgebiet ist die Pelagonische Zone in Griechenland. Dieser Teil der Helleniden ist durch das Auftreten von Grundgebirge (Gneise und Granite im weiteren Sinne), das älter als die alpine Gebirgsbildungsphase ist und in sie mit einbezogen wurde, gekennzeichnet. Für die Altersbestimmung wurde die Zirkon-Datierung gewählt, mit der am ehesten das Intrusionsalter eines granitischen Gesteins oder das des Ausgangsgesteins eines Gneises bestimmt werden kann. Frühere Arbeiten zeigten schon die Existenz von Grundgebirge mit Intrusionsaltern um die 300 Millionen Jahre (Permo-Karbon). Als ein Ergebnis der vorliegenden Studie konnte gezeigt werden, dass diese magmatische Phase ausgedehnt und bestimmend für die Grundgebirgsbildung im Untersuchungsgebiet war. Eine deutliche Mehrheit der datierten Gesteine entstand zu dieser Zeit. Anzeichen für jüngeren Magmatismus sind weitaus seltener, für einige Gesteine wurden Intrusionsalter von ca. 240 Millionen Jahre (Trias, älteres Mesozoikum) bestimmt. Geochemische Untersuchungen zeigen, dass das permo-karbonische Grundgebirge wahrscheinlich entlang eines aktiven Kontinentalrandes, ähnlich den heutigen Anden, entstand. Die triassischen Gesteine dagegen haben ihren Ursprung möglicherweise in einer Dehnungsphase, wie Untersuchungen anderer Autoren an triassischen vulkanischen Gesteinen nahelegen.

Hinweise auf jurassischen Magmatismus (ca. 208-144 Millionen Jahre) sind in der Pelagonischen Zone bislang nur anhand von einer einzigen Probe bekannt. Jurassischer Magmatismus ist hingegen ein Kennzeichen der Vardar Zone, die die Pelagonische Zone nach Osten begrenzt und parallel zu ihr verläuft. Es könnte daher durchaus sein, dass auch der im Nordosten der Pelagonischen Zone gefundene jurassische Gneis aus der Vardar Zone stammt. Die Vardar Zone ist geprägt durch Ophiolithe (erhalten gebliebene ozeanische Kruste), die die Existenz eines ehemaligen Ozeanbeckens anzeigen. Subduktion dieses Ozeanbodens im Jura führte zu Inselbogenvulkanismus und möglicherweise zur Öffnung eines weiteren Ozeanbeckens hinter dem Inselbogen (back-arc Becken). Neben überwiegend jurassischen Gesteinen mit Altern von ca. 164 -155 Millionen Jahre wurden auch in der Vardar Zone ältere Gneise datiert. Ein permo-karbonisches Alter weist darauf hin, dass diese Gesteine ehemals Teil der Pelagonischen Zone waren, denn in der nach Osten an die Vardar Zone angrenzenden Einheit sind solche Alter unbekannt.

Das wichtigste Ergebnis der vorliegenden Studie ist die Entdeckung neoproterozoischen Grundgebirges mit Intrusionsaltern von ca. 700 Millionen Jahren in der nordwestlichen Pelagonischen Zone. Gesteine diesen Alters sind in den Helleniden bisher nicht gefunden worden. Sie sind sehr ähnlich zu Altern, wie sie vom Nordrand Gondwanas, dem neoproterozoischen Superkontinent, bekannt sind. Es wird deshalb angenommen, dass dieses ca. 700 Millionen Jahre alte Grundgebirge die Reste eines Mikrokontinentes darstellt, der von Gondwana wegdriftete und vermutlich im Paläozoikum an den Eurasischen Kontinent andockte (Akkretion). Dieser Mikrokontinent bildete dann einen Teil des Kontinentalrands, an dem später die permo-karbonischen Magmen gebildet wurden. So folgt, dass die vor-alpine Entwicklungsgeschichte, anders als die alpine Gebirgsbildung, durch Magmatismus entlang eines aktiven Kontinentalrands und durch Akkretion von Mikrokontinent(en?) geprägt ist. Die Pelagonische Zone hat offensichtlich Gemeinsamkeiten mit den Varisciden Zentraleuropas, in denen ebenfalls Mikrokontinente auftreten, die vom Nordrand Gondwanas stammen.

Diese Arbeit wäre ohne vielfältige Unterstützung nicht möglich gewesen, angefangen von der Einführung und Betreuung in den verschiedenen Labors und im Gelände bis hin zu den manchmal so wichtigen aufmunternden Worten. Allen, die mir geholfen haben, gilt mein herzlicher Dank!
Besonders bedanken möchte ich mich bei T. R., U. P., D. K., I. R. und W. T., die mir jederzeit mit Rat und Tat zur Seite standen.

Der Weg zum Ziel verläuft nie gerade,
allerdings auch nicht krumm,
genau besehen gibt es ihn gar nicht.

Susan Sontag

Table of Contents:

Summary iii

Zusammenfassung v

Zusammenfassung für Fachfremde vii

Danksagung ix

Preface 1

Chapter 1. Age and origin of granitic rocks of the eastern Vardar Zone, Greece: new constraints on the evolution of the Internal Hellenides 3

1.1 Abstract 3

1.2 Introduction and regional geology 3

1.3 Analytical methods 6

1.4 Sample description and geochemistry 7

1.5 Geochronological results 10

1.6 Isotope Geochemistry 15

1.7 Discussion 16

1.8 Conclusions 19

Chapter 2. The Florina Terrane: first evidence for a Precambrian terrane within the NW Pelagonian Zone 20

2.1 Abstract 20

2.2 Introduction and geological background 20

2.3 Analytical methods 23

2.4 Sample description and geochronological results 23

2.5 Geochemistry 27

2.6 Discussion 30

2.6.a. Permo-Carboniferous rocks 30

2.6.b Neoproterozoic basement rocks 30

2.6.b.1 Neoproterozoic ages 30

2.6.b.2 Post-emplacement processes 30

2.6.c. Derivation and possible linkages of the Pelagonian Neoproterozoic rocks 31

2.6.c.1. Comparison of the Florina Terrane with West Avalonia 32

2.6.c.2. Comparison of the Florina Terrane with East Avalonia 33

2.6.c.3. Comparison of the Florina Terrane with the Armorica Terrane Assemblage 34

2.6.c.4. Comparison of the Florina Terrane with the Arabian-Nubian Shield 34

2.6.c.5. Avalonian Terranes in the Variscan orogeny 34

2.7. Conclusions 35

Chapter 3. Zircon geochronology of basement rocks from the Pelagonian Zone 36

3.1 Abstract 36

3.2 Introduction and regional geology 36

3.3 Sample description and geochronology 38

3.4 Discussion 50

3.5 Conclusions 53

3.A Appendix Analytical methods 54

Chapter 4. Geochemistry of basement rocks from the Pelagonian Zone 55

4.1 Weathering and alteration 55

4.2 Major elements 58

4.3 Trace and rare earth elements 63

4.4 Sr and Nd isotopes 70

4.5 Comparison of the Permo-Carboniferous basement rocks from the Pelagonian Zone with Variscan granitoids from the Alps, the Carpathians and the Moldanubian Zone 72

4.6 The meta-sedimentary rocks 73

4.7 Conclusion 74

Chapter 5. Gondwana-derived terranes in the northern Hellenides 75

5.1 Abstract 75

5.2 Introduction 75

5.3 Regional Geology 76

5.4 Description of the terranes in the Internal Hellenides 79

5.4.a Florina Terrane 79

5.4.b Pirgadikia Terrane 80

5.4.c Vertiskos Terrane 80

5.5 Provenance of Terranes in the Internal Hellenides 82

5.6 Palaeogeographic Reconstructions 84

5.7 Conclusions 85

References 86

Appendix A-1. XRF data 102

Appendix A-2. Replicate XRF trace element analyses 109

Appendix B-1. LA-ICP-MS data 110

Appendix B-2. Method of LA-ICP-MS analyses 111

Appendix C. Sr- and Nd-isotope composition data 120
Appendix D-1. Single-zircon Pb-Pb evaporation data 121
Appendix D-2. PAL reference zircon analyses 123
Appendix E. Single-zircon conventional U-Pb data 124
Appendix F. SIMS zircon data 130
Appendix G. Electron microprobe monazite data 134
Appendix H. Sample localities 138

Preface

The Hellenides constitute a segment of the Alpine-Himalayan mountain chain in the eastern Mediterranean. They were shaped by Cretaceous to Tertiary convergence processes (the Alpine orogeny) and later overprinting by extensional tectonics caused by the roll-back of the Aegean subduction zone in conjunction with extrusion tectonics along the North Anatolian Fault system. These processes concealed the pre-Alpine history of the Hellenides, which is nevertheless essential when dealing with palaeogeographic reconstructions of the eastern Mediterranean.

It is the intention of this study to contribute to the knowledge about the pre-Alpine evolution of the Hellenides. Main emphasis was put on the Pelagonian Zone, which is the westernmost region within the Hellenides dominated by exposed crystalline basement. Additional, research was carried out on basement rocks from the Vardar Zone, which is a suture zone east of the Pelagonian Zone. The aim of the study was to identify pre-Alpine magmatic events and possibly relate them to distinct geodynamic scenarios and specific tectonic contexts. The integrated approach included a geochronological and geochemical study of crystalline basement rocks from the Pelagonian Zone and the Vardar Zone.

In Chapter 1 a study of felsic basement rocks from the Vardar Zone, the suture zone to the east of the Pelagonian Zone, is presented. The results of the zircon geochronology of basement rocks in the eastern part of the Vardar Zone (Peonias Subzone) are described and the possible implications of the identification of Palaeozoic basement in addition to Mesozoic volcanism are discussed. This chapter is largely identical with the manuscript “Age and origin of granitic rocks of the eastern Vardar Zone, Greece: new constraints on the evolution of the Internal Hellenides”, which is accepted for publication in the *Journal of the Geological Society of London* in July 2005. Co-authors are T. Reischmann (Institut für Geowissenschaften, Johannes Gutenberg-Universität Mainz), U. Poller (Max-Planck-Institut für Chemie, Mainz, Abt. Geochemie) and D. Kostopoulos (Department of Mineralogy and Petrology, National and Kapodistrian University of Athens, Greece). Samples for SIMS measurements were analysed with the SHRIMP II at the ANU, Canberra, Australia, by U. Poller and with the SHRIMP II at the Centre of Isotope Research, St. Petersburg, Russia, by T. Reischmann. Data processing with SQUID (Ludwig 2003), data evaluation and interpretation were done by B. Anders. All other analyses were done by B. Anders.

Chapter 2 focuses on the basement geochronology of the northwestern part of the Pelagonian Zone in Greece. It deals with the newly discovered Neoproterozoic basement rocks in the Internal Hellenides and their interpretation as remnants of an exotic terrane. This chapter is largely identical with the manuscript “The oldest rocks of Greece: first evidence for a Precambrian terrane within the Pelagonian Zone”, which is accepted for publication in the *Geological Magazine*. Co-authors are T. Reischmann (Institut für Geowissenschaften, Johannes Gutenberg-Universität Mainz), D. Kostopoulos (Department of Mineralogy and Petrology, National and Kapodistrian University of Athens, Greece) and U. Poller (Max-Planck-Institut für Chemie, Mainz, Abt. Geochemie). One sample for SIMS measurements was analysed with the SHRIMP II at the Centre of Isotope Research, St. Petersburg, Russia, by T. Reischmann. Data processing with SQUID (Ludwig 2003), data evaluation and interpretation as well as all other analyses were done by B. Anders.

Chapter 3 describes the results of a detailed study on zircon geochronology of basement rocks mainly, but not exclusively, from the eastern Pelagonian Zone. It considers the possible existence of different age groups and the implications that stem from this for the pre-Alpine history of the Pelagonian Zone. Chapter 3 is largely identical with the manuscript entitled "Zircon geochronology of basement rocks from the Pelagonian Zone, Greece: constraints on the pre-Alpine evolution of the westernmost Internal Hellenides" submitted to the *International Journal of Earth Sciences*. Co-authors are T. Reischmann (Institut für Geowissenschaften, Johannes Gutenberg-Universität Mainz) and D. Kostopoulos (Department of Mineralogy and Petrology, National and Kapodistrian University of Athens, Greece). Samples for SIMS measurements were analysed with the SHRIMP II at the ANU, Canberra, Australia, by U. Poller. Data processing with SQUID (Ludwig 2003), data evaluation and interpretations were done by B. Anders. All other analyses were done by B. Anders.

Chapter 4 gives an outline on the geochemistry of felsic basement rocks from the Pelagonian Zone. Major- and trace-element XRF analyses, REE analyses with LA-ICP-MS and Sr and Nd isotope composition determinations are used to geochemically characterise the basement rocks. The basement rocks from the Vardar Zone are included in this chapter for comparison, though most of them are also described in Chapter 1.

In Chapter 5, the descriptions of the three exotic terranes recently identified in the Internal Hellenides are combined. This chapter is largely identical to a manuscript entitled "Gondwana-derived terranes in the Internal Hellenides" written by F. Himmerkus, B. Anders, T. Reischmann (all at Institut für Geowissenschaften, Johannes Gutenberg-Universität Mainz) and D. Kostopoulos (Department of Mineralogy and Petrology, National and Kapodistrian University of Athens, Greece). The manuscript was submitted to the *Geological Society of America Memoirs* in February 2005. All parts of the chapter related to the Pelagonian Zone and the Florina Terrane (see also Chapter 2) are the work of B. Anders.

All analytical data are given in the Appendices A to G.

Chapter 1. Age and origin of granitic rocks of the eastern Vardar Zone, Greece: new constraints on the evolution of the Internal Hellenides

This chapter is largely identical to a manuscript entitled “Age and origin of granitic rocks of the eastern Vardar Zone, Greece: new constraints on the evolution of the Internal Hellenides” that is accepted for publication in the Journal of the Geological Society, London. Co-authors are T. Reischmann, U. Poller and D. Kostopoulos.

1.1 Abstract

The Vardar Zone is an integral part of the Internal Hellenides and has long been regarded as an ophiolite-decorated suture zone separating two distinct continental blocks, namely the Pelagonian Zone to the west and the Serbo-Macedonian Massif to the east. Several bodies of granites, gneisses and volcanic rocks are associated with the ophiolitic rocks and can provide additional constraints on the evolution of the suture. Single-zircon and monazite dating of felsic rocks yielded accurate ages for the processes of accretion of the suture. The igneous formation ages obtained range from 155 to 164 Ma, suggesting an important magmatic phase in the Late Jurassic. The chemical and isotopic composition of these rocks is in accord with their formation in a volcanic-arc setting at an active continental margin. Older continental material incorporated in the Vardar Zone is documented by 319 Ma gneisses and by inherited zircons of mainly Mid-Palaeozoic ages. The Late Jurassic magmatic event overprinted such gneisses, as is evident in monazite ages of 158 Ma. The prevalence of Late Jurassic subduction-related igneous rocks indicates that arc formation and accretion orogeny were the most important processes during the evolution of this part of the Internal Hellenides.

1.2 Introduction and regional geology

The Hellenides constitute an integral part of the main Alpine-Himalayan orogenic belt and formed when Apulia and Europe collided in Late Cretaceous to Tertiary times. Traditionally, the Hellenides are subdivided into several tectono-stratigraphic units (Jacobshagen 1986 and references therein). These units, from east to west, are: the Rhodope Massif, the Serbo-Macedonian Massif, the Vardar Zone, the Pelagonian Zone (Internal Hellenides) and the External Hellenides (Fig. 1.1a). Sandwiched between the Pelagonian Zone and the Serbo-Macedonian Massif, the Vardar Zone is an elongated NNW-SSE trending belt (Fig. 1.1a). It is characterised by numerous ophiolitic bodies and is regarded as a suture zone (e.g. Mercier *et al.* 1975; Brown & Robertson 2004). To this date there are no definitive answers concerning the presence of rocks of both Pelagonian and Serbo-Macedonian origin within the Vardar Zone and this is also the case for the age and origin of the basement of the Vardar Zone. The answer to both questions could help to improve reconstructions of the Late Palaeozoic to Mesozoic history of this region, which is characterised by a mosaic of continental fragments with ocean basins in between. Since both the Pelagonian Zone and the Serbo-Macedonian Massif consist of basement of distinctly different age, the dating of remnants of basement blocks from the Vardar Zone would give a clear indication as to their provenance.

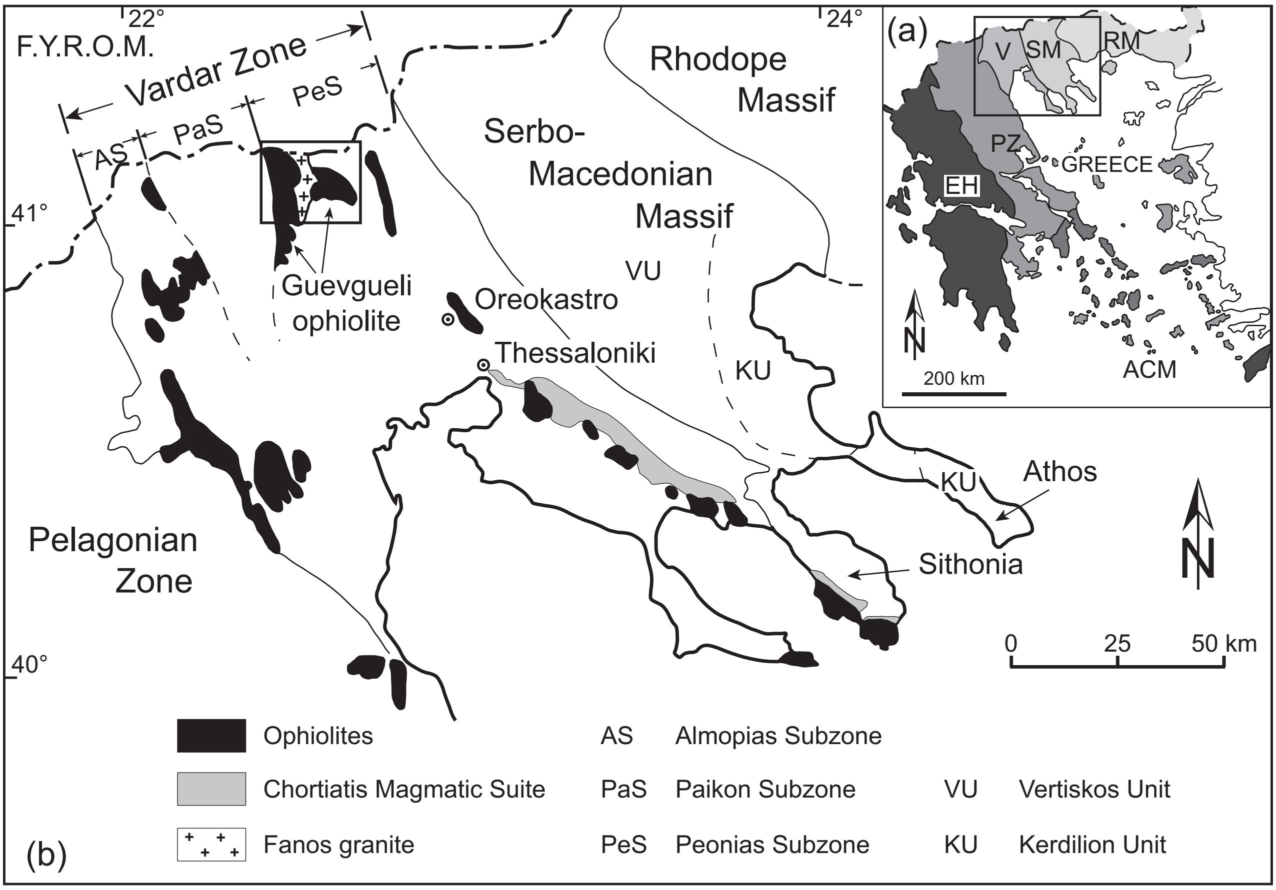

Fig. 1.1. (a) Simplified map of the tectono-stratigraphic zones of Greece modified after the IGME Geological Map of Greece (1983) scale 1:500 000. RM: Rhodope Massif, SM: Serbo-Macedonian Massif, V: Vardar Zone, PZ: Pelagonian Zone, ACM: Attico-Cycladic Massif, EH: External Hellenides. (b) Simplified map of the Vardar Zone, modified after Kockel & Mollat (1977) and Mussallam & Jung (1986b). F.Y.R.O.M.: Former Yugoslav Republic of Macedonia. Kerdilion of Athos after F. Himmerkus (pers. comm. 2005). The box indicates the study area (Fig. 1.2).

In Greece, the Vardar Zone is divided into three units (Fig. 1.1b), which, from east to west, are the Peonias, Paikon and Almopias Subzones (Mercier 1966). The Almopias Subzone consists of ophiolites, meta-volcanic and meta-sedimentary rocks. It is interpreted as a former ocean basin that subducted eastwards underneath the Serbo-Macedonian Massif to form the Paikon volcanic arc in Mid- to Late Jurassic times. During the Late Jurassic, ophiolites from this ocean were obducted westwards onto the Pelagonian Zone (Mercier *et al.* 1975; Brown & Robertson 1994, 2003, 2004; Bébien *et al.* 1994; Sharp & Robertson 1994). During the Cretaceous, however, an ocean basin existed in this area, either as a remnant ocean that had escaped Jurassic obduction or as a small Cretaceous pull-apart basin (Sharp & Robertson 1994). Final closure of the ocean is assumed to have occurred during the Tertiary, accompanied by thrusting of ophiolites eastwards onto the Paikon Subzone (Sharp & Robertson 1994; Brown & Robertson 2004). A different interpretation of the Paikon Subzone as a tectonic window (Godfriaux & Ricou 1991; Ricou & Godfriaux 1991, 1995; Ferrière *et al.* 2001) is highly controversial (e.g. Mercier & Vergély 1994). The Guevgueli ophiolite in the western part of the Peonias Subzone is considered to have formed in an ensialic back-arc basin opening behind (to the east of) the Paikon arc (Bébien 1982; Brown & Robertson 2003). It was then thrusted westwards onto the Paikon Subzone (Mercier *et al.* 1975; Brown & Robertson 1994). Evidence for subduction activity in the eastern Vardar Zone was reported from the Paikon and the eastern Peonias Subzones by Baroz *et al.*

(1987) and Michard *et al.* (1994), respectively, where they found high-Si phengite- and glaucophane-bearing rocks. The Guevgueli ophiolite is itself intruded by a granite pluton, namely the Fanos granite (Mercier 1966; Borsi *et al.* 1966; Bébien 1982; Christofides *et al.* 1990). Sparse and small outcrops of gneisses and granitic rocks are to be found east of the Guevgueli ophiolite; they have been interpreted as remnants of older, pre-back-arc-rift basement rocks of assumed Serbo-Macedonian origin (Zachariadou & Dimitriadis 1994; Fig. 1.2). These are the Pigi block around Pigi village, consisting predominantly of migmatites with subordinate orthogneisses, the Karathodoro block on the eastern side of Axios river, also consisting predominantly of felsic metamorphic rocks, and the anatectic Platania cordierite granite near Platania village (Zachariadou & Dimitriadis 1994).

The south-eastern part of the Peonias Subzone comprises ophiolites together with igneous and sedimentary rocks of the Chortiatis Magmatic Suite (Kockel & Mollat 1977). These ophiolites of the so-called Innermost Hellenic Ophiolite Belt are considered to have been emplaced in a wrench zone (Bébien *et al.* 1986). The Chortiatis Magmatic Suite forms a NW-SE trending belt, extending from Mt. Chortiatis, ESE of Thessaloniki, to Sithonia (Fig. 1.1b) (Kockel & Mollat 1977; Schünemann 1985; Mussallam & Jung 1986a). It is a highly deformed series of rocks interpreted to have formed in an immature volcanic-arc environment (Kockel & Mollat 1977; Mussallam & Jung 1986a).

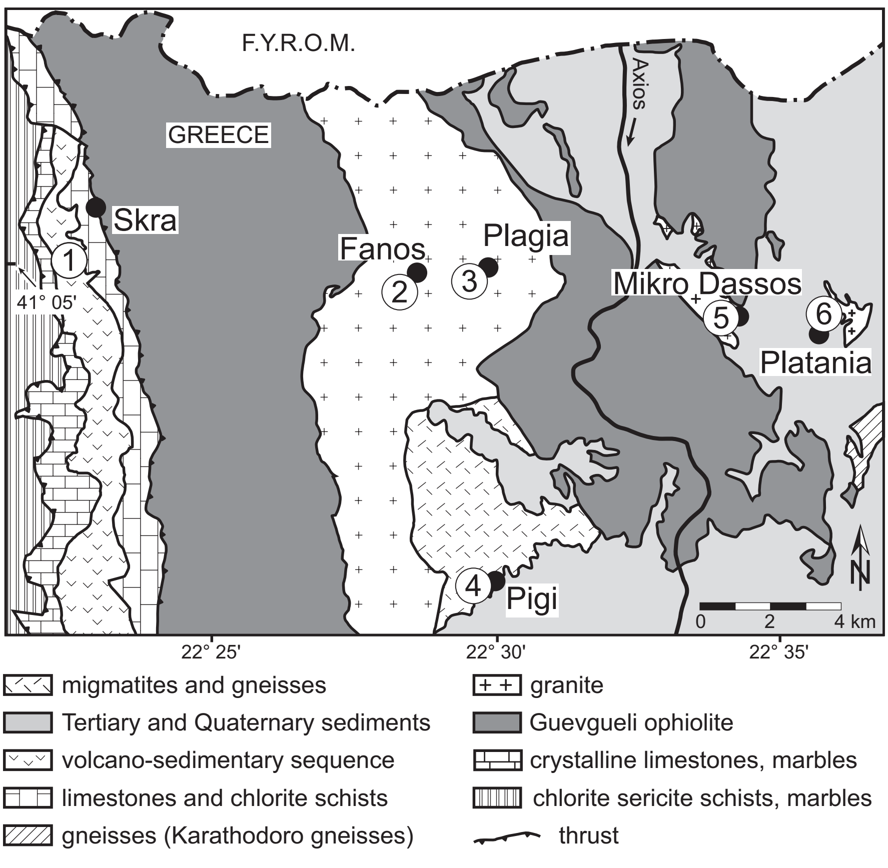

Fig. 1.2. Simplified map of the study area, modified after the IGME Geological Map of Greece, sheet Skra (1982) scale 1:50 000 and sheet Evzoni (1993) scale 1:50 000. Numbers mark the sample locations: 1) Skra mylonites Pl32 and Pl33; 2) Fanos granites Pl35 and Pl36; 3) Fanos granite P5; 4) Pigi orthogneisses P1 and P2; 5) Mikro Dassos rhyolite P6; 6) Platania granites PLT-1 and PLT-2.

In this study we focused our attention on igneous rocks from the Peonias Subzone (Fig. 1.2). The aim was to date the pre-existing basement and correlate it, if possible, with one of the neighbouring zones, i.e. the Serbo-Macedonian Massif to the east or the Pelagonian Zone to the west of the Vardar Zone, in order to locate precisely the Vardar suture. Another aim was to better constrain the age and origin of magmatic activity in this area. To achieve this we used zircon geochronology to date the intrusion event(s) and concentrated on felsic rocks in which zircon is a very common accessory mineral. Additionally, monazite was analysed to constrain the metamorphic history.

1.3 Analytical Methods

Whole-rock samples were analysed on fused glass discs for major elements and on powder pellets for trace elements with a Philips XRF at the Institut für Geowissenschaften, Universität Mainz, Germany. Whole-rock laser-ablation inductively coupled plasma mass-spectrometry (LA-ICP-MS) measurements of REE on fused glass droplets were performed on a ThermoFinnigan Element2 at the Max-Planck-Institut für Chemie, Mainz, Germany. Sample preparation followed the procedure of Gumann *et al.* (2003). For whole-rock Sr- and Nd-isotope composition analyses, powders from five samples were dissolved and the Sr and REE chromatographically separated at 5 ml cation-exchange resin columns, following standard procedures (White & Patchett 1984), including a second clean-up step for Sr at 1ml resin columns. Nd was gathered out of the REE fraction with HDHP-coated Teflon columns. Sr was loaded with TaF_2 on W filaments, while Re filaments in double configuration were used for Nd measurements. Isotopes were measured with a Finnigan MAT 261 thermal-ionisation mass spectrometer (TIMS) in multicollector mode. Mass fractionations were corrected to $^{146}Nd/^{144}Nd$ = 0.7219 and $^{86}Sr/^{88}Sr$ = 0.1194. International standards were also analysed over the period of measurements. For La Jolla, the measured $^{143}Nd/^{144}Nd$ ratio was 0.511819 ± 9 (n = 16), while for NIST SRM 987 (formerly NBS 987) an $^{87}Sr/^{86}Sr$ ratio of 0.710234 ± 12 (n = 16) was obtained.

The conventional U-Pb zircon dating is based on the low-contamination dissolution method of Krogh (1973). Zircon separation followed standard procedures with handpicking as a last step to avoid zircons with visible inclusions. Before dissolution, the zircons were washed in 7N HNO_3 and a mixed ^{205}Pb-^{235}U spike was added. After dissolution with HF, chemical separation of U and Pb with HBr chemistry followed, using 20 µl columns with anion-exchange resin. Pb and U were loaded on single Re filaments with silica gel and analysed with a Finnigan MAT 261 TIMS using an electron multiplier detector. Procedural blanks were < 40 pg Pb; the fractionation factor was determined by repeated measurements of NBS 981 under the same conditions as those of the samples. After correction for fractionation (3‰ per ΔAMU), blank and common Pb (values from Stacey & Kramers 1975), ages were calculated with Isoplot (Ludwig 2003). All TIMS analyses were carried out at the Max-Planck-Institut für Chemie, Mainz, Germany.

Geochronological analyses of zircons with secondary-ionisation mass spectrometry (SIMS), using sensitive high-resolution ion microprobe (SHRIMP), were performed on zircon grains of five samples. The method is described in detail e.g. in Compston *et al.* (1984), Williams (1998) and Compston (1999). Zircons of four samples (P2, P6, Pl33, and PLT-1) were dated with SHRIMP II at the ANU, Canberra, Australia. Zircon standard FC1 (age 1099 Ma; Paces & Miller 1993) was used for calibration of the Pb-U ratios and reference zircon SL13 was used for calibration of the U concentrations. Sample P5 was dated with SHRIMP II at the Centre of Isotopic Research, St. Petersburg, Russia. Here, the TEMORA reference zircon (age 416.75 Ma; Black *et al.* 2003) was used for calibration of the Pb-U ratios and reference zircon 91500 for calibration of the U concentrations (Wiedenbeck *et al.* 1995). Data reduction and age calculations were performed using SQUID (Ludwig 2001). The measured isotopic ratios were corrected for common Pb, based on the measured ^{204}Pb. For each spot analysed, the isotopic composition of the common Pb component was assumed to resemble the values given by Stacey & Kramers (1975) according to the individual age obtained. Concordia diagrams were drawn with Isoplot (Ludwig 2003). Ages were calculated with the built-in concordia age function of SQUID (Ludwig 2001) and include the error of the standard. All ages are given at the 95% confidence level; the MSWD and the probability given include both concordance and equivalence.

Monazites from one sample were dated with an electron microprobe. Monazites were identified in thin section by their very bright back-scattered electron (BSE) images and verified by EDS. Measurements were carried out on a JEOL JXA 8900 RL (Institut für Geowissenschaften, Universität Mainz, Germany) equipped with five wavelength-dispersive spectrometers. Measurement conditions were: acceleration voltage 15 kV, probe current 100 nA, and spot size 5 µm. Analysed lines were Pb*Mß*, U*Mß* and Th*Mα*. Measurement times on peak position were 400s for Pb, 120s for U and 70s for Th. To evaluate monazite purity and the quality of spot analysis the most common elements occurring in monazites (Si, Ca, Nd, Er, Al, P, Ce, Dy, Y, La, Gd, Eu, Sm, Pr) were also analysed. Totals were in the range of 100 - 102 wt.%. Chemical U-Th-Pb ages were calculated by the method described in Montel *et al.* (1996). Errors were based on counting statistics. Errors on ages of individual spots were calculated by error propagation of the U, Th and Pb errors. Systematic errors of the method are not included due to lack of an international monazite standard. Ages were calculated as weighted averages using Isoplot (Ludwig 2003). Additionally, monazite F5 from the Gfoehl granite of the Bohemian Massif with a known age of 341 ± 2 Ma (Finger *et al.* 2003) was analysed to check the quality of the results. An age of 334 ± 4 Ma was obtained as weighted average of 25 spots on three monazite grains and therefore a good external reproducibility was achieved with a deviation < 3%.

1.4 Sample description and geochemistry

The samples of the present study were collected from the eastern Vardar Zone. Sample description is arranged from west to east. It starts with rocks from the easternmost Paikon Subzone and continues into the Peonias Subzone. Sample locations are shown in Fig. 1.2 and GPS coordinates are given in Appendix H.

The westernmost samples are grey mylonitic gneisses sampled from a large shear zone SW of Skra village (Fig. 1.2, location 1; samples PI32 and PI33). Sample PI33 (*Skra mylonite*) is a strongly sheared, very fine-grained rock. It consists mainly of quartz, K-feldspar and white mica. Cube-shaped holes indicate a previously existing, now completely removed mineral that might have been pyrite. PI32 is a coarser-grained grey mylonite taken from the same shear zone. Like PI33, it consists mainly of quartz, feldspar and white mica; plagioclase can also be distinguished under the microscope.

The major intrusion in the study area is the *Fanos granite*. This reddish granite was sampled at two different localities, one west of Fanos village (Fig. 1.2, location 2) and the other west of Plagia village (Fig. 1.2, location 3). At the former locality, the granite forms a coarse-grained and a fine- to medium-grained variety, both of which were sampled (PI35, PI36). At the latter locality a medium-grained sample (P5) was taken. Despite the difference in grain size, the modal and geochemical composition is very much the same, with similar contents of quartz, K-feldspar, plagioclase and biotite.

Good outcrops of migmatites and orthogneisses can be found west of Pigi village. Samples P1 and P2 (*Pigi orthogneiss*), located approximately 200m apart, were collected in this vicinity (Fig. 1.2, location

4). Both are slightly deformed, medium-grained orthogneisses with cm-sized pink K-feldspar crystals. The orthogneisses consist mainly of quartz and feldspar with additional biotite, an opaque phase and minor white mica and epidote. Some of the biotites show incipient alteration to chlorite. Evidence for fluid infiltration can be seen in sample P2 where more leucocratic domains occur and are accompanied by patches of dark minerals. In places mafic dykes crosscut the orthogneisses and the migmatites.

The *Mikro Dassos rhyolite* (P6) is exposed near the village of Mikro Dassos (Fig. 1.2, location 5). It is a light grey, porphyritic volcanic/subvolcanic rock, which shows almost no deformation. The main phenocryst assemblage is quartz and sericitised feldspar together with chlorite pseudomorphs replacing biotite phenocrysts, minor epidote and an opaque phase. The fine-grained matrix consists mainly of quartz and feldspar. Only one remnant of biotite was positively identified and it cannot be ruled out that it is a xenocryst. Dark green to black xenoliths 1-6 cm in size occur in the rhyolite. Moreover, xenoliths of quartz and feldspar 0.5-3 mm in size can be identified under the microscope by their coarser grain size as compared to the fine-grained matrix.

The easternmost sample of this study is the *Platania granite*. Two samples (PLT-1 and PLT-2), located approximately 20m apart, were collected near Platania village (Fig. 1.2, location 6). Sample PLT-1 is a reddish-coloured, medium- to coarse-grained granite. Centimetre-sized layers of different grain size define a weak deformation foliation. K-feldspar dominates the coarser layers while the finer layers are rich in dark minerals. Quartz, feldspar, white mica and biotite are all major constituents. The biotite shows incipient alteration to chlorite. PLT-2 is a grey, fine-grained rock that occurs as xenolithic rafts within PLT-1.

With regard to their geochemical characteristics all samples show a felsic composition with SiO_2 contents > 70 wt.% (Appendix A). On the Ab-An-Or classification diagram (O'Connor 1965) they classify as granites (Fig. 1.3a). The Mikro Dassos rhyolite P6, shown for comparison, plots in the trondhjemite

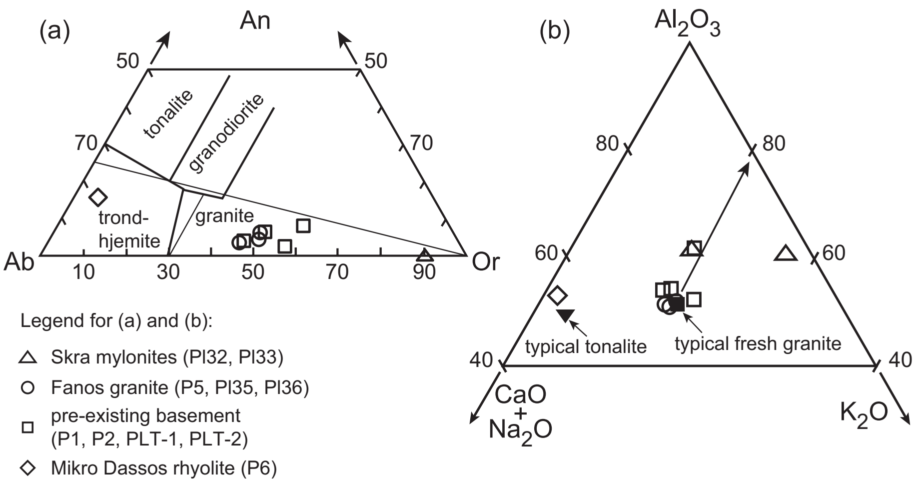

Fig. 1.3. Geochemical classification of the analysed rocks. (a) Classification with normative Ab-An-Or after O'Connor (1965) modified by Barker (1979, heavy lines). (b) A-CN-K diagram after Nesbitt & Young (1989), the long arrow indicates the weathering trend.

field. This is ascribed to its low K_2O content, which is due to the replacement of biotite by chlorite. We therefore continue to classify this sample as a rhyolite. All samples have molecular A/NK and A/CNK ratios between 1.04 and 1.91 and classify as peraluminous (Appendix A). K_2O contents are in the range of 3-5 wt.% with two exceptions. The Mikro Dassos rhyolite (P6), as already mentioned, has a low K_2O content of only 0.6 wt.%, while one Skra mylonite (Pl33) has a very high K_2O concentration of about 7 wt.%. Na_2O concentrations give a similar picture, only this time the Skra mylonite (Pl33) has a rather low concentration of 0.55 wt.% while the Mikro Dassos rhyolite contains as much as 5.4 wt.%. Because secondary alteration processes can lead to severe shifts in sodium and/or potassium contents, the chemical index of alteration (CIA; Nesbitt & Young 1982, 1989) was calculated to evaluate the possible influence of weathering and alteration. For the Fanos granite, the Pigi orthogneiss, the Mikro Dassos rhyolite and one of the Platania granites (PLT-1) the values of the CIA range from 50.9 to 54.1 and therefore these samples still qualify as fresh granites (CIA for average fresh granite: 45-55; Nesbitt & Young 1982). This could indicate that at least part of the high sodium and low potassium concentration of the Mikro Dassos rhyolite is a primary feature. Nevertheless, it only rules out the disturbance of the alkali-content by alteration of feldspar. The low K_2O-content can readily be derived by metamorphism that leads to destruction of biotite. By contrast, alteration is evident for the Skra mylonites and one of the Platania granites (PLT-2). For these rocks higher CIA values of 60.4 to 61.6 were obtained. The samples are also plotted on the A-CN-K diagram of Nesbitt & Young (1989; Fig. 1.3b) where it can be seen that most plot close to the average granite except for the Skra mylonites and the Platania granite PLT-2, which are shifted in the direction of alteration. Therefore, while using classification diagrams that are based on potassium-content it has to be kept in mind that the Skra mylonites are shifted to higher potassium-concentrations in an unknown amount. This alteration will also effect classifications using Rb. On the Nb-Y trace-element discrimination diagram of different tectonic environments for granitic rocks (Pearce *et al.* 1984), all samples plot in the field of syn-collisional (syn-COLG)/volcanic-arc granites (VAG; Fig. 1.4a). Using the Rb-(Y+Nb) classification scheme (Fig. 1.4b), the Fanos granite plots along or slightly below the line that separates the syn-COLG from the VAG field, as noted by previous authors (Christofides *et al.* 1990; Soldatos *et al.* 1993). Therefore, all samples are interpreted to have formed either in a volcanic-arc or in an active continental-margin envi-

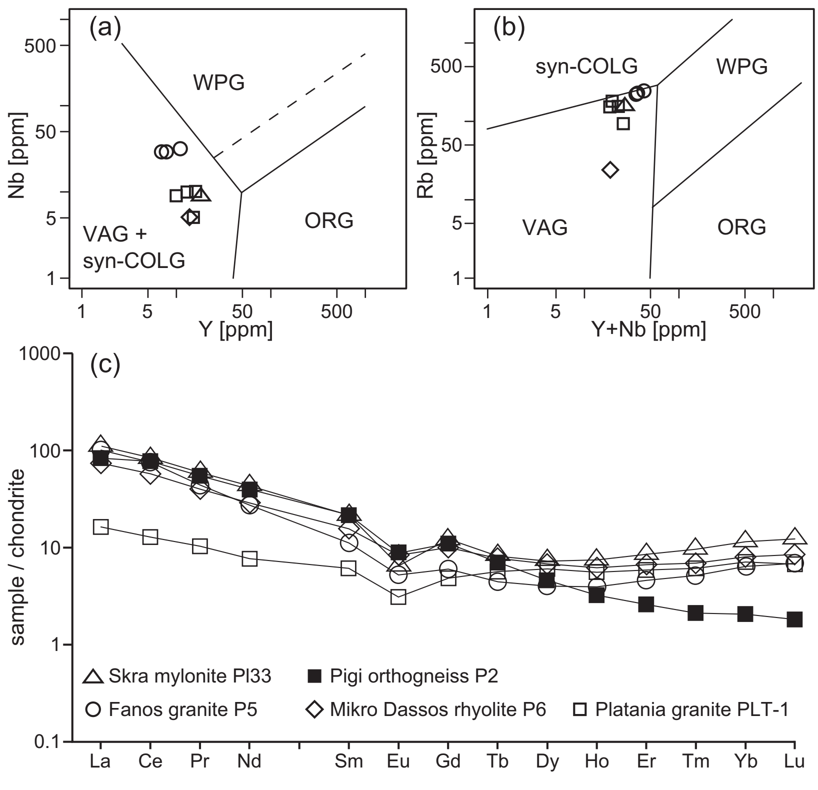

Fig. 1.4. Classification of the sampled rocks using trace elements. (**a**) and (**b**) Geotectonic environment classification after Pearce *et al.* (1984). WPG: within-plate granite; ORG: ocean-ridge granite; VAG: volcanic-arc granite; syn-COLG: syn-collisional granite. Symbols are the same as in Fig. 1.3. (**c**) REE pattern, normalised to chondrite.

ronment. On a chondrite-normalised REE plot the samples show enrichment in the light REE (LREE) and a negative Eu anomaly, again a pattern typical for continental crust (Fig. 1.4c). For Platania granite PLT-1 the LREE enrichment is only weak. A small increase in the heavy REE (HREE) can be seen for the Fanos granite (P5), Mikro Dassos rhyolite (P6), Skra mylonite (Pl33) and Platania granite (PLT-1), while for the Pigi orthogneiss (P2) a constant decrease from LREE to HREE is displayed (Fig. 1.4c).

1.5 Geochronological Results

In this section, the zircon ages are presented according to sample location from west to east; they are followed by the monazite ages. Analytical data are listed in Appendices E-G, concordia plots are shown in Fig. 1.6. Zircon grains of the Platania granite PLT-1 were analysed both by the conventional U-Pb and the SIMS methods, those of Platania granite PLT-2 with the conventional U-Pb method only. All other samples were dated with the SIMS method using SHRIMP.

Secondarily filled crosscutting or radial microcracks that are most clearly visible in SE-images are typical for zircon grains of the *Skra mylonite* (Pl33; Fig. 1.5a, lower part). Wayne & Sinha (1988, 1992) showed that pervasive mylonitic deformation and fracturing of zircons do not necessarily lead to disturbance of the U-Pb system of zircon grains. Nevertheless, fractures may enhance Pb-loss, especially in the case of fluid activity. The above authors argue that disturbance of the U-Pb system of zircon grains in mylonites is mostly related to surface corrosion and overgrowth. Most zircon grains show in cathodoluminescence (CL) images single-phase oscillatory zoning (Fig. 1.5a upper part), even if they are fractured. Single-phase oscillatory zoning is commonly interpreted to reflect growth zoning and ages obtained from such zircons therefore date the growth event (e.g. Vavra 1990; Hanchar & Miller 1993). Applying the SIMS method, we were able to select clear spots on non-fractured zircon grains for analyses. A concordia age of 155 ± 2 Ma (95% confidence, n = 4, MSWD = 0.75, probability (P) = 0.63) is interpreted as the emplacement age (Fig. 1.6a). Two spots were not included in the age calculation: one slightly younger spot (spot 1.1) and one spot that plots discordantly and has a relatively large error (spot 5.2). By contrast, the age of the mylonitisation event remains uncertain.

With regard to the *Fanos granite*, sample P5 was selected for SIMS dating. CL images show clear oscillatory zoning and therefore the obtained age is taken as the emplacement age of the pluton (Fig. 1.5b). Dating with SHRIMP yielded a precise concordia age of 158 ± 1 Ma (95% confidence, n = 5, MSWD = 1.12, P = 0.34; Fig. 1.6b). Three spots do not belong to this coherent age group. One younger spot (spot x) is interpreted to indicate Pb loss. The remaining two spots plot concordantly at slightly older ages (spots xx and 6.x) than those of the coherent age group. This might reflect the existence of a sub-microscopic inherited Pb component, which was to small to be detected by the CL investigation. These three analyses (spots x, xx and 6.x) are not shown in the concordia diagram of Fig. 1.6b but are listed in Appendix F. The zircon age of the Fanos granite is distinctly older than the K-Ar and Rb-Sr ages previously obtained on biotites by Spray *et al.* (1984) and Borsi *et al.* (1966; recalculated in Spray *et al.* 1984), which are in the range 148 ± 3 Ma to 153 ± 2 Ma. As the Rb-Sr system in biotite has a lower closure temperature than the U-Pb system in zircon, these younger ages are considered to reflect cooling of the pluton or later overprint, while the new zircon age dates the emplacement event.

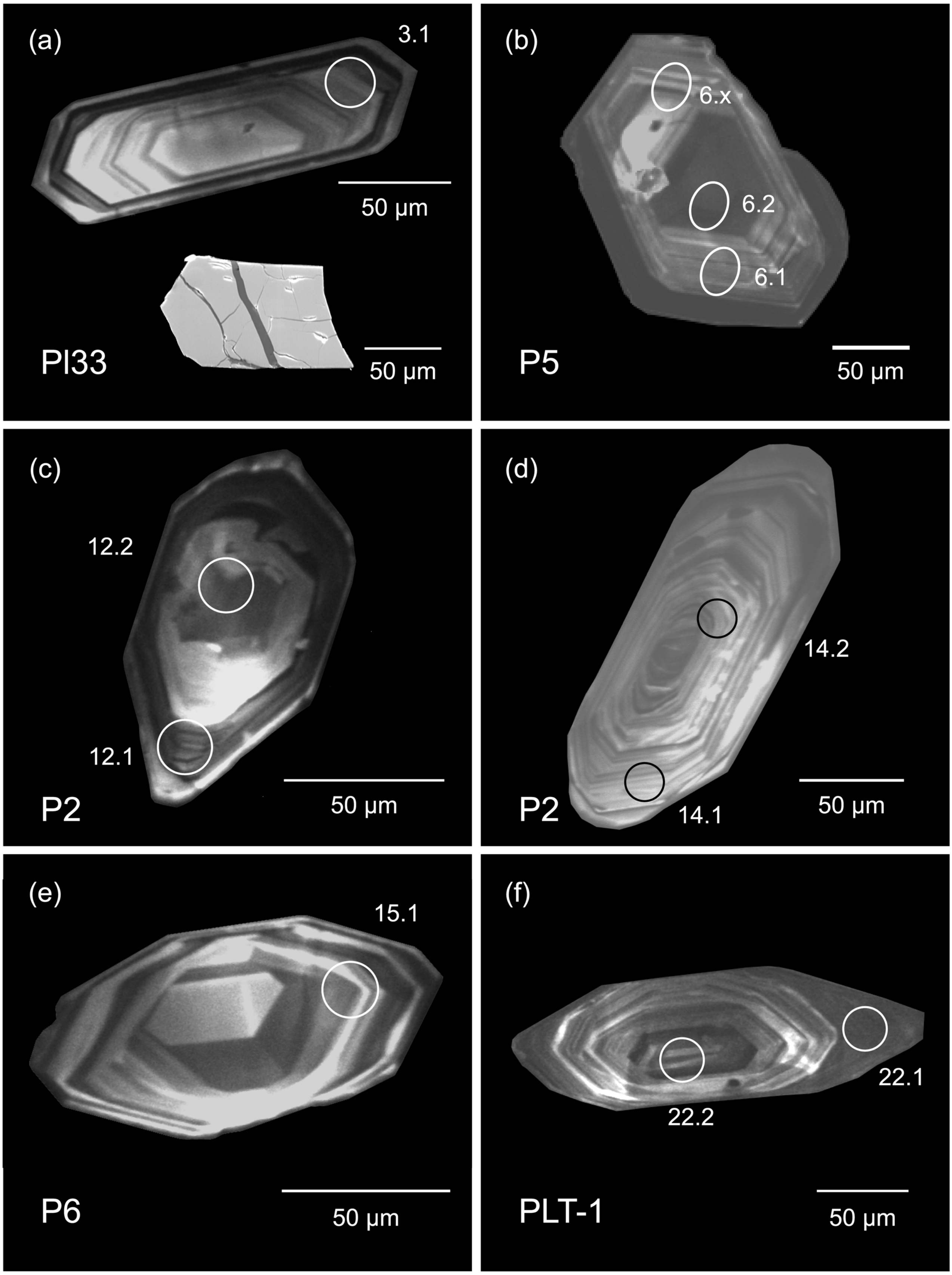

Fig. 1.5. CL images of zircons from the dated samples. (a) The upper part shows a non-fractured zircon with oscillatory zoning in CL image, lower part shows the secondary electron image of a fractured zircon of the same sample; the crack is filled with SiO_2. (a) to (f) White circles indicate the SIMS spots.

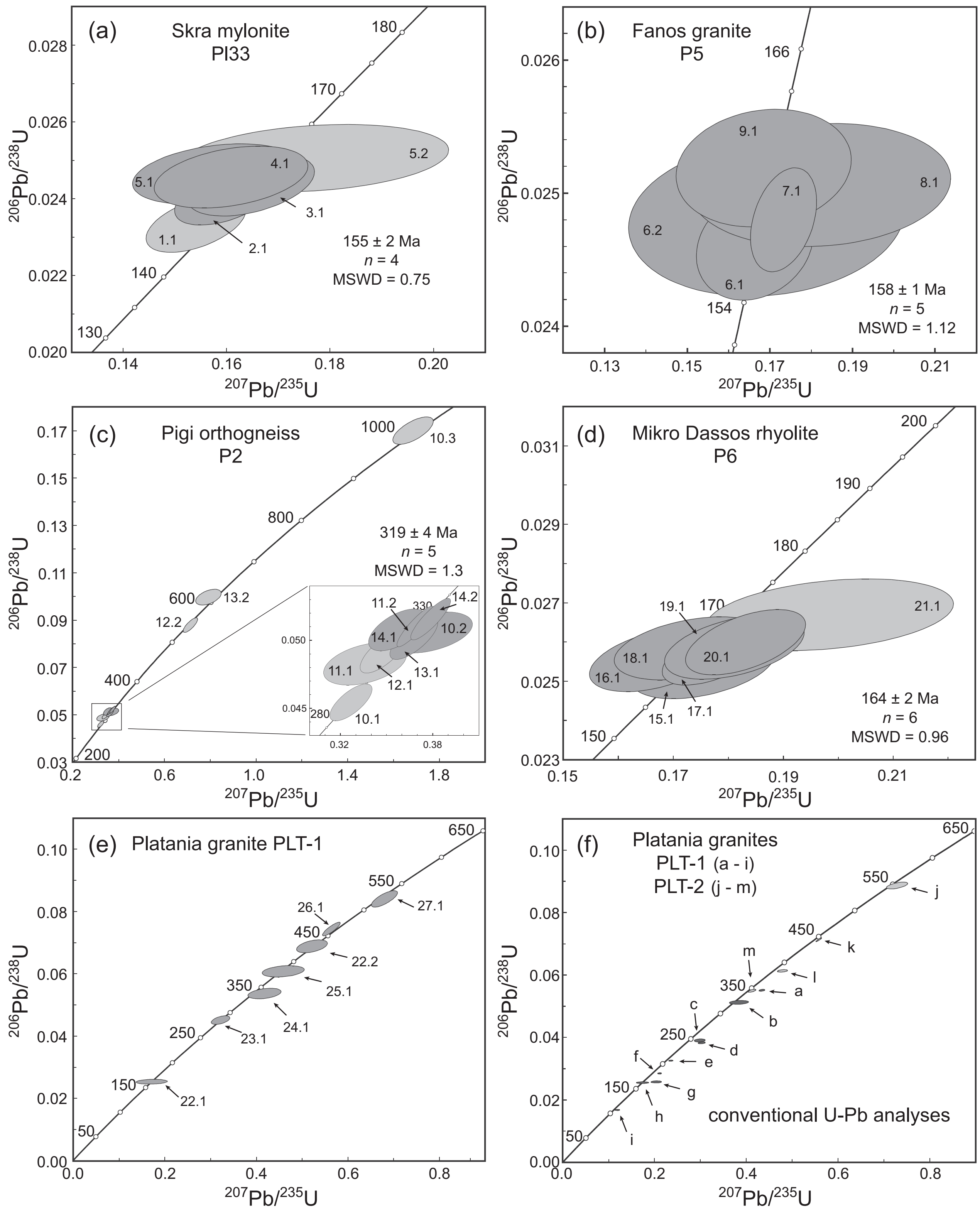

Fig. 1.6. Geochronological results of single-zircon conventional U-Pb and SIMS dating. All errors given are at a 95% confidence level, error ellipses are at 2σ level. (a) to (e): SIMS dating, (f) conventional U-Pb dating.

In CL images most zircons of the *Pigi orthogneiss* (P2) show oscillatory-zoned rims and rounded cores (Fig. 1.5c), but grains with single-phase clear magmatic oscillatory zoning without visible cores also occur (Fig. 1.5d). In addition, some grains show small, very bright overgrowths (Fig. 1.5c). For geochronology, eleven spots on five zircon grains were analysed with SHRIMP; spots were chosen on both core and rim. Five spots resulted in a concordia age of 319 ± 4 Ma (95% confidence, n = 5, MSWD = 1.3, P = 0.25). Of the five spots, three were measured on rims and two on cores. The concordia age of 319 Ma is interpreted as the intrusion age (Fig. 1.6c). Thus, orthogneiss P2 is the oldest rock in the study area. Three spots yielded ages slightly younger than the concordia age of 319 Ma and are interpreted to document Pb loss (spots 10.1, 11.1 and 12.1, Fig. 1.6c). They were therefore excluded from the age calculation. Three older, relatively concordant spots on rounded cores yielded ages of *c.* 540, 600 and 1000 Ma, that point to an inherited component. These three ages are clearly distinct from one another and are an indication that more than one protolith component was involved in granite formation. The bright overgrowths were too small to be analysed. They might have formed, however, during a younger thermal-metamorphic event. Several spots show very low Th/U ratios of ≤ 0.03, often interpreted to reflect metamorphic zircon growth (e.g. Williams & Claesson 1987; Rubatto & Gebauer 2000; Rubatto 2002). These spots belong exclusively to rim measurements that yielded Permo-Carboniferous ages. We nevertheless prefer to interpret the Permo-Carboniferous age as the magmatic intrusion age of the rock. A possible explanation for the extremely low Th/U ratios could be the simultaneous growth of accessory minerals that preferably incorporate Th (monazite, allanite, etc.) together with zircon (Möller *et al.* 2003). Monazite is present in orthogneiss P2, however its primary formation age is unknown. Möller *et al.* (2003) questioned whether it is adequate, at least for high-grade metamorphic rocks, to rely on Th/U ratios when allocating a zircon growth phase to either metamorphism or magmatism. Moreover, a scenario in which the low Th/U ratio is an expression of anatectic melting, as proposed by Zeck & Whitehouse (1999) for a Hercynian orthogneiss from the Betic Cordillera, seems possible. Further support of a Permo-Carboniferous magmatic event comes from three spots with Th/U ratios in the range of 0.17 to 0.77 that reflect igneous growth (spots 11.1, 14.1 and 14.2).

The zircons of the *Mikro Dassos rhyolite* (P6) have a euhedral morphology and a single-phase internal structure in CL images (Fig. 1.5e). Seven spots were analysed on seven grains, covering both the central and outer parts of the crystal. The concordia age of 164 ± 2 Ma (95% confidence, n = 6, MSWD = 0.96, P = 0.48) obtained from SIMS analyses is interpreted as the emplacement age of the rhyolite (Fig. 1.6d). One spot plots discordantly and yielded an older $^{206}Pb/^{238}U$ age, and was therefore not included in the age calculation (spot 21.1, Fig. 1.6d).

Zircons from the *Platania granite* (PLT-1 and PLT-2) show generally rounded cores in CL images, oscillatory zoning is mostly preserved (Fig. 1.5f). They were dated using SIMS and the conventional U-Pb methods. Both concordant and discordant grains scatter variably in the concordia diagram (*c.* 160 to 520 Ma) and render the assignment of a distinct emplacement age impossible (Fig. 1.6e and f). This indicates, as could already be expected from the CL images, that the zircon populations of Platania granites PLT-1 and PLT-2 are dominated by inherited components or grains, possibly of detrital origin. As the heterogeneous zircon population of PLT-1 is indistinguishable from that of PLT-2, an interpretation of granite PLT-2 as the source material from which PLT-1 was derived by partial melting seems plausible. Exactly when this melting episode took place cannot be said from zircon dating as the zircons seem to reflect the source rock only. We suggest that anatexis occurred at medium temperatures, probably under hydrous conditions, and that the duration of the melting episode was not long enough to reset the zircons of these samples completely. Nevertheless, the scatter of the zircon grains in the concordia diagram is in favour of the interpretation that at least one of the contributing sources had an age of around 450 to 400 Ma. The variation in the Th/U ratios reflects the composite structure of the zircons. Some of the rims as well as one core display very low Th/U ratios, which is mostly due to low Th concentrations. These rims also show a tendency towards younger ages, which might be caused by metamorphic growth or recrystallisation.

In order to constrain the age of metamorphism, monazites from the *Pigi orthogneiss* (P2) were dated by the U-Th-Pb chemical-dating method using an electron microprobe (Fig. 1.7, Appendix G). Sixty

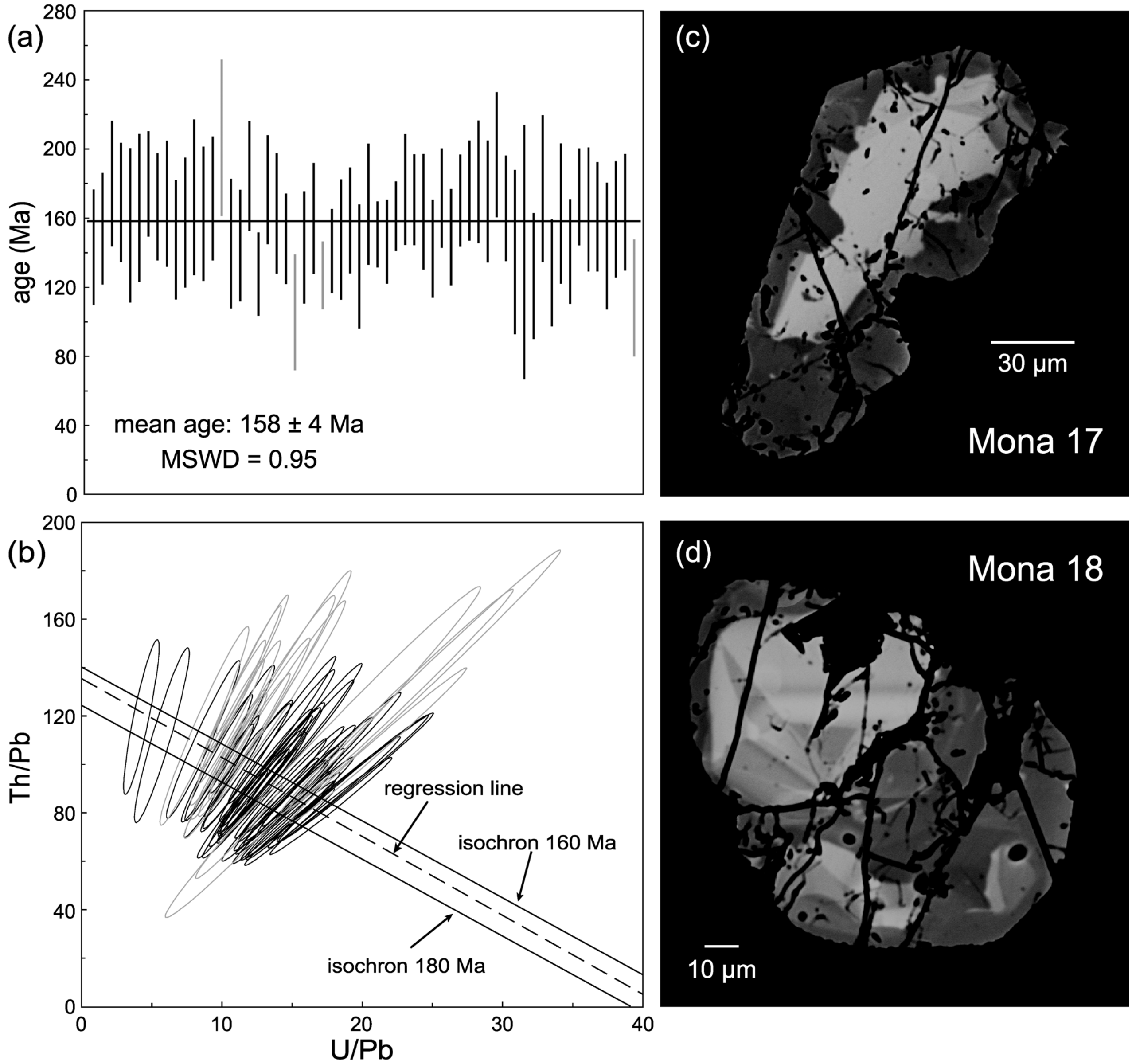

Fig. 1.7. U-Th-Pb monazite ages from the Pigi orthogneiss P2, error bars and error ellipses are at 2σ level. (a) Individual monazite ages, data rejection using a modified 2σ criterion after Ludwig (2003). (b) Th/Pb-U/Pb plot after Cocherie & Albarède (2001) to test if the points fulfil isochron criteria. As can be seen, rejection of 18 points (light grey) out of 60 is required, which could be attributed to Pb loss. The regression line gives a resulting age of *c.* 164 ± 5 Ma and therefore slightly older but within 2σ error with the age of 158 ± 4 Ma calculated as weighted average. (c) and (d) BSE-images of two large monazites. Seven points were measured on Mona 17 and six points on Mona 18.

spots on 25 monazites were analysed, with one to seven spots on individual grains. The monazites showed to be rather homogeneous with respect to the ages (Fig. 1.7a, Appendix G). Only two spots revealed a definitely older (inherited?) Pb component with ages of 197 and 207 Ma, while three spots gave younger ages. Pb loss due to volume diffusion is not very common in monazites (Parrish 1990) and would be extremely slow (Smith & Giletti 1997; Cherniak *et al.* 2004); therefore, these younger ages could be caused either by recrystallisation or continuous/episodic monazite growth over a period of time (Foster *et al.* 2002). Possible indications for recrystallisation or later growth can be seen in BSE-images where darker and brighter zones form a patchy pattern (Fig. 1.7c and d). It can also be argued that the rejection of 18 points on the Th/Pb-U/Pb diagram after Cocherie & Albarède (2001; Fig. 1.7b) in order to fit the regression line to an isochron is necessary because these points have experienced Pb loss. On the other hand, the rather small spread of the ellipses along the regression line and the large error to which each point is subjected by this method, suggest that it would be rather farfetched to distinguish two age groups in this age range, one for metamorphic growth and one for later recrystallisation. Therefore, only one age was calculated as the weighted average of all spots, rejecting the three youngest points and the oldest point (Fig. 1.7a). Rejection was carried out by Isoplot applying a modified 2σ criterion (Ludwig 2003). The age of 158 ± 4 Ma thus obtained is interpreted to reflect either the time of high-grade metamorphism and monazite growth, or in the case that monazite was a primary phase, crystallising concomitantly with zircon, the complete reequilibration and resetting of the U-Th-Pb system of the monazite.

1.6 Isotope geochemistry

Sr- and Nd-isotope compositions were determined for samples P2, P5, P6, Pl33 and PLT-1 (Appendix C). For most samples $^{87}Sr/^{86}Sr_i$ ranges between 0.704734 and 0.707268, indicating that the source rock consisted both of mantle material ($^{87}Sr/^{86}Sr$ of mantle today *c.* 0.702 – 0.706; Faure 1986) and variable amounts of an older crustal component. The lowest $^{87}Sr/^{86}Sr_i$ value of 0.702097 is that of Skra mylonite Pl33. However, the high Rb/Sr ratio of this sample (5.2) implies that small errors in concentration measurements can induce large errors in the Sr initial ratio. An explanation for such a low $^{87}Sr/^{86}Sr_i$ is secondary increase of the Rb/Sr ratio due to Sr loss during metamorphism, as suggested by the very low Sr concentration of 31 ppm. This could have been caused during feldspar alteration, which is considered to have shifted the Skra mylonite towards the A-K boundary in the A-CN-K diagram of Nesbitt & Young (1989; Fig. 1.3b) as discussed earlier. In the case of Mikro Dassos rhyolite P6, secondary alteration led to potassium depletion which is deemed responsible for Rb removal and hence the low Rb/Sr ratio of the sample.

Nevertheless, Nd should be rather unaffected by low-grade alteration. Generally, values of εNd_i vary from -10.7 to +1.7. The calculated model ages (T_{DM}) range from 2.5 to 0.6 Ga. Those samples with the oldest T_{DM} values also show the most negative εNd_i. For example, isotope analysis of the Platania granite PLT-1 yielded the lowest εNd_i value of -10.7 as well as the oldest T_{DM} value of 2.5 Ga. Negative εNd_i and old model ages indicate that either larger quantities of pre-existing continental crust or distinctly older crust contributed to the source from which the magma was derived. Therefore there is good evidence that a larger crustal component was involved in the genesis of the "old basement rocks" P2 and

PLT-1 compared to that of the Late Jurassic rocks, as suggested by their negative εNd_i values and older T_{DM} model ages of 1.3 and 2.5 Ga respectively. This interpretation, especially for the Platania granite, is supported by the abundance of inherited zircon grains, which constitute further evidence for the contribution of an older crustal component in magma genesis. The Nd-isotope characteristics of the Late Jurassic rocks differ distinctly from those described above for the "old basement rocks". Mikro Dassos rhyolite P6 in particular has a rather high εNd_i value of 1.7. This indicates a significant contribution from a mantle source in the genesis of this rock. For the Fanos granite, the εNd_i values of -2.1 to -2.7 indicate that a smaller, yet detectable, amount of mantle material was involved in the genesis of this rock. Skra mylonite Pl33 has an εNd_i of -4.4; here the contribution of crustal material played a more dominant role. The T_{DM} model ages for these younger rocks are between 0.6 Ga and 1.0 Ga suggesting some contribution from a crustal component. The results described above make it unlikely that the Late Jurassic rocks were formed in an intra-oceanic arc, a finding in agreement with the existence of remnants of pre-Jurassic basement in the area.

1.7 Discussion

The geochronological results presented in this paper give clear evidence for a Late Jurassic magmatic and metamorphic event in the eastern Vardar Zone.

In this area, which comprises the western part of the Peonias Subzone and the eastern part of the Paikon Subzone, magmatic activity is documented for a time span from 164 Ma to 155 Ma, as shown by U-Pb dating of zircons from felsic rocks. The rocks are geochemically classified as syn-COLG or VAG, which favours an emplacement in a subduction-related environment. This model is also suggested for the emplacement of the Fanos granite. These felsic rocks are contemporaneous or only slightly younger than rocks from the Guevgueli ophiolite. Spray *et al.* (1984) gave K-Ar determinations for biotite and amphibole separates of gabbros from the Guevgueli ophiolite of Late Jurassic age (163 ± 3 Ma to 149 ± 3 Ma). Danelian *et al.* (1996) reported radiolarian fauna of Oxfordian age (159.4 Ma – 154.1 Ma, Remane *et al.* 2000) in the volcanic part of this complex, greatly supporting the radiometric data. The contemporaneity in ophiolite formation and felsic arc magmatism suggests that intra-oceanic subduction started soon after the opening of the ocean basin. Bébien *et al.* (1986) suggested that the Guevgueli basin commenced as a continental wrench basin. This is indicated by structural and petrological evidence in conjunction with the close association between the ophiolite and crustal basement rocks (Pigi and Karathodoro blocks) in a transtensive dextral strike-slip setting. The Guevgueli ophiolite has been grouped together with the Oreokastro, Thessaloniki and Sithonia ophiolites further southeast as the Innermost Hellenic Ophiolite Belt (Bébien *et al.* 1986), which defines a NW-SE trending belt. This grouping is supported by an age of 172 ± 5 Ma reported for a hornblende gabbro dyke from the Thessaloniki ophiolite (Kreuzer, cited by Mussallam & Jung 1986a, probably K-Ar) and geophysical investigations (Kiriakidis 1989). Along the eastern side of this ophiolite belt (SE of Thessaloniki) a metamorphic suite of mafic to felsic, formerly magmatic, rocks can be found, which is described as the Chortiatis Magmatic Suite (Kockel & Mollat 1977; Schünemann 1985; Mussallam & Jung 1986a; see Fig. 1.1). Among other rocks, the Chortiatis Magmatic Suite comprises tonalitic to trondhjemitic types that are characterised by high Na_2O and low K_2O concentrations (Mussallam &

Jung 1986a) and are geochemically very similar to Mikro Dassos rhyolite P6. Mussallam & Jung (1986a) interpreted the Chortiatis Magmatic Suite as having formed in an immature arc during the subduction prior to ophiolite emplacement. The geochemistry of Mikro Dassos rhyolite P6 fits this interpretation, as its positive εNd_i value of 1.7 indicates a significant mantle component in the source of this rock. The geochemical similarity and the position of the rhyolite in the northwestern extension of the trend of the Chortiatis Magmatic Suite might be taken to indicate that the Chortiatis Magmatic Suite continues into this area, parallel to the Innermost Hellenic Ophiolite Belt. The possible influence of secondary alteration processes on the geochemical characteristics of the Mikro Dassos rhyolite and especially its alkali content has also been considered for some rocks of the Chortiatis Magmatic Suite (Schünemann 1985; Mussallam & Jung 1986a).

On the other hand, the question remains as to whether the Paikon volcanic arc and the Chortiatis Magmatic Suite together with the Mikro Dassos rhyolite represent edifices of the same volcanic chain formed above a single subduction zone and subsequently separated by tectonic/magmatic processes. Skra mylonite Pl33 from the easternmost Paikon Subzone has a lower εNd_i value (-4.4) than Mikro Dassos rhyolite P6, indicating the involvement of a crustal component in its formation. This could be an indication of its formation in a different environment, namely the Paikon arc. Yet it does not rule out the possibility that Skra mylonite Pl33 and Mikro Dassos rhyolite P6, formed in the same arc during different stages of its evolution, i.e. an early immature stage for P6 and a later, more evolved stage for Pl33. No further resolution is possible for the time being. With the data available at present we favour a scenario of arc splitting in the Late Jurassic and formation of the Guevgueli basin.

Brown & Robertson (2003, 2004) developed a model in which rifting occurred in a back-arc setting behind the Paikon volcanic arc, which is suggested to have formed along the continental margin of the Serbo-Macedonian Massif. The development of this back-arc basin stalled soon after its formation (Bébien *et al.* 1986). In this study we have shown that, in the Peonias Subzone, orthogneiss P2 and granites PLT-1 and PLT-2 are hitherto the only evidence for Palaeozoic basement. Zachariadou & Dimitriadis (1994) considered the migmatites and orthogneisses from the Pigi area as representing a sliver of Serbo-Macedonian basement. However, the Carboniferous intrusion age (319 Ma) of the Pigi orthogneiss demonstrated here precludes it from being part of the Vertiskos Unit of the Serbo-Macedonian Massif for which exclusively Silurian ages of granitoids have been reported (426 to 435 Ma, Pb-Pb on zircon, Himmerkus *et al.* 2003). Mercier (1968) determined Permo-Carboniferous Rb-Sr muscovite ages for pegmatites intruding the westernmost margin of the Vertiskos Unit (10-25 km NNE of Thessaloniki), however no zircon ages are available as yet for the host gneisses. It therefore seems much more likely that the Pelagonian Zone, consisting of *c.* 320 Ma to 280 Ma-old Palaeozoic basement (e.g. Vavassis *et al.* 2000; Reischmann *et al.* 2001; Pe-Piper & Piper 2002 and references therein; Anders *et al.* 2002, 2003c), was the region from which the Pigi basement block originated.

The provenance of the detrital zircons of Platania granites PLT-1 and PLT-2 cannot be fully unveiled. However, U-Pb SIMS geochronology yielded ages of rounded cores of zircons of *c.* 284, 430 and 460 Ma, which are a good indication that at least part of the detritus forming the source of this rock came from the Vertiskos Unit in the east. A zircon rim age of *c.* 520 Ma hints to an even older source. Derivation of the bulk detritus from the Pelagonian Zone, where basement ages of around 300 Ma predominate, seems rather unlikely. Young rims with ages of *c.* 160 and 100 Ma surrounding 430 and

460 Ma-old zircon cores might be due to a thermal overprint during the course of Late Jurassic magmatic activity. Late Jurassic thermal overprint and metamorphism is attested to by monazite formation (or complete resetting) in orthogneiss P2 at 158 Ma, and this thermal event possibly also led to the formation of the migmatites.

The results of our study highlight the difficulties in tracing the boundaries of continental units in a region like the eastern Mediterranean, which is characterised by multiple ocean basin formation and closure. The geochronological data of felsic rocks presented here underline the existence of continental basement of Pelagonian affinity in the eastern part of the Vardar Zone (Peonias Subzone) that was formerly interpreted to have once belonged to the Serbo-Macedonian Massif (Zachariadou & Dimitriadis 1994). If we also take into account the above mentioned Permo-Carboniferous Rb-Sr ages of small granite stocks and pegmatites dated by Mercier (1968), the pre-Mesozoic basement identified in the Peonias Subzone seems more closely related to the Pelagonian Zone than to the Vertiskos Unit of the Serbo-Macedonian Massif, although the Lower Palaeozoic inherited zircon ages of Platania granite PLT-1 could indicate a Vertiskos influence. Nevertheless, it raises the question as to how this Pelagonian-type Pigi block came to be situated not only east of the Paikon volcanic arc but even east of the Guevgueli ophiolite. One possibility is that the Pigi block might merely have been separated from the Pelagonian Zone by the opening of the Almopias ocean basin and again later by the opening of the more eastwardly-situated Guevgueli back-arc basin. If this is true, the Paikon arc did not form exclusively on the southern margin of the Serbo-Macedonian Massif as suggested by the model of Brown & Robertson (2003, 2004) but on Pelagonian basement that was rifted during Early Mesozoic opening of the Almopias ocean in the western Vardar Zone. This scenario would suggest a close relation between the Pelagonian Zone and the Serbo-Macedonian Massif in Late Palaeozoic/Early Mesozoic times because Triassic volcanic rocks that are linked to Early Mesozoic rifting in this area are exposed in immediate proximity to the Serbo-Macedonian Massif and Mesozoic extension is recorded in granites intruding the Serbo-Macedonian Massif (Himmerkus *et al.* 2003). Another possibility is that the Pigi block has been transported laterally in a shear zone an unknown distance in an unknown direction to its present location.

Independent of the mechanism by which the Pigi basement block was transported to its present position, it is clear from the monazite dating that it experienced metamorphism in the Late Jurassic, more or less coeval with volcanic activity in the Paikon arc.

A correlation of the Vardar Zone with suture zones in Turkey is still a matter of debate but of importance for palaeogeographic reconstructions. Possible candidates for such a correlation are the Izmir-Ankara Zone and the Intra-Pontide Zone. Around both zones accretionary wedges are indications for Cretaceous subduction. The age groups of the crustal basement blocks that were juxtaposed by the closure of these suture zones, however, are distinctly different from those of both the Pelagonian Zone and the Serbo-Macedonian Massif. Stampfli *et al.* (2004) have, nonetheless, argued that large-scale east-west shortening took place in the eastern Mediterranean domain mainly during the Cretaceous resulting in duplication of sutures, especially in western Turkey. In support of their view they invoked the fact that both borders of the Izmir-Ankara suture zone are not former conjugate passive margins. They further suggested that the Vardar suture in Greece could be correlated with the Izmir-Ankara suture in Turkey. The data obtained in this study are in agreement with such a model.

An alternative model can be derived from new results on the Rhodope Massif, where Late Jurassic gneisses are juxtaposed with Permo-Carboniferous basement along a suture zone (Turpaud & Reischmann 2005). The similarity of these ages with those determined in our study suggests that the Vardar Zone might be correlated to such an intra-Rhodope suture zone.

1.8 Conclusions

The results of this study are in agreement with existing models for the closure of an ocean basin/branch of either the Neotethys or the Palaeotethys in this area (e.g. Mountrakis 1986; Bébien *et al.* 1994; Brown & Robertson 2003, 2004). Zircon geochronology of felsic rocks provided much more accurate and reliable emplacement ages compared to previously employed methods (e.g. K-Ar or Rb-Sr). Our new results show that a major phase of magmatic activity took place in the eastern Vardar Zone from 164 Ma to 155 Ma (Late Jurassic). In this time span, metamorphic overprint (158 Ma) of 319 Ma old Carboniferous basement is intimately associated with the creation of an ensialic back-arc basin (Guevgueli ophiolite) and intrusion of the Fanos granite (158 Ma), all taking place in a subduction zone environment.

The provenance of the Carboniferous basement can be sought in the Pelagonian Zone west of the Vardar Zone. However, ages of inherited zircons (*c*. 520-285 Ma) from an anatectic granite further east suggest derivation of the detritus from the Vertiskos Unit of the Serbo-Macedonian Massif, east of the Vardar Zone.

Geochemical analyses for major and trace elements as well as Sr- and Nd- isotope analyses indicate the formation of the rocks studied here in a volcanic-arc or active continental-margin setting with variable contribution from older crustal material. The Fanos granite intruded into the Guevgueli ophiolite at about 158 Ma. Therefore, obduction of the Guevgueli ophiolite and closure of the Guevgueli ocean basin must have taken place prior to this intrusion.

Arc formation and accretion were the most important geological processes in the Vardar Zone during Late Jurassic times and dominated the igneous evolution of this part of the Internal Hellenides.

Chapter 2. The Florina Terrane: first evidence for a Precambrian terrane within the NW Pelagonian Zone

This chapter is largely identical to a manuscript entitled "The oldest rocks of Greece: first evidence for a Precambrian terrane within the Pelagonian Zone", which is accepted for publication in the Geological Magazine. Co-authors are T. Reischmann, D. Kostopoulos and U. Poller.

2.1 Abstract

The Pelagonian Zone in Greece represents the westernmost belt of the Hellenide hinterland (Internal Hellenides). Previous geochronological studies of basement rocks from the Pelagonian Zone have systematically yielded Permo-Carboniferous ages. In this study we demonstrate, for the first time, the existence of a Precambrian crustal unit within the crystalline basement of the Pelagonian Zone. The U-Pb single-zircon and SHRIMP ages of these orthogneisses vary from 699 ± 7 Ma to 713 ± 18 Ma, which identify them as the oldest rocks in Greece. These Late Proterozoic rocks, which occupy today an area of *c*. 20 x 100 km, are significantly different to the neighbouring rocks of the Pelagonian Zone. They are therefore interpreted as delineating a terrane, named here the Florina Terrane. During the Permo-Carboniferous, Florina was incorporated into an active continental margin, where it formed part of the basement for the Pelagonian magmatic arc. The activity of this arc was dated in this study by single-zircon $^{207}Pb/^{206}Pb$ ages as having taken place at 292 ± 5 Ma and 298 ± 7 Ma. During the Alpine orogeny, Florina, together with the Pelagonian Zone, eventually became a constituent of the Hellenides. Geochemically, the Florina orthogneisses represent granites formed at an active continental margin. Because of the late Proterozoic ages, this arc can be correlated to a Pan-African or Cadomian arc. Since the gneisses contain inherited zircons of Late to Mid-Proterozoic ages, the original location of Florina was probably at the northwestern margin of Gondwana. Similarly to other Gondwana-derived terranes, such as East Avalonia, Florina approached the southern margin of Eurasia during the Palaeozoic, where it became part of an active continental margin above the subducting Palaeotethys. These interpretations further indicate that terrane accretion was already playing an important role in the early pre-Alpine evolution of the Hellenides.

2.2. Introduction and geological background

In the eastern Mediterranean, the Hellenides constitute an integral part of the Alpine-Himalayan orogenic belt. The Hellenides are traditionally divided into the Internal Hellenides (i.e., the Greek hinterland) with abundant occurrences of gneissic and granitic basement rocks and the External Hellenides (i.e., the Greek foreland), built up by Mesozoic and Cainozoic cover rocks (e.g. Aubouin *et al.* 1963; see also Jacobshagen 1986). The Internal Hellenides are further subdivided into several tectonostratigraphic zones which, from NE to SW, are: the Rhodope Massif, the Serbo-Macedonian Massif, the Vardar Zone, the Pelagonian Zone and the Attico-Cycladic Massif (e.g. Aubouin *et al.* 1963; see also Jacobshagen 1986).

The Neoproterozoic to Tertiary evolution of the Mediterranean realm, especially the eastern Mediterranean, includes the opening and closure of multiple ocean basins (e.g. Şengör & Yilmaz 1981; Stampfli

& Borel 2002; von Raumer *et al.* 2003). Subduction-related magmatism is widespread and possible tectonic settings include intra-oceanic volcanic-arc magmatism as well as magmatism at an active continental-margin setting, either along the northern margin of Gondwana or the southern margin of Baltica/Europe. Generally, geochemistry and dating of magmatic rocks can discriminate between different tectonic settings, lead to the identification of distinct terranes and help to constrain their evolutionary history (Pearce *et al.* 1984; Nance & Murphy 1994; Friedl *et al.* 2000). Here, we have used geochemical and geochronological tools to decipher a possible multiphase evolution of the basement rocks from the Pelagonian Zone.

The Pelagonian Zone forms an elongated NNW-SSE trending zone (Fig. 2.1a). Towards the north it continues into the Former Yugoslav Republic of Macedonia (F.Y.R.O.M.), while in the south it is bordered by the Attico-Cycladic Massif (Fig. 2.1a). The Greek part of the Pelagonian Zone consists of granitic and gneissic basement rocks, Mesozoic metasedimentary rocks and Tertiary to recent sediments (e.g. Jacobshagen 1986 and references therein; Pe-Piper & Piper 2002 and references therein). Outcrops of basement rocks are discontinuous, although all geochronological results reported so far show that their ages are rather uniform, ranging from 280-320 Ma (e.g. Yarwood & Aftalion 1976; Mountrakis 1984; Koroneos *et al.* 1993; Katerinopoulos *et al.* 1998; Vavassis *et al.* 2000; Reischmann *et al.* 2001; Anders *et al.* 2003c). Geochemical fingerprinting favours a subduction-zone environment as the origin for the basement rocks of the Pelagonian Zone, most probably in a volcanic-arc or active continental-margin setting (e.g. Pe-Piper *et al.* 1993a, b; Katerinopoulos *et al.* 1998; Vavassis *et al.* 2000; Reischmann *et al.* 2001; Anders *et al.* 2003c). This leads to the interpretation of the Pelagonian Zone as a large Permo-Carboniferous magmatic arc (e.g. Reischmann *et al.* 2001; Anders *et al.* 2003c). However, an active continental-margin setting would require the existence of older, pre-Carboniferous continental basement. To date, only structural and stratigraphic reasoning has indicated the existence of Lower Palaeozoic or older basement in the Pelagonian Zone, e.g. as inferred from intrusive contacts of an Upper Carboniferous granite in gneissic rocks by Mountrakis (1984). Kilias (unpub. Ph.D. thesis, Univ. Thessaloniki 1980) and Marakis (1969) obtained Lower Palaeozoic K-Ar ages for rocks from the northern Pelagonian Zone in Greece and its northward continuation into F.Y.R.O.M., but attributed these old ages to excess Ar. Most (2001, 2003) undertook a geochronological study of rocks from the northwest Pelagonian Zone in southern F.Y.R.O.M. and measured a Silurian K-Ar age (447 ± 17 Ma) for white mica extracted from a granite. However, zircons from the same sample dated by the U-Pb method yielded a Permian age (246 ± 7 Ma). Most (2003) explained this discrepancy by invoking excess $^{40}Ar^{*}$ due to metasomatic alteration. It is therefore clear from the above that the question as to the existence of Lower Palaeozoic or older magmatic rocks in the Pelagonian Zone has not yet been answered. In the Attico-Cycladic Massif, which can be regarded as the southern extension of the Pelagonian Zone, basement rocks show the same range of Permo-Carboniferous ages, clustering around *c.* 300 Ma (Engel & Reischmann 1998; Reischmann 1998). No evidence for older magmatic rocks exists for the Cycladic islands.

In our study we focused on the geochronology and geochemistry of basement rocks from the northwestern part of the Pelagonian Zone in Greece. The aim was to improve geochronological

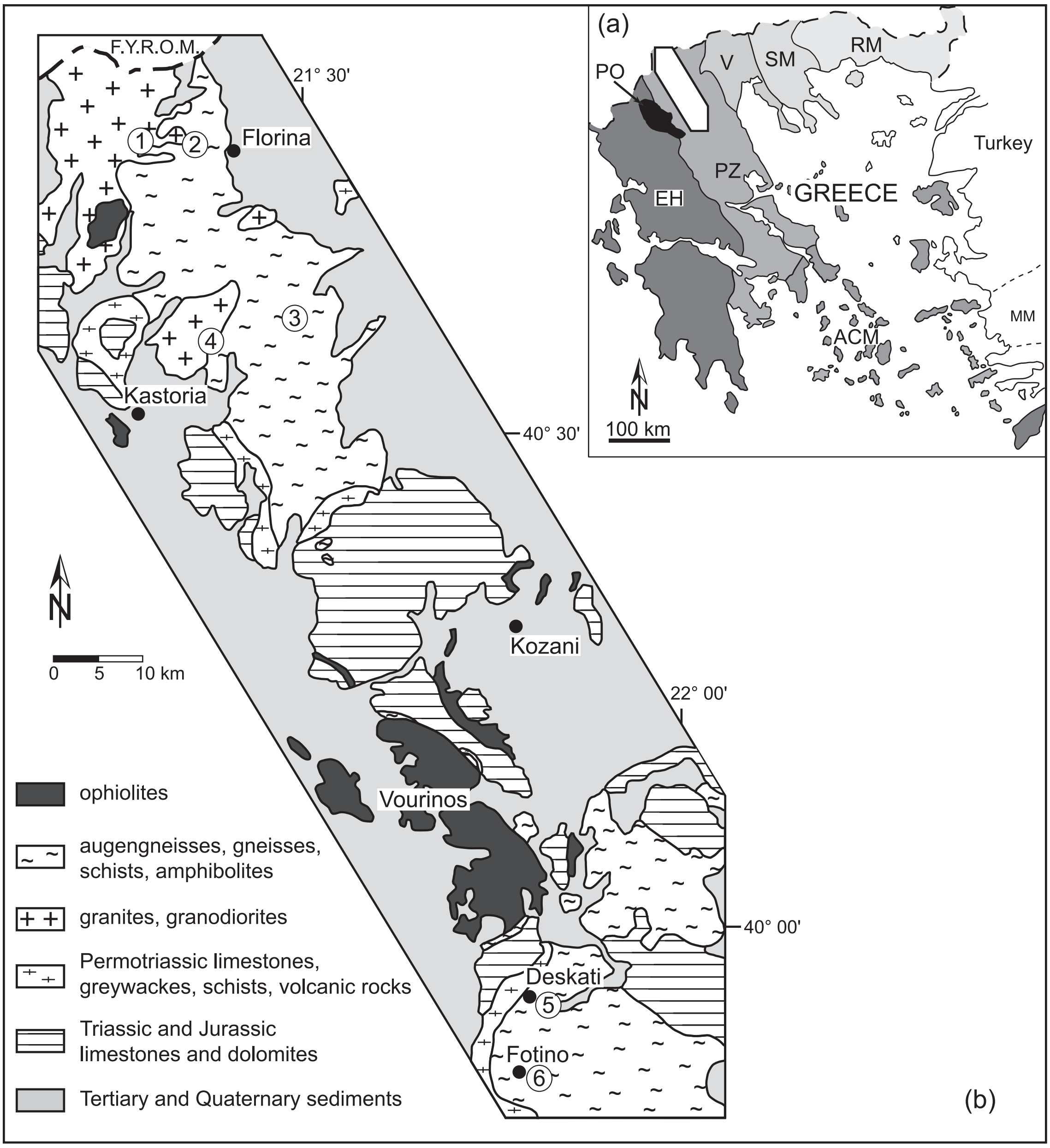

Fig. 2.1. (**a**) Map showing the tectonostratigraphic zones of the Hellenides. RM: Rhodope Massif; SM: Serbo-Macedonian Massif; V: Vardar Zone; PZ: Pelagonian Zone; ACM: Attico-Cycladic Massif; EH: External Hellenides; PO: Pindos ophiolite; MM: Menderes Massif. (**b**) Geological map of the study area, simplified after the geological map of Greece 1:500 000 (IGME, 1983). Sample localities: 1) Varnous granodiorite V1; 2) Varnous orthogneiss V9; 3) Florina orthogneisses Pl58 and Pl59; 4) Kastoria granite Pl61; 5) Deskati orthogneiss Pl70; 6) Fotino granite Pl64-Pl66. F.Y.R.O.M.: Former Yugoslav Republic of Macedonia.

resolution and follow up the question of Early to Mid-Palaeozoic ages of the westernmost Internal Hellenide Zones, as well as to characterise geochemically the basement rocks with regard to their possible tectonic setting. Special emphasis was put on single-zircon dating, as zircons (a) are abundant accessory minerals in felsic rocks, (b) strongly incorporate Th and U but only minor amounts of Pb, thus making them suitable for U-Pb dating, (c) have a high closure temperature for the U-Pb system (e.g. Lee *et al.* 1997; Cherniak & Watson 2000) allowing dating of the intrusion event, (d) are resistant to resetting of the U-Pb isotopic system during later metamorphic events or alteration (e.g. Parrish 2001; Corfu *et al.* 2003). Orthogneisses and granitic basement rocks were sampled from the Florina, Kastoria and Fotino localities (see Fig. 2.1b) and are discussed in detail below.

2.3 Analytical methods

Zircons were dated using the single-zircon Pb-Pb evaporation technique (Kober 1986, 1987), the single-zircon conventional U-Pb method and by sensitive high-resolution ion microprobe (SHRIMP). Dating with the conventional U-Pb method was based on the low-contamination dissolution method of Krogh (1973), two variants of which were used: (a) the vapour-digestion method (Wendt & Todt 1991) and (b) the chemical separation of Pb and U by HBr chemistry following dissolution. The measurements were performed with a Finnigan MAT 261 thermal ionisation mass-spectrometer (TIMS) at the Max-Planck-Institut für Chemie, Mainz, Germany, using an ion multiplier. The measured ratios were corrected for fractionation (3‰ per ΔAMU), blank and common Pb (using the values given by Stacey & Kramers 1975). The fractionation factor was determined by measuring NBS 981 under the same conditions as the samples. Total procedure blanks for Pb were < 10 pg for vapour digestion and < 40 pg for chemical separation. Ages were calculated using Isoplot (Ludwig 2003).

One sample was dated with SHRIMP at the Centre of Isotopic Research, St. Petersburg, Russia. The TEMORA reference zircon (age 416.75 Ma, Black *et al.* 2003) was used for calibration of the Pb-U ratios. Data reduction and age calculations were based on SQUID (Ludwig 2001).

Concordia diagrams were drawn using Isoplot (Ludwig 2003). All ages are given either at the 2σ or 95% confidence level. Calculation of the weighted average was based on Ludwig (2003).

Whole-rock Sr- and Nd-isotope compositions were measured with a Finnigan MAT 261 TIMS in multicollector mode at the Max-Planck-Institut für Chemie, Mainz, Germany. Sample preparation was based on standard procedures as described in White & Patchett (1984). Mass fractionation of Nd and Sr was corrected to $^{146}Nd/^{144}Nd$ = 0.7219 and $^{86}Sr/^{88}Sr$ = 0.1194, respectively. During the course of this study, repeated analyses of La Jolla resulted in a measured $^{143}Nd/^{144}Nd$ value of 0.511823 ± 20 (95% conf., n=7). To allow comparison between samples measured on different days, all $^{143}Nd/^{144}Nd$ values were adjusted to this ratio. For the NBS SRM 987 an $^{87}Sr/^{86}Sr$ value of 0.710234 ± 12 (2σ, n=16) was obtained.

2.4 Sample description and geochronological results

Sample description and geochronological results are arranged in this paper from north to south (Fig. 2.1b). Geochronological data are presented in Appendices D-F.

The northernmost samples are V1 and V9, collected west of Florina town (Fig. 2.1b). Sample V1 is a rather coarse-grained igneous rock from the Varnous pluton. It consists mainly of quartz, K-feldspar, plagioclase and biotite, together with titanite and fine-grained epidote/zoisite. Remnants of amphibole also occur. Secondary alteration is indicated by the partial sericitisation of K-feldspar and partial conversion of titanite to leucoxene. The rock was dated by the single-zircon Pb-Pb evaporation method (Kober 1986, 1987). The analyses of six zircon grains resulted in $^{207}Pb/^{206}Pb$ ages of between 287 ± 4 Ma and 306 ± 2 Ma (Appendix D). There are two possible explanations for the lack of overlap of the ages within error. Firstly, the relatively small errors of the ages are probably underestimated because they are largely dependent on measurement statistics and a large number of $^{207}Pb/^{206}Pb$ ratios measured for each grain will produce small errors. The average age would then be meaningful and, in the case of this sample, date the intrusion event. A second possible explanation for the spread in ages is influence by a younger thermal event resulting in Pb loss and youngening of the $^{207}Pb/^{206}Pb$ ages. In this case the younger ages would reflect stronger Pb loss and only the oldest ages would approximate the intrusion age (assuming that no inherited Pb component exists). In the case of sample V1, evidence for Pb loss is demonstrated in one grain with a significantly younger $^{207}Pb/^{206}Pb$ age of 246 ± 18 Ma. CL images of zircons show clear, fine-scale oscillatory zoning that is interpreted to reflect magmatic growth and changing chemical conditions along zircon grain boundaries (e.g. oversaturation, diffusion rate) in the magma chamber (Vavra 1990; Mattinson *et al.* 1996). Several zircon grains show homogenous, light-grey, low-U domains that irregularly crosscut the oscillatory zoning in CL images (Fig. 2.2b). These zones are possibly due to recrystallisation, either during a late magmatic stage or metamorphism, where Pb-loss is loss is more likely (Connelly 2000). The irregular and sometimes convolute zones in the cores of several zircons are also interpreted as recrystallised parts. They might also indicate zircon domains affected by Pb loss. No indications for inherited cores were seen in CL images. The age group, which may still be regarded as fairly homogenous, implies that possible Pb loss did not severely affect the $^{207}Pb/^{206}Pb$ ratios in six out of seven grains and we suggest that the weighted average minimum age of 298 ± 7 Ma sufficiently approximates the intrusion event (Fig. 2.2a). The relatively large error of ± 7 Ma might then account for this uncertainty. The zircon age of this study is in good agreement with a Rb-Sr errorchron age of 297 ± 25 Ma (whole-rock and biotite) obtained by Koroneos *et al.* (1993) on igneous rocks from the Varnous pluton.

Sample V9 was taken from the country rock into which the Varnous pluton apparently intruded. It is a medium-grained, foliated orthogneiss with small feldspar "augen". The main minerals are

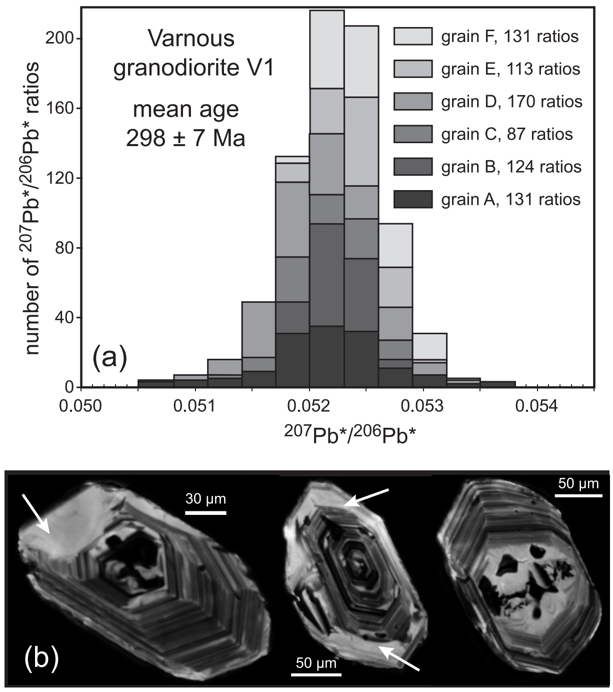

Fig. 2.2. (a) Histogram presenting single-zircon Pb-Pb evaporation analyses for Varnous granodiorite V1. (b) CL images of zircons from granodiorite V1, showing fine-scale magmatic zoning and recrystallised and resorbed parts of the zircons. Arrows indicate regions that crosscut the oscillatory zoning.

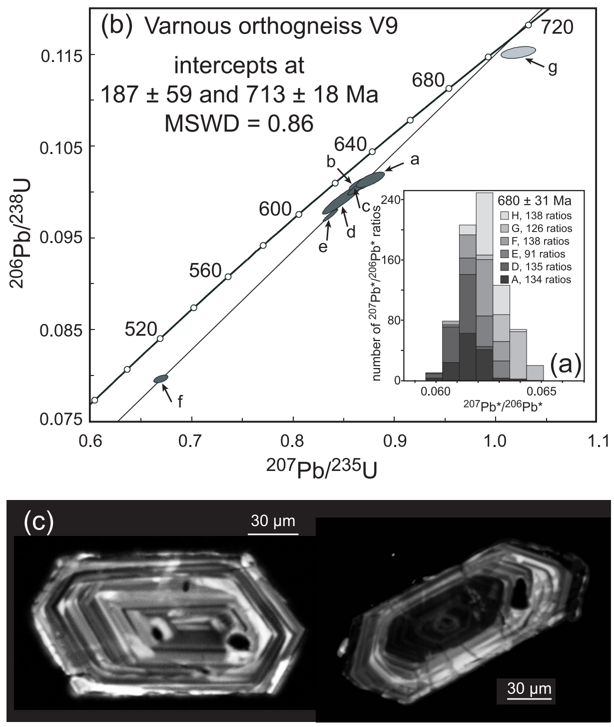

Fig. 2.3. (a) Histogram showing the results of single-zircon Pb-Pb evaporation dating for Varnous orthogneiss V9; two older grains are not shown (see Appendix D). (b) Concordia diagram for Varnous orthogneiss V9 (single-zircon conventional U-Pb measurements). Error ellipses are 2σ. The light-coloured ellipse (grain g) in the concordia diagram displays an inherited grain that was not included in the age calculation. (c) CL images showing clear single-phase magmatic zoning (left grain); rounded parts can also be seen (right grain).

quartz, K-feldspar, white mica, biotite, plagioclase and minor epidote. The rims of the K-feldspars show recrystallisation, which is an indication for metamorphism at upper greenschist to lower amphibolite facies conditions. For this sample the Pb-Pb evaporation method resulted in a wide range of individual zircon ages with a broad peak at about 680 ± 31 Ma (Fig. 2.3a) and distinctly older $^{207}Pb/^{206}Pb$ ages for two zircon grains at 904 ± 7 Ma and 1777 ± 13 Ma respectively (grains V9-B and V9-C, Appendix D). To obtain better accuracy and precision on the age, the conventional single-zircon U-Pb method was also applied. In a concordia diagram, the resulting upper intercept age of 713 ± 18 Ma (MSWD = 0.86) is interpreted as the emplacement age (Fig. 2.3b). The lower intercept age of 187 ± 59 Ma is attributed to Pb loss. One grain (grain g, Fig. 2.3b) has evidently inherited some older component, shown in a $^{207}Pb/^{206}Pb$ age of 754 ± 19 Ma. The existence of inherited components, as indicated by older $^{207}Pb/^{206}Pb$ ages obtained from both the Pb-Pb and the U-Pb method on sample V9, can be seen in CL images of zircons that show rounded cores (Fig. 2.3c).

The area southeast of Florina is characterized by exposures of amphibolites, paragneisses and orthogneisses. A rather coarse-grained orthogneiss was sampled approximately 20 km southeast of Florina. Samples PI58 and PI59 were taken from the same rock unit *c.* 100-200 m apart. The gneisses consist mainly of quartz, K-feldspar, plagioclase, white mica, biotite, and minor epidote. Single-zircon conventional U-Pb dating of both samples resulted in a large scatter of zircon grains in a concordia diagram (Fig. 2.4a) that makes the assignment of an intrusion age impossible. The scatter can be explained by inherited component(s) and one or more thermal/metamorphic events resulting in Pb loss. Inherited cores were not visible under the microscope but are abundant in the CL images. Zircons of orthogneiss PI58 were therefore dated with SHRIMP (Fig. 2.4b). Assuming that the rims reflect the magmatic intrusion event of the rock, SHRIMP measurements focused on analysing the rims of the zircons. Eight analyses resulted in a concordant age of 710 ± 5 Ma (MSWD = 0.98) that is interpreted as the intrusion age of the rock. One discordant spot (1.1) was not included in the age calculation. The analysis of one core (3.2) gave an age of *c.* 1500 Ma that was taken to indicate the age of

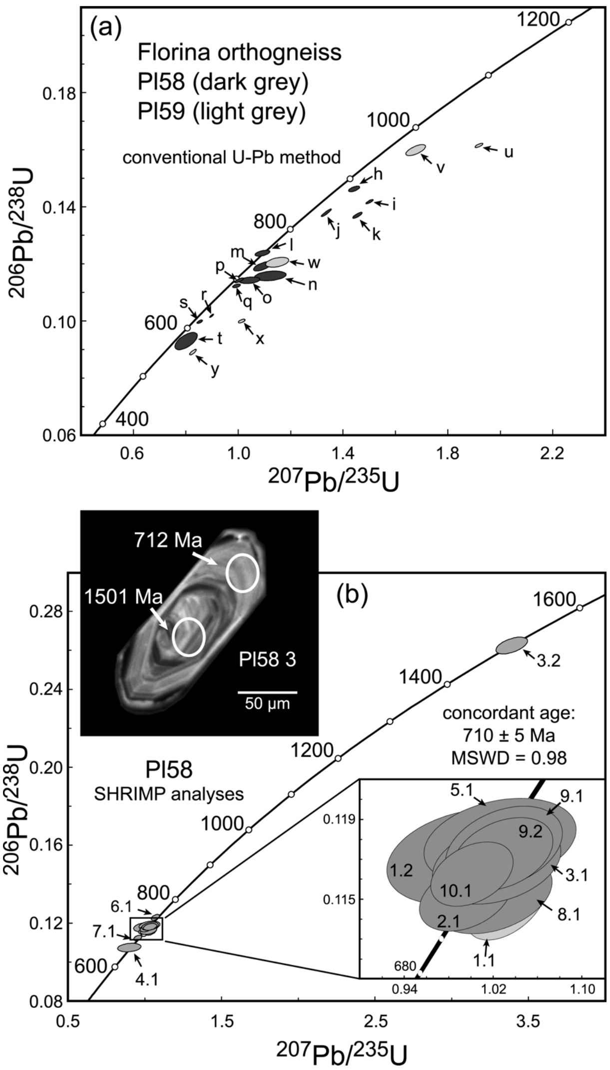

Fig. 2.4. (**a**) Concordia diagram for Florina orthogneisses PI58 and PI59 (single-zircon conventional U-Pb measurements). Note that many single-grain analyses cluster around 700 Ma. (**b**) SHRIMP results for sample PI58. Error ellipses are at the 2σ level. The CL image shows the complex structure of a zircon with Mid- Proterozoic core and Neoproterozoic mantle.

an inherited component. Two younger rim ages of *c.* 650 and 680 Ma (spots 4.1 and 7.1, Fig. 2.4b) are interpreted to reflect Pb loss.

The Kastoria granite is a large, deformed granitic body that is exposed east of the town of Kastoria. The granite was sampled from an outcrop about 10 kilometres west of the localities of Florina orthogneisses Pl58 and Pl59. Deformed granite Pl61 consists mainly of K-feldspar, quartz, saussuritised plagioclase, amphibole, sericite, apatite, titanite, remnants of biotite and epidote. It is a greenish granite with large angular K-feldspar crystals. The granite was dated by the single-zircon Pb-Pb evaporation method. The analyses of six zircons resulted in an age of 292 ± 5 Ma which is interpreted as the intrusion age (Fig. 2.5a). This interpretation is supported by CL images of zircons that show single-stage magmatic-growth oscillatory zoning (Fig. 2.5b). In some CL images, diffuse areas of resorption can be seen. Resorption can take place in a magma chamber during Zr undersaturation (Corfu *et al.* 2003). As this process occurs during growth of the zircon it does not disturb the age information of the U-Pb system of the mineral, which reflects the magmatic event.

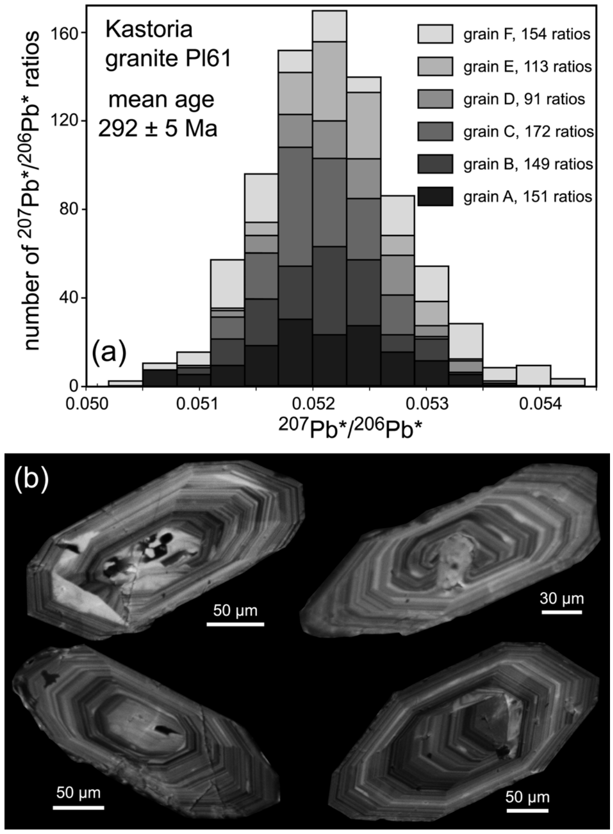

Fig. 2.5. (**a**) Histogram displaying the results of single-zircon Pb-Pb evaporation analyses for the Kastoria granite Pl61. (**b**) CL images showing the predominance of fine-scale magmatic growth zoning and the presence of resorbed and recrystallised areas.

Another part of the Pelagonian Zone that is dominated by granites and gneisses is found about 80 km SSE of Kastoria. Sample Pl70 is a coarse-grained orthogneiss that was taken near the eastern exit of Deskati village. It is a whitish gneiss that consists mainly of quartz, K-feldspar (partly sericitised), biotite, white mica, minor epidote and apatite. The orthogneiss was dated by the single-zircon U-Pb method. An upper intercept age of 699 ± 7 Ma (MSWD = 0.65) is interpreted as the emplacement age, while the scatter along the discordia is attributed to recent Pb loss (Fig. 2.6a). Two grains point to an older inherited component (grains dd and ee, Fig. 2.6a). Inherited components can be seen as rounded

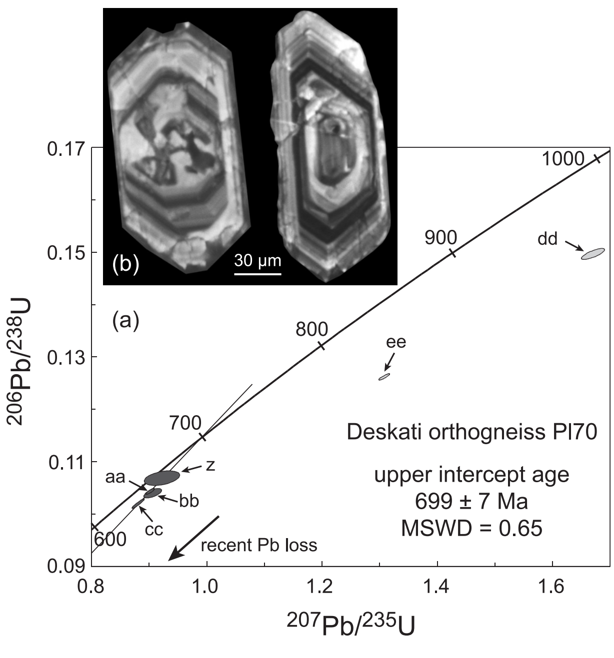

Fig. 2.6. (**a**) Geochronological results for Deskati granite Pl70 (single-zircon conventional U-Pb measurements). Error ellipses are 2σ. The light-coloured ellipses in the concordia diagram display inherited grains that were not included in the age calculation. (**b**) CL images showing typical internal structures of zircons.

cores in some CL images. In the CL images, most zircons show irregular convolute structures in their centres (Fig. 2.6b). We interpret these domains as recrystallised areas. Pb loss is probably correlated with these domains and is most likely reflected in the discordance of the zircon grains. An interpretation of these areas as inherited components seems rather unlikely as such structures are abundant in CL images, while evidence for older components is far less evident in the U-Pb analyses.

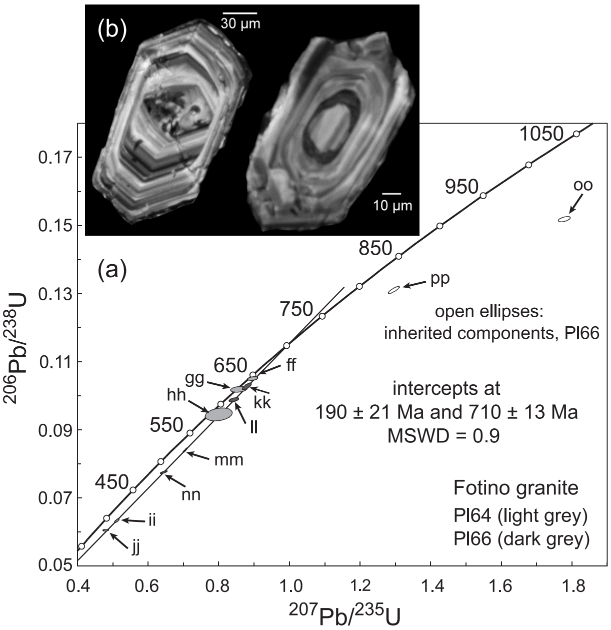

Fig. 2.7. (a) Concordia diagram displaying the geochronological results for the Fotino granite (samples PI64 and PI66). Error ellipses are 2σ. The open error ellipses in the concordia diagram display inherited grains that were not included in the age calculation. (b) CL images of zircons from the Fotino granite showing a grain with a complex internal structure (left grain) and another with a rounded core (right grain).

The Fotino granite is exposed about 10 km further south of Deskati. Three samples of this granite were taken, two for geochronological purposes and one (PI65) for geochemical analysis only. The Fotino granite is a pluton with variable deformation; sample PI64 is a relatively strongly deformed variety of the Fotino granite and shows a gneissic texture, while sample PI66 shows less deformation. The granites are medium-grained and have a greenish appearance. They differ only in their degree of deformation and have a main mineral composition of quartz, K-feldspar, plagioclase, white mica, ± biotite, ± opaque phase, and ± epidote. Tectonometamorphism resulted in subgrain formation and partial recrystallisation of K-feldspar, as well as secondary formation of white mica. For sample PI64, dating by the conventional U-Pb method resulted in an upper intercept age of 685 ± 30 Ma (interpreted as the intrusion age) and a lower intercept age of 177 ± 31 Ma (MSWD = 0.68). Similar ages were obtained for the less deformed granite PI66, i.e. an upper intercept age of 706 ± 26 Ma and a lower intercept age of 178 ± 56 Ma (MSWD = 0.14). Moreover, two grains from this sample indicated an older inherited component. The ages of both PI64 and PI66 are subjected to rather large errors but are identical within analytical error. Taken approximately two kilometres apart from each other along the road south of Fotino village, both samples belong to the same large plutonic body. We have therefore treated the two samples as one in a concordia diagram and extracted an upper intercept age of 710 ± 13 Ma (MSWD = 0.9), interpreted as the emplacement age of the Fotino pluton, and a lower intercept age of 190 ± 21 Ma (Fig. 2.7a). Internal structures of zircons in CL images (Fig. 2.7b) very much resemble those found in samples V9 and PI70, with irregular domains at the centre of grains that otherwise show clear oscillatory zoning.

2.5 Geochemistry

Geochronology revealed two age groups, one with ages of approximately 300 Ma (samples V1 and PI61) and another with ages of around 700 Ma (samples V9, PI58/PI59, PI70, PI64/66). The distinction between the two groups in terms of geochemistry and mineralogy is not as clear though some slight differences are nevertheless apparent (Appendices A-C). These differences principally concern the presence of titanite and white mica in the rocks and the Sr and Eu content.

In regard to the mineralogy of the samples, it can be seen that titanite is a very common accessory mineral in the younger-age group; sample V1 in particular contains abundant titanite crystals with almost euhedral shape. By contrast, titanite was not observed in thin sections in the older-age group, although Katerinopoulos *et al.* (1996) reported fragments of anhedral titanite from the Fotino granite. Instead, the older rocks contain white mica that is absent from the younger ones. This difference indicates that the younger-age-group rocks show I-type granite characteristics while the older-age-group rocks are more akin to S-type granites.

According to their major-element chemistry most of the rocks sampled are classified as granites (Fig. 2.8a). Only sample V1 from the Varnous pluton plots in the granodiorite field in the normative Ab-An-Or classification diagram (O'Connor 1965). This is due to its high CaO content of 4.44 wt.%; all other samples have distinctly lower CaO concentrations.

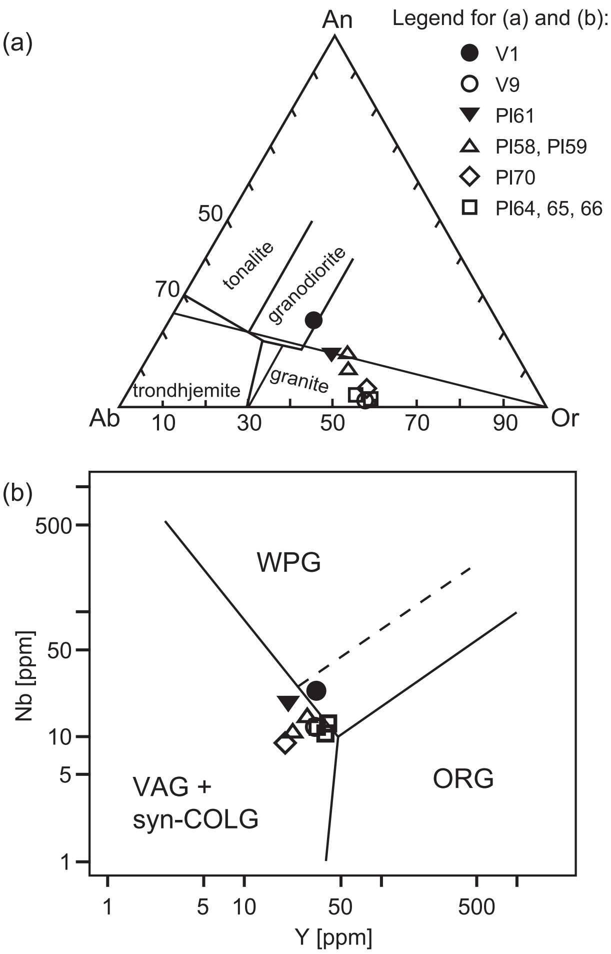

Fig. 2.8. Geochemical classification of the analysed rocks. (a) The normative Ab-An-Or classification diagram of O'Connor (1965), modified by Barker (1979, heavy lines). (b) Geotectonic-environment classification after Pearce *et al.* (1984); WPG: within-plate granite; ORG: ocean-ridge granite; VAG: volcanic-arc granite; syn-COLG: syn-collisional granite.

Almost all samples are peraluminous with A/CNK values between 1.08 and 1.32, the only exception being granodiorite V1 that is classified as metaluminous with an A/CNK of 0.87. The A/NK values range from 1.12 to 1.80. Here, one can discriminate between the younger-age-group samples together with orthogneisses PI58 and PI59 (A/NK = 1.50 - 1.80) and the remaining older-age-group samples (A/NK = 1.12 - 1.21).

A comparison of the geochemistry of the old-age-group rocks with that of Cadomian rocks from central Europe shows that both fall well within the same range, although an extensive comparison is hampered by the restricted range of SiO_2 encountered for the Pelagonian Zone samples together with their limited sample number. Because the old-age-group rocks are characterized by high K_2O and Rb contents accompanied by low Na_2O, Sr and Ba contents, they are clearly different from M- or I-type plutons like, for example, the North Tregor Batholith of NW France (Graviou & Auvray 1990) but similar to Cadomian granitoids with hybrid to S-type characteristics.

Applying the trace-element discrimination diagrams of Pearce *et al.* (1984), a syn-collisional or volcanic-arc origin of the sampled rocks is indicated (Fig. 2.8b). Only sample V1 plots slightly inside the within-plate granite field, which might be an indication for a late- or post-collisional origin.

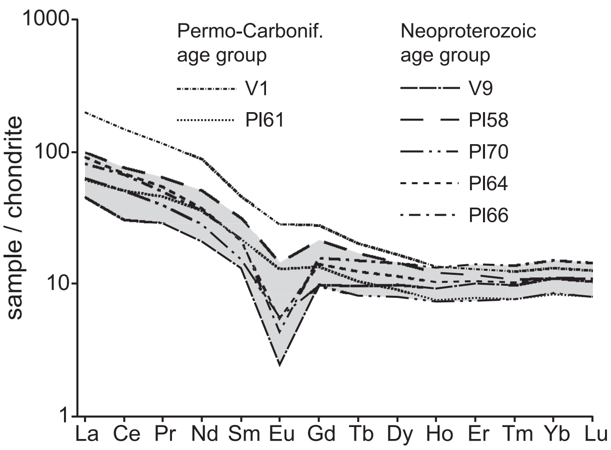

Fig. 2.9. Chondrite-normalised REE patterns (chondrite values from Boynton 1984). Note the pronounced negative Eu-anomaly in the pattern of the Neoproterozoic gneisses (grey area) in comparison to the Carboniferous samples.

The chondrite-normalised REE patterns are typical of rocks formed in a volcanic-arc or active continental margin setting (Fig. 2.9). Light REE are enriched while the heavy REE display a flat pattern. A clear distinction between the older- and the younger-age-group rocks can be seen in the Eu anomaly, which is more pronounced in the older-age-group rocks (Eu/Eu* is between 0.21 and 0.56 as opposed to values of 0.80 and 0.77 for the younger-age-group rocks). Granodiorite V1 shows the largest enrichment of LREE with a $(La/Yb)_n$ of about 15, while for the remainder of the samples this ratio is in the range of 4 to 9.

The Nd-isotope composition analyses resulted in εNd_i values of between +0.9 and -4.8 for the older-age-group rocks, and of between -1.9 and -4.1 for the younger-age-group rocks. This parameter cannot, therefore, discriminate between the two age groups. The same holds true for the depleted-mantle model ages (T_{DM}), which ideally date the time of crust-mantle differentiation but normally reflect the average age of mixed crustal and mantle components that participated in magma genesis (Arndt & Goldstein, 1987). The T_{DM} (1.2 Ga) value for Kastoria granite PI61 is older than that of granodiorite V1 (1.0 Ga) and its εNd_i more negative. This might suggest that the crustal component involved in magma genesis for Kastoria granite PI61 was either larger or older than that for V1. The difference in εNd_i and T_{DM} for the samples from the Fotino granite could reflect heterogeneity within the pluton possibly related to the assimilation of varying amounts of older crustal material. Of the old-age-group rocks, orthogneiss PI58 shows the most negative εNd_i value (-4.8) and the oldest T_{DM} value (1.6 Ga). These values indicate the involvement of a large crustal component and therefore a clear S-type character for the protolith of orthogneiss PI58, which is further confirmed by the abundance of rounded zircon cores that can be seen in CL images.

Contrary to the Nd isotope system, which is unlikely to be disturbed by later thermal events (DePaolo 1981), the Sr isotope system is more readily affected by metamorphism or alteration. Strontium isotope composition analyses clearly show that the Rb-Sr system, at least of the Neoproterozoic rocks from Fotino (PI64, PI66) and Varnous (V9), is disturbed (Appendix C). This is indicated by the high $^{87}Rb/^{86}Sr$ values (*c.* 20) and the unrealistically low $^{87}Sr/^{86}Sr_i$ values (< 0.7000). Such exceptionally low $^{87}Sr/^{86}Sr_i$ values could be an effect of overcorrection due to small errors in Sr concentration measurements and resultant Rb-Sr ratios, as slight changes of very high Rb-Sr ratios significantly affect the initial ratios. Alternatively, they could be related to either secondary Sr loss or Rb gain. The rather low Sr content (*c.* 40 ppm) of the samples with unrealistically low $^{87}Sr/^{86}Sr_i$ values correlates with low Ca concentrations and large negative Eu anomalies; the low Sr concentration could therefore be a primary feature related to plagioclase fractionation. On the other hand, recrystallisation of primary and/or formation of secondary white mica as well as recrystallisation of K-feldspar might be responsible for elevated Rb concentrations. It is worth noting that the Neoproterozoic rocks that yielded the unrealistically low $^{87}Sr/^{86}Sr_i$ values are the ones with the strongest evidence for metamorphic overprint in the form of recrystallised microcline and formation of secondary muscovite. This might indicate that the high concentration of Rb and low concentration of Sr observed is influenced by alteration processes accompanying deformation. An increase of the Rb/Sr due to alteration would consequently result in $^{87}Sr/^{86}Sr_i$ values that are too low. Thus, the $^{87}Sr/^{86}Sr_i$ values we obtained are minimum values. In any case, the $^{87}Sr/^{86}Sr_i$ value of 0.70529 for granodiorite V1 concurs with that of *c.* 07056 reported by Koroneos *et al.* (1993) from the Varnous pluton. It indicates the dominance of mantle material as the source material, with only small amounts of older crustal material being involved. Kastoria granite Pl61 has a higher $^{87}Sr/^{86}Sr_i$ of 0.70831, implying a larger amount of crustal component in the source, as already deduced from the Nd isotopes. The rather high $^{87}Sr/^{86}Sr_i$ of 0.71046 for orthogneiss Pl58 underlines its derivation from a S-type granite involving older crustal material.

2.6 Discussion

The geochronological, geochemical and Sr- and Nd-isotope results of this study shed new light on our knowledge of the Pelagonian Zone. The picture of a single Permo-Carboniferous basement for this zone should be modified to include the existence of a second, distinctly older basement of Neoproterozoic age, identified here for the first time.

2.6.a. Permo-Carboniferous rocks

The Permo-Carboniferous ages of 298 ± 7 Ma for granodiorite V1 from Varnous Mts. and of 292 ± 5 Ma for Kastoria granite Pl61 are zircon ages typical of the basement rocks from the Pelagonian Zone that have been studied to date (e.g. Yarwood & Aftalion 1976; Mountrakis 1984; Koroneos *et al*. 1993; Vavassis *et al.* 2000; Reischmann *et al.* 2001; Anders *et al.* 2003c).

2.6.b. Neoproterozoic basement rocks

2.6.b.1. Neoproterozoic ages

Neoproterozoic ages of basement rocks in the NW Pelagonian Zone are in the range of 699 to 713 Ma. Because of this rather short time span and the fact that they are largely identical within analytical error, one may assume that the rocks formed during a single major magmatic event in the Neoproterozoic. The Neoproterozoic basement rocks of the Pelagonian Zone are the oldest known rocks of Greece.

2.6.b.2. Post-emplacement processes

Due to the igneous zoning of the zircons of the Neoproterozoic rocks, the ages obtained are interpreted as magmatic crystallisation ages. Some of the zircons show evidence of Pb loss during a secondary overprint. Pb loss can be interpreted as recent only in the case of Deskati orthogneiss Pl70. For both samples from the Fotino granite and the orthogneiss from Varnous Mts. (V9), the lower intercept ages are 190 ± 21 Ma and 187 ± 59 Ma respectively (if the two samples from the Fotino granite are considered separately, the resulting lower intercept ages are 177 ± 31 Ma and 178 ± 56 Ma). The geological meaning of these lower intercept ages is not yet clear. Lead loss in zircons is a common phenomenon and mostly attributed to metamictization and later recrystallisation during which Pb is removed from the zircon crystal (Williams 1992; Mezger & Krogstad 1997). This Pb loss can occur either during distinct episodic events or continuously over a large time period, something which is not obvious from the concordia diagram but which will lead to different results. In general, lower intercept ages do not necessarily have a geological meaning and therefore have to be handled with care (Mezger & Krogstad 1997). In the case of the rocks from the NW Pelagonian Zone, a link between the lower intercept ages and regional geology might be suggested when comparing them to ages proposed for the spreading and obduction of the Pindos and Vourinos ophiolites. Liati *et al.* (2004) dated zircons from gabbros and a plagiogranite from the Pindos and Vourinos ophiolites using SHRIMP and obtained ages in the range of 169 ± 2 Ma to 173 ± 3 Ma. Ar-Ar dating of amphibole from the metamorphic sole of the Vourinos ophiolite yielded an age of about 171 ± 4 Ma (Spray *et al.* 1984). However, today at least, the above ophiolites crop out several kilometres away from our sampling positions and there is no definitive proof that spreading or obduction of the ophiolites could have affected the isotopic system of our samples. Mountrakis (1982, 1984, 1986) recognized polyphase deformation in the NW Pelagonian Zone and suggested a pre-Upper Carboniferous and an Upper Jurassic age for the two oldest deformation phases. Yet we see no convincing link between ophiolite obduction and a regional metamorphic overprint. Therefore an attribution of the lower intercept ages to unspecific, episodic Pb loss seems more appropriate. This Pb loss is probably related to thermal/metamorphic events that affected the Pelagonian Zone during Latest Jurassic, Cretaceous and Tertiary times (e.g. Schermer *et al.* 1990; Most 2003).

With regard to the Fotino granite, overprinting by a post-Neoproterozoic event is evident. Katerinopoulos *et al.* (1996) dated white micas and whole-rock from the Fotino granite by the Rb-Sr method and obtained ages in the range of 225 to 273 Ma. The above authors interpret the older ages as intrusion ages and explain the younger ages as Rb-Sr open-system behaviour. The disturbance of the Rb-Sr system of most of the Neoproterozoic rocks, including the Fotino granite, is also evident from the unrealistically low $^{87}Sr/^{86}Sr_i$ values of < 0.7000 (Appendix C). Therefore, in the light of the new zircon ages and Sr isotope measurements of our study, all Rb-Sr ages of Katerinopoulos *et al.* (1996) reflect, at best, a thermal event that occurred between Late Permian and Jurassic times. This thermal event is probably reflected in the lower intercept ages of the zircons from the Fotino granite.

It is noteworthy that the Neoproterozoic zircons do not appear to have been influenced by a Permo-Carboniferous thermal event, despite the fact that this time span is characterised by widespread magmatism. This indicates that the Neoproterozoic rocks sampled did not experience temperatures high enough during Permo-Carboniferous times to affect the U-Pb system of the zircon grains. Whether the absence of a Permo-Carboniferous overprint is a general feature of the Neoproterozoic rocks from the Pelagonian Zone or a consequence of the so far small database will be a matter of future research.

2.6.c. Derivation and possible linkages of the Pelagonian Neoproterozoic rocks

The Neoproterozoic zircon ages of 699 Ma to 713 Ma are the oldest ages of basement rocks known from Greece. Basement rocks with intrusion ages of about 700 Ma are not known from the neighbouring Hellenide Zones. Traditionally, the tectono-stratigraphic zones of the Hellenides are correlated with those of Turkey (e.g. S. Dürr, 1975; Jacobshagen 1986). Zircon dating of granitoid basement from adjacent zones in Turkey so far yielded only Late Neoproterozoic ages of *c.* 520 to 590 Ma for the Menderes Massif (Hetzel & Reischmann 1996; Loos & Reischmann 1999; Gessner *et al.* 2004) and also for the Karadere basement from the Istanbul Zone, NW Turkey (Chen *et al.* 2002). The large difference in ages observed does not support a correlation of the Pelagonian Zone Neoproterozoic basement with either the Menderes Massif or the Karadere basement.

The spatial distribution of the Neoproterozoic rocks in the Pelagonian Zone is not yet accurately known. As our samples were taken several tens of kilometres apart (distributed over an area of about 20 x 100 kilometres), only inferences can be made about their possible contiguity in Neoproterozoic times. Their strong chemical and mineralogical similarities suggest that they once belonged to a single basement unit that was later dissected by Variscan and Alpine tectonomagmatic events. These old basement rocks are interpreted to be remnants of a terrane, which we call here the Florina Terrane, which constituted the continental crust on which the Pelagonian Permo-Carboniferous magmatic arc was built.

The ages yielded (*c.* 700 Ma) support the argument that the Florina Terrane originated in Gondwana but not in Baltica. Neoproterozoic ages of approximately 700 Ma are known from Pan-African Gondwana-derived terranes like West and East Avalonia or the Armorica Terrane Assemblage; they mark an era of widespread subduction-related magmatism along or close to the northern margin of Gondwana. Later, rifting of this Pan-African magmatic arc along the northern margin of Gondwana led to the detachment and dispersal of the terranes. Nowadays, these terranes can be found in NE America (West Avalonia) and in the Variscides of Europe (East Avalonia and the Armorica Terrane Assemblage). Palaeo-reconstructions place the Avalonia Terranes in the western part of the Pan-African magmatic arc and the Armorica Terranes further east (e.g. Nance & Murphy 1994).

Inferences as to which part of the northern margin of Gondwana the Florina Terrane of the Pelagonian Zone comes from can be made by comparing Nd-isotope systematics and the provenance of detrital zircons of these different terrane assemblages, as they display distinct differences. Nd-isotope systematics reveal the characteristics of the source from which the magma is derived (including the contribution of older crustal material). The distribution of ages of inherited zircons, on the other hand, point to the age of the contributing crustal source rocks and the exposed cratons nearby.

2.6.c.1. Comparison of the Florina Terrane with West Avalonia

Ages of about 700 Ma are known from both West and East Avalonia, where an early phase of arc-related magmatism is recognized between 780 and 660 Ma (Murphy *et al.*, 1999 and references therein). A compilation of data by Nance & Murphy (1996) and Murphy & Nance (2002) reveals that West Avalonia Terranes tend to display immature arc characteristics with predominantly positive εNd_i (for Neoproterozoic felsic volcanic rocks it ranges from +0.8 to +3.0) and Nd model ages T_{DM} between 0.9 and 1.2 Ga. The εNd_i values of the Neoproterozoic rocks from the Florina Terrane differ in that they range from about +0.9 to -2.6. Orthogneiss Pl58, which has a strong sedimentary character, shows an even more negative εNd_i value of -4.8. The depleted mantle model ages for the Florina Terrane are also somewhat older than those for West Avalonia, varying mostly between 1.1 and 1.6 Ga. Detrital zircon ages from West Avalonia are distributed over several distinct age groups of about 1.0-1.2 Ga (Grenvillian), 1.5-1.8 Ga, 2.0-2.1 Ga and 2.6 Ga (e.g. Keppie *et al.* 1998). Several workers (e.g. Keppie *et al.* 1998; Murphy & Nance 2002; Nance & Murphy 1994) pointed out that these age groups correspond to age groups known from the Amazonian craton, while at the same time a derivation from NW Africa seems unlikely because ages in the range of 1.0 - 1.8 Ga are virtually absent from this craton.

Therefore, the presence of Grenvillian and older Mesoproterozoic detrital zircon ages imply that West Avalonia originated either adjacent to the Amazonia/South America craton or at least close enough to receive its characteristic detrital zircon assemblage (e.g. Nance & Murphy 1994; Keppie *et al.* 1998; McNamara *et al.* 2001). As for the Florina Terrane of the NW Pelagonian Zone, the Neoproterozoic samples taken as a whole give the following picture. An Early Mesoproterozoic component is evident in both a $^{207}Pb/^{206}Pb$ age of 1777 Ma from Varnous orthogneiss V9 (grain V9-C, Appendix D) and in a SHRIMP analysis of a zircon core from orthogneiss PI58 from which a concordant $^{206}Pb/^{238}U$ age of 1501 ± 9 Ma was obtained (PI58 spot 3.2, Appendix F). All other $^{207}Pb/^{206}Pb$ ages from samples V9, PI58, PI59, PI70 and PI66 range from *c.* 800 to 1340 Ma. It should be noted that $^{207}Pb/^{206}Pb$ ages in the range of 850 to 1150 Ma might indicate a relation to the Grenvillian orogeny. By definition, $^{207}Pb/^{206}Pb$ ages are minimum ages and display the “true” age only if they are concordant. Looking at the concordia diagrams, all of the grains with inherited components are discordant to varying degrees and therefore the “true” age of the protoliths are likely to be older; how much older, however, cannot be said. Assuming that this range of $^{207}Pb/^{206}Pb$ ages reflects a Late Neoproterozoic to Mesoproterozoic source, an affinity of the Florina Terrane to Avalonia is indicated by the detrital zircon ages, though not necessarily by the Nd isotopes.

2.6.c.2. Comparison of the Florina Terrane with East Avalonia

East Avalonia shows a range of Neoproterozoic magmatic ages similar to that of West Avalonia. What distinguishes East from West Avalonia is the range of εNd_i values for the late Neoproterozoic to Cambrian igneous and sedimentary rocks (-2.0 to -8.5), although rocks with εNd_i values up to +4.6 have been reported (Davies *et al.* 1985; Thorogood 1990), the latter resembling West Avalonia lithologies. Depleted-mantle model ages for East Avalonia are slightly older than those for West Avalonia and are of the order of 1.0 to 1.8 Ga (Davies *et al.* 1985; Thorogood 1990). Comparison between East Avalonia and Florina shows good agreement in Nd isotopes (Fig. 2.10). East Avalonia is interpreted by Nance & Murphy (1996) and Murphy & Nance (2002) to have originated in a region along the northern margin of Gondwana that is neither entirely Amazonia-related nor NW-Africa-related, but consists of reworked material of both Amazonia-type and NW-Africa-type crust.

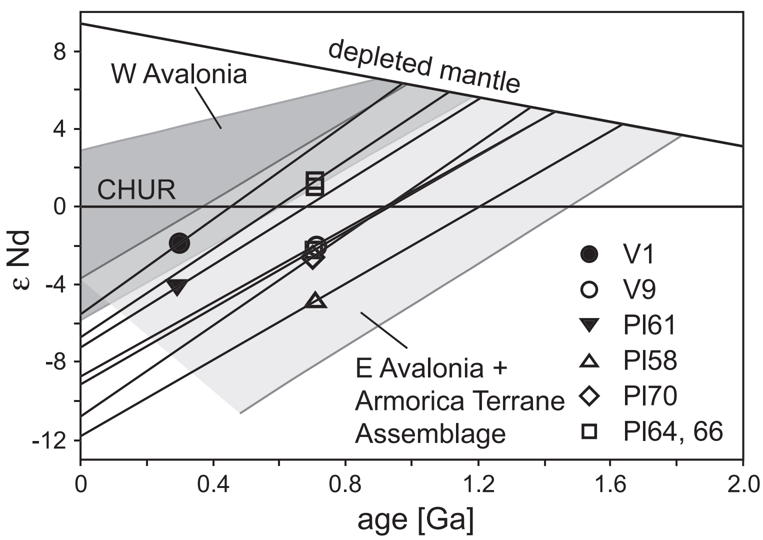

Fig. 2.10. Neodymium-isotope evolution for the basement rocks of the NW Pelagonian Zone. Depleted-mantle evolution line is after Michard *et al.* (1985). Shown for comparison are the fields for West Avalonia (light grey area) and East Avalonia plus Armorica Terrane Assemblage rocks (dark grey area), redrawn after Murphy & Nance (2002). CHUR = chondritic uniform reservoir.

2.6.c.3. Comparison of the Florina Terrane with the Armorica Terrane Assemblage

The Armorica Terrane Assemblage is characterised by basement intrusion ages of about 560-580 Ma (Linnemann *et al.* 2000), although older zircon ages of about 650-670 Ma do exist, e.g. from orthogneiss boulders of the Cesson conglomerate (North Brittany, France; Guerrot & Peucat 1990), and indicate the presence of the same Neoproterozoic magmatic phase that is known from Avalonia. With predominantly negative εNd_i values (+1.6 to -9.9) and T_{DM} values of 1.0 to 1.7 Ga (D'Lemos & Brown 1993), the Late Precambrian-Cambrian Armorica Terrane Assemblage basement rocks show a strong similarity to those known from East Avalonia and the Florina Terrane. However, Mesoproterozoic detrital zircon ages are so far unknown from the Armorica Terrane Assemblage, where Palaeoproterozoic and Archean ages predominate (e.g. Linnemann *et al.* 2000). The absence of Early to Late Mesoproterozoic detrital zircon ages coupled with the presence of Palaeoproterozoic and Archean detrital zircons are in favour of a derivation of the Armorica Terrane Assemblage from close to NW Africa (e.g. Nance & Murphy 1996; Linnemann *et al.* 2000; Murphy & Nance 2002). Despite the similarity in Nd isotopes, the Florina Terrane and the Armorica Terrane Assemblage are clearly different in terms of the distribution of detrital zircon ages.

2.6.c.4. Comparison of the Florina Terrane with the Arabian-Nubian Shield

Neoproterozoic intrusion ages of about 700 Ma are also known from NE Africa and Arabia, especially the Eastern Desert of Egypt, Sinai, Israel, Sudan (Arabian-Nubian Shield) and Ethiopia (e.g. Kröner *et al.* 1994; Teklay *et al.* 1998; Bregar *et al.* 2002; Meert 2003 and references therein). However, an origin of the Florina Terrane from close to Arabia seems unlikely since geochemical analyses indicate formation of large parts of the Arabian-Nubian Shield in an oceanic volcanic-arc setting during the Neoproterozoic (e.g. Kröner *et al.* 1991).

2.6.c.5. Avalonian Terranes in the Variscan orogeny

We conclude that an affinity of the Florina Terrane to Avalonia is supported by the Mesoproterozoic $^{207}Pb/^{206}Pb$ ages of inherited zircons. The existence of a Mesoproterozoic detrital component does not support either a correlation of the Florina Terrane with the Armorica Terrane Assemblage or a derivation from NE Africa and Arabia. A distinction between West and East Avalonia can be made on the basis of Nd isotope analyses; they suggest an East Avalonia affinity for the Florina Terrane.

In a simplified view, in Europe the northern Variscides comprise East Avalonia Terranes (Gibbons & Horák 1996 and references therein) whereas the southern Variscides comprise the Armorica Terrane Assemblage (Tait *et al.* 1997). The Florina Terrane of East Avalonia affinity lies south of the Armorica Terrane Assemblage and does not fit the pattern of terrane distribution in the Variscides described above. However, this simple pattern was questioned in the eastern Variscides (Bohemia; Finger *et al.* 2000), where the basement of the Moravo-Silesicum was re-interpreted as an Avalonia-type terrane on the basis of Nd-isotope systematics (Hegner & Kröner 2000) and detrital zircon dating by SHRIMP (Friedl *et al.* 2000). A basement gneiss of the Silesian domain was dated by the single-zircon Pb-Pb evaporation method at about 685 Ma (Kröner *et al.* 2000). It thus seems plausible that the Neoproterozoic basement of the Pelagonian Zone formed in a similar way to the terranes of the Variscides. Although the Palaeozoic evolution of these Gondwana-derived terranes is different, they nevertheless became involved in the same Permo-Carboniferous orogenic processes that took place at the southern margin of Europe. Geochemical analyses indicate a volcanic-arc or active continental-margin setting for the Permo-Carboniferous magmatism of the Pelagonian Zone (see also Pe-Piper *et al.* 1993a, b; Katerinopoulos *et al.* 1998; Anders *et al.* 2003c). These rocks might therefore be compared to the pre-Alpine I-type granitoids of the Alps, which were interpreted by Finger & Steyrer (1990) to have originated at the South European margin in the course of northward subduction of (a branch of) the Palaeotethys. The alpine tectono-metamorphic overprint onto the Pelagonian Zone basement rocks, however, impedes a direct correlation with this Palaeozoic belt in the Alps.

The discovery of the Florina Terrane and its interpretation as a Gondwana-derived terrane, most probably belonging to East Avalonia, underlines the characterisation of the evolutionary history of the Eastern Mediterranean by arc-accretion processes.

2.7. Conclusions

New information that is essential for unravelling the Late Neoproterozoic-Palaeozoic evolutionary history of the eastern Mediterranean area is presented in this study.

The geochronological and geochemical results support the notion that the pre-alpine basement of the Pelagonian Zone in Greece formed in at least two distinct episodes. The new zircon ages of basement gneisses and granites document the existence of Neoproterozoic crustal rocks in the northwestern part of the Pelagonian Zone in addition to the well-known Permo-Carboniferous basement rocks.

Trace-element geochemistry suggests formation of basement rocks of both age groups in an active continental margin or volcanic-arc setting.

The Neoproterozoic ages of *c.* 699 Ma to 713 Ma for the older-age-group rocks are the oldest recorded ages to this date from the Pelagonian Zone and from Greece in general.

For the Neoproterozoic basement rocks from the Pelagonian Zone the existence of inherited zircons with Mesoproterozoic minimum ages and Mesoproterozoic Nd model ages suggest formation at or close to the continental margin of northern Gondwana. These Neoproterozoic rocks are interpreted as remnants of a Gondwana-derived terrane, named here the Florina Terrane.

Geochronological analyses and Nd isotopes indicate a similarity of the Florina Terrane to Avalonia-type terranes. Therefore a derivation similar to that of East Avalonia is suggested.

The Florina Terrane forms the continental basement on which the Pelagonian Permo-Carboniferous magmatic arc formed and was later incorporated in the Hellenide orogen.

Chapter 3. Zircon geochronology of basement rocks from the Pelagonian Zone

This chapter is largely identical to a manuscript entitled "Zircon geochronology of basement rocks from the Pelagonian Zone, Greece: constraints on the pre-Alpine evolution of the westernmost Internal Hellenides", which was submitted to the International Journal of Earth Sciences. Co-authors are T. Reischmann and D. Kostopoulos.

3.1 Abstract

The Pelagonian Zone of Greece is the westernmost segment of the Internal Hellenides comprising widespread crystalline basement exposures of granites and orthogneisses. We dated these basement rocks in order to identify the major crust-forming episodes and to understand the evolutionary history of the area. In our study we investigated granites, gneisses, meta-rhyolites and mylonites from the major occurrences of the Pelagonian Zone. We applied single-zircon dating techniques such as Pb-Pb evaporation, conventional U-Pb and SHRIMP. The majority of the basement rocks gave Permo-Carboniferous intrusion ages, thus emphasizing the importance of this crust-forming event for the Internal Hellenides of Greece. Triassic intrusion ages were obtained, however, for a meta-rhyolite from the western Pelagonian Zone and two mylonites from the eastern Pelagonian Zone. These ages are interpreted to reflect magmatism accompanying early rifting that led to the subsequent opening of the Pindos Ocean to the west and the Vardar Ocean to the east of the Pelagonian Zone. The geochronological results demonstrate that the magmatic episodes during which most of the Pelagonian Zone crystalline basement formed are predominantly pre-Alpine in age.

3.2 Introduction and regional geology

The Pelagonian Zone is part of the Hellenide orogen, which is, in turn, an eastern Mediterranean segment of the Alpine-Himalayan mountain chain. Together with the Vardar Zone, the Serbo-Macedonian Massif and the Rhodope Massif further east, the Pelagonian Zone belongs to the Internal Hellenides (e.g. Aubouin *et al.* 1963). In terms of rock types, the Pelagonian Zone comprises granites, ortho- and paragneisses (forming the Palaeozoic metamorphic basement), late Palaeozoic to Mesozoic meta-sedimentary rocks (mostly metaclastic sequences and carbonate cover), ophiolites showing Late Jurassic to Early Cretaceous deformation and Tertiary to recent sediments (e.g. Celet & Ferrière 1978; Kilias & Mountrakis 1989; Jacobshagen 1986 and references therein; Pe-Piper & Piper 2002 and references therein). Geochemical studies of Palaeozoic basement rocks indicate that they formed in a subduction-zone environment and mostly favour an active continental-margin setting (e.g. Pe-Piper *et al.* 1993a, b; Katerinopoulos *et al.* 1998; Vavassis *et al.* 2000, Reischmann *et al.* 2001; Anders *et al.* 2002). The Late Precambrian to Mesozoic evolution of the eastern Mediterranean was marked by the opening and closure of ocean basins and continental crust formation in the accompanying subduction zones (e.g. Stampfli & Borel 2002). Orogenic processes due to initial collision of the Apulian plate with the Eurasian plate during Mesozoic and Cainozoic times and subsequent collapse and extension are responsible for the present-day appearance of the Hellenides. These Alpine orogenic processes obscured the pre-Alpine history of the Hellenide region. A geochronological study of what were presumed to be Palaeozoic crustal rocks can help to unravel the pre-Alpine history of the Pelagonian Zone. Pre-

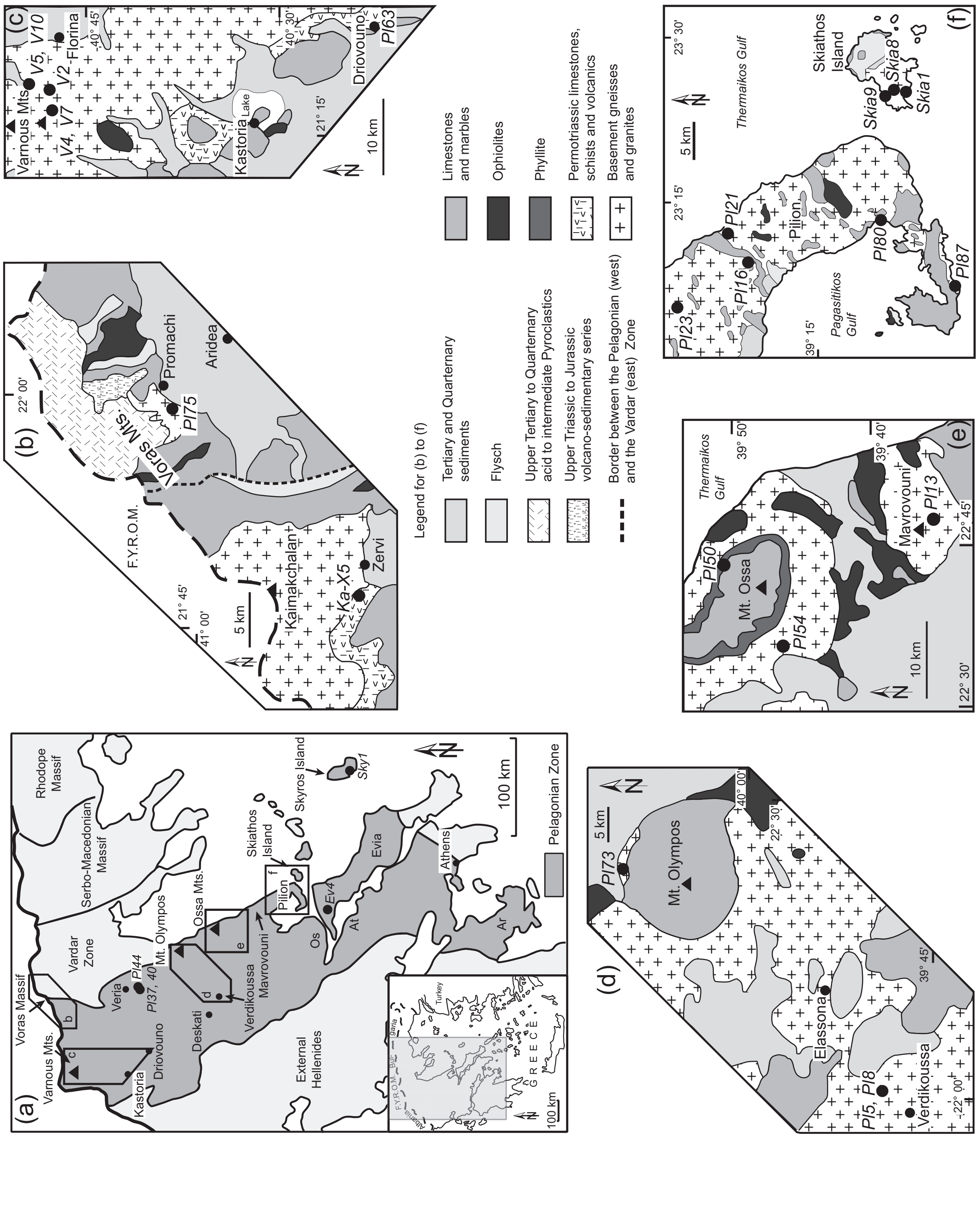

Fig. 3.1. Overview of the study area and the sample locations. (**a**) Map showing the structural zones of northern Greece, simplified after Kondopoulou (2000). The black polygons indicate the blow-ups (b) to (f). At = Atalanti, Ar = Argolis, Os = Othris Sample numbers are shown in italics. (**b**)-(**f**) Geological maps of the main study areas. Simplified after the IGME Geological Map of Greece 1:500 000 (1983).

vious geochronological investigations of the Pelagonian Zone were carried out, for example, by Yarwood & Aftalion (1976), who obtained a U-Pb zircon age of 302 ± 5 Ma from High Pieria Mts., NE Pelagonian Zone. Other studies report results based on the Rb-Sr, K-Ar or Ar-Ar methods of dating (Barton 1976; Schermer 1990; Koroneos *et al.* 1993; Katerinopoulos *et al.* 1998; Lips *et al.* 1998), though these methods are often not suitable for dating primary intrusion events. U-Pb zircon ages of basement rocks from the Pelagonian Zone are so far rather scarce. Apart from the Pieria Mt. age obtained by Yarwood & Aftalion (1976), other U-Pb zircon ages for the Pelagonian Zone include those of the Verdikoussa area (Reischmann *et al.* 2001) and Evia (De Bono 1998; Vavassis *et al.* 2000), where Permo-Carboniferous intrusion ages were found, and those of the NW Pelagonian Zone (Mountrakis 1984; Anders *et al.* 2003b), where Neoproterozoic basement rocks were additionally identified and interpreted in terms of an exotic terrane named Florina Terrane (Anders *et al.* 2003b, see Chapter 2). The aim of this study was therefore to improve our knowledge of basement formation in the Pelagonian Zone. Zircon geochronology is especially suited for obtaining information about intrusion ages and the timing of magmatism, because zircons, apart from being common accessory minerals in felsic rocks, have a high closure temperature that allows dating of the intrusion event, and they are rather resistant against resetting of the U-Pb isotopic system during later metamorphic events or alteration (Lee *et al.* 1997; Cherniak & Watson 2000; Parrish 2001; Corfu *et al.* 2003). Age information on basement rocks from the Pelagonian Zone will give us a more detailed picture of the existence and regional distribution of distinct magmatic episodes, information necessary for palinspastic reconstructions. For example, a northward younging of the Permo-Carboniferous subduction-zone magmatism was proposed by Reischmann *et al.* (2001). A detailed geochronological study will provide important clues regarding the evolution of the Pelagonian Zone and will shed ample light on the pre-Alpine history of the Internal Hellenides.

3.3 Sample description and geochronology

Samples were collected from major basement exposures along the length of the Pelagonian Zone (see Fig. 3.1a). In the northern part of the Pelagonian Zone, sampling areas include the Voras Mountains in the northeast, close to the border with the Former Yugoslav Republic of Macedonia (F.Y.R.O.M.) (Fig. 3.1b), and the Varnous Mts. in the northwest (Fig. 3.1c). Progressing southwards sampling localities include outcrops south of Veria (Fig. 3.1a), a basement exposure NE of Mt. Olympos (Fig. 3.1d), the Verdikoussa area (Fig. 3.1d), Mt. Ossa and Mavrovouni (Fig. 3.1e), Mt. Pilion and Skiathos Island (the westernmost island of the N. Sporades; Fig. 3.1f). The southernmost samples were taken from the northern part of Evia Island and from Skyros Island (Fig. 3.1a). Description of the samples is arranged from north to south. Three different methods of single-zircon dating were applied, namely the Pb-Pb evaporation method (Kober 1986, 1987), the conventional U-Pb method (isotope dilution; Krogh 1973; Wendt & Todt 1991) and the sensitive high-resolution ion microprobe (SHRIMP) method (e.g. Compston *et al.* 1984). SHRIMP dating was performed on samples for which both the Pb-Pb and the conventional U-Pb methods failed to produce satisfactory results. Cathodoluminescence (CL) images typical for zircons from Pelagonian Zone basement rocks are shown in Fig. 3.2. Analytical results are listed in Appendices D to F and shown in Figs. 3.3-3.9. Pb-Pb evaporation data are shown as histograms, while

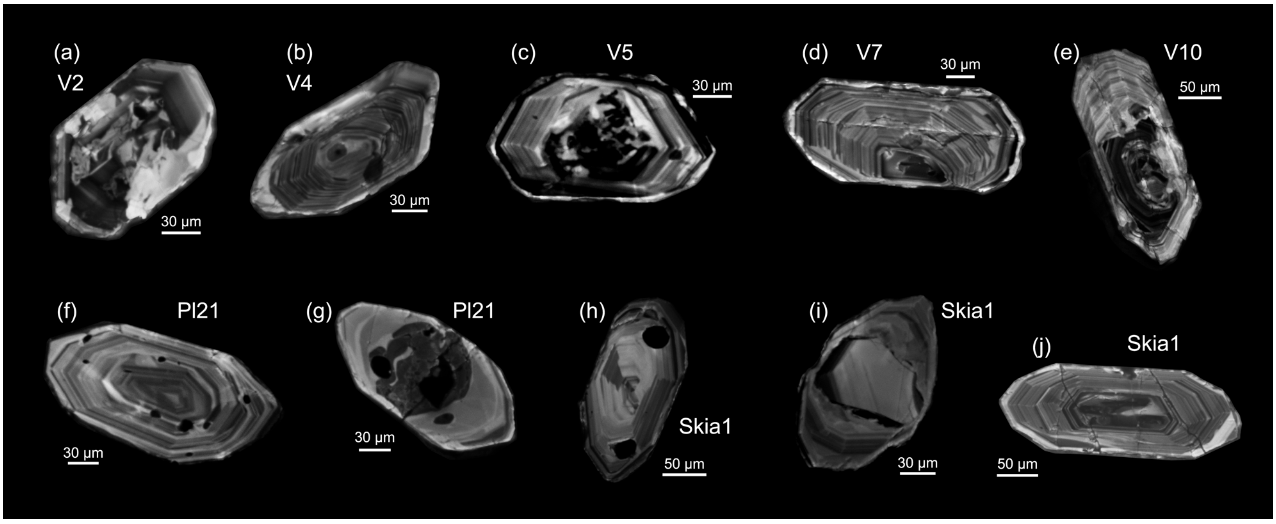

Fig. 3.2. CL images of zircons from the Varnous Mts., Mt. Pilion and Skiathos Island.

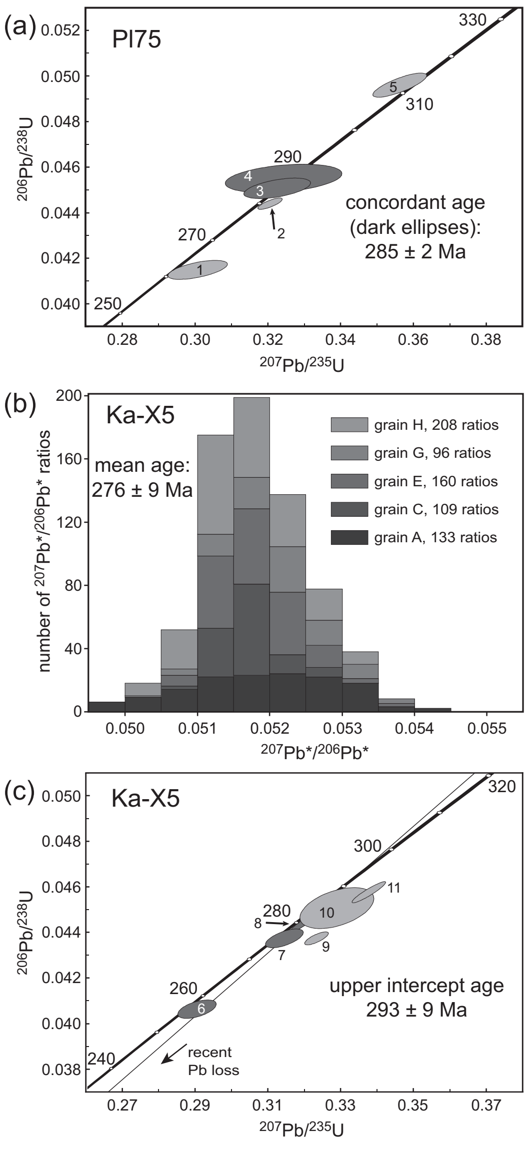

Fig. 3.3. Geochronological results for the basement rocks from the Voras Mts. The histogram shows the results of single-zircon Pb-Pb evaporation analyses while the concordia diagrams illustrate the results of the conventional U-Pb method. The discordia line in part (c) was calculated through the origin.

conventional U-Pb and SHRIMP results are displayed as concordia diagrams. Details of analytical procedures are given in the appendix.

Voras Mts. The Voras Mts. in northern Greece stretch from the Pelagonian Zone in the west eastwards into the Vardar Zone (Fig. 3.1a). They are recognised as a pile of westward-stacked thrust sheets (Brown & Robertson 2004). The westernmost part of the chain, forming the footwall onto which the lowermost thrust sheet was thrust, is the Kaimakchalan Massif, which belongs to the Pelagonian Zone (Mountrakis 1982, 1984; Jacobshagen 1986). One granite (Ka-X5) was sampled from this westernmost part, while one orthogneiss (Pl75) was taken further east in the Voras Mts., west of Promachi village (Likostomo-Promachi Unit of Brown & Robertson 2004) (Fig. 3.1b).

Pl75 is a light-coloured granitic gneiss and consists mainly of quartz, K-feldspar, plagioclase, white mica and epidote. Pl75 was dated with the single-zircon conventional U-Pb method (Fig. 3.3a). Two zircon grains define a concordant age of 285 ± 2 Ma (MSWD of concordance = 0.039). This age is interpreted to date the intrusion event. Two grains display Pb-loss and one grain falls on the reverse side of the concordia line.

Granite Ka-X5 was sampled in the western part of the Voras Mts. The main minerals are quartz, severely sericitised plagioclase, K-feldspar, biotite and epidote. Dating with the single-zircon Pb-Pb evaporation method did not yield clear-cut results (Fig. 3.3b). One grain contains an older Pb component and yielded an age of *c.* 418 Ma, while two other grains show signs of Pb loss. Nevertheless, the majority of the zircon grains cluster at 276 ± 9 Ma (MSWD = 9.5). Therefore, an Upper Carboniferous / Lower Permian intrusion age can be assumed. This assumption is also supported by the result of the single-zircon conventional U-Pb dating approach (Fig. 3.3c) that yielded an upper intercept age of about 293 ± 9 Ma (MSWD = 0.43).

Varnous Mts. The Varnous Mts. in the NW Pelagonian Zone consist of intrusive rocks, ranging in composition from mafic to felsic. Deformation is absent or only weak. Some of the mafic rocks occur as enclaves in the felsic rocks. Five plutonic rocks were sampled from the Varnous Mts. (V10, V2, V4, V5, V7; Fig. 3.1c). Differences in grain size and relative proportions, as well as in the degree of alteration of the minerals quartz, K-feldspar, plagioclase (often showing saussuritisation), biotite, titanite, apatite and epidote/clinozoisite are obvious. V2 and V4 are fine-grained mafic rocks, while V5, V7 and V10 are coarse-grained and of intermediate (V7, V10) or felsic (V5) composition. Titanite occurs mostly as large euhedral grains up to 2.5 mm in length, but in sample V5 only remnants of titanite are found. Zircons from all samples were dated by the single-zircon Pb-Pb evaporation method. Moreover, zircons from sample V7 were additionally dated by the single-zircon conventional U-Pb method. The resulting ages are: 282 ± 8 Ma (V2), 296 ± 6 Ma (V4), 289 ± 8 Ma (V5), 290 ± 6 Ma (V10) and 294 ± 4 Ma / 282 ± 1 Ma (V7, Pb-Pb evaporation method / conventional U-Pb method respectively). The ages thus cover a narrow range from 282 ± 1 Ma to 296 ± 6 Ma (Fig. 3.4a-f) and indicate a time span of about 14 Ma for igneous activity. Ages of individual zircon grains for each sample form a homogeneous group, the only exception being sample V2, where two age groups were found. An older age of 282 ± 8 Ma is calculated as the mean age of four grains (grains V2 B, C, F and D; Fig. 3.4a) and interpreted to reflect the intrusion event. The other four grains gave a mean age of 262 ± 8 Ma (grains V2 A, E, G and H, not shown in Fig. 3.4). This age most likely reflects Pb loss. Generally, Pb loss seems more likely to have occurred during a later thermal event than during a late magmatic pulse and zircon growth at 262 Ma because CL images show the patchy pattern often obtained during recrystallisation (Fig. 3.2a). For sample V7, there is a discrepancy in the ages obtained using the Pb-Pb evaporation (294 ± 4 Ma) and the conventional U-Pb methods (concordant age of 282 ± 1 Ma). This might be explained by the different response of these two dating methods to the existence of small overgrowths on zircon grains, which are visible as bright rims in CL images (Fig. 3.2d). Such overgrowths could have led to the slightly younger age obtained by conventional U-Pb analyses when the whole grain was dissolved and analysed. Applying the Pb-Pb evaporation method, such a rim could have been evaporated during the first phase of the heating procedure, before the deposition of Pb on the ionisation filament. Bright overgrowths, visible in CL images, are a common feature of the zircon grains in most of the Varnous pluton samples, e.g. samples V4 and V5 (Fig. 3.2b and c). Complex internal structures are also typical (e.g. V5, Fig. 3.2c; V10, Fig. 3.2e). They are, however, unlikely to point to an older inherited component because this feature is relatively common and there is no indication for an older inherited Pb component from the geochronological analyses. The only indication for a minor inherited component would be an age of *c.* 312 Ma obtained from a zircon grain of sample V4 (grain B, Appendix D); no older ages were obtained from the Varnous pluton samples.

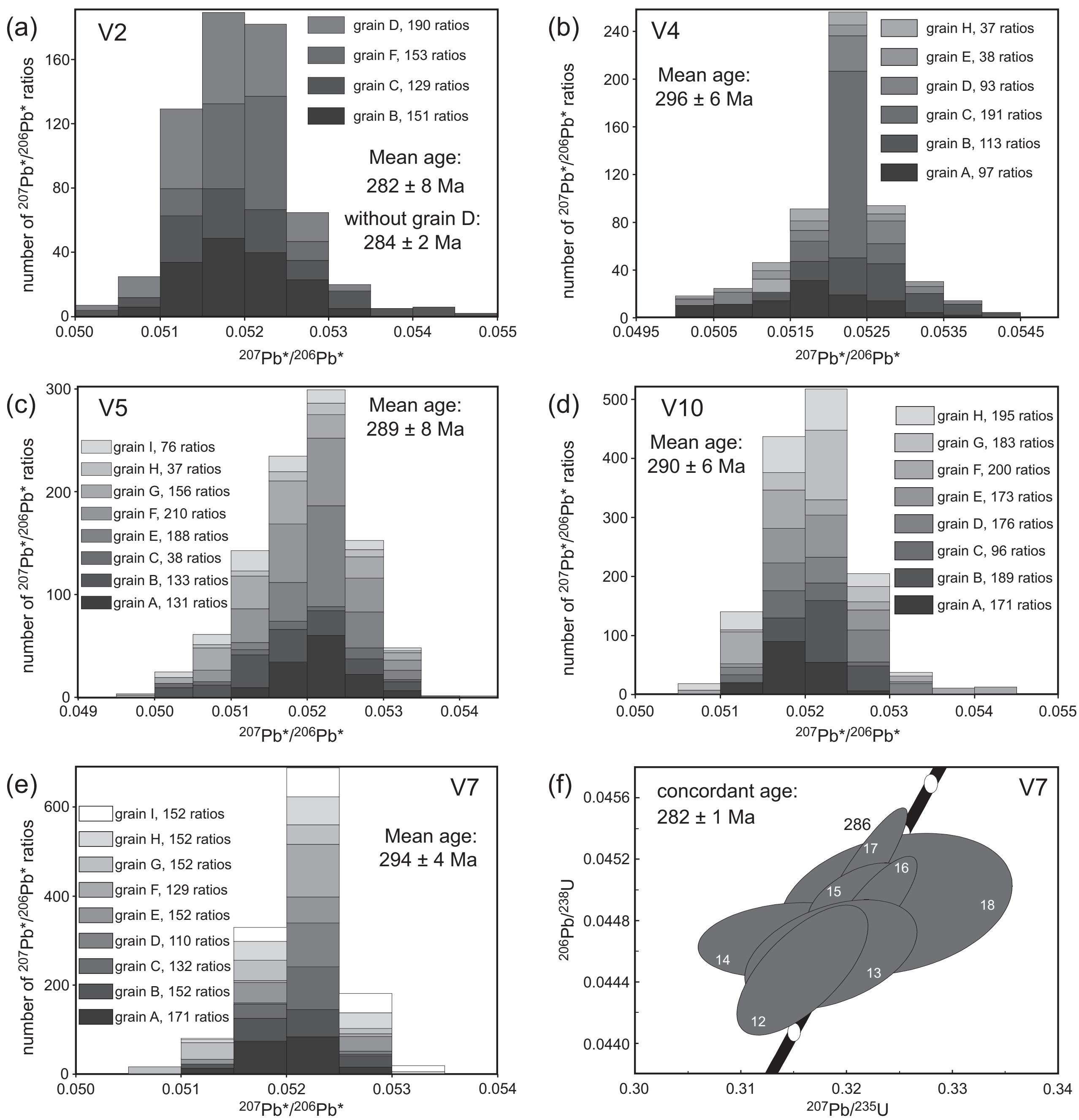

Fig. 3.4. Geochronological results from the Pb-Pb evaporation dating of basement rocks from the Varnous Mts. are displayed as histograms (**a-e**). Sample V7 was additionally dated by the conventional U-Pb method (**f**).

Driovouno. Along the northwestern margin of the Pelagonian Zone Permo-Triassic metaclastic sequences occur with rhyolite flows embedded in their upper parts, which are overlain by Triassic-Jurassic carbonates (Mountrakis *et al.* 1987). Sample Pl63 (the westernmost sample of this study; Fig. 3.1c) was taken close to Driovouno village. The red meta-rhyolite consists of feldspar crystals in a matrix of spherulitic intergrowth of quartz and feldspar (devitrified glass?). Meta-rhyolite Pl63 was dated by the conventional U-Pb method (Fig. 3.5a). As the size of the zircon grains was small (mostly about 50 µm), fractions of two to three grains were analysed. Two fractions yielded a concordant age of 244 ± 1 Ma (MSWD of concordance = 1.14). One fraction displays Pb-loss while another fraction plots slightly reversely discordant in the concordia diagram.

Veria region. About 15 km south of the town of Veria (Fig. 3.1a) there are large exposures of granitic basement rocks. Deformation is variable and ranges from foliated gneisses to almost undeformed granites.

Pl44 is a grey mylonitic gneiss with small feldspar "augen". Its main minerals are quartz, K-feldspar, plagioclase and white mica. Very minor biotite and minor epidote also occur. Mylonite Pl44 was dated by the single-zircon conventional U-Pb method (Fig. 3.5b). Four zircon grains define a concordant age of 137 ± 1 Ma (95% conf. level, MSWD of concordance = 0.2). Two grains plot concordantly at

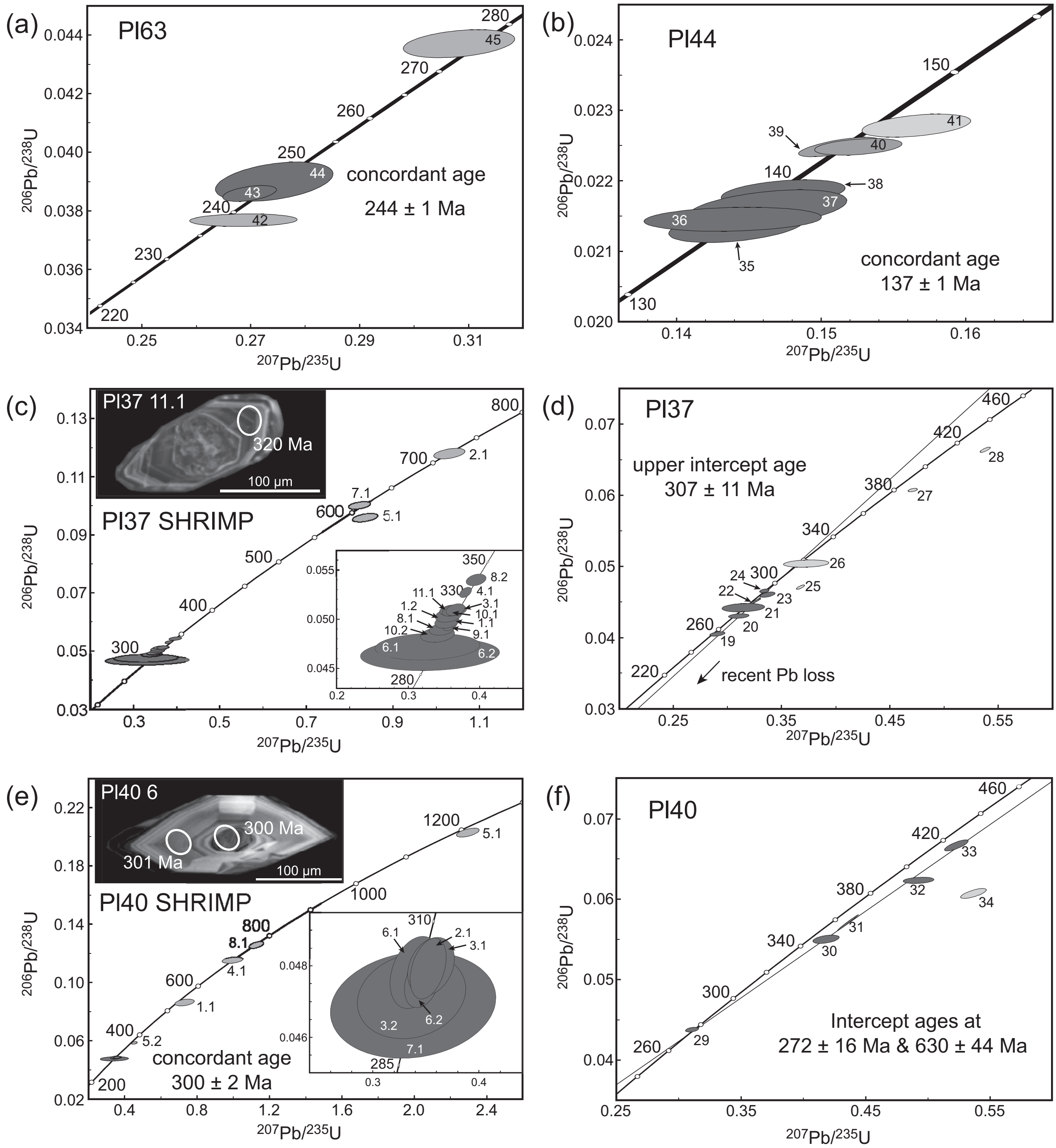

Fig. 3.5. Geochronological results of basement rocks from Driovouno (a) and the area south of Veria (b-f). The lower intercept age of sample Pl38 was assumed to be at the origin (d).

143 ± 1 Ma (MSWD of concordance = 0.02). It is not possible to decide whether the younger age represents the intrusion age and the older age the existence of a subordinate inherited component or whether the older age dates the intrusion event and the younger age is caused by Pb loss. The discordance of a zircon grain that plots close to the older age group in the concordia diagram could be taken to indicate the existence of an inherited component. We interpret these data, nevertheless, to be a strong indication for a magmatic event at about 140 Ma.

Pl37 and Pl40 (Fig. 3.1a) are light-coloured granites that vary in their degree of deformation. They were sampled along road cuts approximately 500 m apart. Pl37 is less deformed than Pl40. Both granites consist mainly of quartz, K-feldspar, plagioclase, white mica and garnet < 0.5 mm across. Minor epidote and remnants of biotite also occur. The plagioclase shows severe alteration to epidote and white mica. Zircons from both samples show several events of growth and inheritance in CL images. These characteristics complicate the dating of the zircons and the interpretation of the resulting age. For instance, SHRIMP dating of sample Pl37 resulted in a continuous spread of concordant ages from 339 ± 3 Ma to 292 ± 8 Ma (Fig. 3.5c). A precise intrusion age cannot be inferred from this range in ages, which seems too long to reflect continuous magmatism. However, as the two youngest ages could reflect minor Pb loss (being measured on a narrow grain) and the two oldest ages are probably mixing ages between the young zircon rim and an older core, the age range can be narrowed down to about 300 to 320 Ma. This age range is assumed to reflect the intrusion age. A similar result was obtained applying the conventional U-Pb method (Fig. 3.5d), where 6 grains define a discordia with an upper intercept age of 307 ± 11 Ma (MSWD = 1.14) while the lower intercept (assumed at 0 Ma) reflects recent Pb loss. Dating by SHRIMP revealed two concordant ages for inherited grains; the obtained ages were 614 ± 6 Ma and 719 ± 9 Ma.

For Pl40, SHRIMP dating yielded a concordant age of 300 ± 2 Ma (MSWD of concordance = 0.8) that is interpreted as the intrusion age (Fig. 3.5e). This age is distinctly older than the one obtained from the single-zircon conventional U-Pb analyses, which is a lower intercept age of 272 ± 16 Ma (MSWD = 1.3; Fig. 3.5f). One grain, however, plots concordantly at 275 ± 2 Ma. This younger age could be caused by Pb loss that led to a shift towards younger ages but was not severe enough to result in discordance. Information about the ages of inherited components by the conventional U-Pb method is mostly imprecise. The upper intercept age of about 630 ± 44 Ma gives only the range of the inherited age, if no more than two components, inherited core and newly grown zircon at *c.* 275 Ma, are present. This, however, is rather unlikely because partial Pb loss is assumed to have affected at least the youngest of the grains. SHRIMP analyses resulted in two concordant ages of 701 ± 10 Ma and 764 ± 11 Ma, and in three slightly discordant ages that plot close to 365, 535 and 1200 Ma respectively.

Mt. Olympos region. Strongly deformed, greenish “augen” gneisses crop out northeast of Mt. Olympos (Fig. 3.1d). The area of orthogneiss exposures is limited to the SW by the Mt. Olympos carbonates and to the north and east by Tertiary to recent sediments. A coarse- and a fine-grained variety of this orthogneiss (samples Pl74 and Pl73, respectively) were sampled close to the monastery of Agios Nicolaos (not shown on the map). The mylonitic orthogneisses consist mainly of quartz, K-feldspar, chlorite, plagioclase and remnants of biotite and epidote. In the fine-grained variety, the feldspar “augen” have more or less disappeared. Zircons from the fine-grained orthogneiss Pl73 were dated by the conventional single-zircon U-Pb method. Seven discordant and three slightly reversely discordant zircon grains define a discordia line (Fig. 3.6a). The upper intercept age is 245 ± 8 Ma (MSWD = 1.5). The (forced) lower intercept age of about 0 Ma is interpreted as recent Pb loss. Two older grains seem to reflect an inherited component.

Thessaly/Verdikoussa. The area around Verdikoussa (Fig. 3.1d) is characterised by large exposures of granites and gneisses. Deformation ranges from undeformed granites to variably deformed augen-gneisses and to highly sheared rocks in the east ("Ambelakia unit"). Pl5 and Pl8 are orthogneisses sampled east of Verdikoussa. They consist mainly of quartz, saussuritised plagioclase, K-feldspar, white mica and epidote/clinozoisite ± titanite. Pl8 additionally contains biotite and apatite; the feldspar is severely altered to sericite or epidote.

Zircon grains from orthogneiss Pl5 were initially analysed using the Pb-Pb evaporation method. Four ages are in the range of 296-270 Ma, while five older grains scatter from 1469 Ma to 492 Ma (Appendix D). This age distribution makes it impossible to identify the intrusion age of the rock. Therefore, orthogneiss Pl5 was dated by the single-zircon conventional U-Pb method (Fig. 3.6b). Two concordant grains define an age of 279 ± 2 Ma (MSWD of concordance = 3.7) that is interpreted as the protolith intrusion age. A wide scatter of discordant grains that are older than 279 Ma demonstrates the existence of inherited components in the zircon grains. Several discordia lines can be fitted through groups of these zircon grains. This method does not yield unequivocal results because it assumes that only two events are reflected in the analysis, namely the protolith component and the magmatic intrusion that led to new zircon growth. The method of fitting discordia lines through groups of grains with inherited components might nevertheless give some good indications about the age groups of source rocks contributing to magma genesis. The youngest age for a source component is obtained by three grains that define a discordia with an upper intercept age of 702 ± 36 Ma (MSWD = 1.5). The lower intercept age of 273 ± 18 Ma is identical, within analytical error, to the magmatic intrusion age. Four zircon grains roughly define a discordia with an upper intercept age of 1320 ± 78 Ma (MSWD = 5.7). The lower intercept age of 299 ± 27 Ma is again close, within analytical error, to the magmatic intrusion age. Two zircon grains indicate an even older source component, for which an upper intercept age of 1505 ± 21 Ma and a lower intercept age of 301 ± 7 Ma were obtained. One zircon grain did not fit on either of the described discordia lines. If calculated through an age of 279 Ma (intrusion event), an upper intercept age of *c.* 880 Ma is obtained. This age, however, could reflect the mixture of more than two components. One young zircon grain fits on a discordia line between the magmatic event at 279 Ma and present day, demonstrating recent Pb loss.

Zircon grains from orthogneiss Pl8 were analysed using the Pb-Pb evaporation method. The ages obtained show a heterogeneous distribution that does not allow us to calculate an intrusion age. Some grains scatter around 280 Ma (Appendix D), indicating a relation to the Permo-Carboniferous magmatic phase identified in several samples from the Pelagonian Zone. Four grains are older, ranging from 416 Ma to 1875 Ma, thus indicating the contribution from an older source.

Mt. Ossa. The region of Mt. Ossa (Fig. 3.1e), south of Mt. Olympos, comprises mostly basement gneisses and phyllites as well as a thick marble succession. Two samples were taken from this region. Sample Pl50 is a strongly deformed mylonite taken from the eastern flank of Mt. Ossa. The main minerals are quartz, K-feldspar, plagioclase, white mica and chlorite after mica, epidote, and minor

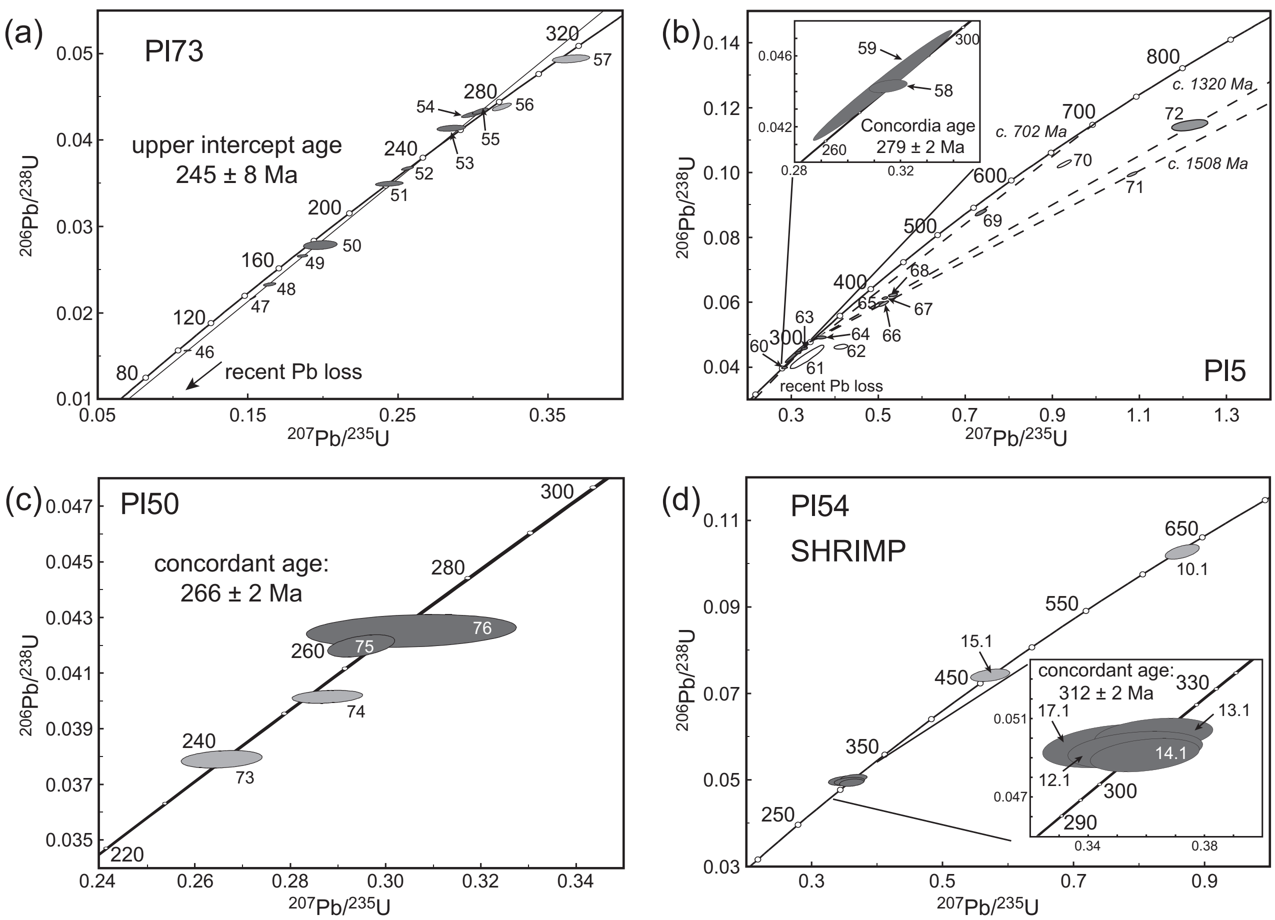

Fig. 3.6. Geochronological results of basement rocks from the Mt. Olympos and the Mt. Ossa areas. Concordia diagrams display the results of the conventional U-Pb method, unless stated otherwise. The lower intercept age of sample PI73 was assumed to be at the origin (**a**).

opaques. Five zircon grains of this mylonite were analysed using the conventional single-zircon U-Pb method (Fig. 3.6c). Two grains yielded a concordant age of 266 ± 2 Ma (MSWD of concordance = 1.15) while a third concordant grain yielded an age of 240 ± 2 Ma (MSWD of concordance = 0.039). One zircon grain plots slightly discordant between 260 and 240 Ma, a feature that is interpreted as Pb loss. Another grain with a $^{207}Pb/^{206}Pb$ age of about 2076 Ma (not shown in Fig. 3.6e) clearly displays an inherited component.

PI54 is a greenish, strongly foliated mylonite sampled west of Mt. Ossa (Fig. 3.1e). Plagioclase, K-feldspar and quartz “augen” occur in a matrix of mainly quartz. White mica is concentrated in the foliation planes. Some minor epidote and opaques also occur. Mylonite PI54 was dated with SHRIMP (Fig. 3.6d) and a concordant age of 312 ± 2 Ma (MSWD of concordance = 0.29) was obtained. This age is interpreted as the intrusion age. Two older concordant ages of 461 ± 10 Ma and 632 ± 13 Ma indicate the involvement of an older crustal source in magma genesis.

Mavrovouni. Mavrovouni is another region of the Pelagonian Zone characterised by gneissic basement (Fig. 3.1e). PI13 is a light-coloured, medium-grained orthogneiss that shows strong foliation. It consists of K-feldspar and large, deformed flakes of white mica in a fine-grained matrix of quartz, minor opaques and apatite. The Mavrovouni orthogneiss PI13 was dated with the single-zircon conventional U-Pb method (Fig. 3.7a). For three grains a concordant age of 280 ± 2 Ma (MSWD of concordance = 7) was obtained. This age is interpreted as the intrusion age. An almost concordant age of *c.* 252 ± 12 Ma is attributed to a Pb-loss event, possibly during Lower Triassic times. Two zircon grains that plot strongly reversely in the concordia diagram were not used for the age calculation.

Pilion peninsula. The geology of the Pilion peninsula (Fig. 3.1f) is characterised by large occurrences of felsic to intermediate basement gneisses and schists in northern and southeastern Mt. Pilion. In central and southwest Pilion marbles and limestones prevail. On the very southwestern tip of the Pilion peninsula gneisses are once more exposed. Basement rocks are often severely deformed mylonites. Marbles and remnants of ophiolites are tectonically intercalated with the basement rocks (Wallbrecher 1976; Jacobshagen 1986).

The northernmost sample (Pl23) was taken from an orthogneiss occurrence along the road east of Andraki hill (not shown in Fig. 3.1f). The orthogneiss consists mainly of quartz, feldspar, white mica, chlorite, titanite and epidote. Single-zircon dating with the conventional U-Pb method for orthogneiss Pl23 resulted in an upper intercept age of 546 ± 10 Ma (MSWD = 0.96) that is interpreted as the intrusion age (Fig. 3.7b). Three older grains demonstrate the existence of an older inherited component. For the two younger grains showing inheritance, a discordia can be calculated that intersects with the concordia at 529 ± 39 Ma and 1292 ± 170 Ma (though two-point discordias are of doubtful reliability). Because the lower intercept is identical, within analytical error, to the obtained intrusion age of 546 ± 10 Ma, the upper intercept age of *c.* 1300 Ma could indicate the age of one of the contributing source rocks. The third of the grains showing inheritance has a $^{207}Pb/^{206}Pb$ age of *c.* 2062 Ma and therefore reflects a second, even older source component.

Orthogneiss Pl21 was sampled on a road-cut approximately 4 km NE of the village of Milies (not shown in Fig. 3.1f). It consists mainly of sparse porphyroblasts of feldspar and white mica set in a fine-grained matrix containing quartz, K-feldspar, plagioclase, epidote and small garnets. Pl21 was dated by the single-zircon conventional U-Pb method (Fig. 3.7c). Four grains are slightly discordant and yielded an upper intercept age of 279 ± 14 Ma (MSWD = 0.43) that is interpreted as intrusion age. It is also possible to calculate concordant ages for each of these grains separately, but this results in a spread of the concordant ages from 260 ± 2 Ma for the youngest grain to 277 ± 2 Ma for the oldest grain. We interpret the younger ages as the probable result of very slight Pb loss and favour the oldest age as most likely resembling the intrusion age. This age is identical, within error, to the more imprecise upper intercept age, which supports our interpretation. One older grain is interpreted to reflect an older inherited component. Inheritance can be seen in CL images of zircons, where zircons with rounded cores and discordances in the zoning pattern occur beside those showing fine-scale, single-phase oscillatory zoning (Fig. 3.2g and f).

A rather dark green mylonite (sample Pl16) with small feldspar “augen” was also collected in northern Pilion (Fig. 3.1f). This mylonite consists mainly of quartz, K-feldspar, white mica, chlorite and epidote and was sampled approximately 1.5 km east of Milies. Zircons from mylonite Pl16 were dated using SHRIMP. Although most spots plot slightly reversely discordant in a concordia diagram, a relatively concordant age of 241 ± 6 Ma (MSWD of concordance = 13) was obtained (Fig. 3.7d). Two spots on an older zircon grain yielded a concordant age of 352 ± 7 Ma (MSWD = 0.72).

Orthogneisses from southern Pilion are represented by two samples (Fig. 3.1f). Sample Pl80 was collected from a road cut in southwestern Pilion. It is a fine-grained greenish mylonitic orthogneiss and contains small feldspar “augen” and white mica flakes in a very fine-grained matrix of quartz, some

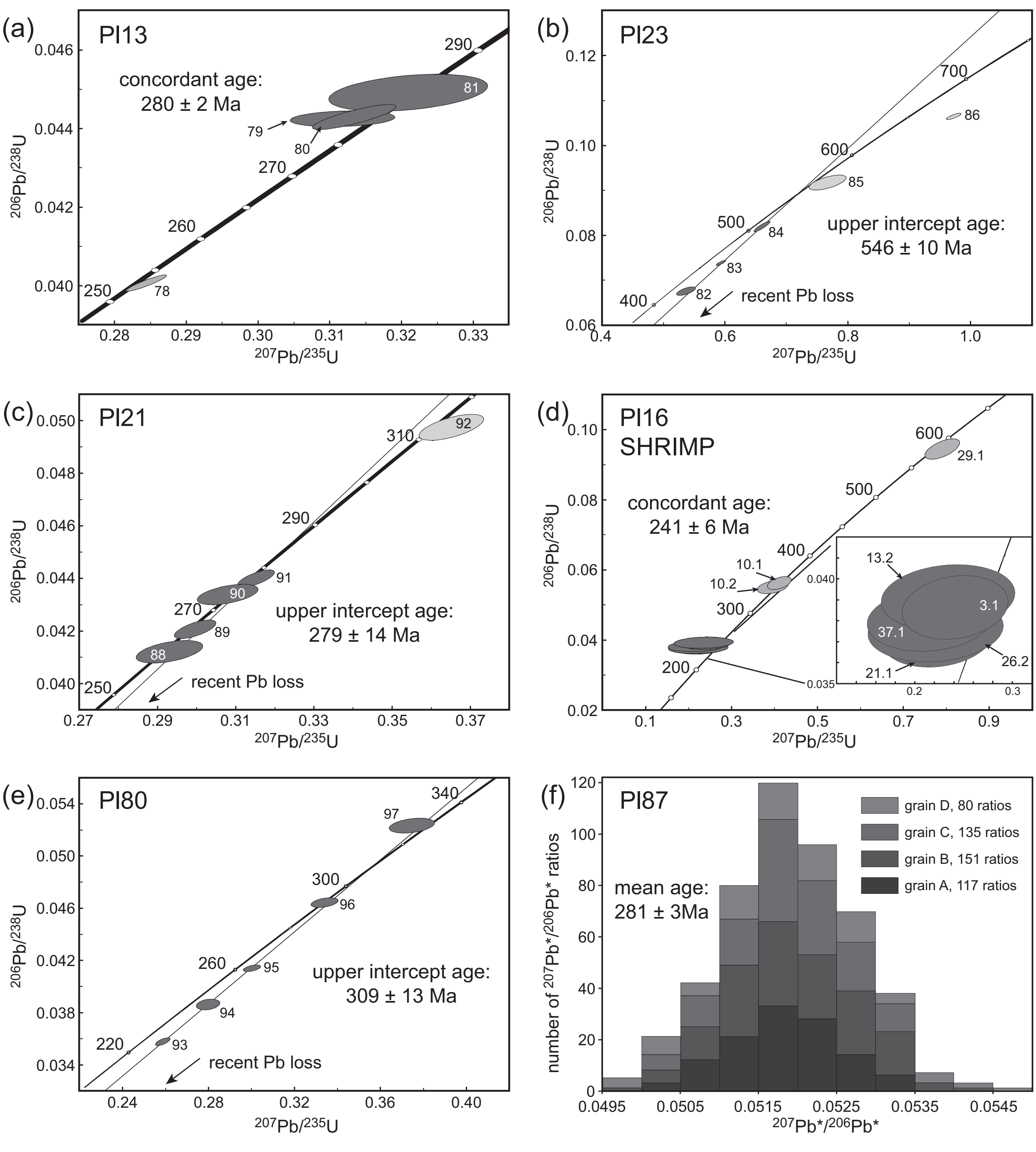

Fig. 3.7. Geochronological results of basement rocks from the Mavrovouni and Mt. Pilion areas. Concordia diagrams (**a-e**) display the results of the conventional U-Pb method, unless stated otherwise. Histogram (**f**) shows the results of the single-zircon Pb-Pb evaporation method. If no lower intercept age is given (**b**, **c** and **e**), the discordia was calculated through the origin.

feldspar, white mica and minor epidote. Mylonitic gneiss Pl80 was dated using the single-zircon conventional U-Pb method (Fig. 3.7e). Five zircon grains define a discordia. The upper intercept of the discordia with the concordia line at 309 ± 13 Ma (MSWD = 0.63) is interpreted as the emplacement age.

A coarse-grained mylonite (Pl87) was collected from the southern coast of the Pilion peninsula (Fig. 3.1f). Large, centimetre-sized, feldspar “augen” occur in bands of quartz, K-feldspar, plagioclase, biotite, epidote, white mica and apatite. Orthogneiss Pl87 was dated using the single-zircon Pb-Pb

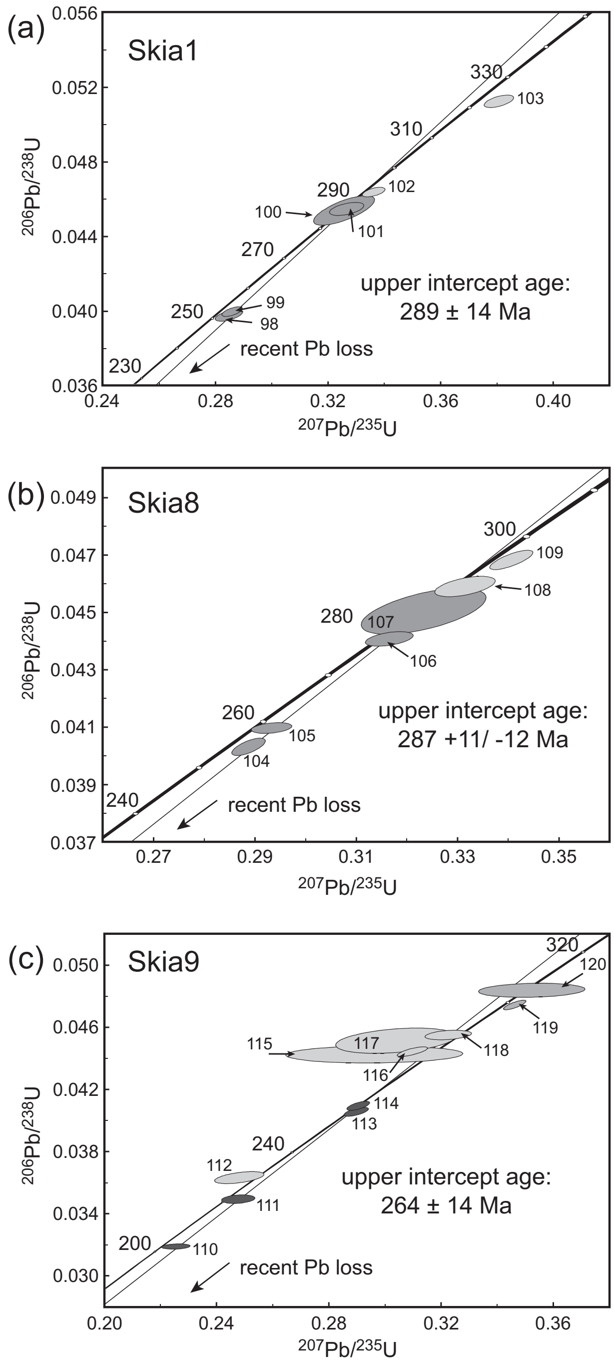

Fig. 3.8. Results of single-zircon conventional U-Pb analyses of basement rocks from Skiathos Island. Discordia lines for all samples were calculated through the origin.

evaporation method (Fig. 3.7f). Four grains yielded an age of 281 ± 3 Ma, which is perceived to closely resemble the intrusion age of the protolith of the orthogneiss.

Skiathos Island. The crystalline basement of western Skiathos Island comprises schists, para- and orthogneisses. Eastern Skiathos Island is dominated by Mesozoic limestones and marbles as well as Upper Cretaceous to Tertiary flysch. Three orthogneisses from western Skiathos Island (Fig. 3.1f) were dated using the single-zircon conventional U-Pb method. The southernmost orthogneiss Skia1 was sampled *c.* 300 m SE of Maratha village and consists mainly of quartz, sericitised and saussuritised feldspar (K-feldspar and plagioclase), biotite, white mica, minor epidote/clinozoisite and minor apatite. Four zircon grains define a discordia with an upper intercept age of 289 +13/ -14 Ma (MSWD = 0.038; Fig. 3.8a), which is interpreted as the emplacement age. Two of the four grains display recent Pb loss while the other two grains fall on the concordia curve. From these latter two grains a concordant age of 286 ± 2 Ma (MSWD of concordance = 0.23) can be calculated. Two zircon grains that were not included in the age calculation plot discordantly towards older ages and are interpreted to have incorporated an older inherited component. This interpretation is reinforced by CL images of zircons that show relics of old detrital zircon in the core of the zircon (Fig. 3.2i). However, most zircons show single-phase magmatic oscillatory zoning in CL images (Fig. 3.2h and j).

Orthogneiss Skia8 was sampled from the central part of the basement complex of Skiathos Island. The main minerals are quartz, K-feldspar, saussuritised plagioclase and white mica. Remnants of biotite occur in addition to minor epidote/clinozoisite. Zircons of orthogneiss Skia8 yielded an upper intercept age of 287 +11/-12 Ma (MSWD=0.047; Fig. 3.8b) that is taken as the intrusion age and that is identical, within error, to the intrusion age obtained for orthogneiss Skia1. For one concordant grain a concordant age of 284 ± 4 Ma can be calculated.

Skia9 is a medium-grained, garnet-bearing orthogneiss from the NW coast of Skiathos Island. It was sampled at the northeastern end of Mikro Aselinos Bay. Zircons were dated by the conventional single-zircon U-Pb method (Fig. 3.8c). A discordia line defined by four grains was calculated through the origin, representing recent Pb loss, and yielded an upper intercept age of 264 ± 14 Ma (MSWD = 0.6). Three older grains (grains 119-121, grain 121 not shown in Fig. 3.8c) are interpreted to reflect the incorporation of an older, inherited component in the zircons. Grain 121 has a $^{207}Pb/^{206}Pb$ age of *c.* 1518 Ma (Appendix E). Five grains, however, fall on the left-hand side of the concordia line and plot reversely discordant in the concordia diagram. Four of those grains plot in the same range, close to the age of *c.* 280 Ma on the concordia line. These results can be interpreted in two possible ways. The first approach is to reject all grains that fall on the left-hand side of the concordia, because this is caused by the analytical process in the laboratory and hampers the extraction of age information. Then the upper intercept age of *c.* 264 Ma would most likely be interpreted as the intrusion age. A second way to interpret the results is to attribute the old group of reversely plotting zircon grains to analytical difficulties yet accept that they belong to an age group of about 270 to 290 Ma because they plot close to the concordia line. If the age of *c.* 280 Ma were interpreted as the intrusion age, the protolith of orthogneiss Skia9 would have formed during the same time span as that of orthogneisses Skia1 and Skia8. A possible interpretation for the age of 264 Ma could then be a metamorphic overprint in the Upper Permian that only affected the U-Pb isotopic system of zircons in rocks from northern Skiathos Island.

Evia. One of the southernmost samples from the Pelagonian Zone was collected from northern Evia Island (Fig. 3.1a). Apart from the prevailing Mesozoic sedimentary successions, the northern part of Evia exhibits a small number of outcrops of crystalline basement rocks. Sample Ev4 is a dark-green gneiss that was taken from an outcrop at a road cut between Rovies and Marouli. It consists mainly of quartz, sericitised feldspar, and chlorite after mica, calcite, apatite and epidote. Orthogneiss Ev4 was dated using SHRIMP (Fig. 3.9a). A concordant age of 303 ± 2 Ma (MSWD of concordance = 0.53) was obtained from the analyses of four spots. This age is interpreted to be the intrusion age of the protolith of this orthogneiss.

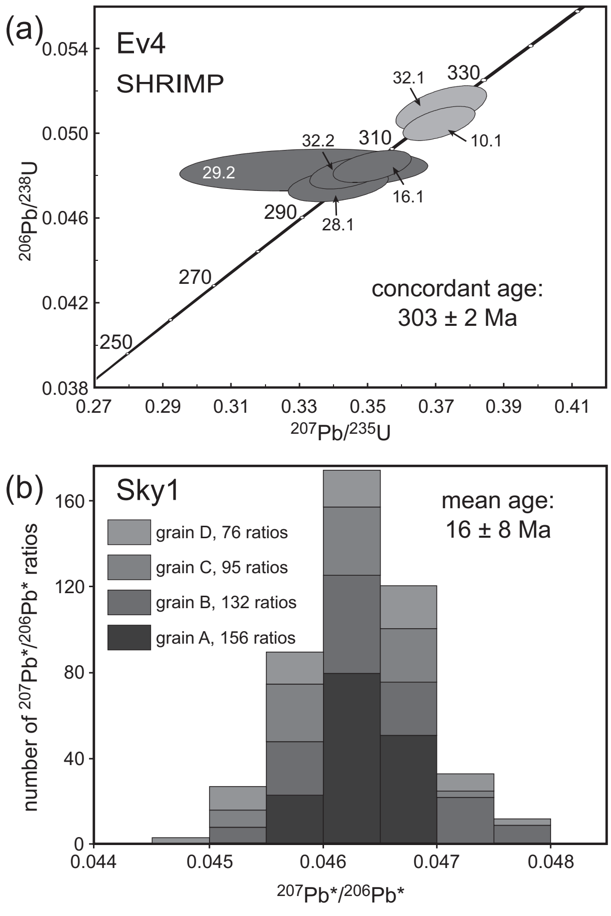

Fig. 3.9. Results for SHRIMP dating of Ev4 (**a**) and Pb-Pb evaporation dating of Sky1 (**b**).

Skyros Island. The geology of Skyros Island is dominated by metaclastic rocks of Permo-Triassic age as well as metaclastics of probably Mesozoic age and Mesozoic marbles (Melentis 1973; Harder *et al.*, c.f. Pe-Piper 1991). In southwestern Skyros Island some severely altered granitoids of presumed Mesozoic age (Pe-Piper 1991) are exposed along small road cuts and one of them was sampled for geochronology (Fig. 3.1a). Zircons were dated with the single-zircon Pb-Pb evaporation method (Fig. 3.9b). The zircons turned out to be very young, and a Miocene intrusion age of 16 ± 8 Ma is assumed. A precise age cannot be given because the limit of this dating method is reached by such a young age (low radiogenic Pb concentration and large measurement errors).

3.4 Discussion

The geochronological results described above show the presence of at least five age groups for magmatic rocks in the western part of the Internal Hellenides. These igneous events are discussed in the following paragraphs.

Tertiary. Tertiary magmatism is clearly indicated by the Skyros Island granitoid rock, although no precise intrusion age could be obtained because of the limits of dating young zircons by the Pb-Pb evaporation method. The Tertiary age supports the assumption of Fytikas *et al.* (1980) that these intrusive rocks are Cainozoic in age and do not have, as Pe-Piper (1991) suggested, a Mesozoic age.

Jurassic/Cretaceous. The second age group is represented by the Upper Jurassic/Lower Cretaceous meta-granite Pl44 sampled south of Veria, which could be a rock of the westernmost Vardar Zone. Jurassic magmatism in the Vardar Zone as a result of ocean spreading and subduction-zone volcanism (Paikon Massif) is well known (e.g. Mercier *et al*. 1975; Anders *et al*. 2003a; see Chapter 1). The Upper Jurassic age of this orthogneiss might either reflect an independent igneous pulse that has so far gone undetected in the Pelagonian Zone, or it might be related to Jurassic igneous activity in the Vardar Zone, in which case the granite was tectonically emplaced in its present position at the eastern margin of the Pelagonian Zone. There is abundant evidence for such tectonic movements in the area east of the Pelagonian Zone as shown by eastward thrusting of ophiolites and strike-slip faulting (e.g. Mercier *et al*. 1975; Mountrakis 1984; Bébien *et al*. 1986; Brown & Robertson 2004).

Triassic. Two different types of Triassic rocks from the Pelagonian Zone were dated in this study: a meta-rhyolite in the NW Pelagonian Zone (Pl63) and mylonitic orthogneisses in the Eastern Pelagonian Zone. Mountrakis *et al*. (1987) described meta-rhyolites that crop out near Driovouno village in the northwestern Pelagonian Zone and proposed an Early Triassic intrusion age for these rocks, because they lay stratigraphically below Middle Triassic limestones and intrusion contacts between the rhyolites and the limestones are absent. The Early Triassic age of the rhyolites inferred by Mountrakis *et al*. (1987) is now confirmed by our U-Pb dating of zircons from a rhyolite close to Driovouno village, which resulted in an intrusion age of *c.* 244 Ma. A Cretaceous age obtained by K-Ar geochronology of K-feldspar phenocrysts of the Driovouno rhyolites was ascribed by Mountrakis *et al*. (1987) to metasomatic overprint. The Triassic volcanic rocks in the western Pelagonian Zone are interpreted to be related to rifting in the realm of the later Pindos Ocean (e.g. Robertson *et al*. 1991), although some authors argue in favour of all ophiolites being derived from one single ocean east of the Pelagonian Zone (e.g. Bortolotti *et al*. 2003).

Triassic magmatism is also known from the eastern part of the Pelagonian Zone. Northeast of Mt. Olympos and in northern Mt. Pilion two rocks were dated at 245 ± 8 Ma (mylonitic orthogneiss Pl73) and 241 ± 6 Ma (mylonite Pl16) respectively. Other samples from the East Pelagonian Zone also seem to have been affected by a Late Permian to Triassic thermal event. For example, orthogneiss Skia9 from northern Skiathos Island either intruded during the latest Permian or a metamorphic event at that time led to resetting of the U-Pb system of zircons from this sample. Another example is mylonite Pl50 from the eastern flank of Mt. Ossa that is interpreted to have intruded at *c.* 266 Ma and to have been overprinted at *c.* 240 Ma. Interpretation of these Triassic rocks in a geodynamic context is difficult, because Triassic magmatism is considered to be related to post-Variscan extension, rifting and spreading of Neotethyan ocean basins (e.g. Mountrakis 1987; Pe-Piper 1982, 1998; Pe-Piper & Piper 2002). For example, Sub-Pelagonian and Pelagonian Zone Triassic volcanic rocks are exposed in Argolis (e.g. Bortolotti *et al.* 2001, 2003), Chios Island (Pe-Piper 1982 and references therein), Evia (De Bono 1998; Pe-Piper 1998 and references therein; De Bono *et al.* 2001), Atalanti (Kauffmann 1976) and Mt. Othris (e.g. Kauffmann 1976). Most of the Triassic volcanic rocks in the Pelagonian Zone are basaltic in composition with rhyolites occurring rather rarely. Triassic rift-related magmatism is also known from the easternmost part of the Vardar Zone, where Triassic basalts and rhyolites have been reported (Kockel & Mollat 1977; Dimitriadis & Asvesta 1993), and from the Serbo-Macedonian Massif where the Triassic within-plate Arnaea granite has intruded Silurian basement orthogneisses (*Himmerkus et al.* 2004*b*). The Vardar Zone constitutes proof of a Mesozoic ocean basin east of the Pelagonian Zone; in its western part early Triassic spreading was suggested by Stais & Ferriére (1991) and Brown & Robertson (2003). Therefore, an extensional tectonic setting for the late Permian / early Triassic magmatism in the east Pelagonian Zone is suggested.

Permo-Carboniferous. The majority of the samples in this study belong to basement rocks that have Permo-Carboniferous intrusion ages. Since the pioneering work of Yarwood & Aftalion (1976) the Permo-Carboniferous period is regarded as an era of major magmatism in the region. The importance of this magmatic phase for the evolution of the Pelagonian Zone basement is further underscored by the results of this study. We have demonstrated that Permo-Carboniferous magmatism was widespread throughout the Pelagonian Zone and that for some areas, where basement rocks had hitherto been interpreted as belonging to the Pelagonian Zone on a structural or stratigraphic basis only these interpretations are correct on the basis of intrusion ages. For example, the Permo-Carboniferous protolith ages of gneisses from Skiathos Island determined here are in accordance with the suggestion of Ferentinos (1973) who claimed that the metamorphic basement of western Skiathos Island is part of the Pelagonian Zone. Similarly, the gneisses of the Likostomo-Promachi Unit in the central part of the Voras Mts. were interpreted by Migiros & Galeos (1990) and Brown & Robertson (2004) as showing affinity to the Pelagonian Zone and not to the Serbo-Macedonian Massif. This interpretation is now confirmed by the age of 285 Ma obtained for orthogneiss Pl75, because Permo-Carboniferous intrusion ages are absent from the neighbouring parts of the Serbo-Macedonian Massif (Himmerkus *et al.* 2003).

Magmatic ages of Permo-Carboniferous basement rocks in the Pelagonian Zone range from *c.* 320 Ma (De Bono 1998; Vavassis *et al.* 2000) to *c.* 280 Ma (Reischmann *et al.* 2001; this study), indicating long-lived subduction-zone magmatism. A systematic northward younging of intrusion ages, as suggested by Reischmann *et al.* (2001), would indicate that the commencement of subduction-zone magmatism varied laterally. However, although most of the older ages are found in the southern parts of the Pelagonian Zone this hypothesis could not be confirmed by the ages obtained in our study. The active continental margin was possibly situated at the southern European margin (Stampfli & Borel 2002).

The Varnous pluton in the northwestern Pelagonian Zone occupies an area where magmatism started at about 290 Ma and continued probably up until *c.* 280 Ma. This is indicated by the spread of ages obtained for the various rocks from the Varnous pluton. The majority of the zircon ages are interpreted to represent the time of magmatic growth of the zircons, although some young ages clearly reflect Pb loss. The internal structure of zircons from the Varnous pluton, which are visible in CL images (Fig. 3.2), show diffuse areas of resorption, complex structures of cores or lighter-coloured rims. Geochronology provided no evidence for inherited components, therefore these structures are interpreted mostly as syn- to late magmatic, suggesting multiple intrusion events in a long-lived magma chamber system, or as post-magmatic, in which case recrystallisation can cause Pb loss and result in younger ages.

Precambrian. Rocks older than Upper Carboniferous were not encountered in this study except for gneiss PI23 from northern Pilion, although in the western part of the Pelagonian Zone Neoproterozoic basement rocks were identified (Anders *et al.* 2003b, see Chapter 2). Inherited cores in zircon grains from granites PI37, PI40 and possibly PI5, however, indicate that Neoproterozoic rocks were incorporated in magma genesis during the Permo-Carboniferous magmatic event. Zircons grown during late Precambrian to Cambrian magmatism were also found in gneiss PI23 from northern Pilion. It is, however, unclear whether the obtained age of *c.* 545 Ma does really reflect the intrusion age of a magmatic protolith of the gneiss or if it, in fact, reflects the age of a sedimentary source component. All in all, inherited zircon components were found in several samples, mostly hinting at a Mesoproterozoic to Palaeoproterozoic source contribution.

Magmatic crystallisation ages of about 300 Ma are not only widespread in the Pelagonian Zone but also in the Attico-Cycladic Massif in the southeastern continuation of the Pelagonian Zone (Engel & Reischmann 1998, 1999; Reischmann 1998). This led Reischmann *et al.* (2001) to propose the presence of a huge Permo-Carboniferous magmatic arc in this region of the eastern Mediterranean. Other regions in the eastern Mediterranean in which Permo-Carboniferous basement rocks occur are the Sakarya Complex in NW Anatolia, Turkey, (Özmen & Reischmann 1999), the Rhodope Massif of both NE Greece and S Bulgaria (Peytcheva & von Quadt 1995; Turpaud & Reischmann 2003; Peytcheva *et al.* 2004) and the Strandja Massif in E Thrace, Turkey (Okay *et al.* 2001). By contrast, Permo-Carboniferous basement rocks are not known from the Menderes Massif, which is the eastern prolongation of the Attico-Cycladic Massif in Turkey. Here, granitic rocks with magmatic ages of *c.* 540 Ma prevail (e.g. Hetzel & Reischmann 1996; Loos & Reischmann 1999). It is therefore highly unlikely that the Menderes Massif forms the eastern continuation of the Pelagonian Zone and the Attico-Cycladic Massif, as was suggested by Dürr (1975). The geodynamic correlation of the different regions dominated by Permo-Carboniferous magmatism in the Eastern Mediterranean is a matter of ongoing discussion. With regard to the origin of gneiss PI23 from northern Pilion, for which a zircon age of 545 Ma was obtained, one could argue that it is somehow related to the Menderes Massif. If this were the case, it would have been tectonically emplaced onto the eastern Pelagonian Zone along the Vardar Zone. A second explanation is that this rock formed part of the basement on which the Pelagonian Permo-Carboniferous magmatic arc developed, as is the case for the Florina-Terrane in the NW

Pelagonian Zone (see Chapter 2). Apart from the Menderes Massif, latest Precambrian magmatism has also been recorded in the Istanbul Zone of NW Turkey (Chen *et al.* 2002), the Serbo-Macedonian Massif of northern Greece (Himmerkus *et al.* 2003) and the Kraište region of western Bulgaria, where Graf (2001) obtained magmatic ages of about 550 Ma for basement rocks. So far it is not possible to draw a clear correlation between orthogneiss Pl23 from northern Pilion and rocks from any of the above regions of Latest Precambrian basement exposures.

3.5 Conclusions

Permo-Carboniferous basement rocks occur throughout the entire Pelagonian Zone and form the predominant age group. Among the different crust-forming events in the western Internal Hellenides this episode of magmatism is by far the most important and is related to a continental magmatic-arc setting. Permo-Carboniferous magmatism occurred over a relatively large time span from *c.* 320 to *c.* 280 Ma. Commencement of magmatism does not vary systematically throughout the Pelagonian Zone. The assumption of systematic northward younging of arc magmatism could not be confirmed.

Inherited zircon components identified in orthogneisses from the eastern Pelagonian Zone (e.g. south of Veria and in Verdikoussa area), indicate the previous existence of Neoproterozoic basement in the region into which the Permo-Carboniferous magmas had intruded. Inheritance is a widespread feature of zircon populations in orthogneisses from the Pelagonian Zone and signifies the contribution of Precambrian basement to the source of the Palaeozoic and Mesozoic magmatic rocks.

Triassic magmatism was demonstrated both by a meta-rhyolite from the northwestern Pelagonian Zone as well as by mylonites from the eastern Pelagonian Zone. Triassic metamorphism appears to have affected the U-Pb system of zircons in several samples, resulting in sporadic Triassic ages of individual grains.

The Upper Jurassic/Lower Cretaceous age obtained for an orthogneiss in the area south of Veria is exceptional for the Pelagonian Zone. Tentatively, this orthogneiss is assigned an Almopias Zone origin (i.e. western part of the Vardar Zone).

Tertiary magmatism in the Pelagonian Zone is of minor significance.

In conclusion, the results of the present study clearly demonstrate that the major crust-forming events in the Pelagonian Zone are predominantly of pre-Alpine age.

3.Appendix: Analytical Methods

For geochronology sample weights were between 8 and 12 kg. The rocks were crushed and sieved to a grain size smaller than 500 µm using standard procedures, followed by mineral separation using a Wilfley table, a Frantz magnetic separator and heavy liquids. In a final step, the zircons were hand-picked under a binocular to avoid grains with visible inclusions.

Three different methods were used for zircon geochronology, namely the Pb-Pb evaporation method (Kober 1986, 1987), the conventional U-Pb method and SHRIMP (e.g. Compston *et al.* 1984; Compston 1999).

For zircon grains that were analysed using the Pb-Pb evaporation method, ages were calculated from the $^{207}Pb/^{206}Pb$ values after correction for common Pb using the values of Stacey & Kramers (1975). Sample ages were calculated as weighted averages, using Isoplot (Ludwig 2003).

The application of the single-zircon conventional U-Pb method is based on the low contamination method of Krogh (1973). Before dissolution, the zircons were washed in 7n HNO_3 and a mixed ^{205}Pb-^{235}U spike was added. The zircon grains were dissolved with HF in Teflon bombs at 200°C. Chemical separation of U and Pb with HBr chemistry followed, using 20µl columns with anion-exchange resin. Some zircon grains of sample V7 were analysed following the vapour digestion method of Wendt & Todt (1991) in which Pb and U are not chemically separated after dissolution but measured from the same Re filament. Pb and U were loaded on single Re filaments with silica gel. Thermal ionisation mass spectrometer (TIMS) measurements were performed on a Finnigan MAT 261 equipped with a secondary electron multiplier at the Max-Planck-Institut für Chemie, Mainz, Germany. After correction for fractionation, blank and common Pb (using the values of Stacey & Kramers 1975), ages were calculated using Isoplot (Ludwig 2003). Procedure blanks were < 40 pg Pb, the fractionation factor (3‰ per ΔAMU) was determined by repeated measurements of NBS 981 under the same conditions as the samples.

Three samples (Pl54, Pl16 and Ev4) were dated by sensitive high-resolution ion microprobe (SHRIMP) at the ANU, Canberra, Australia. For calibration of the Pb-U ratios the zircon standard FC1 (age 1099 Ma; Paces & Miller 1993) was used. U concentrations were calibrated using the SL13 zircon standard. Two samples (Pl37 and Pl40) were dated by SHRIMP at the Centre of Isotopic Research, St. Petersburg, Russia. The TEMORA reference zircon (age 416.75 Ma; Black *et al.* 2003) was used for calibration of the Pb-U ratios and zircon standard 91500 for U concentration calibration (Wiedenbeck *et al.* 1995). Data reduction and age calculations were based on SQUID (Ludwig 2001). Concordia diagrams were drawn with Isoplot (Ludwig 2003). All ages are given either at 2σ or 95% confidence level.

Chapter 4. Geochemistry of basement rocks from the Pelagonian Zone

The results of the geochemical analyses of the westernmost Internal Hellenide basement rocks are presented in this chapter. To avoid extensive cross-references between different chapters the rocks that were already described in previous chapters are also included. Although this chapter focuses on the Pelagonian Zone, the samples from the Vardar Zone will be shown for comparison.

Geochemical analyses on whole-rocks for major and trace elements were performed for all samples with XRF (Appendix A). Additionally selected samples were analysed for REE with LA-ICP-MS (Appendix B-1) and for Sr- and Nd-isotope composition analyses with TIMS (Appendix C). Details of the analytical procedures for LA-ICP-MS are given in Appendix B-2.

Sampling was carried out throughout the whole Pelagonian Zone, most samples, however, where taken in its the eastern part since in the western part the basement gneisses are largely covered by meta-sediments. Sample-regions from N to S are the Varnous pluton and the western Voras Massif in the north of the Pelagonian Zone close to the border with the Former Yugoslav Republic of Macedonia (F.Y.R.O.M.). More southward sampling areas were the area south of Veria and NE of Mt. Olympos in the east and the Kastoria region to Fotino and Deskati in the west of the Pelagonian Zone. Further samples were taken around Verdikoussa and Ambelakia village, Ossa Mts., Mt. Mavrovouni, Mt. Pilion, Skiathos Island, northern Evia Island and Skyros Island. The approximate sample localities are shown in Fig. 4.1, GPS coordinates are given in Appendix H. Additionally, some samples were taken in the Vardar Zone east of the Pelagonian Zone; most of these samples are already discussed in Chapter 1. For sample locations of the samples from the Vardar Zone see Chapter 1 Fig. 1.2 and Appendix H.

Sampling of basement rocks from the Pelagonian Zone focused on felsic (ortho-) gneisses and granites (Fig. 4.2). The basement rocks are variably deformed, ranging from relatively undeformed or only slightly deformed granites to augengneisses and to severely deformed mylonites. Especially for the highly deformed basement rocks an unambiguous distinction between ortho- and para-rocks is difficult. In this study, only rocks that could be identified as meta-sediments with some confidence in the field (samples V8, Pl39, Pl17, Pl52, Skop, and Sky4) are grouped together, while those of ambiguous origin, for the time being, are regarded as meta-igneous rocks. Besides the felsic basement rocks, some rocks of intermediate composition were additionally sampled, as were few samples of basaltic composition. Among the felsic samples are two (P6, Pl63) volcanic rocks. The mafic rocks will not be discussed but the results are given in Appendix A for completeness; they are also included in Figures 4.2 and 4.3. The meta-sedimentary rocks will be shortly described in paragraph 4.7.

4.1 Weathering and alteration

The climate in Greece and the conditions of outcrops made sampling of very fresh basement rocks difficult. Most samples show more or less signs of secondary alteration and weathering. This is evident by the alteration of feldspars and the mobility of alkalis and LIL elements such as Rb. Figure 4.3 shows the chemical index of alteration (CIA) after Nesbitt & Young (1982) for all sampled rocks, which is defined as the molecular ratio of $[Al_2O_3/(Al_2O_3+CaO+Na_2O+K_2O)]*100$. Values between 45 and 55 are in the range of fresh granite and granodiorite while values between 30 and 45 are typical for fresh basalt

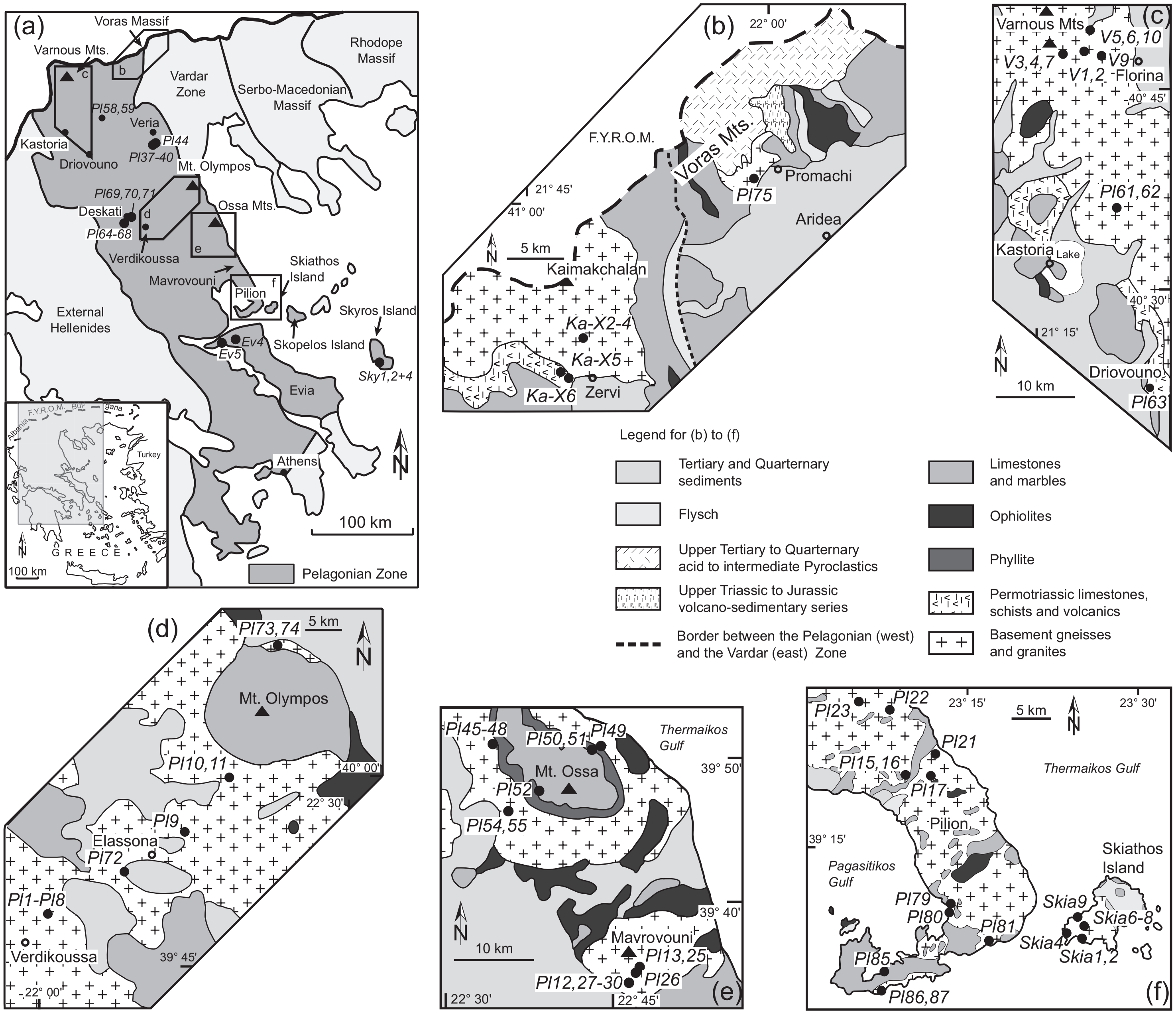

Fig. 4.1. Overview of the study area and the sample locations. (**a**) Map showing the structural zones of northern Greece, simplified after Kondopoulo (2000). The black polygons indicate the blow-ups (**b**) to (**f**). Sample numbers are shown in italics. (**b**) to (**f**) Geological maps for the main study areas. Simplified after the IGME Geological Map of Greece 1:500 000 (1983).

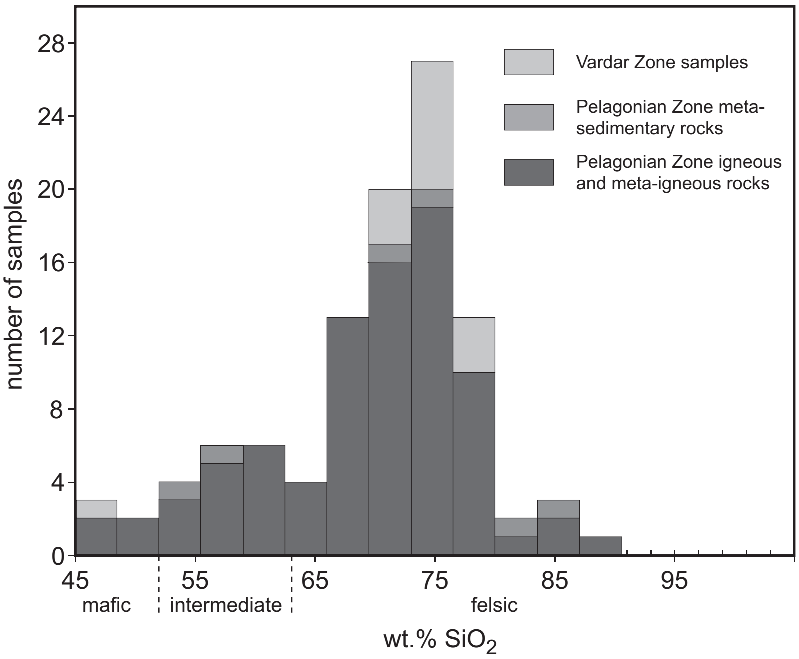

Fig. 4.2. Histogram underlining that mostly felsic basement rocks were sampled. Pelagonian Zone (PZ): mafic rocks (45-52 wt.% SiO_2) = 4, intermediate rocks (52-63 wt.% SiO_2) n = 15, felsic rocks (> 63 wt.% SiO_2) n = 65; sediments: mafic rocks n = 0, intermediate rocks n = 2, felsic rocks n = 4; Vardar Zone: mafic rocks n = 1, intermediate rocks n = 0, felsic rocks n = 13.

(Nesbitt & Young 1982). Higher values indicate influence of weathering or earlier secondary alteration (hydrothermal or metasomatic). CaO was left uncorrected for the Ca bound in apatite or carbonate because of the difficulty of quantification. This will result in slightly to low values for CIA but the negative deviation is estimated to be in most cases smaller than 1 (because carbonate is generally rare in the (meta-) igneous rocks and apatite occurs as an accessory mineral) and therefore does not affect the overall interpretation. The weathering trend can also be graphically illustrated by a molecular (CaO + Na_2O) - Al_2O_3 - K_2O diagram after Nesbitt & Young (1984, 1989, Fig. 4.4). The arrow indicates the typical weathering trend; it is predominantly caused by the decomposition of feldspar and leads to an enrichment in aluminium relative to the alkali elements and CaO. However, only relatively few samples show this trend, most rocks just scatter in their relative concentrations of K_2O vs. CaO + Na_2O at fairly similar Al_2O_3 concentrations, which might reflect the variation of the primary composition of Pelagonian Zone basement rocks. According to these diagrams most sampled basement rocks seem to be reasonably fresh rocks.

Besides weathering, deformation and metamorphism can change the chemical composition of a rock, especially during mylonitization, the effects of which are, however, difficult to recognize and quantify (e.g. Tobisch *et al.* 1991). Solution and removal of Si and the alkali elements are possible processes, although enrichment of Si along with removal of the alkali elements is also reported. This would mean that a change in chemical composition during metamorphism could lead to a decrease of alkali elements relative to aluminium, and therefore the effects of metasomatism should lead to increased CIA values just as weathering does.

The remainder of the discussion of the geochemical characteristic of Pelagonian Zone basement rocks in this chapter concentrates on those ortho-rocks, whose geochemistry is most likely to reflect that of the igneous protolith. Therefore, all samples with CIA values > 60 are not taken into consideration. Additionally left out are those with SiO_2 > 80 wt.% (PI68), one sample with an extremely high K_2O/Na_2O value of about 50 (PI34), and one sample (PI30) which geochemistry strongly differs from a typical

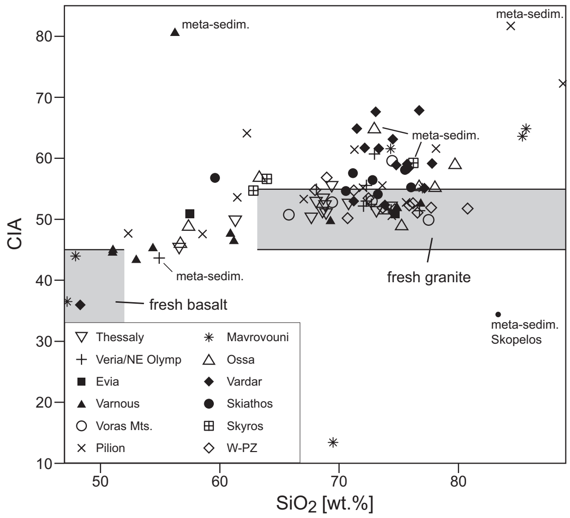

Fig. 4.3. Diagram showing the chemical index of alteration (CIA) after Nesbitt & Young (1982) plotted against SiO_2 content. Grey fields indicate the range of CIA for fresh basalt and fresh granite, respectively.

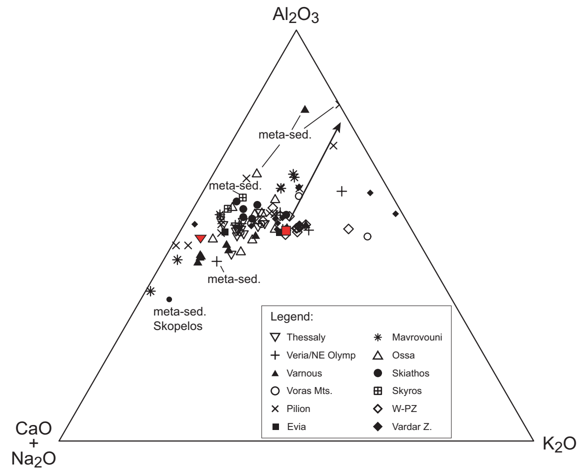

Fig. 4.4. Molecular ($CaO + Na_2O$) - Al_2O_3 - K_2O diagram of Nesbitt & Young (1984, 1989). The arrow indicates the typical weathering trend. Indicated in red are a typical fresh tonalite and a typical fresh granite.

granitoid (Al_2O_3 < 0.5 wt.%, Fe_2O_{3tot} *c.* 26 wt.% at SiO_2 69.5 wt.%). These restrictions have the additional advantage that most of the potentially para-rocks will not be considered either. However, in paragraph 4.5, in which the Sr- and Nd-isotope characteristics of the basement rocks are discussed, basement rocks with CIA > 60 are included in the discussion. For some of these rocks the Sr- and Nd-isotope compositions were also determined to see if the inferred alteration is also evident with regard to isotopes. Those for which REE analyses were performed are included in the respective paragraph. That the chosen restriction has its drawbacks is evident from the samples Sky1 and Sky2 from Skyros Island, which, according to the CIA, belong to the reasonably fresh rocks while in the field the rocks were so so disintegrated that the expression "hard rock" is somewhat misleading. Nevertheless, in the absence of a perfect classification scheme the chosen one seems reasonably well working and is therefore used, keeping its drawbacks in mind.

4.2 Major elements

Harker diagrams for the orthogneisses and granitoids from the Pelagonian Zone and the Vardar Zone (Fig. 4.5) show relatively smooth negative trends for most elements, such as TiO_2, Al_2O_3, MgO, Fe_2O_{3tot}, and CaO. For Na_2O a negative trend can be anticipated, but generally, like for K_2O, the samples scatter widely. A distinction of samples from different areas of the Pelagonian Zone or the Vardar Zone is not possible on the basis of those major elements vs. SiO_2 plots. The overall geochemical composition of the granitoids is similar in all areas of the Pelagonian Zone. Both samples from Skyros Island show slightly higher Al_2O_3 concentrations, which might be an effect of the alteration seen in the field, although a CIA value of about 57 and 55, respectively, indicates relatively fresh granites. Regarding the different age groups there are also no striking geochemical differences. All Neoproterozoic rocks belong to the basement rocks with the highest SiO_2 contents (generally > 70 wt.%) and they ap-

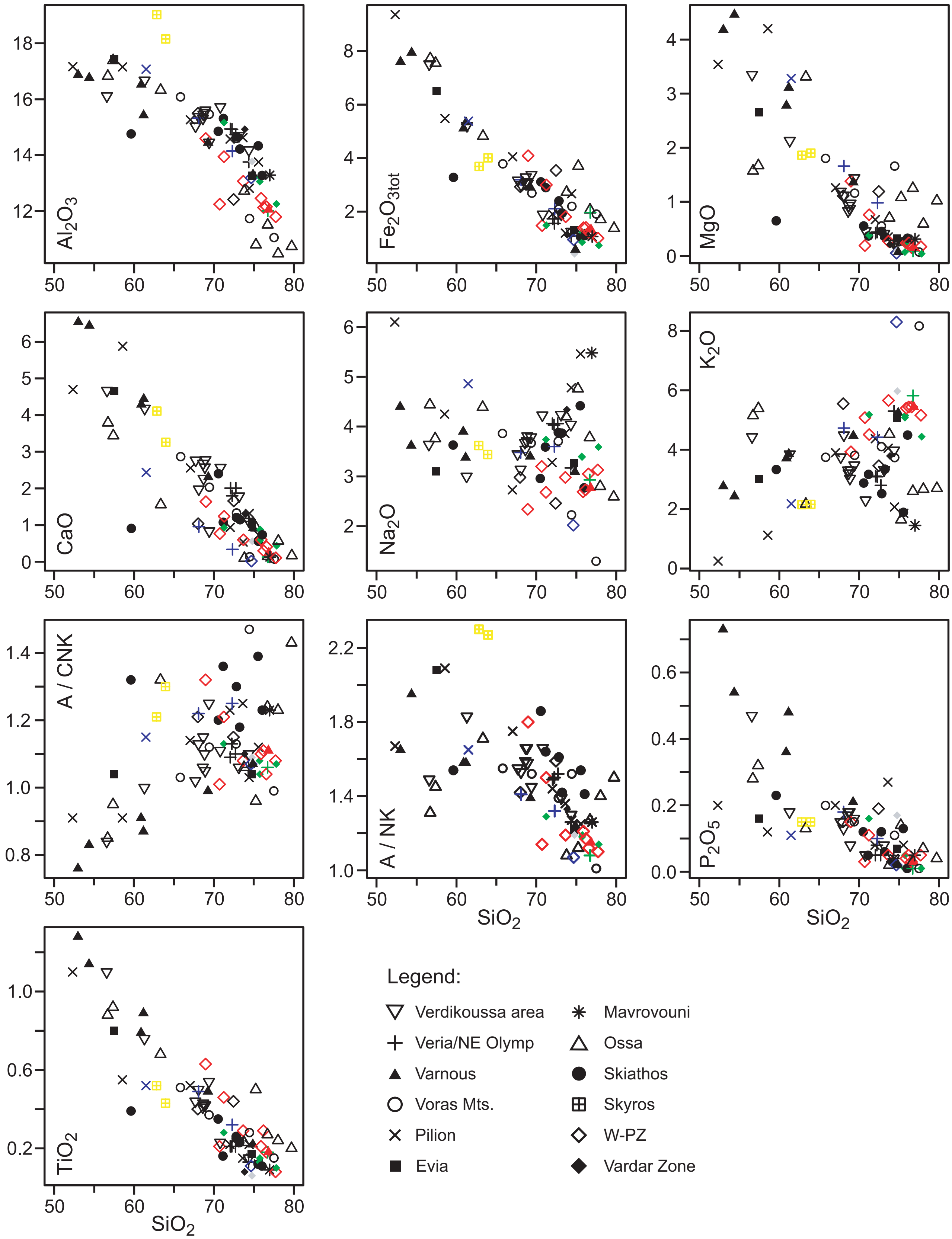

Fig. 4.5. Harker variation diagram of major element vs. SiO_2 for basement rocks from the Pelagonian Zone and the Vardar Zone. Elements are given as wt.%. Colours indicate the different age groups: Neoproterozoic = red; Permo-Carboniferous = black; Triassic = blue; Jurassic = green; Tertiary = yellow. For those samples that were not dated an intrusion age was assumed for this classification. Sample PLT-1, which belongs to the pre-Mesozoic basement of the Vardar Zone, is shown in grey.

pear to have slightly higher K_2O and lower Na_2O concentrations than the Permo-Carboniferous basement rocks.

A closer look can be taken at the Varnous pluton, which is the largest plutonic body in the Pelagonian Zone and occurs in its northwestern part, west of Florina town. Besides a suite of igneous rocks (V1-7, V10), two samples were taken from the surrounding basement into which the pluton intruded (orthogneiss V9 and paragneiss V8). One of the granites from the pluton (V1) and one of the samples from the surrounding basement (V9) were already described in Chapter 2. For completeness, however, they are again included in the following discussion. The igneous rocks are relatively undeformed and show only slight deformation. The SiO_2 content of the plutonic samples varies from *c.* 51 to *c.* 75 wt.%.

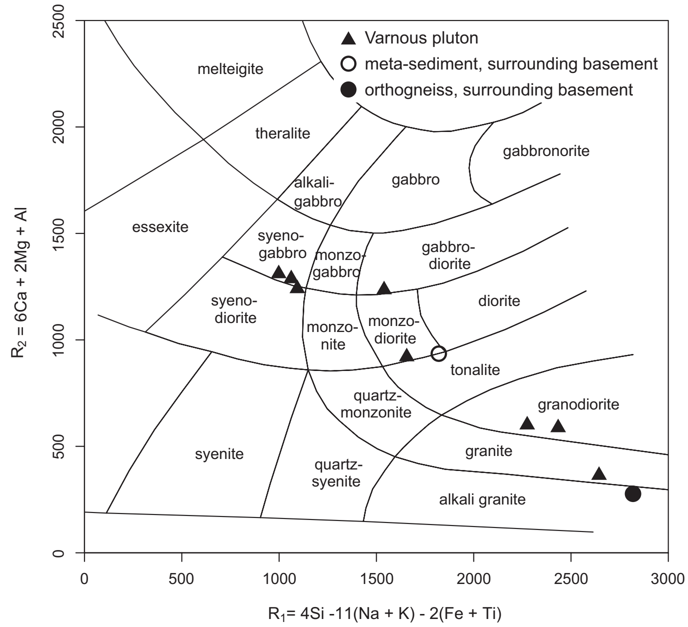

Fig. 4.6. R1-R2 classification after De la Roche *et al.* (1980) for the Varnous plutonic suite. Two analyses of rocks of the basement into which the Varnous pluton has intruded are also shown.

In a R1-R2 classification diagram (De la Roche *et al.* 1980) the rocks range from syeno-gabbro to monzo-diorite, granodiorite and granite (Fig. 4.6). The paragneiss (V8) from the surrounding basement has a granodioritic composition while the orthogneiss (V9) is classified as alkali granite. Mafic to intermediate rocks can occur as enclaves in the felsic rocks. Monzogabbro V2 is taken from an enclave in the tonalitic granite from which sample V1 was sampled. Increasing SiO_2 contents in the plutonic samples correlate with decreasing contents of Al_2O_3, CaO, Na_2O, P_2O_5 and MgO as well as with increasing K_2O contents and fit well with literature data from the Varnous pluton as well as the Baba pluton, which is suggested to be the northern continuation of the Varnous pluton into F.Y.R.O.M. (Katerinopoulos & Kyriakopoulos 1989; Katerinopoulos *et al.* 1992) (Fig. 4.7). The high P_2O_5 concentration corresponds to the abundance of apatite seen in the thin sections. The mylonitic gneiss V8 from the surrounding basement does not fit in the trends defined by the major element vs. SiO_2 Harker diagrams. Therefore this rock clearly does not belong to the pluton suite of magmatites. Its extremely high ASI of > 4 and the high Al_2O_3 concentration supports its classification as a meta-sediment. The literature data for several rocks, especially from the Baba Mts., show scatter of the alkali elements Na_2O and K_2O. For the evolved samples with high SiO_2 concentrations this might indeed indicate same geochemical differ-

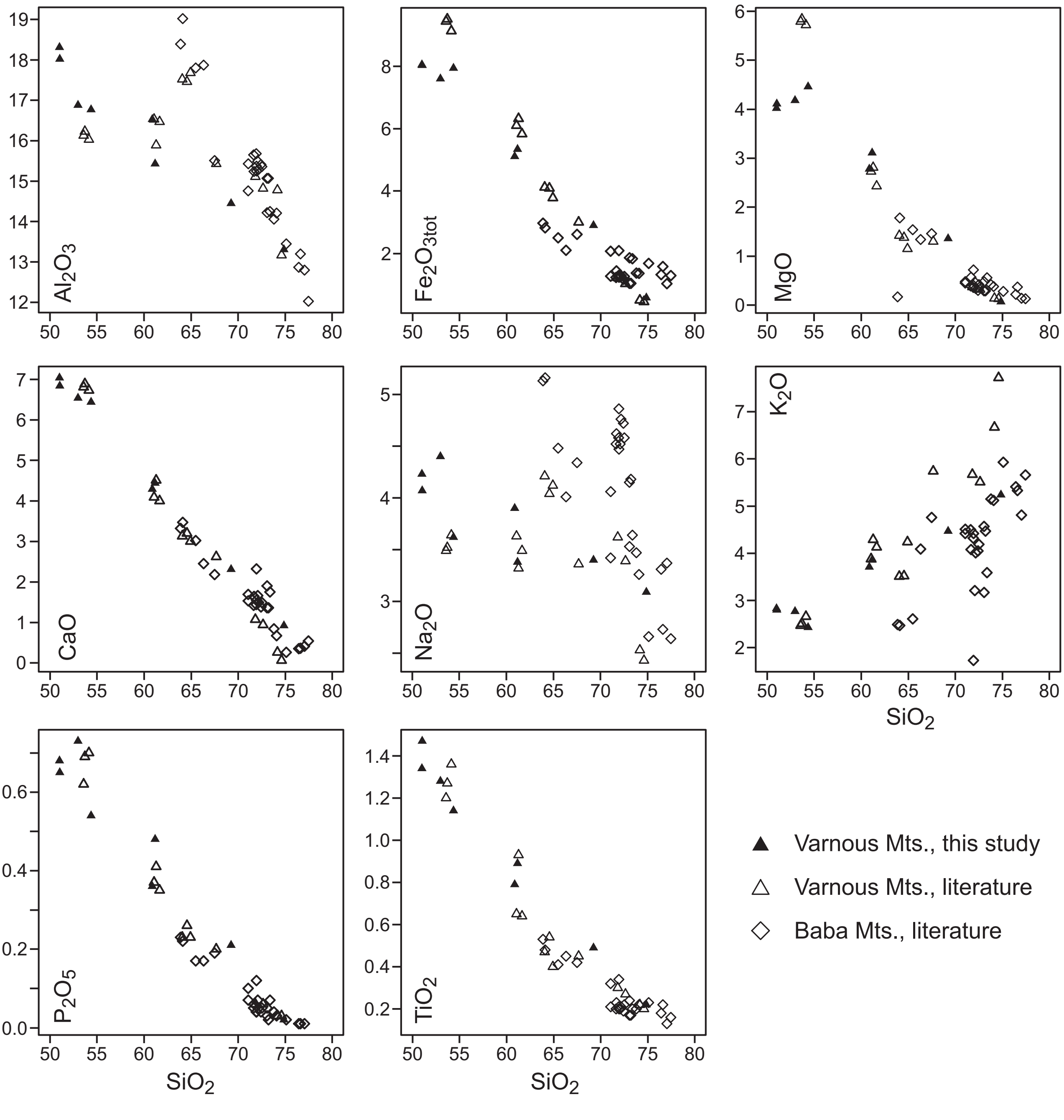

Fig. 4.7. Major element vs. SiO_2 Harker diagrams for the Varnous plutonic suite. Elements are given as wt.%. Additionally plotted are data from the Varnous pluton and the plutonic rocks from the Baba Mts. (southern F.Y.R.O.M.) of Katerinopoulos & Kyriakopoulos (1989) and Katerinopoulos *et al.* (1992).

ence between the Varnous and the Baba Mts. rocks. Several rocks from the Baba Mts. have additionally high Al_2O_3 concentrations at intermediate SiO_2 and therefore might be affected by alteration.

In an attempt to classify the granitoid basement rocks from the Pelagonian Zone and the Vardar Zone and to possibly identify distinct groups not distinguishable from the Harker diagrams, the granite classification scheme of Frost *et al.* (2001) was applied. Frost *et al.* (2001) developed this classification scheme for granitoids with the aim that it should be based on easily accessible and precisely determinable parameters, accommodate the wide range of possible geochemical compositions of granites, that it is unaffected by chemical parameters that do not unambiguously reflect the original melt composition, and is independent of assumptions concerning the tectonic environment. They therefore used major element geochemistry and classified the granitoids according to the Fe- (or Fe*-) number (FeO_{tot}/(FeO_{tot} + MgO) as an indication for the differentiation history), the modified alkali-lime index (Na_2O + K_2O - CaO, which is related to the magma source), and the aluminium-saturation index (ASI) (which allows inferences of the magma sources and the conditions of melting). Applying this granite classification scheme of Frost *et al.* (2001) to the basement rocks from the westernmost Internal Hellenides, the majority of the samples can be classified as magnesian in the FeO_{tot}/(FeO_{tot} + MgO) vs. SiO_2 diagram (Fig. 4.8a), calc-alkalic to alkali-calcic in a MALI (modified alkali index) vs. SiO_2 diagram (Fig. 4.8b) and peraluminous (Fig. 4.8c and d). According to Frost *et al.* (2001), Cordilleran-type granitoids tend to be calcic to calc-alkalic while Caledonian-type granitoids fall largely into the alkali-calcic field. The peraluminous, ferroan granitoids with a high SiO_2 content belong to the S-type rocks of a Cordilleran-type suite or the collisional granitoids, and contain large contributions of continental crust. The basement rocks from the Pelagonain Zone and Vardar Zone are therefore similar to granitoids formed in a subduction-related volcanic arc or collisional setting. The ferroan and alkalic granitoids have similarities to within-plate granites (Frost *et al.* 2001). Three of the Pelagonian Zone basement rocks fall into this group but as two of these rocks belong to the highly deformed Ambelakia Unit, which has experienced blueschist metamorphism, it is doubtful if these rocks really form a distinct group different from the bulk of the Pelagonian Zone basement rocks.

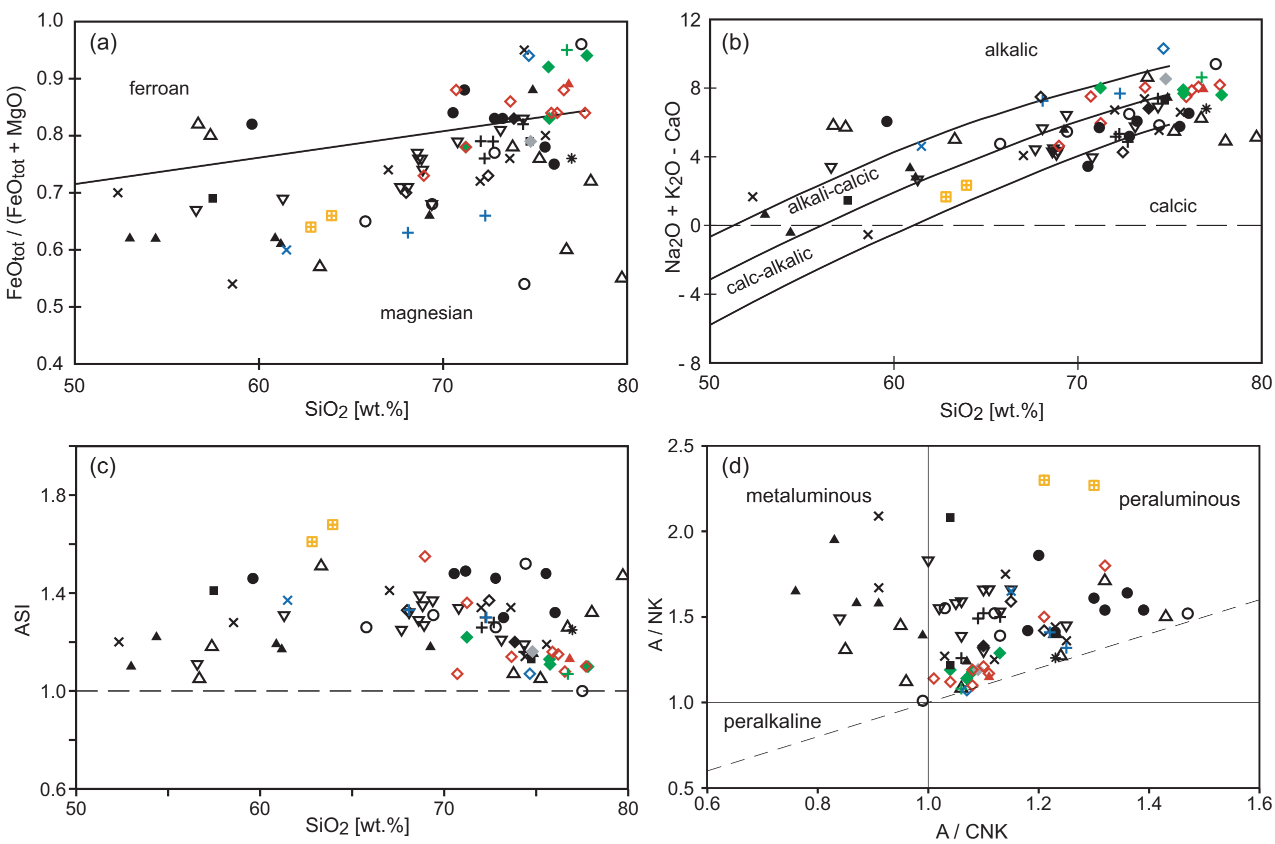

Fig. 4.8. Classification diagrams for granites using major elements (after Frost *et al.* 2001). It shows that most basement rocks can be characterised as magnesian-type (a), calcic to alkali-calcic (b) and peraluminous (c). (d) Classification after Shand (1951). For legend see Fig. 4.5.

4.3 Trace and rare earth elements

Trace element vs. SiO_2 Harker diagrams display only weak trends (Fig. 4.9), with the exception of V and Ga and perhaps Sr and Zr, and again do not allow clear distinctions to be made between rocks from different regions of the Pelagonian Zone. The Jurassic Fanos granite samples from the Vardar Zone together with the Triassic meta-rhyolite from the NW Pelagonian Zone and intermediate granitoids from the Varnous pluton differ from the bulk of the basement rocks by higher Nb concentrations. The Neoproterozoic rocks display relatively high Rb and Y concentrations and belong to the rocks with high Rb/Sr values. The samples from the Varnous pluton correspond again with the data from the literature for the Varnous and the Baba pluton (Katerinopoulos & Kyriakopoulos 1989; Katerinopoulos *et al*. 1992), (Fig. 4.10). Negative trends for Sr, Ba, Ni, V, Sc, and Zr and a positive trend for Rb can be seen, while Nb and Y scatter more widely. The relatively high V concentrations might be explained with the abundant occurrence of titanite in these rocks, a mineral that can incorporate vanadium.

In the Nb-Y discrimination diagram for geodynamic environments (Pearce *et al.* 1984) most samples fall inside the volcanic-arc granite (VAG) / syn-collisional granite (syn-COLG) field (Fig. 4.11). Applying the Rb-(Y+Nb) diagram after Pearce *et al*. (1984), these samples are classified as VAG. The majority of the VAG rocks plot in the upper right corner of the VAG field, which is typical for granitoids that formed in a continental margin, continental arc or mature volcanic arc environment (Förster *et al*. 1997). A minority of the basement rocks from the Pelagonian Zone falls inside the WPG field (Pl43, Pl63, Pl55, Pl65, Pl67, Pl72, V1, V2, V7) in either one or both of the diagrams. For the Triassic meta-rhyolite Pl63 this could in fact indicate a within-plate origin because the Triassic rocks of the Pelagonian Zone have previously been interpreted to have originated in an extensional regime (e.g. Mountrakis *et al*. 1987; Pe-Piper 1998), although subduction-related formation in a back-arc environment was also considered (Pe-Piper 1982). For the Permo-Carboniferous and the Neoproterozoic samples it might suggest a late to post-collisional origin, as these diagrams cannot discriminate late or post-collisional granites, which might fall well within any of the syn-COLG, VAG or WPG field (Pearce *et al.* 1984). Evolved rocks from continental margins or rocks formed during the waning stages of continental arc magmatism can occasionally fall in the WPG field (Förster *et al*. 1997) as can differentiation cause arc-granites to plot in the WPG field (Pearce *et al*. 1984; Förster *et al*. 1997). The Varnous samples V2 and V7 have SiO_2 contents < 56 wt.% and therefore do not strictly belong to the range of rocks considered in the discrimination diagrams. While for all of the Neoproterozoic and Permo-Carboniferous rocks an origin in a continental environment, at an active continental margin or during arc-continent collision seems plausible, the geotectonic origin of the Upper Jurassic samples Pl43 and Pl44 remains unknown. Because they might have been derived from the Vardar Zone, a “true” WPG origin cannot be ruled out as can their formation in an arc- or collision-related environment.

Additionally to the samples already described in previous chapters twenty-one samples were analysed for REE using LA-ICP-MS, so that coverage of basement rocks from a wide area of the Pelagonian Zone was achieved. The REE pattern normalised to chondrite is that of typical continental crust (Fig. 4.12). The majority of the samples show enrichment of the light REE and a flat pattern for the heavy REE as well as a negative Eu-anomaly. Therefore, fractionation of plagiclase played a significant role in magma genesis. For those basement rocks for which a strong contribution of older crustal rocks to the magma source is indicated the negative Eu-anomaly can be at least partly inherited. Almost no nega-

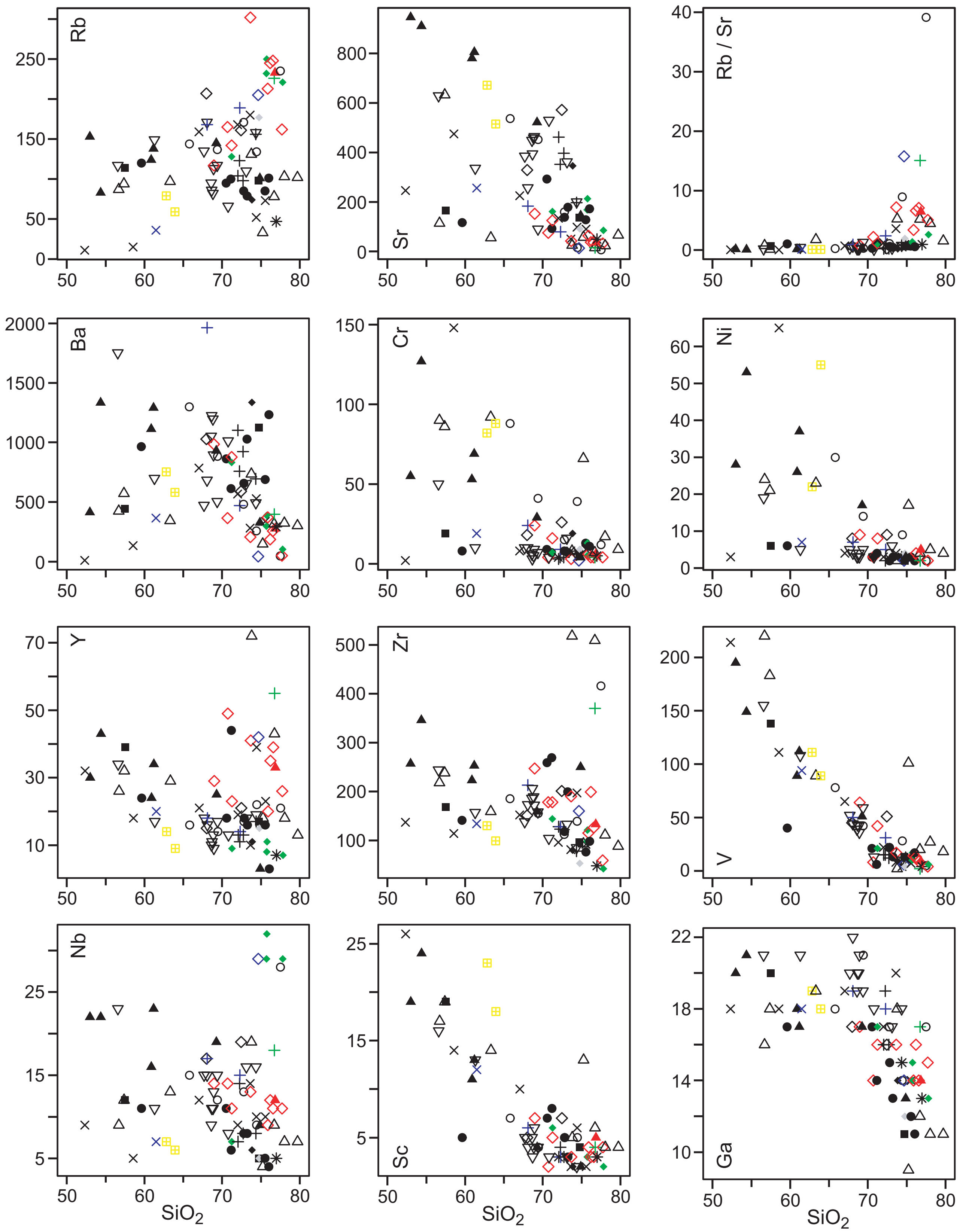

Fig. 4.9. Trace element vs. SiO_2 Harker variation diagrams of basement rocks from the Pelagonian Zone and the Vardar Zone. SiO_2 is given as wt.% and trace elements as ppm. For legend see Fig. 4.5.

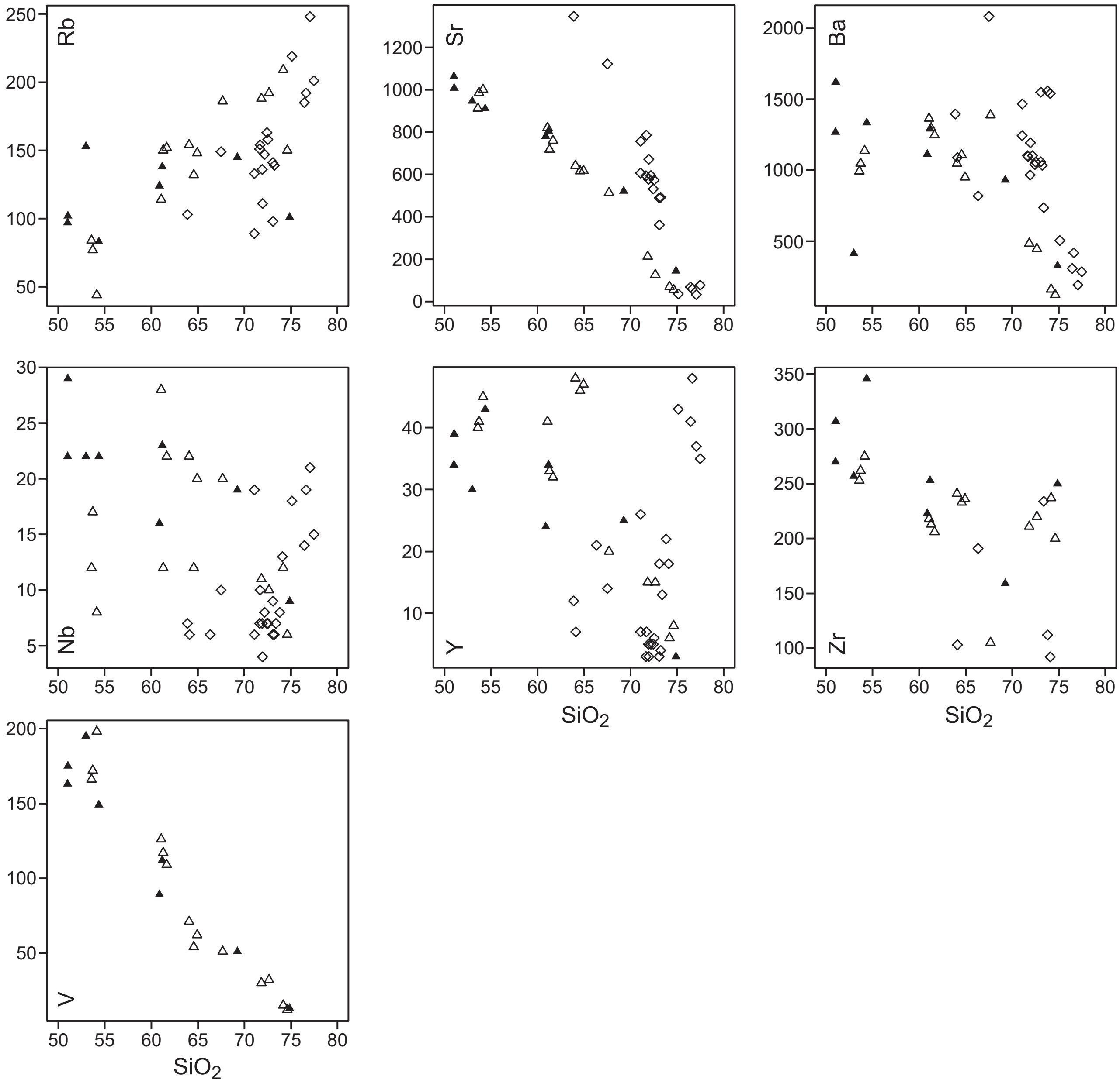

Fig. 4.10. Trace element vs. SiO_2 Harker variation diagrams for the Varnous plutonic suite and the Baba Mts. (Katerinopoulos & Kyriakopoulos 1989; Katerinopoulos *et al.* 1992). SiO_2 is given as wt.% and trace elements as ppm. For legend see Fig. 4.7.

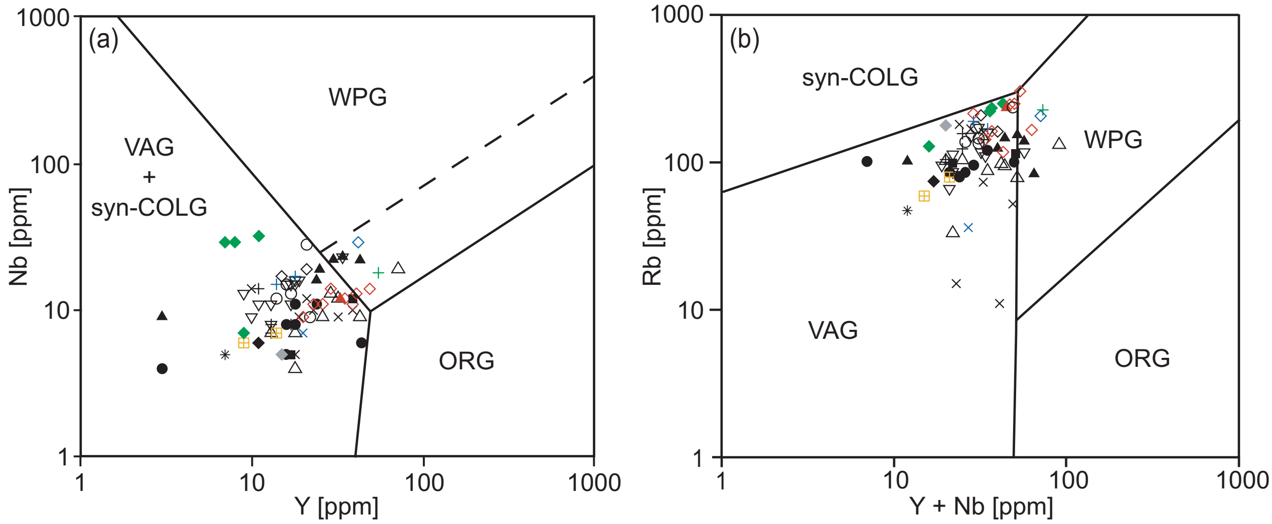

Fig. 4.11. Discrimination diagrams for the geotectonic environment after Pearce *et al.* (1984). VAG: volcanic-arc granite; syn-COLG: syn-collisional granite; WPG: within-plate granite; ORG: ocean-ridge granite. For legend see Fig. 4.5.

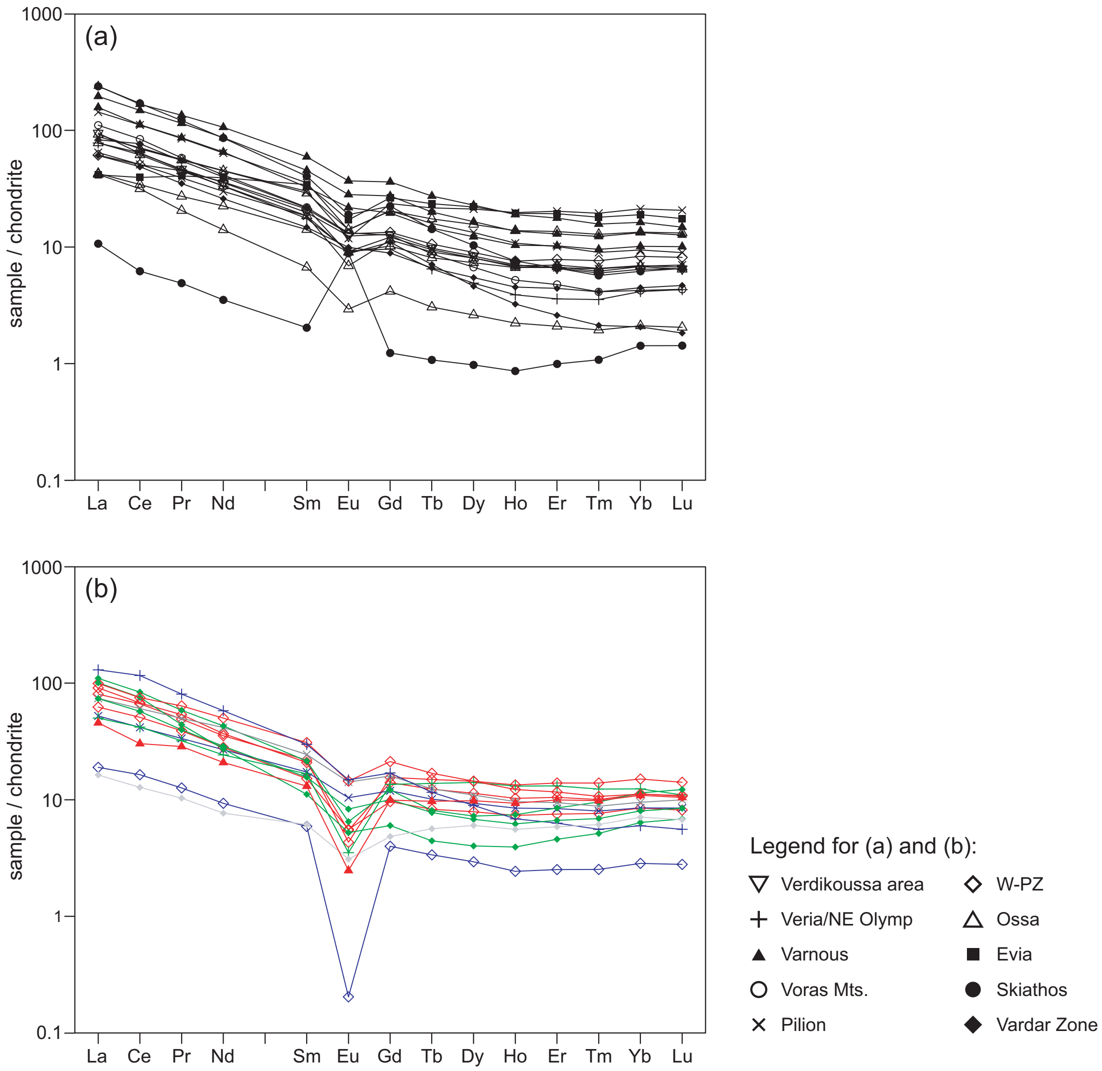

Fig. 4.12. RE element pattern for basement rocks from the Pelagonian Zone and the Vardar Zone, normalised to chondrite (values from Boynton 1984). The REE were analysed by LA-ICP-MS. (a) Permo-Carboniferous rocks. (b) Other age groups. Colours indicate the different age groups: Neoproterozoic = red; Permo-Carboniferous = black; Triassic = blue; Jurassic = green. For those samples that were not dated, an intrusion age was assumed for this classification. Sample PLT-1, which belongs to the pre-Mesozoic basement of the Vardar Zone, is shown in light grey. Sample Pl23 from northern Pilion, for which a Late Neoproterozoic / Early Cambrian age is indicated, is shown in dark grey.

tive Eu-anomaly or only a very small one is found for the Permo-Carboniferous samples from the northern Pelagonian Zone (Fig. 4.12), e.g. the samples from the Varnous pluton and the two samples from the western Voras Massif (Ka-X5, Pl75). This is an indication that fractionation of plagioclase did not play an important role in the genesis of these rocks. The Permo-Carboniferous samples taken from Ossa Mts., Pilion and Skiathos Island (except Skia8) display a more pronounced negative Eu-anomaly. The largest negative Eu-anomalies are found in the Triassic rhyolite Pl63 and the Late Jurassic/Early Cretaceous granite Pl43 and to some extent in the Neoproterozoic basement rocks from the NW Pelagonian Zone (see Chapter 2). Different from the bulk of the samples is the pattern of sample Skia8, which displays a strong positive Eu-anomaly. This seems to suggest its formation as a cumulate. Ev4 shows only a flat pattern for both the light and the heavy REE. It can be stated that samples Skia8 and Pl63, and to some extent sample Pl51, have lower total REE concentrations than the rest of the samples.

Trace element pattern in so-called spider-diagrams are typical for continental crust. They show characteristic negative anomalies of Nb and Ti for all rocks from the Pelagonian Zone and the Vardar Zone (Fig. 4.13). These anomalies suggest that a subduction-related environment played a role in the evolutionary history of the basement rocks, because magmas formed in subduction zones display negative Nb and Ti (or HFS elements in general) anomalies probably caused by residual rutile or amphibole in the restite. Other prominent anomalies visible in the spider-diagrams are negative Sr or P anomalies, indicating that fractionation of plagioclase or apatite, respectively, played a role during rock formation. Mostly the negative Sr anomalies seem to parallel the negative Eu anomaly seen in the REE pattern, supporting the notion that plagioclase fractionation was an important process, although this statement is hampered by the fact that REE analyses are not available for all rocks. Assimilation or anatexis and incorporation of older crustal material is another possible process that can lead to anomalies in spider-diagrams. If a rock with pronounced anomalies is molten, the pattern can be inherited by the newly formed rock obscuring the effects of other processes. Especially in the basement rocks that show a strong S-type characteristic parts of the pattern might be inherited. Meta-rhyolite Pl63 from the north-western part of the Pelagonian Zone might be an example for a rock with an inherited pattern. Like the other Pelagonian Zone basement rocks it displays the negative Nb anomalie and therefore an subduction-environment origin is indicated. Geochronology, however, yielded a Triassic age for this rock and from several regional studies it is suggest that during the Triassic an extensional regime prevailed with beginning of rifting that later led to formation of ocean basins. Therefore this rock might have inherited the subduction-zone characteristic from one of its sources. Comparison of the different age groups (for those rocks that were not dated an age was assumed) shows that generally the Neoproterozoic rocks display the most pronounced negative Sr anomaly, although some of the Permo-Carboniferous rocks especially from the Mt. Ossa region also show strong negative Sr anomalies.

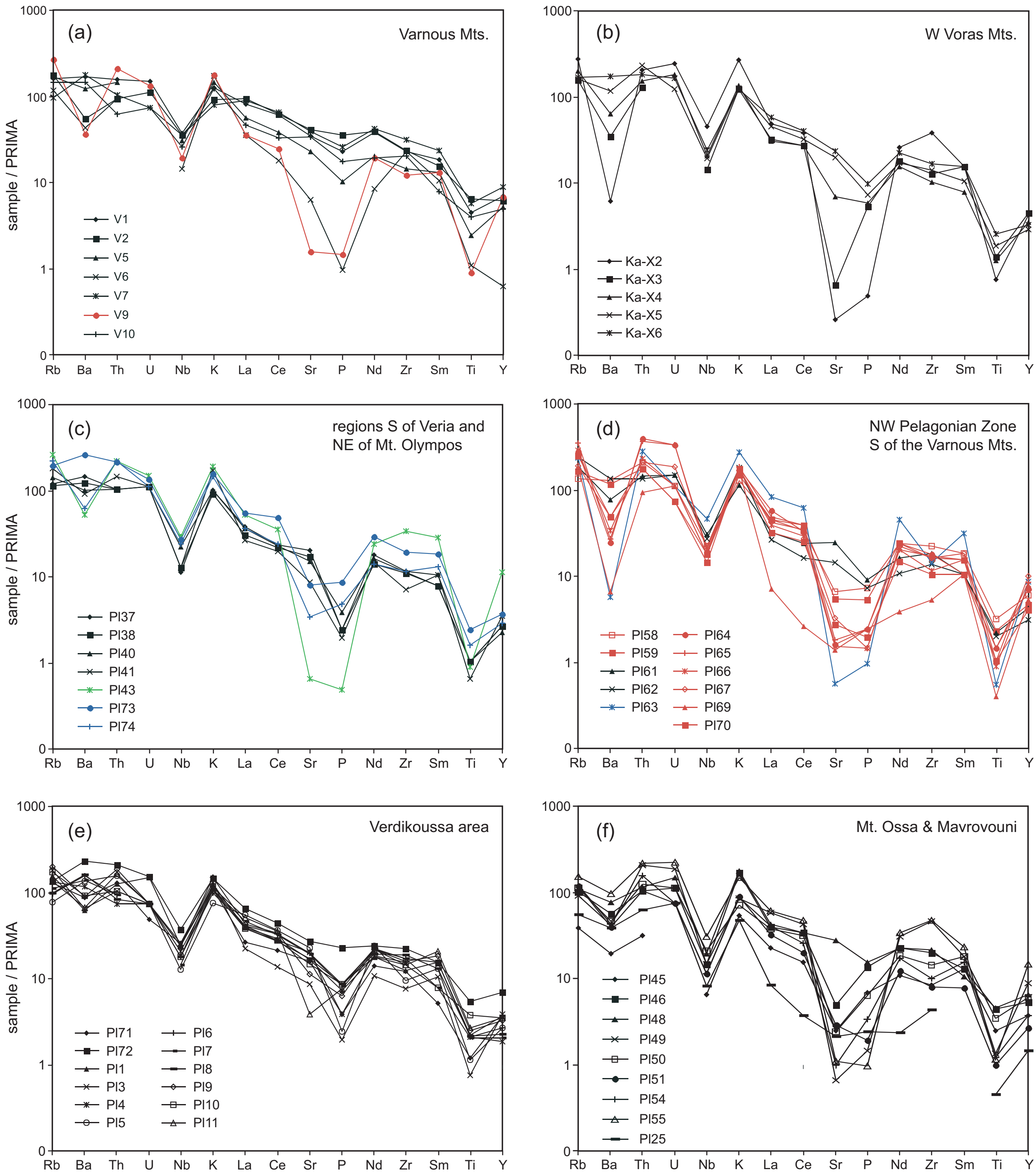

Fig. 4.13. Spider-diagrams, rocks are grouped by region. All elements were analysed by XRF and are normalised to primitive mantle (PRIMA) using the values of Wood *et al.* (1979, 1981). The order of the elements follows approximately increasing compatible behaviour during melting of the mantle (from left to right) (Rollinson 1993). Colours are according to age group (dated or assumed intrusion age): Neoproterozoic = red; Permo-Carboniferous = black; Triassic = blue; Jurassic = green; Tertiary = yellow. Sample PLT-1, which belongs to the pre-Mesozoic basement of the Vardar Zone, is shown in grey.

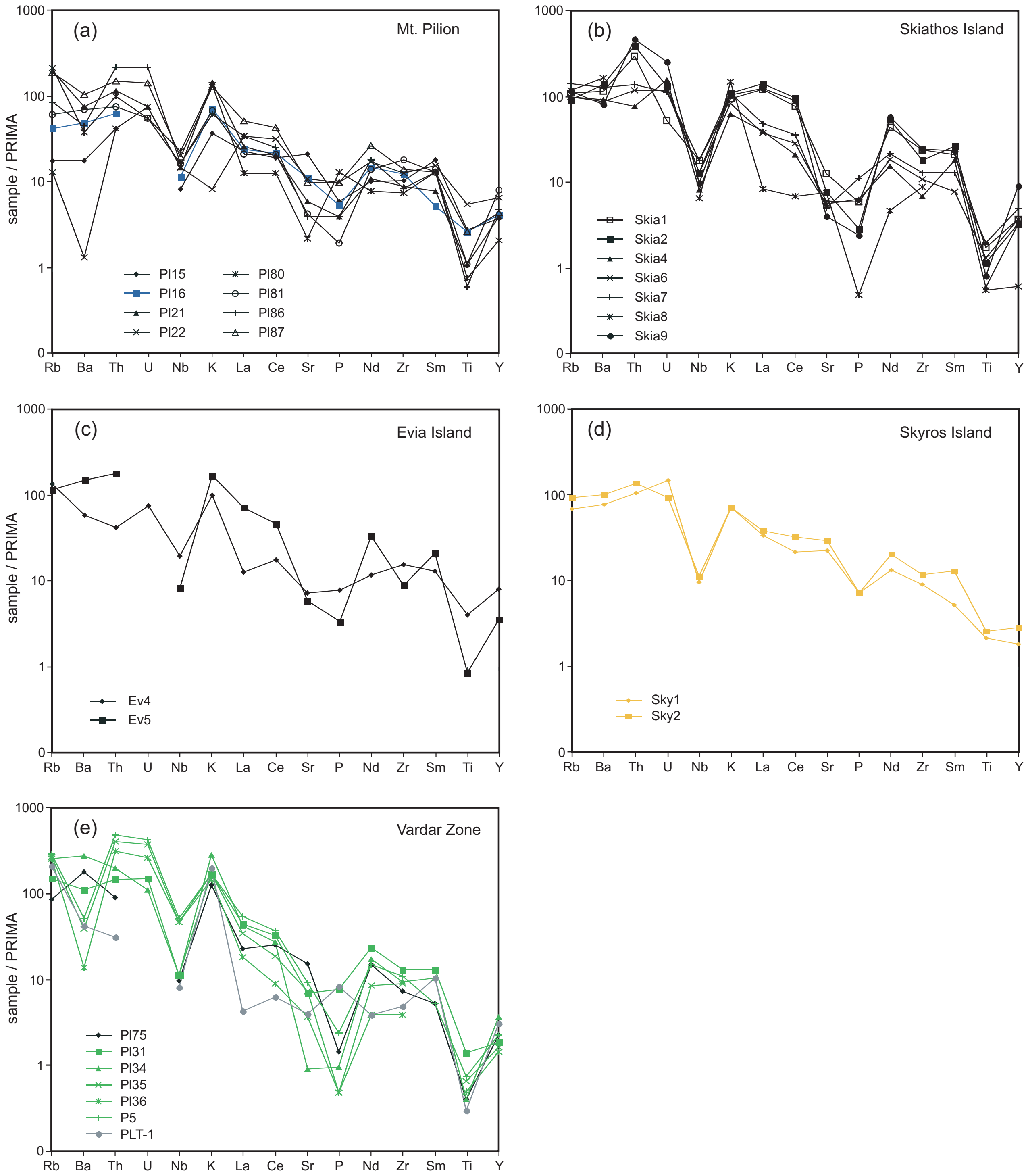

Fig. 4.13. *continued*

4.4 Sr- and Nd-isotopes

Additional to the isotope analyses for samples from the Vardar Zone and the northwestern and western Pelagonian Zone, which were already discussed in Chapters 1 and 2, Sr- and Nd-isotope composition analyses were performed for 25 samples, mainly from the eastern Pelagonian Zone.

Most of these samples were dated in the course of this study (see previous chapters). The intrusion age for sample Pl10 of *c.* 283 ± 7 Ma is taken from Reischmann *et al.* (2001). Because Pl43 was sampled from the same outcrop as sample Pl44 an identical intrusion age is assumed. For the remaining samples (Pl45, Pl51, Pl81 and Pl86) an intrusion age of 300 Ma was assumed. Still an open question is whether the zircon age of *c.* 545 Ma for sample Pl23 is the age of the magmatic event that formed the rock or the inherited age of one of the contributing source rocks. Therefore initial ratios were calculated for both the Cambrian age and a possible "magmatic" age of 300 Ma. To allow comparison of Nd isotope results that were measured on different days, all $^{143}Nd/^{144}Nd$ values were corrected to an average measured $^{143}Nd/^{144}Nd$ value for La Jolla of 0.511823. An exception are those samples of the Vardar Zone that were already described in Chapter 1. For those samples a correction will not result in relevant changes, i.e. they would be undetectable in the used diagrams, and for reason of consistency with the submitted manuscript they are left uncorrected.

Epsilon Nd_i ratios of Pelagonian Zone basement rocks range from -8.2 to -1.1 (if an intrusion age of 300 Ma is assumed for Pl23) or even to +1.4 in the case that a Cambrian intrusion age is accepted for Pl23. The variation in εNd_i is rather continuous so that no groups can be identified regarding either region or age (Fig. 4.14a). It nevertheless shows clearly the crustal character of the basement rocks from the Pelagonian Zone and indicates a varying but distinct contribution of older crustal rocks to the source from which the Pelagonian Zone basement formed (Fig. 4.14b). The Nd depleted mantle model ages (T_{DM}) support this picture (Fig. 4.14c and d). T_{DM} for basement rocks from the Pelagonian Zone range mainly from 1.0 to 1.6 Ga, only sample Ev4 gives a much older T_{DM} of 2.5 Ga. The youngest T_{DM} values are obtained for the samples from the Varnous pluton (V1, V7, V10). This supports the suggestion already made in Chapter 2 (on the basis of V1) that Permo-Carboniferous magmatism in this region can be characterised as predominantly I-type magmatism; only small amounts of older crustal rocks contributed to magma genesis. Even younger T_{DM} were obtained for Jurassic basement rocks from the Vardar Zone (Chapter 1). Beside the samples from the Varnous pluton and the Jurassic rocks from the Vardar Zone no grouping of T_{DM} values either with regard to region or age of the basement rock is possible. Relatively young T_{DM} values of 1.0 to 1.2 Ga can be found both in the northern and central Pelagonian Zone (e.g. Varnous pluton, Ka-X5 from the western Voras Massif, sample Pl73 NE of Mt. Olympos) and in the southern parts of the Pelagonian Zone, like sample Pl23 from northern Pilion and Skia1 from Skiathos island. The range of T_{DM} for the Permo-Carboniferous basement rocks is similar to those of 1.4-1.7 Ga obtained for middle European Variscan basement rocks (Liew & Hofmann 1988).

Sr-isotope analyses give similar results. A group of samples have $^{87}Sr/^{86}Sr_i$ values between 0.705 and 0.706, which indicates a dominance of a mantle source and only lesser amounts of older crustal rocks in the source of the magma. To this group belong the samples from the Varnous pluton, confirming the I-type characteristic already inferred from their Nd isotopic ratios. A second large group displays $^{87}Sr/^{86}Sr_i$ values between 0.708 and 0.709. This indicates the incorporation of either larger amounts of

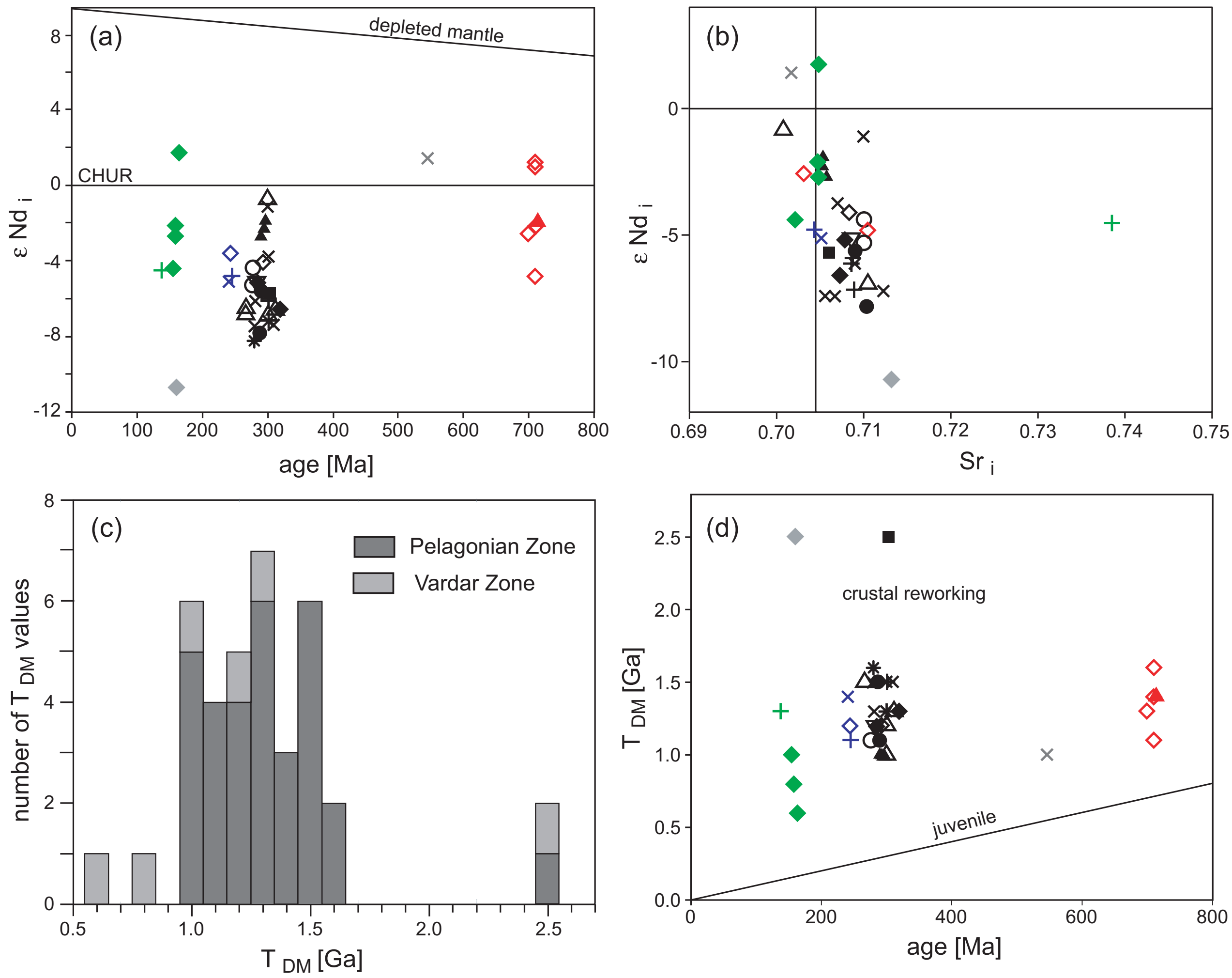

Fig. 4.14. Different diagrams showing the results of Sr- and Nd-isotope analyses. The basement rocks show variable influence of the contribution of older continental crust in magma genesis. (**c**) The Jurassic rocks from the Vardar Zone show the youngest model ages while The Permo-Carboniferous rocks show model ages similar to Pelagonian Zone rocks. The cordierite granite PLT-1 from the eastern Vardar Zone has the highest model age (see also Chapter 1). For legend see Fig. 4.5. Duplicates are included in (**a**) and (**b**) but not in (**c**) and (**d**).

pre-existing crust or older crust in the magma genesis. Several samples show a strong S-type characteristic with $^{87}Sr/^{86}Sr_i$ values above 0.710. Again these groups do not coincide with groups based on region or intrusion age. Generally, the results of the Sr-isotope analyses have to be taken with care because the Rb-Sr system, unlike the Sm-Nd system, is more readily affected by secondary alteration and weathering. Additionally, several samples show extreme Rb/Sr ratios, this means that either Rb or Sr occurs in concentrations smaller than 30 ppm. The unrealistic low $^{87}Sr/^{86}Sr_i$ values < 0.700 obtained for several samples are probably caused by alteration. Taking a look at those samples that were excluded from the discussion because of their high CIA it shows that there is no strong correlation. Samples with CIA > 60 are among the samples with the anomalously low $^{87}Sr/^{86}Sr_i$ values as are several samples with CIA < 60. Even more, some samples belonging to the group with CIA > 60 yielded $^{87}Sr/^{86}Sr_i$ values that seem to be undisturbed. The extremely high $^{87}Sr/^{86}Sr_i$ value of 0.738 for sample Pl43 cannot be explained so far. Possible explanations include alteration, an erroneous assumption for the intrusion age or the derivation from an extremely crustal source.

4.5 Comparison of the Permo-Carboniferous basement rocks from the Pelagonian Zone with Variscan granitoids from the Alps, the Carpathians and the Moldanubian Zone

Figure 4.15a shows the Variscan basement rocks from the Pelagonian Zone (data from both this study and the literature) in a Na_2O vs. K_2O diagram. Fields for special granitoid-types are indicated (drawn after Finger & Steyrer 1990); the Californian batholith is an example for a magmatic suite along an active continental margin, while the Lachlan Fold Belt of southwestern Australia is the locality were Chapell & White (1974, 2001) defined I- and S-type granitoids and the Himalayan granites are those of a typical collision orogen. The majority of the samples is similar to Lachlan or Californian I-type granitoids, only few samples plot inside the S-type granite field. Similarly few samples fall inside the “Moldanubian S-type granitoids” or the “Himalayan collision granites” field. The Pelagonian Zone basement rocks are compared with Variscan basement rocks from SE Europe, namely the Alps, the Carpathians and the Moldanubian (Fig. 4.15b). It can be seen that the Variscan rocks from the Alps are similar to Himalayan-type granitoids and therefore distinctly different from the Pelagonian Zone basement rocks. Those Moldanubian granitoids that plot in the I-type field overlap with the Pelagonian Zone basement rocks although the S-type rocks are different. The basement rocks from the Carpathians on the contrary demonstrate a clear similarity to the Pelagonian Zone basement rocks.

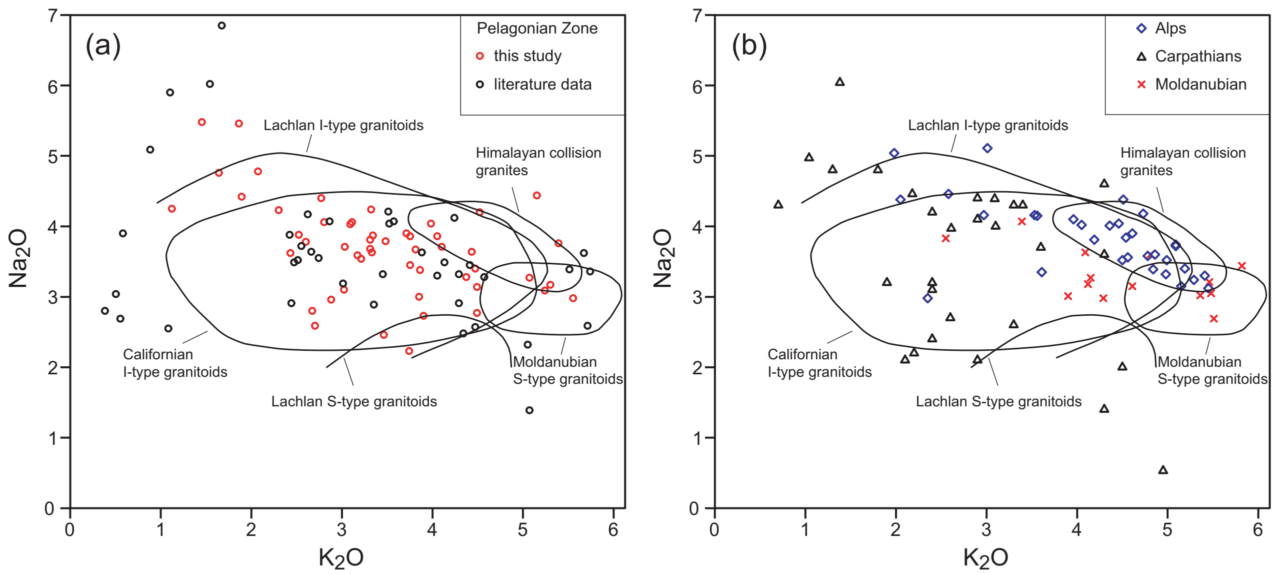

Fig. 4.15. (a) Comparison of the Permo-Carboniferous basement rocks from the Pelagonian Zone (red circles) with different granite types (after Finger & Steyrer 1990). Additional geochemical data of Pelagonian Zone granitoids from the literature are plotted (black circles; data from Katerinopoulos *et al.* 1992; Koroneos *et al.* 1993; Pe-Piper *et al.* 1993a, b; Kotopouli *et al.* 2000; Vavassis *et al.* 2000). (b) Same diagram showing Variscan granitoids from the Alps, the Carpathians and the Moldanubian Zone. Data are taken from the literature. Alps: Marro 1988; Schermaier *et al.* 1997; Bertrand *et al.* 1998; Moldanubian: Liew *et al.* 1989; Carpathians: Poller *et al.* 2000, 2001.

4.6 The meta-sedimentary rocks

Only six meta-sedimentary rocks were sampled from the Pelagonian Zone, therefore general conclusions and interpretations concerning the meta-sedimentary basement of the Pelagonian Zone are not possible. This is especially true as the only age constraint is their metamorphic character indicating that they were most likely deposited before the alpine orogeny. For reason of completeness, however, they shall be shortly described in this paragraph.

Sample V8 is a mylonitic basement rock taken from the NW Pelagonian Zone into which the Varnous pluton intruded. It has an intermediate composition and is characterised by a high Al_2O_3 concentration > 20 wt.%. CaO and Na_2O concentrations are low (< 1 wt.%) but K_2O content is about 3 wt.%. With regard to the trace elements it shows relatively high concentrations of Ba, La, Ce, Y, and Nb compared to the other meta-sediments. Sample Pl39 is a highly sheared dark rock (possibly country rock) taken from the same outcrop as orthogneisses Pl37 and Pl38. Though Pl39 has an intermediate (*c.* 55 wt.% SiO2) composition like V8 it has a lower Al_2O_3 concentration and higher MgO, CaO, Na_2O and K_2O contents than V8. Phyllite Pl52 is a foliated relatively weathered sampled at the western flank of Mt. Ossa W of Spilia. It has a felsic composition and a relatively high MgO content of *c.* 3 wt.% compared to the other felsic meta-sediments. It is characterised by low Sr and Ba concentrations and high Cr and Ni contents. Pl17 is a fine grained foliated quartzite taken from northern Pilion. It occurs in an outcrop together with phyllite and marble, indicating sedimentation in a subsiding basin. One coarse-grained meta-sediment (Skop) was sampled on Skopelos Island. It has a felsic composition (SiO_2 > 80 wt.%) with extremely low Al_2O_3 (*c.* 5 wt.%) and MgO concentrations (*c.* 0.5 wt.%), and the CaO content is

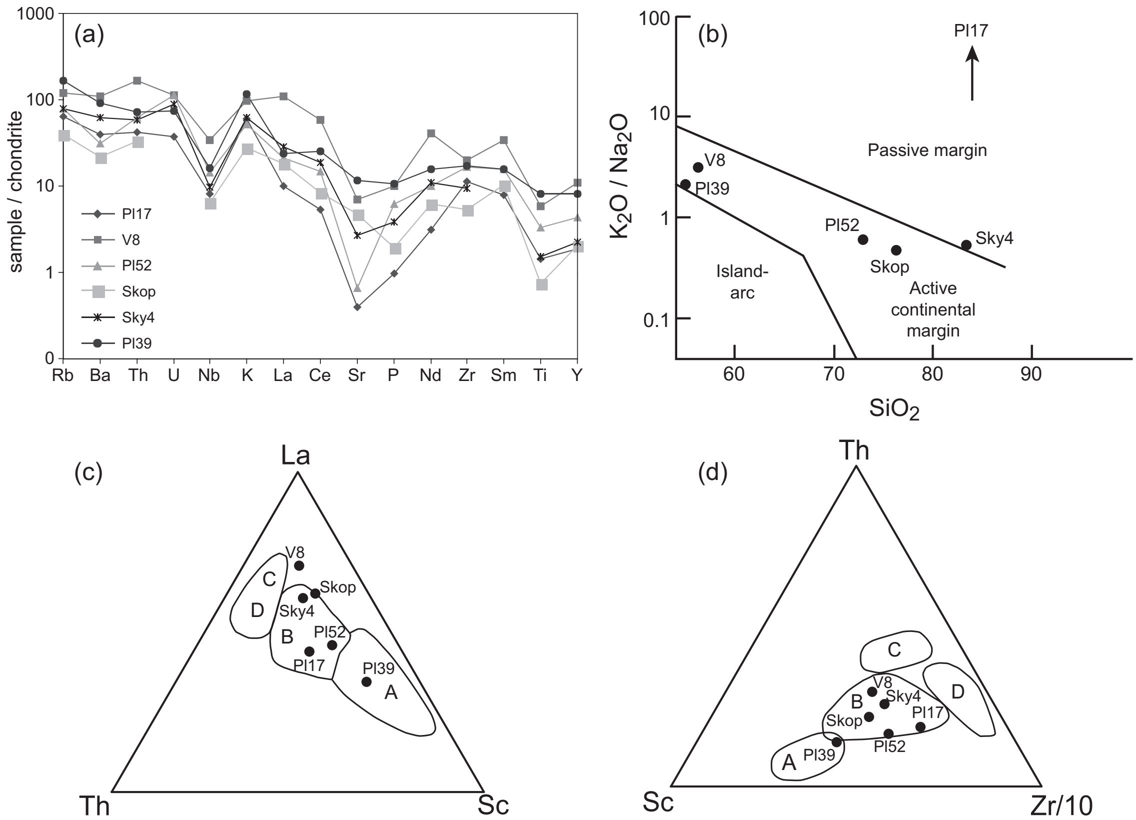

Fig. 4.16. (a) Spider-diagram of the meta-sedimentary basement rocks from the Pelagonian Zone. (b) Classification diagrams after Roser & Korsch (1986). (c) and (d) Bathia & Crook (1986) for the meta-sedimentary rocks. A = oceanic island arc; B = continental island arc; C = active continental margin; D = passive margins. All elements used in the diagrams were analysed with XRF.

higher than Na_2O and K_2O contents. Trace element concentrations are generally low, only Sr contents is about 100 ppm. Sky4 is a medium grained, foliated rock sampled from the northern part of the road cut on Skyros Island from which granites Sky1 and Sky2 were taken. It has a felsic composition and Na_2O content is higher than K_2O or CaO. Trace element concentration are relatively low, only Ba is about 400 ppm.

In a spider-diagram (normalised to PRIMA) (Fig. 4.16a) all meta-sediments show a negative Nb anomaly and most show also a negative Ti anomaly (not Pl39). Sample Pl39 generally forms the smoothest pattern with only the negative Nb anomaly showing clearly and a small negative K anomaly might be indicated. Sample V8 deviates from the other meta-sediments by its relatively high Th, La, Ce, Nd and Sm contents.

Discrimination diagrams to classify between different tectonic environment after Roser & Korsch (1986) and Bathia & Crook (1986) favour a sedimentary environment in a subduction zone environment either at an active continental margin or a continental island arc (Fig. 4.16b-d). For sample Pl17 a passive margin origin in the classification after Roser & Korsch (1986) is indicated, caused by Na_2O concentrations below the detection limit, and sample Sky4 just falls within the passive-margin field. In the classification after Bathia & Crook (1986) no sample plots close to the passive margin field.

4.7 Conclusion

Geochemical analyses have shown that granitoid composition despite their variability between single samples is relatively homogenous throughout the Pelagonian Zone. The only exception might be the Varnous-pluton of the NW Pelagonian Zone with its distinct I-type composition. Most other granitoids show variably hybrid characteristics ranging from predominantly I-type characteristics to those with more or less S-type influence. Sr- and Nd-isotope composition investigations underline this view. Depleted mantel model ages between 1.0 and 1.6 Ga are typical for central European Variscan basement rocks. The REE and the spider-diagram pattern resemble those of typical continental crust. Major and trace element data suggest an origin in a continental-arc or an active continental-margin setting, only a limited number of samples might have originated during arc-continent collision or post-collision.

The Pelagonian Zone can be traced northward into F.Y.R.O.M. but the question remains if it could possibly form the southern or southeastern extension of one of the Central European Variscan belts, like e.g. the Alps or the Carpathians. In comparison to other Variscan orthogneiss basement rocks in southeastern Europe the Permo-Carboniferous basement rocks from the Pelagonian Zone are similar to those from the Carpathians but not so much to the Variscan rocks from the Alps. This might be a hint that a possible continuation of the Pelagonian active continental margin should not be sought in the Alps but more eastward in the Carpathians.

Chapter 5. Gondwana-derived terranes in the northern Hellenides

This chapter is largely identical to a manuscript entitled "Gondwana-derived terranes in the northern Hellenides" written by Himmerkus, F., Anders, B., Reischmann, T. & Kostopoulos, D., which was submitted to the Geological Society of America Memoirs.

5.1 Abstract

The Hellenides constitute an integral part of the Alpine orogenic system in southeastern Europe. Despite the recognition of several sub-parallel zones, which are interpreted as terranes s.l. separated by ophiolitic sutures (e.g. Pindos and Vardar sutures), the classical view of an orogen with a foreland fold-and-thrust belt, a central crystalline zone and a rather undeformed hinterland is still in discussion. This paper concentrates on basement terranes of exotic provenance in two of the internal zones of the Hellenides, supporting the interpretation of the Hellenides as an accretionary orogen, which formed by amalgamation of crustal segments during the subduction of oceanic basins of the Tethys.

The oldest of these exotic terranes is the Florina Terrane in the Pelagonian Zone. It is composed of Neoproterozoic arc-related orthogneisses. The two other terranes occur east of the Vardar Zone within the Serbo-Macedonian Massif. The Pirgadikia Terrane is a micro-terrane in the southern Chalkidiki peninsula. It is built by Pan-African mylonitic orthogneisses, which originated, according to trace-element geochemistry and Sr isotopic composition, in a magmatic-arc environment. The entire northwestern part of the Serbo-Macedonian Massif is composed of the Silurian predominantly coarse-grained peraluminous orthogneisses with a magmatic-arc signature, interpreted here as the Vertiskos Terrane.

These terranes are exotic in relation to the other parts of the Hellenides. Because of the similarity of ages, the provenance of the late Proterozoic Pan-African terranes is assumed to be Gondwana. The Vertiskos Terrane may have been part of the so-called Hun superterrane, which formed at the northern active continental margin of Gondwana in the early Palaeozoic.

5.2 Introduction

After the establishment in the 1960's of the paradigm of plate tectonics with its fundamental processes of creation and subduction of oceanic crust, the Wilson cycle was considered the pace of orogenic processes (Miyashiro *et al.* 1982). In this scenario, an orogenic cycle was defined as the opening and closure of an ocean starting off with rifting, then passing through a sea-floor spreading phase that ended in eventual destruction of the oceanic crust in a subduction zone, to final lock-up during continental collision. However, this cycle does not take into account the pre-existing geology of the plates involved in the system and movements parallel to the plate boundaries. The recognition of smaller fault-bounded crustal blocks led to the refinement of the ideas on orogeny. The terrane concept was defined in the western American Rocky Mountains, where similar crustal segments occur along the strike of the orogen (e.g. Coney *et al.* 1980). These crustal units were accreted to the American continent by eastward subduction during the Mesozoic and later displaced by major left lateral faults. A terrane is defined as a distinct fault-bounded crustal unit with a geological evolution that is significantly different from that of the neighbouring regions (e.g. Howell *et al.* 1985). In the case of a terrane comprising mainly sedimentary sequences the differences in facies and faunal diversity can be used to identify different terranes. In the case of crystalline basement units, geochemical and isotopic characteristics, primary intrusion ages, age and grade of metamorphism and deformation, and palaeomagnetic approaches can be used for terrane discrimination.

This paper is dedicated to the basement occurrences of the northern Hellenides of Greece. Primary intrusion ages and the geochemical and isotopic characteristics of the basement rocks are used in conjunction with structural information to identify different terranes and their origin in the internal part of the Hellenides and to constrain the pre-Alpine to early Alpine history of the Hellenic orogen.

5.3 Regional Geology

The Hellenides are an Alpine mountain chain in Greece and constitute the link between the Dinarides/Albanides to the northwest and the Taurides to the southeast in Asia Minor. This orogenic belt formed upon the closure of the different branches/oceans of the Tethys Sea and the resultant accretion of variably sized continental fragments that were separated by them. The Hellenides are an elongated and strongly arcuate orogen, which present appearance is influenced by large-scale extension due to retreat of the Hellenic subduction zone since the Miocene (Le Pichon & Angelier 1979, 1981; Le Pichon *et al.* 1995; Gautier & Brun 1994; Gautier *et al.* 1999; Jolivet 2001). This extension resulted in submergence of large parts of the central and internal units of the Hellenides in the Aegean Sea and the exhumation of metamorphic core complexes and gneiss domes along flat-lying detachment faults (Lister *et al.* 1984; Brun & Sokoutis 2004).

In the past 25 years, the Hellenides have become the focus of scientific attention mainly because of the well-preserved high-pressure and ultra high-pressure rocks in the metamorphic units of the Internal Hellenides (Altherr *et al.* 1979; Jacobshagen 1986; Kostopoulos *et al.* 2000; Mposkos & Kostopoulos 2001).

Also scientific interest was concentrated on neotectonics, which monitors the ongoing tectonic processes in the retreating Aegean subduction zone, as well as the extending continental crust in the Aegean Sea and along the North Anatolian Fault Zone (Le Pichon *et al.* 1995; Davies *et al.* 1997; Reilinger *et al.* 1997; Kahle *et al.* 2000; Jolivet 2001; Royden & Papanikolaou 2004). The pre-Alpine history, however, remained largely untouched. It is nevertheless an important field for research concerned with establishing a geological framework for the evolution of the Hellenides, and the palaeogeographic reconstructions of the eastern Mediterranean. Hence our study contributes to this field of research.

The Hellenides trend approximately NNW-SSE and can be subdivided into several sub-parallel units or terranes s.l., which are separated by large fault zones (Jacobshagen 1986 and references therein; Papanikolaou 1997). These units are grouped in two large zones, which are the External Hellenides, which are mainly built by supracrustal rocks and the Internal Hellenides comprising predominantly basement units, namely the Pelagonian Zone, the Attico-Cycladic Massif, the Vardar Zone, the Serbo-Macedonian Massif and the Rhodope Massif.

The westernmost zone is the External Hellenide Platform (comprising the Paxon, Ionian and Gavrovo-Tripolis Zones) consisting mainly of thick neritic Mesozoic carbonates and fewer clastic sediments and representing part of the passive continental margin of southern Tethys (Apulian promontory of northern Gondwana).

This is separated from the Pelagonian Zone to the east by the remnants of the Pindos Ocean containing Mesozoic ophiolites and their accompanying pelagic sedimentary cover (Brun 1956; Kostopoulos 1988).

The Pelagonian Zone is composed of crystalline basement (schists, ortho- and paragneisses, amphibolites and granitoids) in addition to Permo-Triassic volcano-sedimentary series, Mesozoic limestones, ophiolitic rocks s.l. and abundant Tertiary to Quaternary sediments (e.g. Mountrakis 1982, 1984; Jacobshagen 1986 and references therein; Kilias & Mountrakis 1989; Pe-Piper & Piper 2002 and references therein). Geochronology of basement rocks revealed widespread Permo-Carboniferous mag-

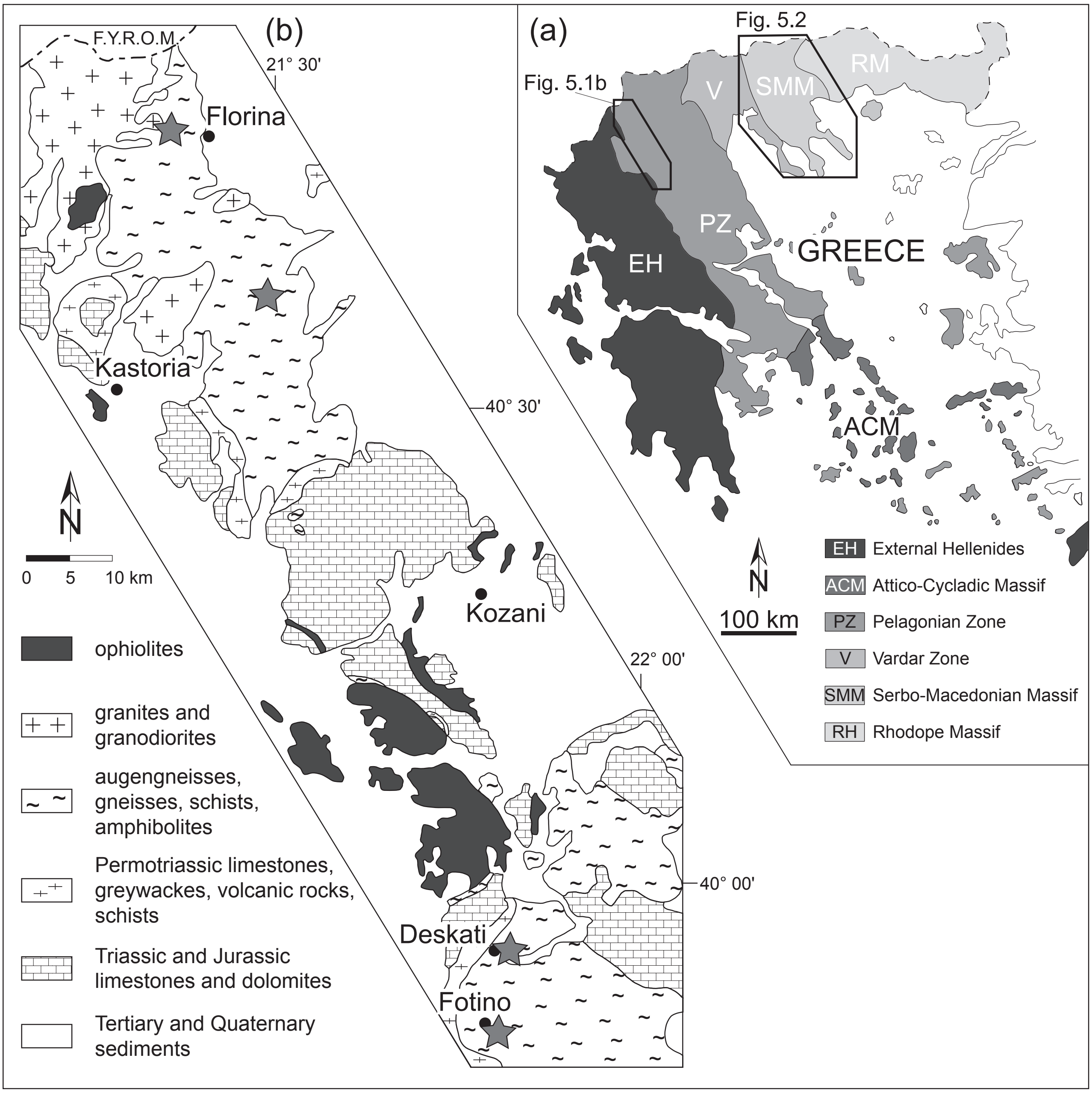

Fig. 5.1. (a) Tectono-stratigraphic overview of the Hellenides in Greece and the adjacent areas after Kondopoulou (2000). The External Hellenides are mainly built by meta-sediments, whereas the Internal Hellenides are composed of several sub-parallel zones of basement rocks. (b) Geological map of the northwestern part of the Greek Pelagonian Zone (simplified from the IGME Geological Map of Greece, 1:500 000, 1983), the occurrences of Late Neoproterozoic rocks are indicated with stars.

matism with ages in the range of about 280 to 320 Ma (Yarwood & Aftalion 1976; Schermer 1990; Koroneos *et al.* 1993; Vavassis *et al*. 2000; Reischmann *et al.* 2001; Anders *et al*. 2003c, see Chapter 3). These ages are similar to intrusion ages found in the Attico-Cycladic Massif (Engel & Reischmann 1998; Reischmann 1998), which borders the Pelagonian Zone to the south. Because of this similarity the Pelagonian Zone and the Attico-Cycladic Massif were interpreted as parts of a large Permo-Carboniferous magmatic arc (Reischmann *et al.* 2001). In the northwestern Pelagonian Zone, pre-Permo-Carboniferous basement was inferred by Mountrakis (1984) on the basis of field observations. Recently crystalline basement of Late Proterozoic age was identified by Anders *et al.* (see Chapter 2) and interpreted as remnants of an exotic terrane.

East of the Pelagonian Zone is the ophiolitic Vardar Zone (Figs. 5.1 and 5.3), which is interpreted as a major suture zone on the basis of outcrops further north in former Yugoslavia (Robertson & Karamata 1994 and references therein; Dimitrijevic 1997). The Vardar zone has also been equated to the Izmir-Ankara suture zone further east in Asia Minor (e.g. Stampfli *et al.* 2004).

The so-called Hellenic hinterland comprises two discrete massifs east of the Vardar Zone, namely the Serbo-Macedonian Massif (SMM) and the Rhodope Massif. The SMM is an elongated polymetamorphic basement terrane, which is largely build by orthogneisses (Kockel & Mollat 1977; Jacobshagen 1986; Kilias *et al.* 1999). Metasedimentary rocks and amphibolites occur only in mélange zones, bordering the basement complexes. The metasedimentary unit bordering the SMM to the adjacent Vardar Zone was formerly termed Circum Rhodope Belt (Kauffmann *et al.* 1976). This nomenclature, however, was already abandoned by Ricou *et al.* (1998), because it was describing a greenschist-facies mélange zone, which occurs in different positions in the Internal Hellenides.

The SMM is not a crustal entity but consists of four main basement units, which are the Pan-African Pirgadikia Unit, the Silurian Vertiskos Unit, the Triassic Arnea Unit, and the Upper Jurassic Kerdillion Unit. These basement units are separated by two major mélange zones (Fig. 5.2), which contain mafic and ultramafic rocks as well as marbles and clastic metasediments and slivers of the adjacent basement units. The northwestern part of the SMM is characterized by the association of the Silurian augengneisses of the Vertiskos Unit with the Triassic leucogranites of the Arnea Unit. The Kerdillion Unit (Kockel & Mollat 1977), in the east of the SMM, is lithologically related to the adjacent Rhodope Massif. The Kerdillion Unit consists of banded biotite gneisses, which are intruded by a large amount of leucocratic dykes and pegmatites. For this reason the gneisses were traditionally regarded as migmatites. This unit is exposed in three large gneiss domes. In the south of the SMM the Pirgadikia Unit occurs within the ophiolitic mélange zone, which separates the Vertiskos Unit from the Vardar Zone. The Pirgadikia Unit is composed of leucocratic mylonitic gneisses, which originated in the Late Neoproterozoic in a magmatic arc setting.

The Rhodope Massif is the easternmost unit of the Hellenides and consists of an association of granitic gneisses, metapelites, eclogites, amphibolites and very thick units of marbles (Burg *et al.* 1996; Ricou *et al.* 1998; Barr *et al.* 1999). It is situated east of the Strimon river basin (Fig. 5.2) and is built by a pile of nappes. Two principal units have been distinguished here (Papanikolaou & Panagopoulos 1981). The Lower Tectonic Unit is composed of a Permo-Carboniferous basement overlain by massive marbles of considerable thickness. The Upper Tectonic Unit contains Upper Jurassic gneisses similar to the Kerdillion Unit and Tertiary granites (Turpaud & Reischmann 2003).

5.4 Description of the terranes in the Internal Hellenides

In the following paragraphs the crustal units of the Internal Hellenides recently identified as exotic terranes are described. As these areas comprise crystalline basement rocks, terrane identification was accomplished using zircon geochronology and whole-rock isotope geochemistry, combined with fieldwork and petrographic studies.

5.4.a Florina Terrane

The westernmost terrane so far identified in the region of the Internal Hellenides is the Florina Terrane, situated in the northwestern area of the Greek part of the Pelagonian Zone. Recent geochronological studies of the crystalline basement of the Pelagonian Zone revealed that although Permo-Carboniferous magmatism predominates the whole Pelagonian Zone, a well-defined group of orthogneisses and granites with Neoproterozoic intrusion ages of about 700 Ma also exists in its northwestern part (Fig. 5.1) (Anders *et al.* 2003b, see Chapter 2). The ages of the Neoproterozoic basement rocks vary in a narrow range between 699 Ma and 713 Ma (single-zircon U-Pb TIMS and SIMS geochronology, Anders *et al.* 2003b, see Chapter 2), and hence these rocks are interpreted to have formed during the same magmatic event. The identification of pre-Permo-Carboniferous basement supports Mountrakis (1984), who proposed the existence of Early Palaeozoic or even older basement rocks in the Pelagonian Zone on the basis of intrusive contacts and contact metamorphism of a Permo-Carboniferous granite (Kastoria granite) with the surrounding basement. Mountrakis (1986) considered this pre-Permo-Carboniferous basement as being part of the Cimmerian continent, which rifted away from Gondwana in the Triassic thus proposing the existence of far-travelled crustal units in the Pelagonian Zone.

The Neoproterozoic basement rocks vary in colour, grain size, degree of deformation and development of feldspar “augen”, and are indistinguishable from the neighbouring Permo-Carboniferous granites and gneisses. Based on intrusion ages, however, these rocks are clearly distinct from all other basement rocks of the Internal Hellenides. Consequently, Anders *et al.* (see Chapter 2) proposed that these gneisses are remnants of a terrane. Geochemically, the Florina-terrane basement rocks have the composition of felsic peraluminous granites with volcanic-arc/syn-collisional characteristics (see Chapter 2). Epsilon Nd_i values vary between +0.9 and -4.8 and Nd model age (T_{DM}) values from 1.2 to 1.7 Ga (see Chapter 2), which is in agreement with a formation in an active continental margin setting.

The spatial distribution of the Neoproterozoic basement rocks is not exactly known. Their northernmost exposure is west of Florina town (Fig. 5.1) close to the Permo-Carboniferous Varnous pluton (Koroneos *et al.* 1993; see Chapters 2 and 3), while their southernmost outcrop is the Fotino granite south of Fotino village (Fig. 5.1). The Neoproterozoic rocks are thus distributed across an area of *c*. 20 x 100 km. Inherited components in zircon grains with ages of *c*. 700 Ma were also identified in orthogneisses further east (S of Veria town) and southeast (close to Verdikoussa village) in the Pelagonian Zone (not shown on Fig. 5.1) Based on the chemical and mineralogical similarities between the Neoproterozoic basement rocks, Anders *et al.* (see Chapter 2) proposed that they once belonged to a single basement unit that was dissected during later tectonic events.

5.4.b Pirgadikia Terrane

This basement unit is a micro-terrane exposed in southeastern Chalkidiki north of Sithonia peninsula (Fig. 5.2). The rocks are mylonitic gneisses, which are restricted to the bay of Pirgadikia village and further inland to an area around the village of Taxiarchis (Himmerkus *et al.* 2004a, submitted). The two outcrops occur within a major mélange zone bordering the Vertiskos Terrane to the southwest (Fig. 5.2). The gneisses form tectonic slivers floating within the metasedimentary rocks of the mélange zone. The rocks of the Taxiarchis occurrence are mylonitic quartzites, whereas those of Pirgadikia are leucocratic orthogneisses characterized by a strong lineation and grain-size reduction due to mylonitic deformation. The rocks at the shore of Pirgadikia are in tectonic contact with massive marbles to the north and south. Two of the orthogneisses gave ages of 570 and 587 Ma as determined by the single-zircon Pb-Pb evaporation method (Himmerkus *et al.* 2004a, submitted). The $^{87}Sr/^{86}Sr$ initial ratios calculated using the zircon ages are 0.70644 and 0.70734 respectively. The εNd_i values are -7.59 and -6.24 respectively and show a strong contribution from a pre-existing crustal material in the source. The metaquartzite contains zircons with a uniform age of 555 Ma. This indicates proximal sedimentation conditions. The rocks of the Pirgadikia Terrane differ from their country rocks in terms of rock type and metamorphic grade as well as structural characteristics. The entire SMM and the western Rhodope Massif show a very consistent top-to-the-SW sense of shear (Burg *et al.* 1995, 1996; Kilias *et al.* 1999), which is also present in the metasedimentary and orthogneissic country rocks of the Pirgadikia Terrane. By contrast, the mylonitic gneisses of Pirgadikia are sheared top-to-the-east. All contacts to the country-rocks of the Vertiskos Unit and the mélange zone are of tectonic nature and do therefore not allow any correlations.

The basement unit of Pirgadikia is small in extent yet very important in putting together the pieces of the tectonic puzzle of the area, as it relates the Greek part of the SMM to similar units of the Bulgarian SMM and the Menderes Massif in western Turkey (see below).

5.4.c Vertiskos Terrane

The Vertiskos Terrane occurs in the northwestern part of the SMM and is restricted to this massif. The name derives from the Vertiskos Mountains northeast of Thessaloniki (Fig. 5.2). Kockel & Mollat (1977) defined the Vertiskos Unit as one of the principal units of the SMM on the basis of its lithology, which is mostly augengneisses. These basement gneisses are intruded by a series of leucocratic granites termed the Arnea Suite after the main body, the Arnea Granite east of Thessaloniki (Himmerkus *et al.* 2004b). The association of these two rock units defines the Vertiskos Terrane, which is bordered by two large-scale shear zones interpreted as mélange zones: the Vardar Zone (including the Circum-Rhodope Belt of Kauffmann *et al.* 1976) to the west and the Athos-Volvi Suture Zone (TVG Zone of Dixon & Dimitriadis 1984) to the east (Himmerkus *et al.* 2005). As previously mentioned, the rocks of the Vertiskos Terrane are orthogneisses, which form several groups according to their mineralogy and texture. The most prominent group comprises very coarse-grained augengneisses with K-feldspars up to 10 cm in size. These rocks are mainly biotite gneisses with little white mica and are characterized by a strong non-coaxial deformation. A second group comprises fine-grained gneisses with small augen and a prominent C/S fabric. These gneisses are mainly two-mica gneisses. The third major group

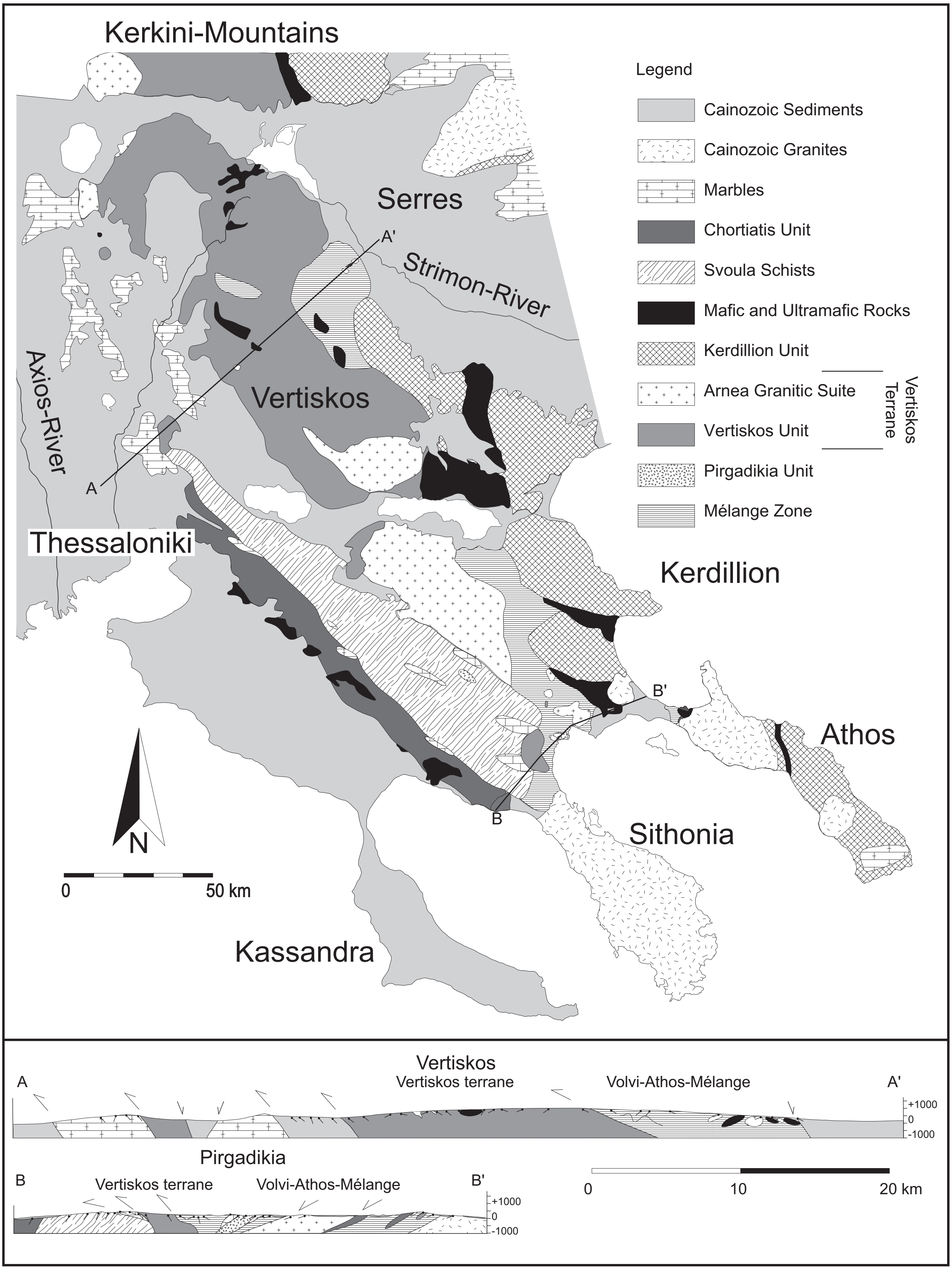

Fig. 5.2. Geological-tectonical map of the Greek Serbo-Macedonian Massif with interpretative cross sections, simplified after Kockel & Mollat (1977). Scale of sections is 5 times scale of the map but to scale. The Circum-Rhodope Belt after Kauffmann *et al.* (1976) comprises the Chortiatis Unit and the Svoula Schists.

comprises leucocratic muscovite gneisses, which represent the most fractionated rocks of the succession. The rocks are peraluminous and classify as volcanic-arc granites in the discriminant diagrams of Pearce *et al.* (1984). The ages of the orthogneisses of the Vertiskos Terrane vary between 425.9 ± 4.2 Ma and 443.4 ± 5.5 Ma with a mean of 432.2 Ma (Himmerkus *et al.* 2003). It was determined by the single-zircon Pb-Pb evaporation method and conventional U-Pb dating on a total of 22 samples. Cathodoluminescence imaging of representative zircon grains shows clear magmatic zoning suggesting that the ages obtained are primary intrusion ages of the granitic precursor to the gneisses. The $^{87}Sr/^{86}Sr$ initial ratio of whole-rock samples is 0.70924 indicating a significant contribution from a pre-existing continental crust material in the source region of the granites. The individual samples also form an errorchron with an age of 430 ± 24 Ma (MSWD = 28), which agrees with the zircon age. The εNd_i values of two coarse-grained augengneisses (−4.61 and −6.46) also suggest a strong contribution from old crustal material. The data show that the orthogneisses of the Vertiskos Terrane originated in Silurian times in a magmatic arc environment that was built on pre-existing continental crust, a situation comparable to the modern Andean active continental margin.

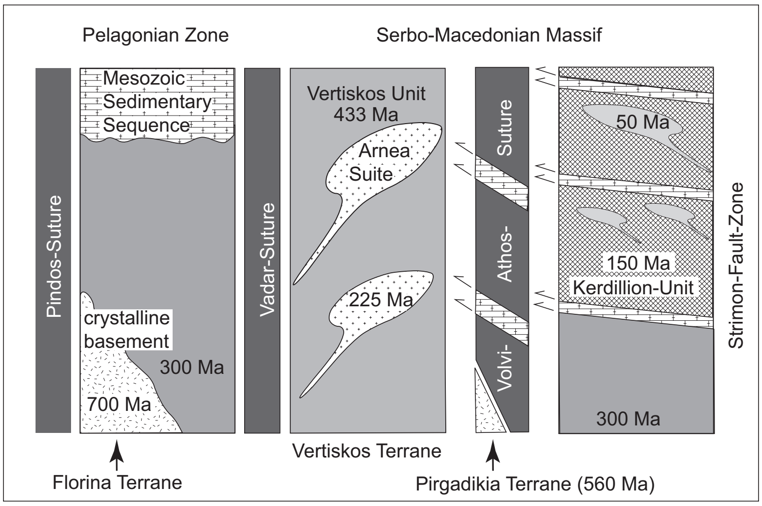

Fig. 5.3. Schematic tectono-stratigraphic columns of the units of the Pelagonian Zone and the Serbo-Macedonian Massif in the Internal Hellenides. The basement units are separated by mélange zones containing ophiolitic material. The Kerdillion Unit is related to the adjacent Rhodope Massif east of the Strimon-Fault Zone, which shows the same spectrum of ages. The Vertiskos Terrane comprises two lithological units (the Silurian Vertiskos and the Triassic Arnea Unit), which are both exotic to the Internal Hellenides, as well as the Late Neoproterozoic terranes of Florina and Pirgadikia.

5.5 Provenance of Terranes in the Internal Hellenides

The Precambrian and Silurian intrusion ages of the above-described terranes from the Internal Hellenides deviate distinctly from those of the surrounding basement units, which are essentially younger and have Permo-Carboniferous or even Mesozoic ages (Yarwood & Aftalion 1976; Engel & Reischmann 1998; Reischmann 1998; Vavassis *et al.* 2000; Reischmann *et al.* 2001; Anders *et al.* 2003c, see Chapter 3; Turpaud & Reischmann 2003, 2005). Two of these terranes, the Vertiskos and the Pirgadikia Terrane, form crustal blocks with a distinct tectono-metamorphic history separated by major faults, in places containing ophiolites. They are interpreted as exotic terranes accreted to the Hellenide orogen. The occurrence of the Pirgadikia and Vertiskos Terranes in close proximity to the Vardar Zone supports this notion. For the Florina Terrane, clear definition of the limits and contacts to the surrounding rocks is still indistinct. The intrusion ages of about 700 Ma, however, render a derivation from the neighbouring rock units unlikely, and because of the singularity of these ages in the Hellenides the interpretation as a far-travelled exotic terrane is plausible (see Chapter 2).

Having agreed that the three crustal units described above are exotic terranes in their present surrounding, the question arises from where these terranes originated.

The Late Neoproterozoic intrusion ages for the Florina Terrane of the Pelagonian Zone favour a derivation from the northern margin of Gondwana instead from the East European Craton and Baltica. The question remains from which area along the northern margin of Gondwana the Florina Terrane was the most likely derived. Anders *et al.* (see Chapter 2) pointed out that an affinity to East Avalonia is indicated by means of Nd isotopes and inherited zircon components. Zircon geochronology infers the existence of Proterozoic contributions. Several geochronological and geochemical studies led to the identification of crustal units in central Europe as Avalonia-type terranes (e.g. Finger *et al.* 2000; Friedl *et al.* 2000; Hegner & Kröner 2000). The Florina Terrane might be compared with these Avalonia-type terranes.

The age and the chemical and isotopic characteristics of the Pirgadikia Terrane are not unique in the eastern Mediterranean. Similar Pan-African ages and isotopic characteristics of old recycled crust have been reported from basement units in the SMM of Bulgaria and in the Menderes Massif in western Turkey (Hetzel & Reischmann 1996; Loos & Reischmann 1999). Late Precambrian basement in the SMM of western Bulgaria (Kraište region) occurs in the Osogovo-Lisets Complex and the Struma Unit and has intrusion ages between *c.* 544 Ma and 568 Ma (von Quadt *et al.* 2000; Graf 2001; Neubauer 2002 and references therein). In the Menderes Massif the predominant rock types are orthogneisses with a magmatic-arc signature. Their intrusion ages range from 520 to 570 Ma with a mean of 550 Ma (Hetzel & Reischmann 1996; Loos & Reischmann 1999). Large exposures of basement rocks with Pan-African ages are known from the Arabian-Nubian Shield (e.g. Reischmann 2000) and other parts of N Africa.

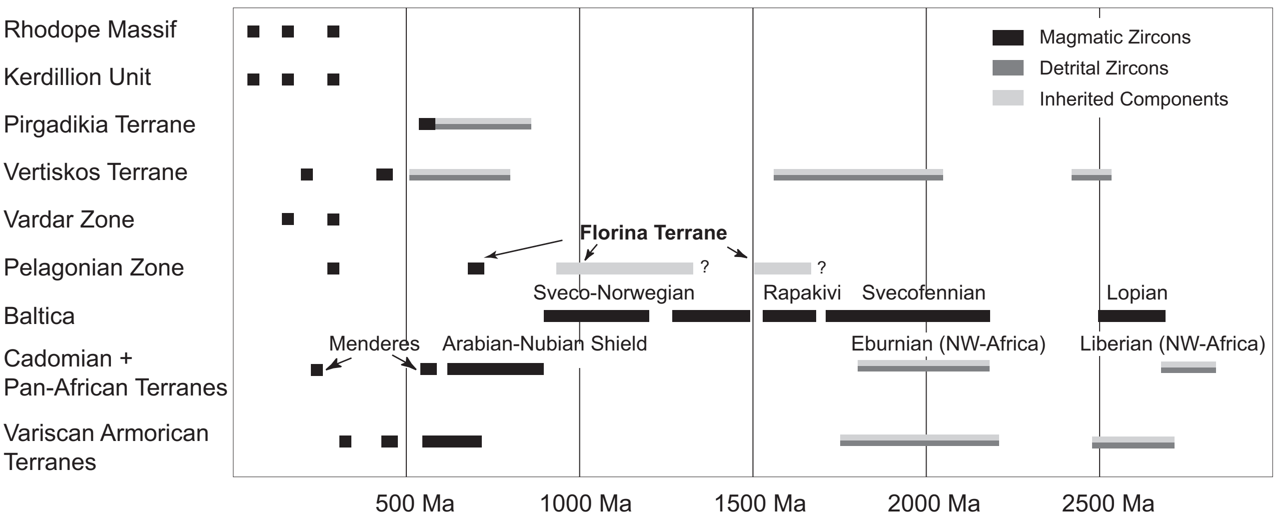

Fig. 5.4. Compilation of age distributions of parts of the Alpine and Variscan belts in comparison to ages in the shields of Baltica and northern Gondwana. The terranes of the SMM differ in the age spectrum to the Florina Terrane in the Mesoproterozoic. The Florina Terrane is more related to the Avalonian Terranes of the central European Variscides, whereas the Vertiskos and Pirgadikia Terranes contain no Mesoproterozoic inheritance. This lack of Grenvillian ages indicates a relation to the Cadomian Terranes, and excludes a provenance from Baltica and western Gondwana (Fig. 5.5). Data compiled by T. Reischmann.

The Vertiskos Terrane has a different history and there are no basement rocks of similar lithology and age known from the Hellenides and western Turkey. The terrane continues north into Bulgaria where it is known as the Ograzhden Block (Titorenkova *et al.* 2003), but there it vanishes south of Blagoevgrad. Ordovician and Silurian ages however can be found throughout the entire Alpine-Variscan Chain (Neubauer 2002; von Raumer *et al.* 2002, 2003). The age and tectonic environment of the Vertiskos augengneisses indicate that this terrane may have been part of the so-called Hun superterrane defined by Stampfli & Borel (2002). This superterrane is composed of a series of basement and supracrustal rocks formed during Cambrian to Silurian times at the northern active continental margin of Gondwana. Here, an island arc was built on an archipelago of pre-existing Cadomian crust that had been rifted away from Gondwana in the Earliest Cambrian during initial opening of the Rheic ocean (von Raumer *et al.* 2003). Subduction beneath Gondwana created peraluminous granitoids, which are representative of this environment. Parts of this superterrane are present in the Alpine and Variscan orogens from Western Europe to China. The basement units of the Pirgadikia and Vertiskos Terranes as well as the Pan-African rocks of the Osogovo-Lisets dome in the Bulgarian SMM match this scenario as they represent the Pan-African basement and the Ordovician-Silurian magmatic arc that formed by southward-directed subduction beneath Gondwana. Analyses of detrital zircons in metasediments of the mélange zones of the SMM and of inherited components in the magmatic zircons combined with the Nd model ages of the basement units of the SMM show a strong contribution from Pan-African crust. Grenvillian ages of around 1 Ga are completely missing in the Vertiskos terrane whereas few grains show ages of 1.5 to 2 Ga and a well-defined inheritance of 2.4 Ga to 2.5 Ga. This age spectrum of inherited components excludes western Gondwana and Baltica as sources of sediments and crustal material for the granites as no Grenvillian ages of around 1000 Ma are present (Linnemann *et al.* 2004; see Fig. 5.4).
Though a definitive allocation of the original positions of the Hellenide terranes along the northern margin of Gondwana is not possible from the present data, some inferences can be made.

5.6 Palaeogeographic Reconstructions

The study of the Alps and related young orogenic belts resulted in a large data set on different parts of the Tethys Ocean, which comprised different basins separating micro-continents or terranes. Palaeogeographic reconstructions of the Mediterranean realm (Robertson & Dixon 1984; Şengör *et al.* 1984; Stampfli & Borel 2002) favour two large oceanic basins termed the Palaeo- and Neotethys. In this scenario the Palaeo-Tethys closed during the Cimmerian Orogeny in the Triassic or Upper Jurassic (depending on the model) and the Neotethys during the Alpine Orogeny in the Eocene. In Greece and the entire Balkan area this simple subdivision is hard to apply, as there is a variety of sub-parallel ophiolitic zones and indications for several small ocean basins. This mosaic of several micro-continents was accreted to the south European margin during closure of the ocean basins in between.
With regard to the Palaeozoic, we favour the reconstructions of Stampfli & Borel (2002) and von Raumer *et al.* (2003) as the finding of exotic terranes can most easily be brought in agreement with these scenarios (Fig. 5.5). We follow these models with regard to the fact that a piece of Pan-African crust rifted off from northern Gondwana in the Lower Palaeozoic and that a magmatic arc formed in the Ordovician and Silurian. We propose that the Vertiskos and the Pirgadikia Terranes are part of this rifted continental fragment. For the Florina Terrane we suggest that it can be correlated with the Avalonian-

type terranes of southeastern Europe (e.g. Bruno-Vistulikum, Finger *et al.* 2000) and tentatively place it next to the Bruno-Vistulikum in the reconstruction of von Raumer *et al.* (2003) (Fig. 5.5).

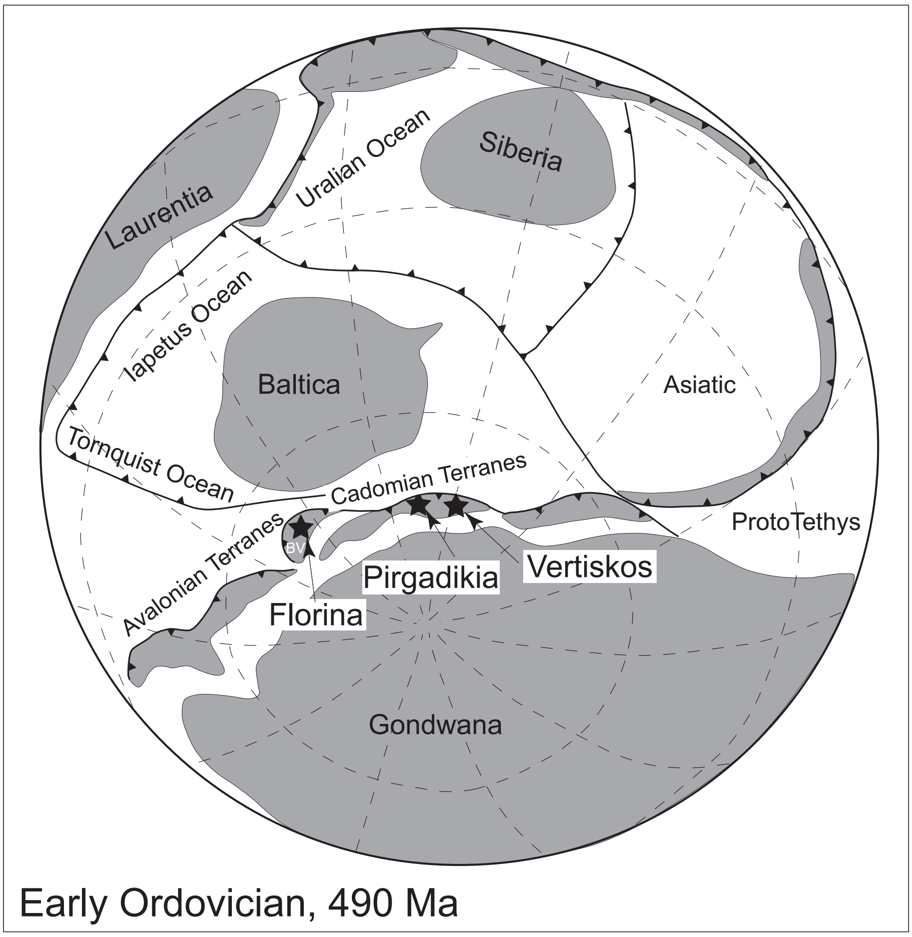

Fig. 5.5. Palaeogeographic reconstruction of the northern margin of Gondwana in Early Ordovician times at around 490 Ma, modified after von Raumer *et al.* (2003). The Florina Terrane has similarities with western Gondwana and the Avalonian Terranes of the central European Variscides. The two terranes from the SMM are placed in the vicinity of the Cadomian Terranes as the Pirgadikia Terrane as well as the Bulgarian SMM show a strong influence of the Pan-African orogeny. The Vertiskos Terrane was mostly built by the Ordovician-Silurian south-directed subduction under the active continental margin north of the Gondwana mainland. The Vertiskos Terrane originated in an Andean-type setting on pre-existing Pan-African crust with little sedimentary input from the cratons. BV: Bruno-Vistulikum

5.7 Conclusions

The presence of Gondwana-derived terranes in different zones of the Internal Hellenides highlights the allochtonous character of parts of the Hellenide orogen. Distinct crustal units in the different zones were accreted to the European craton during closure of Tethyan oceanic basins. The Vardar Zone is interpreted to represent a major suture and the discovery of the exotic Vertiskos Terrane in the neighbouring basement units supports this view. The ubiquitous top-to-the-SW sense of shear in the SMM and the western Rhodope Massif, as well as the transport direction of the western zones of the orogen (the External Hellenide Platform and the Sub-Pelagonian), indicate NE-directed accretion of various units in the Late Palaeozoic and Mesozoic. In the Tertiary, lateral movements parallel to the trend of the orogen due to flexure of the arc and extension in the central Aegean overprinted the structure of amalgamated terranes. The pre-Alpine to early Alpine history of the Hellenides is far more multifaceted than previously thought, as the main parts of the Greek orogen came into being during this period. It can be compared with that of the central European Variscides, expanding the region of Palaeozoic accretion orogeny and terrane amalgamation along the southern European margin to the southeast.

References

ALTHERR, R., SCHLIESTEDT, M., OKRUSCH, M., SEIDEL, E., KREUZER, H., HARRE, W., LENZ, H., WENDT, I. & WAGNER, G. A. 1979: Geochronology of High-pressure Rocks on Sifnos (Cyclades, Greece). *Contributions to Mineralogy and Petrology,* **70**, 245-255.

ANDERS, B., REISCHMANN, T. & POLLER, U. 2002: Geochronology and Isotope Analysis of Basement Rocks from the Pelagonian Zone, Greece. *Geochimica et Cosmochimica Acta*, **66**, A19.

ANDERS, B., REISCHMANN, T., POLLER, U. & KOSTOPOULOS, D. 2003a: Age and origin of granitic rocks within the Vardar Zone, N Greece. Geological Survey of Japan, Interim-Report 29, Hutton Symposium V, 2.

ANDERS, B., REISCHMANN, T., POLLER, U. & KOSTOPOULOS, D. 2003b: The oldest rocks in Greece: Geochronological evidence for remnants of a Precambrian basement within the central Hellenides. *Geochimica et Cosmochimica Acta*, **67**, A18.

ANDERS, B., REISCHMANN, T., POLLER, U. & KOSTOPOULOS, D. 2003c: First zircon ages from South Pilion and Skiathos Island, Greece. *Berichte der Deutschen Mineralogischen Gesellschaft, Beiheft zum European Journal of Mineralogy,* **15**, 5.

ARNDT, N. T. & GOLDSTEIN, S. L. 1987: Use and abuse of crust-formation ages. *Geology*, **15**, 893-895.

AUBOUIN, J., BRUNN, J. H., CELET, P., DERCOURT, J., GODFRIAUX, I. & MERCIER, J. 1963: Esquisse de la Géologie de la Grèce. *Livre Mémoire Professeur Fallot, Mémoires Société géologique de France*, 383-610.

BARKER, F. 1979: Trondhjemite: Definition, environment and hypotheses of origin. In *Trondhjemites, dacites and related rocks*. (ed. F. Barker), pp. 1-12. Elsevier, Amsterdam.

BAROZ, F., BEBIÉN, J. & IKENNE, M. 1987: An example of high-pressure low-temperature metamorphic rocks from an island arc: the Paikon Series (Innermost Hellenides, Greece). *Journal of Metamorphic Petrology*, **5**, 509-527.

BARR, S. R., TEMPERLEY, S. & TARNEY, J. 1999: Lateral growth of the continental crust through deep level subduction–accretion: a re-evaluation of central Greek Rhodope. *Lithos*, **46**, 69-94.

BARTON, C. M. 1976: The tectonic vector and emplacement age of an allochthonous basement slice in the Olympos are, N.E. Greece. *Bulletin de la Société Géologique de France*,**18**, 253-258.

BATHIA, M. R. & CROOK, K. A. W. 1986: Trace element characteristics of graywackes and tectonic setting discrimination of sedimentary basins. *Contributions to Mineralogy and Petrology,* **92**, 181-193.

BÉBIEN, J. 1982: *L'association ignée de Guévguéli (Macédoine grecque). Expression d'un magmatisme ophiolitique dans une déchirure continentale*. D.Sc. thesis, Université de Nancy I, Nancy, France.

BÉBIEN, J., DUBOIS, R. & GAUTHIER, A. 1986: Example of ensialic ophiolites emplaced in a wrench zone: Innermost Hellenic ophiolite belt (Greek Macedonia). *Geology*, **14**, 1016-1019.

BÉBIEN, J., PLATEVOET, B. & MERCIER, J. 1994: Geodynamic significance of the Paikon Massif in the Hellenides : contribution of the volcanic rock studies. *Bulletin of the Geological Society of Greece*, **30**, 63-67.

BERTRAND, J.-M., GUILLOT, F., LETERRIER, J., PERRUCHOT, M. P., AILLÈRES, L. & MACAUDIÈRE, J. 1998: Granitoides de la zone houillère brianconnaise en Savoie et en Val d'Aoste (Alpes occidentales): géologie et géochonologie U-Pb sur zircon. *Geodinamica Acta (Paris),* **11**, 33-49.

BLACK, L. P., KAMO, S. L., ALLEN, C. M., ALEINIKOFF, J. N., DAVIS, D. W., KORSCH, R. J. & FOUDOULIS, C. 2003: TEMORA 1: a new zircon standard for Phanerozoic U-Pb geochronology. *Chemical Geology,* **200**, 155-170.

BOYNTON, W. V. 1984: Cosmochemistry of the rare earth elements: meteorite studies. In *Rare Earth Element Geochemistry* (ed. P. Henderson), pp 63-114. Elsevier, Amsterdam.

BORSI, S., FERRARA, G., MERCIER, J. & TONGIORGI, E. 1966: Age stratigraphique et radimétrique Jurassique Supérieur d´un granite des Zones Internes Hellénides (Granite de Fanos, Macédoine, Grèce). *Revue de Géographie Physique et de Géologie Dynamic (2)*, **VIII**, 279-287.

BORTOLOTTI, V., CHIARI, M., MARCUCCI, M., PHOTIADES, A. & PRINCIPI, G. 2001: Triassic radiolarian assemblages from the cherts associated with pillow lavas in Argolis peninsula (Greece). *Ofioliti,* **26**, 75.

BORTOLOTTI, V., CARRAS, N., CHIARI, M., FAZZUOLI, M., MARCUCCI, M., PHOTIADES, A. & PRINCIPI, G. 2003: The Argolis peninsula in the palaeogeographic and geodynamic frame of the Hellenides. *Ofioliti*, **28**, 79-94.

BREGAR, M., BAUERNHOFER, A., PELZ, K., KLOETZLI, U., FRITZ, H. & NEUMAYR, P. 2002: A late Neoproterozoic magmatic core complex in the Eastern Desert of Egypt: emplacement of granitoids in a wrench-tectonic setting. *Precambrian Research* **118**, 59-82.

BROWN, S. A. M. & ROBERTSON, A. H. F. 1994: New structural evidence from the Mesozoic-Early Tertiary Paikon Unit, Northern Greece. *Bulletin of the Geological Society of Greece*, **30**, 159-170.

BROWN, S. A. M. & ROBERTSON, A. H. F. 2003: Sedimentary geology as a key to understanding the tectonic evolution of the Mesozoic-Early Tertiary Paikon Massif, Vardar suture zone, N Greece. *Sedimentary Geology,* **160**, 179-212.
DOI: 10.1016/S0037-0738(02)00376-7

BROWN, S. A. M. & ROBERTSON, A. H. F. 2004: Evidence for Neotethys rooted within the Vardar suture zone from the Voras Massif, northernmost Greece. *Tectonophysics*, **381**, 143-173.

BRUN, J.-P. 1956: Contribution a l' étude Géologique du Pinde Septentrional et d'une partie de la Macédoine Occidental. *Annales Géologiques des Pays Helleniques*, **7**, 1-358.

BRUN, J.–P. & SOKOUTIS, D. 2004: North Aegean extension: From the Rhodope Core Complex to Neogene basins. In *Proceedings of the 5th International Symposium on Eastern Mediterranean Geology* (eds. A. A. Chatzipetros and S. B. Pavlides) Thessaloniki, Greece, April 14-20, 2004, Ref: T1-26.

BURG, J.-P., GODFRIAUX, I., & RICOU, L. -E., 1995: Extension of the Mesozoic Rhodope thrust units in the Vertiskos-Kerdillion Massifs (Northern Greece). *Comptes Rendus de l'Academie des Sciences, Serie II. Sciences de la Terre et des Planetes*, **320**, 889–896.

BURG, J. -P., RICOU, L. -E., IVANOV, Z., GODFRIAUX, I., DIMOV, D., & KLAIN, L. 1996: Syn-metamorphic nappe complex in the Rhodope Massif. Structure and Kinematics. *Terra Nova*, **8**, 6–15.

CHAPPELL, B. W. & WHITE, A. J. R. 1974: Two contrasting granite types. *Pacific Geology*, **8**, 173-174.

CHAPPELL, B. W. & WHITE, A. J. R. 2001: Two contrasting granite types: 25 years later. *Australian Journal of Earth Sciences*, **48**, 489-499.

CELET, P. & FERRIÈRE, J. 1978: Les Hellénides internes: Le Pèlagonien. *Eclogae Geologicae Helvetiae*, **73**, 467-495.

CHEN, F., SIEBEL, W., SATIR, M., TERZIOGLU, M. N. & SAKA, K. 2002: Geochronology of the Karadere basement (NW Turkey) and implications for the geological evolution of the Istanbul Zone. *International Journal of Earth Sciences* **91**, 469-481.

CHERNIAK, D. J. & WATSON, E. B. 2000: Pb diffusion in zircon. *Chemical Geology*, **172**, 5-24.

CHERNIAK, D. J., WATSON, E. B., GROVE, M. & HARRISON, T. M. 2004: Pb diffusion in monazite: A combined RBS/SIMS study. *Geochimica et Cosmochimica Acta*, **68**, 829-840.

CHRISTOFIDES, G., SOLDATOS, T. & KORONEOS, A. 1990: Geochemistry and Evolution of the Fanos Granite, N. Greece. *Mineralogy and Petrology*, **43**, 49-63.

COCHERIE, A. & ALBAREDE, F. 2001: An improved U-Th-Pb age calculation for electron microprobe dating of monazite. *Geochimica et Cosmochimica Acta*, **65**, 4509-4522.

COMPSTON, W. 1999: Geological age by instrumental analysis: the 29th Hallimond Lecture. *Mineralogical Magazine*, **63**, 297-311.

COMPSTON, W., WILLIAMS, I. S. AND MEYER, C. 1984: U-Pb geochronology of zircons from lunar breccia 73217 using a sensitive high mass-resolution ion microprobe. *Journal of Geophysical Research*, **89** supplement, B525-B534.

CONEY, P. J., JONES, D. L. & MONGER, J. W. H. 1980: Cordilleran suspect terranes. *Nature*, **270**, 329-333.

CONNELLY, J. N. 2000: Degree of igneous zonation in zircon as a signpost for concordancy in U/Pb geochronology. *Chemical Geology*, **172**, 25-39.

CORFU, F., HANCHAR, J. M., HOSKIN, P. W. O. & KINNY, P. 2003: Atlas of zircon textures. In *Zircon* (eds. J. M. Hanchar and P. W. O. Hoskin), pp. 468-500. Reviews in Mineralogy and Geochemistry 53.

DANELIAN, T., ROBERTSON, A. H. F. & DIMITRIADIS, S. 1996: Age and significance of radiolarian sediments within basic extrusives of the marginal basin Guevgueli Ophiolite (northern Greece). *Geological Magazine*, **133**, 127-136.

DAVIES, G., GLEDHILL, A. & HAWKESWORTH, C. 1985: Upper crustal recycling in southern Britain: evidence from Nd and Sr isotopes. *Earth and Planetary Science Letters*, **75**, 1-12.

DAVIES, R., ENGLAND, P., PARSONS, B., BILLIRIS, H., PARADISSIS, D. & VEIS, G. 1997: Geodetic strain of Greece in the interval 1892-1992. *Journal of Geophysical Research*, **102**, 24571-24588.

DE BONO A. 1998: *Pelagonian margins in central Evia Island (Greece). Stratigraphy and geodynamic evolution*. Unpublished PhD thesis, Lausanne University, 114 pp.
http://www-ss.unil.ch/publications/pdf/phd_debono.pdf

DE BONO A., MARTINI R., ZANINETTI L., HIRSCH F., STAMPFLI G. M. & VAVASSIS I. 2001: Permo-Triassic stratigraphy of the pelagonian Zone in central Evia island (Greece). *Eclogae Geologicae Helvetiae*, **94**, 289-311.

DE LA ROCHE, H., LETERRIER, J., GRANDE CLAUDE, P. & MARCHAL, M. 1980: A classification of volcanic and plutonic rocks using R1-R2 diagrams and major element analyses – its relationship and current nomenclature. *Chemical Geology*, **29**, 183-210.

DEPAOLO, D. J. 1981: Neodymium isotopes in the Colorado Front Range and crust-mantle evolution in the Proterozoic. *Nature*, **291**, 193-196.

Dimitriadis, S. & Asvesta, A. 1993: Sedimentation and magmatism related to the Triassic rifting and later events in the Vardar-Axios Zone. *Bulletin of the Geological Society of Greece*, **28**,149-168.

DIMITRIJEVIC, M. D. 1997: *Geology of Yugoslavia*. Special publication – Geological Institute GEMINI, Belgrade, 187 pp.

DIXON, J. E. & DIMITRIADIS, S. 1984: Metamorphosed ophiolitic rocks from the Serbo-Macedonian Massif, near lake Volvi, North-east Greece. In *The geological evolution of the Eastern Mediterranean* (eds. J. E. Dixon and A. H. F. Robertson), pp. 603–618. Geological Society of London Special Publication no. 17.

D'LEMOS, R. S. & BROWN, M. 1993: Sm-Nd isotope characteristics of late Cadomian granite magmatism in northern France and the Channel Islands. *Geological Magazine*, **130**, 797-804.

DÜRR, S. 1975: *Über Alter und geotektonische Stellung des Menderes-Kristallins/SW-Anatolien und seine Aequivalente in der mittleren Aegaeis*. Habilitations-Schrift, Universität Marburg.

DULSKI, P. 2001: Reference materials for geochemical studies: new analytical data by ICP-MS and critical discussion of reference values. *Geostandards Newsletter*, **25**, 87-125.

ENGEL, M. & REISCHMANN, T. 1998: Single-zircon Geochronology of the orthogneisses from Paros, Greece. *Bulletin of the Geological Society of Greece*, **32**, 91-99.

ENGEL, M. & REISCHMANN, T. 1999: Geochronology of the pre-alpine basement of the central Cyclades, Greece. *Journal of Conference Abstracts*, **4**, 806, EUG 10.

FERENTINOS, G. C. 1973: The Geology - Petrology of the Island of Skiathos. *Bulletin of the Geological Society of Greece*, **10**, 323-358.

FAURE, G. 1986: *Principles of isotope geology*. 2nd edition, John Wiley & Sons, New York, 589 pp.

FERRIÈRE, J., BONNEAU, M., CARIDROIT, M., BELLIER, J.-P., GORICAN, S. & KOLLMANN, H. 2001: Les nappes tertiaires du Paikon (zone du Vardar, Macédoine, Grèce): arguments stratigraphiques pour une nouvelle interprétation structurale. *Comptes Rendues de l'Académie des Sciences (Paris), Earth and Planetary Sciences*, **332**, 695-702.

FINGER, F. & STEYRER, H. P. 1990. I-type granitoids as indicators of a late Paleozoic convergent ocean-continent margin along the southern flank of the central European Variscan orogen. *Geology*, **18**, 1207-1210.

FINGER, F., HANŽL, P., PIN, C., VON QUADT, A. & STEYRER, H. P. 2000: The Brunovistulian: Avalonian Precambrian sequence at the eastern end of the Central European Variscides? In *Orogenic Processes: Quantification and Modelling in the Variscan Belt* (eds. W. Franke, V. Haak, O. Oncken and D. Tanner), pp.103-112. Geological Society of London Special Publication no. 179.

FINGER, F., BROSKA, I., HAUNSCHMID, B., HRASKO, L., KOHÚT, M., KRENN, E., PETRÍK, I., RIEGLER, G. & UHER, P. 2003: Electron-microprobe dating of monazites from Western Carpathian basement granitoids: plutonic evidence for an important Permian rifting event subsequent to Variscan crustal anatexis. *International Journal of Earth Sciences*, **92**, 86-98.

FÖRSTER, H.-J., TISCHENDORF, G. & TRUMBULL, R. B. 1997: An evaluation of the Rb vs. (Y + Nb) discrimination diagram to infer tectonic setting of silicic igneous rocks. *Lithos*, **40**, 261-293.

FOSTER, G., GIBSON, H.D., PARRISH, R., HORSTWOOD, M., FRASER, J. & TINDLE, A. 2002: Textural, chemical and isotopic insights into the nature and behaviour of metamorphic monazite. *Chemical Geology*, **191**, 183-207.

FRIEDL, G., FINGER, F., MCNAUGHTON, N. J. & FLETCHER, I. R. 2000: Deducing the ancestry of terranes: SHRIMP evidence for South America derived Gondwana fragments in central Europe. *Geology*, **28**, 1035-1038.

FROST, B. R., BARNES, C. G., COLLINS, W. J., ARCULUS, R. J., ELLIS, D. J. & FROST, C. D. 2001: A geochemical classification for granitic rocks. *Journal of Petrology*, **42**, 2033-2048.

FYTIKAS, M., GIULIANI, O., INNOCENTI, F., MANETTI, P., MAZZUOLI, R., PECCERILLO, A. & VILLARI, L. 1980: Neogene volcanism of the northern and central aegean region. *Annales Géologiques des Pays Helleniques*, **30**, 106-129.

GAUTIER, P. & BRUN, J.–P. 1994: Crustal-scale geometry and kinematics of late-orogenic extension in the central Aegean (Cyclades and Ewia Island. *Tectonophysics*, 238, 399-424.

GAUTIER, P., BRUN, J.–P., MORICEAU, R., SOKOUTIS, D., MARTINOD, J. & JOLIVET, L. 1999: Timinig, kinematics and cause of Aegean extension : a scenario based on a comparison with simple analogue experiments. *Tectonophysics*, 315, 31-72.

GESSNER, K., COLLINS, A. S., RING, U. & GÜNGÖR, T. 2004: Structural and thermal history of poly-orogenic basement: U-P geochronology of granitoid rocks in the southern Menderes Massif, Western Turkey. *Journal of the Geological Society, London*, 161, 93-101.

GIBBONS, W. & HORÁK, J. M. 1996: The Evolution of the Neoproterozoic Avalonian Subduction System: Evidence from the British Isles. In *Avalonia and related peri-Gondwana terranes of the circum-North Atlantic* (eds. R. D. Nance and M. D. Thompson), pp. 269-280. Geological Society of America Special Papers 304.

GODFRIAUX, I. & RICOU, L.-E. 1991: Le Paikon, une fenêtre tectonique dans les Hellénides Internes (Macédoine, Grèce). *Comptes Rendues de l'Académie des Sciences (Paris)*, 313, Série II, 1479-1484.

GOVINDARAJU, K. 1994: 1994 compilation of working values and sample description for 383 geostandards. *Geostandards Newsletter*, 18, special issue, 158 pp.

GRAF, J. 2001: Alpine tectonics in western Bulgaria: Cretaceous compression of the Kraište region and Cenozoic exhumation of the crystalline Osogovo-Lisec Complex. Thesis, Dissertation Naturwissenschaften ETH Zürich, Nr. 14238, 185 pp.
http://e-collection.ethbib.ethz.ch/show?type=diss&nr=14238

GRAVIOU, P. & AUVRAY, B. 1990. Late Precambrian M-type granitoid genesis in the Cadomian belt of NW France. In *The Cadomian orogeny* (eds. R. S. D'Lemos, R. A. Strachan and C. G. Topley), pp. 231-244. Geological Society of London Special Publication no. 51.

GUERROT, C. & PEUCAT, J. J. 1990: U-Pb geochronology of the Upper Proterozoic Cadomian orogeny in the northern Armorican Massif, France. In *The Cadomian orogeny* (eds. R. S. D'Lemos, R. A. Strachan & C. Topley), pp. 13-26. Geological Society of London Special Publication no. 51.

GUEVARA, M., VERMA, S. P. & VALESCO-TAPIA, F. 2001: Evaluation of GSJ intrusive rocks JG1, JG2, JG3, JG1a, and JGb1 by an objective outlier rejection statistical procedure. *Revista Mexicana de Ciencias Geológicas*, 18, 74-88.

GUMANN, S., LAHAYE, Y. & BREY, G. P. 2003: Iridium-Strip – Rhyolite enthüllen ihre Details. *Berichte der Deutschen Mineralogischen Gesellsch*aft, *Beiheft zum European Journal of Mineralogy*, 15, 72.

HANCHAR, J. M. & MILLER, C. F. 1993: Zircon zonation patterns as revealed by cathodoluminescence and backscattered electron images : Implications for interpretation of complex crustal histories. *Chemical Geology*, 110, 1-13.

HEGNER, E. & KRÖNER, A. 2000: Review of Nd isotopic data and xenocrystic and detrital zircon ages from the pre-Variscan basement in the eastern Bohemian Massif: speculations on palinspastic reconstructions. In *Orogenic Processes: Quantification and Modelling in the Variscan Belt* (eds. W. Franke, V. Haak, O. Oncken and D. Tanner), pp.113-129. Geological Society of London Special Publication no. 179.

HETZEL, R. & REISCHMANN, T. 1996: Intrusion age of Pan-African augen gneisses in the southern Menderes Massif and the age of cooling after Alpine ductile extensional deformation. *Geological Magazine*, 133, 565-572.

HIMMERKUS, F., REISCHMANN, T. & KOSTOPOULOS, D. 2003: The Serbo-Macedonian Massif, the oldest crustal segment of the Internal Hellenides, identified by zircon ages. *Geophysical Research Abstracts*, 5, 05671.

HIMMERKUS F., REISCHMANN T. & KOSTOPOULOS D. 2004a: The Pirkadikia Unit, the oldest crustal segment in the Serbo-Macedonian terrane assemblage. In *Proceedings of the 5th International Symposium on Eastern Mediterranean Geology* (eds. A. A. Chatzipetros and S. B. Pavlides) Thessaloniki, Greece, April 14-20, 2004, Ref: T1-63.

HIMMERKUS, F., REISCHMANN, T. & KOSTOPOULOS, D. 2004b: Triassic rifting recorded in Gondwana derived Tethyan terranes, Serbo-Macedonian Massif, northern Greece. *Berichte der Deutschen Mineralogischen Gesellschaft, Beiheft zum European Journal of Mineralogy*, **16**, 57.

HIMMERKUS F., ZACHARIADIS, P., REISCHMANN T. & KOSTOPOULOS D. 2005: The mafic complexes of the Athos-Volvi-Zone – a suture zone between the Serbo-Macedonian Massif and the Rhodope Massif? *Geophysical Research Abstracts*, **7**, 10240.

HIMMERKUS F., REISCHMANN T. & KOSTOPOULOS D. (submitted): Late Proterozoic and Silurian basement units within the Serbo-Macedonian Massif, Greece: the significance of terrane accretion in the Hellenides. Submitted for publication in *Geological Society of London Special Publication*.

HOWELL, D. G., JONES, D. L. & CHERMER, E. R. 1985: Tectonostratigraphic terranes of the Circum-Pacific region. In *Tectonostratigraphic terranes of the Circum-Pacific region* (ed. D. G. Howell), pp.3-31. Circum-Pacific Council for Energy and Mineral Resources, Earth Science Series, 1.

IGME 1982: Geological Map of Greece, sheet Skra, scale 1:50 000, Institute of Geology and Mineral Exploration, Athens.

IGME 1983: Geological Map of Greece, scale 1:500 000, Institute of Geology and Mineral Exploration, Athens.

IGME 1993: Geological Map of Greece, sheet Evzoni, scale 1:50 000, Institute of Geology and Mineral Exploration, Athens.

IMAI, N., TERASHIMA, S., ITHO, S. & ANDO, A. 1995: 1994 compilation of analytical data for minor and trace elements in seventeen GSJ geochemical reference samples, "Igneous Rock Series". *Geostandards Newsletter*, **19**, 135-213.

JACOBSHAGEN, V. 1986: *Geologie von Griechenland*. Gebrueder Borntraeger, Berlin/Stuttgart, 363 pp.

JOCHUM, K. P., STOLL, B., HERWIG, K. & AMINI, M. (submitted): Trace element and isotope analyses of geo- and cosmochemical samples by laser ablation-sector field-ICPMS. Submitted in October 2004 for publication in *High Resolution ICP-MS* (ed. C. B. Douthitt).

JOLIVET, L. 2001: A comparison of geodetic and finite strain pattern in the Aegean, geodynamic implications. *Earth and Planetary Science Letters*, **187**, 95-104.

KAHLE, H. G., COCARD, M., PETER, Y., GEIGER, A., REILINGER, R., BARKA, A. & VEIS, G. 2000: GPS-derived strain rate fixed within the boundary zones of the Eurasian, African and Arabian Plates. *Journal of Geophysical Research*, **105**, 23353-23370.

KATERINOPOULOS, A. & KYRIAKOPOULOS, K. 1989: Petrographic and petrochemical study of the plutonic rocks from the Baba Mountain (Yugoslavia). *Bulletin of the Geological Society of Greece*, **23**, 561-576 (in greek with english abstract).

KATERINOPOULOS, A., KYRIAKOPOULOS, K., DEL MORO, A., MITROPOULOS, P. & GIANNOTTI, U. 1992: Comparative study of Hercynian granitoids from N.W. Greece and S. Yugoslavia. *Chemie der Erde*, **52**, 261-276.

KATERINOPOULOS, A., KOKKINAKIS, A. & KYRIAKOPOULOS, K. 1996: Mineralogy, Petrology and Geochemistry of the Fotino Granitic Rocks, Thessaly, Central Greece. *Slovak Geological Magazine*, **2**, 87-101.

KATERINOPOULOS, A., KYRIAKOPOULOS, K., DEL MORO, A., KOKKINAKIS, A. & GIANNOTTI, U. 1998: Petrology, Geochemistry and Rb/Sr Age Determination of Hercynian Granitic Rocks from Thessaly, Central Greece. *Chemie der Erde*, **58**, 64-79.

KAUFFMANN, G. 1976: Perm und Trias im östlichen Mittelgriechenland und auf einigen ägäischen Inseln. *Zeitschrift der Deutschen Geologischen Gesellschaft*, **127**, 387-398.

KAUFFMANN, G., KOCKEL, F. & MOLLAT, H. 1976: Notes on the stratigraphic and palaeogeographic position of the Svoula Formation in the Innermost Zone of the Hellenides (Northern Greece). *Bulletin de la Société Géologique de France*, **18**, 225–230.

KEPPIE, J. D., DAVIS, D. W. & KROGH, T. E. 1998: U-Pb geochronological constraints on Precambrian stratified units in the Avalon Composite Terrane of Nova Scotia, Canada: tectonic implications. *Canadian Journal of Earth Sciences*, **35**, 222-236.

KILIAS, A. 1980: *Geologische und tektonische Untersuchung des Gebietes von östlichen Varnous (NW Makedonian)*. unpublished Ph.D. thesis, University of Thessaloniki, Greece, 271 pp.

KILIAS, A. & MOUNTRAKIS, D. 1989: The Pelagonian Nappe. Tectonics, metamorphism and magmatism. *Bulletin of the Geological Society of Greece*, **23**, 29-46 (in greek with english abstract).

KILIAS, A., FALALAKIS, G. & MOUNTRAKIS, D. 1999: Cretaceous-Tertiary structures and kinematics of the Serbomacedonian metamorphic rocks and their relation to the exhumation of the Hellenic hinterland (Macedonia, Greece). *International Journal of Earth Sciences*, **88**, 513–531.

KIRIAKIDIS, L. G. 1989: The Vardar ophiolite: a continuous belt under the Axios basin sediments. *Geophysical Journal International*, **98**, 203-212.

KOBER, B. 1986: Whole-grain evaporation for $^{207}Pb/^{206}Pb$-age-investigations on single zircons using a double-filament thermal ion source. *Contributions to Mineralogy and Petrology*, **93**, 482-490.

KOBER, B. 1987: Single-zircon evaporation combined Pb^{+}emitter-bedding for $^{207}Pb/^{206}Pb$-age investigations using thermal ion mass spectrometry, and applications to zirconology. *Contributions to Mineralogy and Petrology*, **96**, 63-71.

KOCKEL, F. & MOLLAT, H. (mit einem Beitrag von H. W. Walther) 1977: *Erläuterungen zur Geologischen Karte der Chalkidiki und angrenzender Gebiete 1:100 000, Nordgriechenland*. Bundesanstalt für Geowissenschaften und Rohstoffe, Hannover, 119 pp.

KONDOPOULOU, D. 2000: Palaeomagnetism in Greece: Cenozoic and Mesozoic components and their geodynamic implications. *Tectonophysics*, **326**, 131-151.

KORONEOS, A., CHRISTOFIDES, G., DEL MORO, A. & KILIAS, A. 1993: Rb-Sr geochronology and geochemical aspects of the Eastern Varnountas plutonite (NW Macedonia, Greece). *Neues Jahrbuch für Mineralogie, Abhandlungen*, **165**, 297-315.

KOSTOPOULOS, D. K. 1988: *Geochemistry, petrogenesis and tectonic setting of the Pindos Ophiolite, NW Greece*. Unpublished Ph.D. Thesis, University of Newcastle-upon-Tyne, UK, 528 pp.

KOSTOPOULOS, D. K., IOANNIDIS, N. M. & SKLAVOUNOS, S. A. 2000: A new occurrence of ultrahigh-pressure metamorphism, central Macedonia, northern Greece: evidence from graphitized diamonds? *International Geology Review*, **42**, 545-554.

KOTOPOULI, C. N., PE-PIPER, G. & PIPER, D. J. W. 2000: Petrology and evolution of the Hercynian Pieria granitoid complex (Thessaly, Greece); paleogeographic and geodynamic implications. *Lithos*, **50**, 137-152.

KRÖNER, A., LINNEBACHER, P., STERN, R. J., REISCHMANN, T., MANTON, W. & HUSSEIN, I. M. 1991: Evolution of Pan-African island arc assemblages in the southern Red Sea Hills, Sudan, and in southwestern Arabia as exemplified by geochemistry and geochronology. *Precambrian Research*, **53**, 99-118.

KRÖNER, A., KRÜGER, J. & RASHWAN, A. A. A. 1994: Age and tectonic setting of granitoid gneisses in the Eastern Desert of Egypt and south-west Sinai. *Geologische Rundschau*, **83**, 502-513.

KRÖNER, A., STIPSKA, P., SCHULMANN, K. & JAECKEL, P. 2000: Chronological constraints on the pre-Variscan evolution of the northeastern margin of the Bohemian Massif, Czech Republic. In *Orogenic Processes: Quantification and Modelling in the Variscan Belt* (eds. W. Franke, V. Haak, O. Oncken and D. Tanner), pp. 175-197. Geological Society of London Special Publication no. 179.

KROGH, T. E. 1973: A low-contamination method for hydrothermal decomposition of zircon and extraction of U and Pb for isotopic age determinations. *Geochimica et Cosmochimica Acta*, **37**, 485-494.

LEE, J. K. W., WILLIAMS, I. S. & ELLIS, D. J. 1997: Pb, U and Th diffusion in natural zircon. *Nature*, **390**, 159-161.

LE PICHON, X. & ANGELIER, J. 1979: The Hellenic arc and trench system: a key to the neotectonic evolution of the Eastern Mediterranean area. *Tectonophysics*, **60**, 1-42.

LE PICHON, X. & ANGELIER, J.,1981: The Aegean Sea. *Philosophical Transactions of the Royal Society of London, A 300*, 1454, 357-372.

LE PICHON, X., CHAMOT-ROOKE, N., LALLEMENT, S., NOOMEN, B. & VEIS, G., 1995. Geodetic determination of the kinematics of central Greece with respect to Europe: Implications for Eastern Mediterranean tectonics. *Journal of Geophysical Research*, **100**, 12675-12690.

LIATI, A., GEBAUER, D. & FANNING, C. M. 2004: The age of ophiolitic rocks of the Hellenides (Vourinos, Pindos, Crete): first U-Pb ion microprobe (SHRIMP) zircon ages. *Chemical Geology*, **207**, 171-188.

LIEW, T. C. & HOFMANN, A. W. 1988: Precambrian crustal components, plutonic associations, plate environment of the Hercynian Fold Belt of central Europe: Indications from a Nd and Sr isotopic study. *Contributions to Mineralogy and Petrology,* **98**, 129-138.

LIEW, T. C., FINGER, F. & HÖCK, V. 1989: The Moldanubian granitoid plutons of Austria: Chemical and isotopic studies bearing on their environmental setting. *Chemical Geology*, **76**, 41-55.

LINNEMANN, U., GEHMLICH, M., TICHOMIROWA, M., BUSCHMANN, B., NASDALA, L., JONAS, P., LÜTZNER, H. & BOMBACH, K. 2000: From Cadomian subduction to Early Palaeozoic rifting: the evolution of Saxo-Thuringia at the margin of Gondwana in the light of single-zircon geochronology and basin development (Central European Variscides, Germany). In *Orogenic Processes: Quantification and Modelling in the Variscan Belt* (eds. W. Franke, V. Haak, O. Oncken and D. Tanner), pp. 131-153. Geological Society of London Special Publication no. 179.

LINNEMANN, U., MCNAUGHTON, N. J., ROMER, R. L., GEHMLICH, M., DROST, K. & TONK, C. 2004: West African provenance for Saxo-Thuringia (Bohemian Massif): Did Armorica ever leave the pre-Pangean Gondwana? – U/Pb-SHRIMP zircon evidence and the Nd-isotopic record. *International Journal of Earth Sciences*, **93**, 683-705.

Lips, A. L. W., White, S. H. & Wijbrans, J. R. 1998: $^{40}Ar/^{39}Ar$ laserprobe dating of discrete deformational events: a continuous record of early Alpine tectonics in the Pelagonian Zone, NW Aegean area, Greece. *Tectonophysics*, **298**, 133-153.

LISTER, G. S., BANGA, G. & FEENSTRA, A. 1984: Metamorphic core complexes of cordilleran type in the Cyclades, Aegean Sea, Greece. *Geology*, **12**, 221-225.

LOOS, S. & REISCHMANN, T. 1999: The evolution of the Menderes Massif in SW Turkey as revealed by zircon dating. *Journal of the Geological Society, London*, **156**, 1021-1030.

LUDWIG, K. R. 2001: SQUID 1.02. Berkeley Geochronological Center, Special Publication No. 2.

LUDWIG, K. R. 2003: Isoplot/Ex 3.00. A geochronological toolkit for Microsoft Excel. Berkeley Geochronological Center, Special Publication No. 4.

MARAKIS, G. 1969: Geochronological studies of some granites from Macedonia (in greek with english summary). *Annales Géologiques des Pays Helleniques*, **21**, 121-152.

MARRO, C. 1988: Organisation géochimique et intrusion du granite du Mont Blanc et de deux leucogranites. *Schweizerische Mineralogische und Petrographische Mitteilungen*, **68**, 521-529.

MATTINSON, J. M., GRAUBARD, C. M., PARKINSON, D. L. & MCLELLAND, W. C. 1996: U-Pb reverse discordance in zircons: the role of fine-scale oscillatory zoning and sub-microscopic transport of Pb. *American Geophysical Union, Geophysical Monograph*, **95**, 355-370.

MCNAMARA, A. K., NIOCAILL, C. M., VAN DER PLUIJM, B. A. & VAN DER VOO, R. 2001: West African proximity of the Avalon terrane in the latest Precambrian. *Geological Society of America Bulletin*, **113**, 1161-1170.

MEERT, J. G. 2003: A synopsis of events related to the assembly of eastern Gondwana. *Tectonophysics*, **362**, 1-40.

MELENTIS, J. K. 1973: Die Geologie der Insel Skyros. *Bulletin of the Geological Society of Greece*, **10**, 298-322. (in greek with german summary)

MERCIER, J. 1966: Mouvements orogeniques et magmatisme d'age Jurassique Supérieur-Éocrétacé dans les Zones Internes des Hellénides (Macédoine, Grèce): *Revue de Geographie Physique et de Géologie Dynamique (2)*, **VIII**, 265-278.

MERCIER, J. 1968: Étude géologique des zones internes des Hellénides en Macédoine centrale (Grèce). Contribution a l'étude du métamorphisme et de l'évolution magmatique des zones internes des Hellénides. *Annales Géologiques des Pays Helléniques,* **20**, 1-792.

MERCIER, J. & VERGÉLY, P. 1994: Is the Paikon Massif a tectonic window in the Axios-Vardar Zone? (Internal Hellenides, Macedonia, Greece). *Bulletin of the Geological Society of Greece*, **30**, 115-120.

MERCIER, J., VERGÉLY, P. & BÉBIEN, J. 1975: Les ophiolites hellénique «obductées» au Jurassique supérieur sont-elles les vestiges d'un Océan téthysien ou d'une mer marginale péri-européene? *Comptes Rendues sommaires de la Société Géologique de France*, **17**, 108-112.

MEZGER, K. & KROGSTAD, E. J. 1997: Interpretation of discordant U-Pb zircon ages: An evaluation. *Journal of Metamorphic Geology*, **15**, 127-140.

MICHARD, A., GURRIET, P., SOUDANT, M. & ALBAREDE, F. 1985: Nd isotopes in French Phanerozoic shales: external vs. internal aspects of crustal evolution. *Geochimica et Cosmochimica Acta*, **49**, 601-610.

MICHARD, A., GOFFÉ, B., LIATI, A. & MOUNTRAKIS, D. 1994: Blueschist-facies assemblages in the peri-Rhodopian zone, and hints for an eohellenic HP-LT belt in northern Greece. *Bulletin of the Geological Society of Greece*, **30**, 185-192.

MIGIROS, G. & GALEOS, A. 1990: Tectonic and stratigraphic significance of the Ano Garefi ophiolitic rocks, (Northern Greece). In *Ophiolites, oceanic crustal analogues: proceedings of the symposium "Troodos 1987"* (eds. J. Malpas, E. M. Moores, A. Panayiotou and C. Xenophontos), pp. 279-284. Geological Survey Department, Cyprus.

MIYASHIRO, A., AKI, K. & ŞENGÖR, A. M. C. 1982: *Orogeny*. John Wiley & Sons, 242 pp.

MÖLLER, A., O'BRIEN, P. J., KENNEDY, A. & KRÖNER, A. 2003: The use and abuse of Th-U ratios in the interpretation of zircon. *Geophysical Research Abstracts*, **5**, 12113.

MONTEL, J.-M., FORET, S., VESCHAMBRE, M., NICOLLET, C. & PROVOST, A. 1996. Electron microprobe dating of monazite. *Chemical Geology*, **131**, 37-53.

MOST, T., FRISCH, W., DUNKL, I., KADOSA, B., BOEV, B., AVGERINAS, A. & KILIAS, A. 2001: Geochronological and structural investigations of the Northern Pelagonian Crystalline Zone. Constraints from K/Ar and zircon and apatite fission track dating. *Bulletin of the Geological Society of Greece*, **34**, 91-95.

MOST, T. 2003: *Geodynamic Evolution of the Eastern Pelagonian Zone in northwestern Greece and the Republic of Macedonia. Implications from U/Pb, Rb/Sr, K/Ar, $^{40}Ar/^{39}Ar$ geochronology and fission track thermochronology*. published Ph.D. thesis, Universität Tübingen.
URN: urn:nbn:de:bsz:21-opus-7057, URL: http://w210.ub.uni-tuebingen.de/dbt/volltexte/2003/705/

MOUNTRAKIS, D. 1982: Étude géologique des terrains métamorphiques de Macédoine occidentale (Grèce). *Bulletin de la Société Géologique de France*, **24**, 697-704.

MOUNTRAKIS, D. 1984: Structural evolution of the Pelagonian Zone in Northwestern Macedonia, Greece. In *The geological evolution of the Eastern Mediterranean* (eds. J. E. Dixon and A. H. F. Robertson), pp. 581-590. Geological Society of London Special Publication no. 17.

MOUNTRAKIS, D. 1986: The Pelagonian Zone in Greece: a polyphase-deformed fragment of the Cimmerian Continent and its role in the geotectonic evolution of the eastern Mediterranean. *Journal of Geology*, **94**, 335-347.

MOUNTRAKIS, D., ELEFTHERIADIS, G., CHRISTOFIDES, G., KILIAS, A. & SAPOUNTZIS, E. 1987: Silicic Metavolcanics in the Western Pelagonian Margin of Greece Related to the Opening of Neo-Tethys. *Chemie der Erde*, **47**, 167-179.

MPOSKOS, E. D. & KOSTOPOULOS, D. K. 2001: Diamond, former coesite and supersilicic garnet in metasedimentary rocks from the Greek Rhodope: A new ultrahigh-pressure metamorphic province established. *Earth and Planetary Science Letters*, **192**, 497-506.

MURPHY, J. B. & NANCE, R. D. 2002: Sm-Nd isotopic systematics as tectonic tracers: an example from West Avalonia in the Canadian Appalachians. *Earth-Science Reviews*, **59**, 77-100.

MURPHY, J. B., KEPPIE, J. D., DOSTAL, J. & NANCE, R. D. 1999: Neoproterozoic-early Palaeozoic evolution of Avalonia. In *Laurentia-Gondwana Connections before Pangea* (eds. V. A. Ramos and J. D. Keppie), pp. 253-266. Geological Society of America Special Papers 336.

MUSSALLAM, K. & JUNG, D. 1986a: Petrology and Geotectonic Significance of Salic Rocks Preceding Ophiolites in the Eastern Vardar Zone, Greece. *Tschermaks Mineralogische und Petrographische Mitteilungen*, **35**, 217-242.

MUSSALLAM, K. & JUNG, D. 1986b: Geologie und Bau des Sithonia-Ophiolits (Chalkidiki, NE-Griechenland): Anmerkungen zur Bildung ozeanischer Krusten. *Geologische Rundschau*, **75**, 383-409.

NANCE, R. D. & MURPHY, J. B. 1994: Contrasting basement isotopic signatures and the palinspastic restoration of peripheral orogens: Example from the Neoproterozoic Avalonian-Cadomian belt. *Geology*, **22**, 617-620.

NANCE, R. D. & MURPHY, J. B. 1996: Basement isotopic signatures and Neoproterozoic paleogeography of Avalonian-Cadomian and related terranes in the circum-North Atlantic. In *Avalonia and related peri-Gondwana terranes of the circum-North Atlantic* (eds. R. D. Nance and M. D. Thompson), pp. 333-346. Geological Society of America Special Papers 304.

NESBITT, H. W. & YOUNG, G. M. 1982: Early Proterozoic climates and plate motions inferred from major element chemistry of lutites. *Nature*, **299**, 715-717.

NESBITT, H. W. & YOUNG, G. M. 1984: Prediction of some weathering trends of plutonic and volcanic rocks based on thermodynamic and kinetic considerations. *Geochimica et Cosmochimica Acta*, **48**, 1523-1543.

NESBITT, H. W. & YOUNG, G. M. 1989: Formation and diagenesis of weathering profiles. *Journal of Geology*, **97**, 129-147.

NEUBAUER, F. 2002: Evolution of late Neoproterozoic to early Paleozoic tectonic elements in central and Southeast European Alpine mountain belts: review and synthesis. *Tectonophysics*, **352**, 87–103.

O'CONNOR, J. T. 1965. A classification of quartz-rich igneous rocks based on feldspar ratios. *U.S. Geological Survey Professional Paper*, **525B**, B79-B84.

Okay, A.I., Satir, M., Tüyüz, O., Akyüz, S. & Chen, F. 2001: The tectonics of the Strandja Massif: late Variscan and mid-Mesozoic deformation and metamorphism in the northern Aegean. *International Journal of Earth Sciences*, **90**, 217-233.

ÖZMEN, F. & REISCHMANN, T. 1999: The age of the Sakarya continent in W Anatolia: Implications for the evolution of the Aegean region. *Journal of Conference Abstracts*, **4**, 805, EUG 10.

PACES, J. B. & MILLER, J. D. 1993: Precise U-Pb Ages of Duluth Complex and related mafic intrusions, northeastern Minnesota: Geochronological insights to physical, petrogenetic, paleomagnetic and tectonomagmatic processes associated with the 1.1 Ga midcontinent rift system. *Journal of Geophysical Research*, **98/B8**, 13997-14013.

PAPANIKOLAOU, D. 1997: The tectonostratigraphic terranes of the Hellenides. *Annales Géologiques des Pays Helleniques*, **37**, 495-514.

PAPANIKOLAOU, D. & PANAGOPOULOS, A. 1981: On the structural style of Southern Rhodope. *Geologica Balcanica*, **11**, 13-22.

PARRISH, R. 1990: U-Pb dating of monazite and its application to geological problems. *Canadian Journal of Earth Sciences*, **27**, 1431-1450.

PARRISH, R. 2001: The response of mineral chronometers to metamorphism and deformation in orogenic belts. In *Continental Reactivation and Reworking* (eds. J. A. Miller, R. E. Holdsworth, I. S. Buick and M. Hand), pp. 289-301. Geological Society of London Special Publications no. 184.

PEARCE, J. A., HARRIS, N. B. W. & TINDLE, A. G. 1984: Trace element discrimination diagrams for the tectonic interpretation of granitic rocks. *Journal of Petrology*, **25**, 956-983.

PE-PIPER, G. 1982: Geochemistry, tectonic setting and metamorphism of mid-Triassic volcanic rocks of Greece. *Tectonophysics*, **85**, 253-272.

PE-PIPER, G. 1991: Petrology and origin of ?Mesozoic dioritic rocks from the island of Skyros, Greece. *Ofioliti*, **16**, 111-119.

PE-PIPER, G. 1998: The nature of Triassic extension-related magmatism in Greece: evidence from Nd and Pb isotope geochemistry. *Geological Magazine*, **135**, 331-348.

PE-PIPER, G. & PIPER, D. J. W. 2002: *The igneous rocks of Greece. The anatomy of an orogen*. Gebrueder Borntraeger, Berlin/Stuttgart, 573 pp.

PE-PIPER, G., DOUTSOS, T. & MIJARA, A. 1993a: Petrology and Regional Significance of the Hercynian Granitoid rocks of the Olympiada Area, Northern Thessaly, Greece. *Chemie der Erde*, **53**, 21-36.

PE-PIPER, G., DOUTSOS, T. & MPORONKAY, C. 1993b: Structure, geochemistry and mineralogy of Hercynian granitoid rocks of the Verdikoussa area, Northern Thessaly, Greece and their regional significance. *Neues Jahrbuch für Mineralogie, Abhandlungen*, **165**, 267-296.

PEYTCHEVA, I. & VON QUADT, A. 1995: U-Pb zircon dating of metagranites from Byala-Reka region in the east Rhodopes, Bulgaria. *Special Publications of the Geological Society of Greece*, **4**, 637-642.

PEYTCHEVA, I., VON QUADT, A., OVTCHAROVA, M., HANDLER, R., NEUBAUER, F., SALNIKOVA, E., KOSTITSYN, Y., SAROV, S. & KOLCHEVA, K. 2004: Metagranitoids from the eastern part of the Central Rhodopean Dome (Bulgaria): U-Pb, Rb-Sr and $^{40}Ar/^{39}Ar$ timing of emplacement and exhumation and isotope-geochemical features. *Mineralogy and Petrology*, **82**, 1-31.

POLLER, U., JANÁK, M., KOHÚT, M. & TODT, W. 2000: Early Variscan magmatism in the Western Carpathians: U-Pb zircon data from granitoids and orthogneisses of the Tatra Mountains (Slovakia). *International Journal of Earth Sciences*, **89**, 336-349.

POLLER, U., TODT, W., KOHÚT, M. & JANÁK, M. 2001: Nd, Sr, Pb isotope study of the Western Carpathians: implications for Palaeozoic evolution. *Schweizerische Mineralogische und Petrographische Mitteilungen*, **81**, 159-174.

RACZEK, I., STOLL, B., HOFMANN, A. W. & JOCHUM, K. P. 2001: High-precision trace element data for the USGS reference materials BCR-1, BCR-2, BHVO-1, BHVO-2, AGV-1, AGV-2, DTS-1, DTS-2, GSP-1 and GSP-2 by ID-TIMS and MIC-SSMS. *Geostandards Newsletter*, **25**, 77-86.

RACZEK, I., JOCHUM, K. P. & HOFMANN, A. W. 2003: Neodymium and strontium isotope data for USGS reference materials BCR-1, BCR-2, BHVO-1, BHVO-2, AGV-1, AGV-2, GSP-1, GSP-2 and eight MPI-DING reference glasses. *Geostandards Newsletter*, **27**, 173-179.

REMANE, J., CITA, M. B., DERCOURT, J., BOUYSSE, P., REPETTE, F. & FAURET-MURET, A. (eds.) 2000: *International Stratigraphic Chart*. International Union of Geological Sciences, International Commission on Stratigraphy, UNESCO, Commission on the Geological Map of the World.

REILINGER, R., MCCLUSKY, S., ORAL, M., KING, R., TOKSOZ, N., BARKA, A., KINIK, I., LENK, O. & SANLI, I. 1997: Global Positioning System measurements of present day crustal movements in the Arabia–Africa–Eurasia plate collision zone. *Journal of Geophysical Research*, **102**, 9983-9999.

REISCHMANN, T. 1995: Precise U/Pb age determination with baddeleyite (ZrO_2), a case study from the Phalaborwa Igneous Complex, South Africa. *South African Journal of Geology*, **98**, 1-4.

REISCHMANN, T. 1998: Pre-alpine origin of tectonic units from the metamorphic complex of Naxos, Greece, identified by single-zircon Pb/Pb dating. *Bulletin of the Geological Society of Greece*, **32**, 101-111.

REISCHMANN, T. 2000: Ophiolites and island arcs in the late Proterozoic Nubian shield. *Ofioliti*, **25**, 1-13.

REISCHMANN, T., KOSTOPOULOS, D. K., LOOS, S., ANDERS, B., AVGERINAS, A., & SKLAVOUNOS, S. A. 2001: Late Palaeozoic magmatism in the basement rocks southwest of Mt. Olympos, Central Pelagonian Zone, Greece: remnants of a Permo-Carboniferous magmatic arc. *Bulletin of the Geological Society of Greece*, **34**, 985-993.

RICOU, L.-E. & GODFRIAUX, I. 1991: Une coupe à travers les ophiolites et gneiss allochtones entre le massif Pélagonien et la fenêtre du Paikon (Grèce du Nord). *Comptes Rendues de l'Académie des Sciences (Paris)*, **313**, Série II, 1595-1601.

RICOU, L.-E. & GODFRIAUX, I. 1995: Mise au point sur la fenêtre multiple du Paikon at la structure du Vardar en Grèce. *Comptes Rendues de l'Académie des Sciences (Paris)*, **321**, Série II a, 601-608.

RICOU, L.-E., BURG, J.-P., GODFRIAUX, I. & IVANOV, Z. 1998: Rhodope and Vardar: the metamorphic and the olistostromic paired belts related to the Cretaceous subduction under Europe. *Geodinamica Acta*, **11**, 285–309.

ROBERTSON, A. H. F. & DIXON, J. E. 1984: Introduction: aspects of the geological evolution of the eastern Mediterranean. In *The geological evolution of the Eastern Mediterranean* (eds. J. E. Dixon and A. H. F. Robertson), pp. 1-74. Geological Society of London Special Publication no. 17.

ROBERTSON, A. H. F. & KARAMATA, S. 1994: The role of subduction accretion processes in the tectonic evolution of the Mesozoic Tethys in Serbia. *Tectonophysics*, **234**, 73–94.

Robertson, A. H. F., Clift, P. D., Degnan, P. J. & Jones, G. 1991: Palaeogeographic and palaeotectonic evolution of the Eastern Mediterranean Neotethys. *Palaeogeography, Palaeoclimatology, Palaeoecology*, **87**, 289-343.

ROLLINSON, H. 1993: *Using geochemical data: evaluation, presentation, interpretation*. Longman, UK, 352 pp.

ROSER, B. P. & KORSCH, R. J. 1986: Determination of tectonic setting of sandstone-mudstone suites using SiO_2 content and K_2O/Na_2O ratio. *Journal of Geology*, **94**, 635-650.

ROYDEN, L. H. & PAPANIKOLAOU, D. 2004: Buoyancy of subducted lithosphere and the recent evolution of the Hellenic subduction system. *Geological Society of America, Abstracts with Programs*, **36**, 482.

RUBATTO, D. 2002: Zircon trace element geochemistry: partitioning with garnet and the link between U-Pb ages and metamorphism. *Chemical Geology,* **184**, 123-138.

RUBATTO, D. & Gebauer, D. 2000: Use of Cathodoluminescence for U-Pb Zircon Dating by Ion Microprobe: Some examples from the Western Alps. In *Cathodoluminescence in Geosciences* (eds. M. Pagel, V. Barbin, P. Blanc and D. Ohnenstetter), pp. 373-400. Springer, Heidelberg.

SCHERMAIER, A., HAUNSCHMID, B. & FINGER, F. 1997: Distribution of I- and S-type granites in the Eastern Alps: a possible clue to unravel pre-Alpine basement structures. *Tectonophysics*, **272**, 315-333.

SCHERMER, E. R. 1990: Mechanisms of blueschist creation and preservation in an A-type subduction zone, Mount Olympos region, Greece. *Geology*, **18**, 1130-1133.

SCHERMER, E. R., LUX, D. R. & BURCHFIEL, B. C. 1990: Temperature-time history of subducted continental crust, Mount Olympos region, Greece. *Tectonics*, **9**, 1165-1195.

ŞENGÖR, A. M. C. & YILMAZ, Y. 1981: Tethyan evolution of Turkey: a plate tectonic approach. *Tectonophysics*, **75**, 181-241.

ŞENGÖR, A. M.C., YILMAZ, Y. & SUNGURLU, O. 1984: Tectonics of the Mediterranean Cimmerides: nature and evolution of the western termination of Palaeo-Tethys. In *The geological evolution of the Eastern Mediterranean* (eds. J. E. Dixon and A. H. F. Robertson), pp. 603-618. Geological Society of London Special Publication no. 17.

SCHÜNEMANN, M. 1985: *Contributions to the geology, geochemistry and tectonics of the Chortiatis Series metamorphic calc-alkaline suite, Chalkidiki, Northern Greece*. PhD thesis, University of Hamburg.

SHAND, S. J. 1951: *Eruptive rocks*. 4th edition, New York, John Wiley, 488 pp.

SHARP, I. & ROBERTSON, A. 1994: Late Jurassic – Lower Cretaceous oceanic crust and sediments of the eastern Almopias Zone, NW Macedonia (Greece) ; implications for the evolution of the eastern "Internal" Hellenides. *Bulletin of the Geological Society of Greece*, **30**, 47-61.

SMITH, H. A. & GILETTI, B. J. 1997: Lead diffusion in monazite. *Geochimica et Cosmochimica Acta*, **61**, 1047-1055.

SOLDATOS, T., KORONEOS, A. & CHRISTOFIDES, G. 1993: Origin and evolution of the Fanos granite (Macedonia, northern Greece): Trace and REE modelling constraints. In *Special Volume in honour of Professor A. G. Panagos* (ed. N. Konispoliatis), pp. 789-812. National Technical University of Athens Scientific Publications, Athens, Greece, volume B.

SPRAY, J. G., BÉBIEN, J., REX, D. C. & RODDICK, J. C. 1984: Age constraints on the igneous and metamorphic evolution of the Hellenic-Dinaric ophiolites. In *The geological evolution of the Eastern Mediterranean* (eds. J. E. Dixon and A. H. F. Robertson), pp. 619-627. Geological Society of London Special Publication no. 17.

STACEY, J. S. & KRAMERS, J. D. 1975: Approximation of terrestrial lead isotope evolution by a two-stage model. *Earth and Planetary Science Letters*, **26**, 207-221.

STAIS, A. & FERRIÉRE, J. 1991: Nouvelles donnees sur la paleogeographie mesozoique du domaine Vardarien: Les bassins d'Almopias et de Peonias (Macédoine, Helleniques Internes Septentrionales). *Bulletin of the Geological Society of Greece*, **25**, 491-507

STAMPFLI, G. M. & BOREL, G. D. 2002: A plate tectonic model for the Paleozoic and Mesozoic constrained by dynamic plate boundaries and restored synthetic oceanic isochrons. *Earth and Planetary Science Letters*, **196**, 17-33.

STAMPFLI, G. M., ROSSELET, F., & BAGHERI, S. 2004: Tethyan oceans and sutures. In *Proceedings of the 5th International Symposium on Eastern Mediterranean Geology* (eds. A. A. Chatzipetros and S. B. Pavlides) Thessaloniki, Greece, April 14-20, 2004, Ref: T1-21.

TAIT, J. A., BACHTADSE, V., FRANKE, W. & SOFFEL, H. C. 1997: Geodynamic evolution of the European Variscan fold belt: palaeomagnetic and geological constraints. *Geologische Rundschau*, **86**, 585-598.

TEKLAY, M., KRÖNER, A., MEZGER, K. & OBERHÄNSLI, R. 1998: Geochemistry, Pb-Pb single-zircon ages and Nd-Sr isotope composition of Precambrian rocks from southern and eastern Ethiopia: implications for crustal evolution in East Africa. *Journal of African Earth Sciences*, **26**, 207-227.

THOROGOOD, E. J. 1990: Provenance of pre-Devonian sediments of England and Wales: Sm-Nd isotopic evidence. *Journal of the Geological Society, London*, **147**, 591-594.

TITORENKOVA, R., MACHEVA, L. ZIDAROV, N., VON QUADT, A. & PEYTCHEVA, I. 2003: Metagranites from SW Bulgaria as a part of the Neoproterozoic to Early Paleozoic system in Europe: New insight from zircon typology, U-Pb isotope data and Hf-tracing. *Geophysical Research Abstracts*, **5**, 08963.

TOBISCH, O. T., BARTON, M. D., VERNON, R. H. & PATERSON, S. R. 1991: Fluid-enhanced deformation: transformation of granitoids to banded mylonites, western Sierra Nevada, California, and southeastern Australia. *Journal of Structural Geology*, **13**, 1137-1156.

TURPAUD, P. & REISCHMANN, T. 2003: Zircon ages of granitic gneisses from the Rhodope (N. Greece), determination of basement age and evidences for a Cretaceous intrusive event. *Geophysical Research Abstracts*, **5**, 04435.

TURPAUD, P. & REISCHMANN, T. 2005: Relationships between crustal blocks and UHP relics, an example from Northern Greece. *Geophysical Research Abstracts*, **7**, 04353.

USGS: United States Geological Survey Certificate of Analysis, Granodiorite, Silver Plume, Colorado, GSP-2. Preliminary. http://minerals.cr.usgs.gov/geo_chem_stand/granodiorite.html

VAVASSIS, I., DE BONO, A., STAMPFLI, G. M., GIORGIS, D., VALLOTON, A. & AMELIN, Y. 2000: U-Pb and Ar-Ar geochronological data from the Pelagonian basement in Evia (Greece): geodynamic implications for the evolution of Palaeotethys. *Schweizerische Mineralogische und Petrographische Mitteilungen*, **80**, 21-43.

VAVRA, G. 1990: On the kinematics of zircon growth and its petrogenetic significance: a cathodoluminescence study. *Contributions to Mineralogy and Petrology*, **106**, 90-99.

VON QUADT, A., GRAF, J. & BERNOULLI, D. 2000: Pre-Variscan and Tertiary magmatism in western Bulgaria (Kraište) based on U-Pb single zircon analyses, trace and REE element distribution and Sm/Nd - Rb/Sr investigation. *Terra Nostra*, **2000/1**, 87.

VON RAUMER, J. F., STAMPFLI, G. M., BOREL, G. & BUSSY, F. 2002: Organization of pre-Variscan basement areas at the north-Gondwana margin. *International Journal of Earth Sciences*, **91**, 35-52.

VON RAUMER, J. F., STAMPFLI, G. M. & BUSSY, F. 2003. Gondwana-derived microcontinents – the constituents of the Variscan and Alpine collisional orogens. *Tectonophysics*, **365**, 7-22.

WALLBRECHER, E. 1976: Geologie und Tektonik auf dem Südteil der Magnesischen Halbinsel (Nord-Griechenland). *Zeitschrift der Deutschen Geologischen Gesellschaft*, **127**, 365-371.

WASSERBURG, G. J., JACOBSEN, S., B., DEPAOLO, D. J., MCCULLOCH, M. T. & WEN, T. 1981: Precise determination of Sm/Nd ratios, Sm and Nd isotopic abundances in standard solutions. *Geochimica et Cosmochimica Acta*, **45**, 2311-2323.

WAYNE, D. M. & SINHA, A. K. 1988: Physical and chemical response of zircons to deformation. *Contributions to Mineralogy and Petrology*, **98**, 109-121.

WAYNE, D. M. & SINHA, A. K. 1992: Stability of zircon U-Pb systematics in a greenschist-grade mylonite: an example from the Rockfish Valley Fault Zone, Central Virginia, USA. *Journal of Geology*, **100**, 593-603.

WENDT, J. I. & TODT, W. 1991: A vapour digestion method for dating single zircons by direct measurement of U and Pb without chemical separation. *Terra abstracts,* **3**, 507-508.

WHITE, W. M. & PATCHETT, J. 1984: Hf-Nd-Sr isotopes and incompatible element abundances in island arcs: implications for magma origins and crust-mantle evolution. *Earth and Planetary Science Letters,* **67**, 167-185.

WIEDENBECK, M., ALLÉ, P., CORFU, F., GRIFFIN, W. L., MEIER, M., OBERLI, F., VON QUADT, A., RODDICK, J. C. & SPIEGEL, W. 1995: Three natural zircon standards for U-Th-Pb, Lu-Hf, trace element and REE analyses. *Geostandards Newsletter*, **19**, 1-23.

WILLIAMS, I. S. 1992: Some observations on the use of zircon U-Pb geochronology in the study of granitic rocks. *Transactions of the Royal Society of Edinburgh: Earth Sciences,* **83**, 447-458.

WILLIAMS, I. S. 1998: U-Th-Pb Geochronology by Ion Microprobe. In *Applications of microanalytical techniques to understanding mineralization processes* (eds. M. A. McKibben, W. C. Shanks III & W. I. Ridley), pp. 1-35. Reviews in Economic Geology, 7.

WILLIAMS, I. S. & CLAESSON, S. 1987: Isotopic evidence for the Precambrian provenance and Caledonian metamorphism of high grade paragneisses from the Seve Nappes, Scandinavian Caledonides. 2. Ion microprobe zircon U-Th-Pb. *Contributions to Mineralogy and Petrology*, **97**, 205-217.

WOOD, D. A., JORON, J. L., TREUIL, M., NORRY, M. & TARNEY, J. 1979: Elemental and Sr isotope variations in basic lavas from Iceland and the surrounding ocean floor. *Contributions to Mineralogy and Petrology*, **70**, 319-339.

WOOD, D. A., TARNEY, J. & WEAVER, B. L. 1981: Trace element variations in Atlantic ocean basalts and Proterozoic dykes from Northwest Scotland: their bearing upon the nature and geochemical evolution of the upper mantle. *Tectonophysics*, **75**, 91-112.

YARWOOD, G. A. & AFTALION, M. 1976: Field relations and U-Pb geochronology of a granite from the Pelagonian Zone of the Hellenides (High Pieria, Greece). *Bulletin de la Société Géologique de France*, **18**, 259-264.

ZACHARIADOU, S. & DIMITRIADIS, S. 1994: Crustal extension and partial melting possibly related to the opening of a marginal basin. The pelitic migmatites of Piyi and Karathodoro, Macedonia, Greece. *Bulletin of the Geological Society of Greece*, **30**, 271-284.

ZECK, H. P. & WHITEHOUSE, M. J. 1999: Hercynian, Pan-African, Proterozoic and Archean ion-microprobe zircon ages for a Betic-Rif core complex, Alpine belt, W Mediterranean – consequences for its P-T-t path. *Contributions to Mineralogy and Petrology*, **134**, 134-149.

Appendix A-1. Major and trace element analyses (XRF) of the investigated rocks

sample	V1	V2	V3	V4	V5	V6	V7	V9	V10	Ka-X2	Ka-X3	Ka-X4	Ka-X5	Ka-X6	Pl37
region	Varnous	Varnous	Varnous	Varnous	Varnous	Varnous	Varnous	Varnous	Varnous	Voras	Voras	Voras	Voras	Voras	S Veria
age [1] [Ma]	**298**	**282**	300	**296**	**289**	300	**294**	**713**	**290**	300	300	300	**276**	300	**307**
major elements [wt.%]															
SiO_2	61.18	52.98	51.01	51.04	69.26	74.88	54.37	76.83	60.88	77.51	74.43	72.79	69.41	65.78	72.05
TiO_2	0.89	1.28	1.34	1.47	0.49	0.22	1.14	0.18	0.79	0.15	0.28	0.25	0.37	0.51	0.21
Al_2O_3	15.43	16.88	18.31	18.02	14.45	13.31	16.77	12.06	16.53	11.06	11.74	14.61	15.47	16.09	14.94
$Fe_2O_{3\ tot}$	5.34	7.60	8.05	8.03	2.90	0.58	7.94	1.33	5.11	1.91	2.20	2.09	2.69	3.79	1.73
MnO	0.10	0.13	0.12	0.13	0.05	0.01	0.14	0.02	0.10	0.01	0.02	0.07	0.05	0.08	0.03
MgO	3.11	4.18	4.02	4.11	1.36	0.07	4.46	0.15	2.78	0.07	1.66	0.55	1.16	1.80	0.42
CaO	4.44	6.54	7.04	6.84	2.31	0.92	6.44	0.25	4.29	0.08	0.14	1.33	2.03	2.87	2.01
Na_2O	3.38	4.40	4.23	4.07	3.40	3.09	3.62	2.77	3.90	1.30	2.23	3.71	3.67	3.86	4.06
K_2O	3.86	2.77	2.83	2.80	4.47	5.24	2.43	5.44	3.71	8.17	3.74	4.10	3.81	3.75	3.11
P_2O_5	0.48	0.73	0.68	0.65	0.21	0.02	0.54	0.03	0.36	0.01	0.11	0.12	0.15	0.20	0.05
Cr_2O_3	n.d.	0.01	0.01	0.01	n.d.	n.d.	0.02	n.d.	n.d.	n.d.	n.d.	n.d.	n.d.	n.d.	n.d.
NiO	n.d.	0.00	0.00	0.00	n.d.	n.d.	0.01	n.d.	n.d.	n.d.	n.d.	n.d.	n.d.	n.d.	n.d.
LOI	0.98	1.75	1.44	1.92	0.31	0.36	1.17	0.42	0.59	0.06	1.43	0.97	1.19	1.03	0.71
Total	99.19	99.25	99.08	99.09	99.21	98.70	99.04	99.48	99.04	100.33	97.98	100.59	100.00	99.76	99.32
MALI	2.80	0.63	0.02	0.03	5.56	7.41	-0.39	7.96	3.32	9.39	5.83	6.48	5.45	4.74	5.16
Fe*	0.61	0.62	0.64	0.64	0.66	0.88	0.62	0.89	0.62	0.96	0.54	0.77	0.68	0.65	0.79
ASI	1.17	1.10	1.17	1.19	1.18	1.15	1.22	1.13	1.19	1.00	1.52	1.26	1.31	1.26	1.26
A/CNK	0.87	0.76	0.80	0.81	0.99	1.07	0.83	1.11	0.91	0.99	1.47	1.13	1.12	1.03	1.09
A/NK	1.58	1.65	1.83	1.85	1.39	1.24	1.95	1.15	1.58	1.01	1.52	1.39	1.52	1.55	1.49
CIA	46.42	43.27	44.52	44.85	49.69	51.71	45.25	52.53	47.55	49.85	59.56	52.99	52.76	50.73	52.17
trace elements [ppm]															
Sc	13	19	18	20	4	2	24	5	11	b.d.	5	5	4	7	3
V	112	195	163	175	51	13	149	9	89	5	28	22	42	78	15
Cr	69	55	56	47	29	4	127	6	53	12	39	15	41	88	3
Co	14	54	9	41	98	98	23	3	14	b.d.	5	5	5	12	b.d.
Ni	37	28	30	28	17	3	53	5	26	2	9	4	14	30	b.d.
Cu	3	78	4	11	7	4	16	4	b.d.	b.d.	11	2	3	7	2
Zn	64	88	88	87	40	9	89	20	60	20	56	41	44	58	43
Ga	17	20	20	21	17	13	21	14	18	17	14	17	21	18	16
Rb	138	153	97	102	145	101	83	233	124	235	134	171	137	144	104
Sr	806	947	1063	1008	522	145	911	36	781	6	15	160	452	537	462
Y	34	30	34	39	25	3	43	33	24	21	22	17	14	16	13
Zr	253	257	270	307	159	250	346	133	223	416	139	112	155	185	128
Nb	23	22	22	29	19	9	22	12	16	28	9	13	12	15	7
Ba	1291	414	1268	1620	931	327	1334	277	1113	46	259	482	884	1300	1102
Pb	13	14	13	14	14	36	9	16	12	23	10	29	25	25	28
Th	15	9	9	11	14	9	10	20	6	20	12	15	22	18	10
U	4	3	2	2	b.d.	b.d.	2	4	2	7	b.d.	5	3	5	b.d.
La	58	66	48	62	40	25	64	25	33	35	23	22	32	41	27
Ce	114	118	93	125	72	34	125	47	63	73	51	52	61	76	45
Pr	9	13	7	15	6	1	7	7	5	8	5	7	4	8	4
Nd	49	51	39	56	26	11	54	25	25	33	23	20	22	29	23
Sm	7	6	8	8	5	4	9	5	3	6	6	3	4	6	4

LOI: loss on ignition

MALI: Na_2O+K_2O-CaO

Fe*: FeO_{tot} / (FeO_{tot} + MgO)

ASI: Al/(Ca-1.67*P+Na+K)

A/CNK: molecular Al_2O_3/(CaO+K_2O+Na_2O)

A/NK: molecular Al_2O_3/(K_2O+Na_2O)

CIA: molecular [Al_2O_3/(Al_2O_3+CaO+Na_2O+K_2O)]*100

n.d.: not determined; b.d.: below detection limit

[1] ages obtained from zircon geochronology are shown in bold while for the remaining samples an age was assumed; ages for samples Pl4, Pl7, Pl9, Pl10 and Pl11 are from Reischmann *et al.* (2001)

Appendix A-1. (*continued*)

sample	PI38	PI40	PI41	PI43	PI44	PI73	PI74	PI58	PI59	PI61	PI62	PI63	PI64	PI65	PI66
region	S Veria	S Veria	S Veria	S Veria	S Veria	N-Olymp	N-Olymp	NW-PZ	NW-PZ	NW-PZ	NW-PZ	NW-PZ	Fotino	Fotino	Fotino
age [Ma]	300	**300**	300	137	**137**	**245**	245	**710**	**710**	**292**	300	**244**	**710**	700	**710**
								major elements [wt.%]							
SiO_2	72.71	72.25	74.35	76.73	72.97	68.08	72.29	68.96	71.24	72.45	67.99	74.66	76.20	73.66	76.56
TiO_2	0.21	0.21	0.13	0.18	0.22	0.49	0.32	0.63	0.46	0.44	0.40	0.11	0.29	0.29	0.18
Al_2O_3	14.74	14.93	13.76	12.01	12.94	15.33	14.15	14.60	13.95	12.42	15.50	13.19	12.13	13.07	12.16
$Fe_2O_{3\,tot}$	1.73	1.56	1.09	1.97	2.91	3.19	2.11	4.09	3.00	3.54	2.93	0.95	1.41	1.81	1.23
MnO	0.04	0.05	0.02	0.02	0.05	0.06	0.04	0.05	0.03	0.07	0.06	0.00	0.01	0.02	0.02
MgO	0.42	0.44	0.22	0.09	1.45	1.66	0.98	1.38	0.76	1.19	1.11	0.05	0.24	0.27	0.15
CaO	2.01	1.80	1.10	0.13	0.04	0.96	0.34	1.64	1.24	1.66	1.04	0.02	0.30	0.60	0.41
Na_2O	4.06	4.03	3.17	2.93	1.28	3.48	3.60	2.34	2.68	2.46	2.98	2.02	2.73	2.98	3.05
K_2O	2.80	3.09	5.30	5.82	5.72	4.73	4.42	3.93	4.51	3.46	5.55	8.30	5.44	5.66	5.44
P_2O_5	0.05	0.08	0.04	0.01	0.02	0.18	0.10	0.15	0.11	0.19	0.15	0.02	0.05	0.05	0.03
Cr_2O_3	n.d.	n.d.	n.d.	n.d.	n.d.	n.d.	n.d.	n.d.	n.d.	n.d.	n.d.	n.d.	n.d.	n.d.	n.d.
NiO	n.d.	n.d.	n.d.	n.d.	n.d.	n.d.	n.d.	n.d.	n.d.	n.d.	n.d.	n.d.	n.d.	n.d.	n.d.
LOI	0.81	0.89	0.63	0.28	1.74	1.96	1.38	1.87	1.18	1.50	1.62	0.24	0.58	0.68	0.62
Total	99.58	99.33	99.81	100.17	99.34	100.12	99.73	99.64	99.16	99.38	99.33	99.56	99.38	99.09	99.85
MALI	4.85	5.32	7.37	8.62	6.96	7.25	7.68	4.63	5.95	4.26	7.49	10.30	7.87	8.04	8.08
Fe*	0.79	0.76	0.82	0.95	0.64	0.63	0.66	0.73	0.78	0.73	0.70	0.94	0.84	0.86	0.88
ASI	1.28	1.30	1.16	1.07	1.56	1.33	1.30	1.55	1.36	1.37	1.33	1.07	1.15	1.14	1.08
A/CNK	1.10	1.13	1.06	1.06	1.55	1.22	1.25	1.32	1.21	1.15	1.21	1.07	1.11	1.08	1.04
A/NK	1.52	1.50	1.26	1.08	1.56	1.41	1.32	1.80	1.50	1.59	1.42	1.07	1.17	1.19	1.12
CIA	52.45	52.99	51.51	51.40	60.72	54.91	55.55	56.84	54.72	53.47	54.77	51.66	52.61	51.89	51.07
								trace elements [ppm]							
Sc	3	4	b.d.	4	3	6	3	7	5	7	5	b.d.	3	3	3
V	12	15	9	2	3	50	31	64	42	51	45	6	13	17	9
Cr	4	4	b.d.	4	2	24	9	24	16	26	18	2	4	3	4
Co	b.d.	2	b.d.	b.d.	3	6	b.d.	8	7	7	4	b.d.	3	3	3
Ni	b.d.	2	3	2	2	7	5	9	8	9	8	2	4	b.d.	3
Cu	b.d.	b.d.	2	4	b.d.	9	2	8	7	2	b.d.	4	9	3	3
Zn	38	41	23	51	92	65	42	57	41	49	49	13	22	29	34
Ga	16	19	15	17	23	19	18	17	16	16	17	14	16	16	14
Rb	98	123	156	226	300	168	189	117	142	161	207	205	245	302	248
Sr	397	352	197	15	8	183	79	152	125	572	329	13	37	42	35
Y	13	11	17	55	58	18	14	29	23	21	15	42	35	41	39
Zr	122	123	78	370	340	213	128	247	178	201	151	160	199	190	126
Nb	8	14	8	18	24	17	15	14	11	19	17	29	12	13	11
Ba	923	758	694	397	368	1963	470	985	877	590	1028	43	186	206	257
Pb	18	20	23	21	40	13	23	19	16	14	15	30	35	17	24
Th	10	10	14	21	25	21	21	20	17	14	13	27	38	35	22
U	3	3	3	4	5	4	3	3	2	4	4	3	9	9	3
La	22	26	19	37	46	39	26	32	32	23	19	59	41	35	28
Ce	41	44	38	67	75	92	46	64	74	46	31	118	63	75	56
Pr	3	b.d.	2	3	8	9	b.d.	5	5	3	b.d.	12	6	3	5
Nd	18	21	19	31	45	38	18	31	31	21	14	58	31	26	26
Sm	3	3	4	11	10	7	5	7	6	4	4	12	4	6	6

LOI: loss on ignition

MALI: Na_2O+K_2O-CaO

Fe*: FeO_{tot} / (FeO_{tot} + MgO)

ASI: Al/(Ca-1.67*P+Na+K)

A/CNK: molecular $Al_2O_3/(CaO+K_2O+Na_2O)$

A/NK: molecular $Al_2O_3/(K_2O+Na_2O)$

CIA: molecular $[Al_2O_3/(Al_2O_3+CaO+Na_2O+K_2O)]*100$

n.d.: not determined; b.d.: below detection limit

Appendix A-1. *(continued)*

sample	Pl67	Pl68	Pl69	Pl70	Pl71	Pl72	Pl1	Pl3	Pl4	Pl5	Pl6	Pl7	Pl8	Pl9	Pl10
region	Fotino	Fotino	Deskati	Deskati	Thessaly	Thessaly	Thessaly	Thessaly	Thessaly	Thessaly	Thessaly	Thessaly	Thessaly	Thessaly	Thessaly
age [Ma]	700	700	700	**699**	300	300	300	300	**284**	**279**	300	**285**	**280**	**284**	**283**
major elements [wt.%]															
SiO_2	70.71	80.78	77.72	75.89	73.12	56.58	67.68	74.36	68.91	70.79	68.83	68.61	68.67	68.07	61.30
TiO_2	0.21	0.12	0.08	0.21	0.24	1.10	0.44	0.15	0.42	0.23	0.42	0.41	0.43	0.50	0.76
Al_2O_3	12.25	10.49	11.80	12.46	14.70	16.12	15.04	14.19	15.61	15.73	15.53	15.32	15.46	15.38	16.68
$Fe_2O_{3\ tot}$	1.48	0.80	1.01	1.40	1.90	7.51	3.17	1.26	3.06	1.90	3.12	3.06	3.29	3.00	5.21
MnO	0.02	0.00	0.01	0.02	0.05	0.13	0.07	0.06	0.06	0.03	0.05	0.06	0.06	0.05	0.11
MgO	0.19	0.08	0.17	0.24	0.41	3.35	1.19	0.23	0.97	0.46	0.87	0.83	0.93	1.12	2.13
CaO	0.77	0.02	0.11	0.60	1.79	4.67	2.77	1.10	2.78	2.57	2.58	2.68	2.27	1.98	4.18
Na_2O	3.20	2.95	3.13	2.69	4.24	3.64	3.45	4.04	3.81	4.23	3.71	3.68	3.54	3.14	3.00
K_2O	5.08	4.52	5.16	5.40	3.32	4.43	3.75	3.98	3.31	2.30	3.03	3.31	3.21	4.49	3.85
P_2O_5	0.03	0.02	0.05	0.04	0.08	0.47	0.15	0.04	0.08	0.05	0.18	0.17	0.18	0.13	0.18
Cr_2O_3	n.d.	n.d.	n.d.	n.d.	n.d.	0.01	n.d.	n.d.	n.d.	n.d.	n.d.	n.d.	n.d.	n.d.	n.d.
NiO	n.d.	n.d.	n.d.	n.d.	n.d.	0.00	n.d.	n.d.	n.d.	n.d.	n.d.	n.d.	n.d.	n.d.	n.d.
LOI	0.47	0.45	0.35	0.60	0.79	1.73	1.63	0.75	0.48	1.17	1.31	1.19	1.44	1.56	2.24
Total	94.41	100.23	99.59	99.55	100.64	99.74	99.34	100.16	99.49	99.46	99.63	99.32	99.48	99.42	99.64
MALI	7.51	7.45	8.18	7.49	5.77	3.40	4.43	6.92	4.34	3.96	4.16	4.31	4.48	5.65	2.67
Fe*	0.88	0.90	0.84	0.84	0.81	0.67	0.71	0.83	0.74	0.79	0.76	0.77	0.76	0.71	0.69
ASI	1.07	1.08	1.10	1.16	1.21	1.11	1.25	1.19	1.27	1.34	1.35	1.29	1.39	1.32	1.31
A/CNK	1.01	1.07	1.08	1.10	1.06	0.84	1.02	1.10	1.05	1.11	1.10	1.06	1.15	1.13	1.00
A/NK	1.14	1.08	1.10	1.21	1.39	1.49	1.55	1.30	1.58	1.66	1.66	1.59	1.66	1.53	1.83
CIA	50.18	51.75	51.90	52.31	51.54	45.55	50.45	52.28	51.16	52.70	52.46	51.36	53.52	53.02	49.97
trace elements [ppm]															
Sc	2	b.d.	4	4	3	16	5	2	6	3	4	5	3	4	13
V	8	5	4	14	18	155	52	10	36	13	42	39	43	44	108
Cr	4	41	4	6	16	50	10	6	9	4	5	6	3	10	10
Co	2	b.d.	b.d.	b.d.	2	17	66	35	56	60	54	33	70	62	50
Ni	3	b.d.	2	b.d.	6	19	5	3	3	3	4	3	3	4	5
Cu	3	3	b.d.	3	b.d.	15	b.d.	4	b.d.	3	b.d.	b.d.	b.d.	b.d.	b.d.
Zn	15	7	15	26	41	80	52	37	61	36	48	57	64	62	75
Ga	14	13	15	14	17	21	20	18	21	18	20	19	20	22	21
Rb	165	125	162	213	110	117	135	158	113	66	82	95	86	171	149
Sr	75	38	32	63	362	629	385	200	464	530	458	449	394	257	336
Y	49	21	26	20	18	34	18	19	9	13	13	10	11	16	17
Zr	178	122	59	115	133	244	138	85	172	104	189	186	206	173	157
Nb	14	22	11	9	16	23	15	16	13	8	11	9	11	15	11
Ba	365	208	50	371	654	1752	472	493	895	1013	1196	1052	1225	683	698
Pb	18	67	14	17	16	15	18	13	16	18	27	17	16	22	18
Th	20	11	9	17	12	20	12	10	7	15	9	9	8	18	10
U	5	3	3	2	1	4	4	2	2	2	b.d.	b.d.	2	2	2
La	30	28	5	23	19	46	28	16	29	39	29	33	27	31	27
Ce	66	55	5	48	40	84	55	26	53	69	62	61	51	64	53
Pr	4	6	b.d.	5	3	11	2	b.d.	4	6	8	7	5	11	6
Nd	29	23	5	19	18	31	23	14	24	31	28	29	25	28	23
Sm	7	5	4	4	2	6	6	4	b.d.	5	6	3	5	7	3

LOI: loss on ignition

MALI: Na_2O+K_2O-CaO

Fe*: FeO_{tot} / (FeO_{tot} + MgO)

ASI: Al/(Ca-1.67*P+Na+K)

A/CNK: molecular $Al_2O_3/(CaO+K_2O+Na_2O)$

A/NK: molecular $Al_2O_3/(K_2O+Na_2O)$

CIA: molecular $[Al_2O_3/(Al_2O_3+CaO+Na_2O+K_2O)]*100$

n.d.: not determined; b.d.: below detection limit

Appendix A-1. *(continued)*

sample	PI11	PI45	PI46	PI48	PI49	PI50	PI51	PI54	PI55	PI12	PI13	PI25	PI26	PI27	PI29
region	Thessaly	Mt. Ossa	Mt. Ossa	Mt. Ossa	Mt. Ossa	Mt. Ossa	Mt. Ossa	Mt. Ossa	Mt. Ossa	Mavro.	Mavro.	Mavro.	Mavro.	Mavro.	Mavro.
age [Ma]	**282**	300	300	300	300	**266**	300	**312**	300	300	**280**	300	300	300	300
major elements [wt.%]															
SiO_2	69.38	75.24	56.70	57.37	76.71	63.31	79.72	78.03	73.78	47.90	74.33	76.98	85.35	85.68	47.21
TiO_2	0.54	0.50	0.88	0.92	0.27	0.68	0.20	0.24	0.23	1.35	0.22	0.09	0.17	0.20	1.51
Al_2O_3	14.46	10.80	16.83	17.39	11.51	16.33	10.74	10.48	12.72	18.62	14.52	13.29	7.80	5.09	14.31
$Fe_2O_{3\ tot}$	3.38	3.70	7.72	7.55	2.07	4.82	1.38	1.71	2.73	7.49	1.84	1.07	1.49	2.68	12.05
MnO	0.07	0.05	0.12	0.11	0.02	0.08	0.02	0.03	0.04	0.12	0.03	0.01	0.01	0.16	0.16
MgO	1.44	1.08	1.57	1.67	1.25	3.31	1.02	0.59	0.70	7.04	0.55	0.31	0.28	1.39	7.97
CaO	0.84	0.93	3.79	3.44	0.15	1.56	0.17	0.57	0.10	9.50	0.12	0.13	0.04	0.51	11.87
Na_2O	3.79	4.76	4.44	3.76	3.78	4.39	2.59	2.80	4.20	3.16	3.09	5.48	1.34	0.33	1.77
K_2O	3.48	1.64	5.15	5.39	2.60	2.17	2.70	2.67	4.52	1.17	3.47	1.45	2.02	1.19	0.37
P_2O_5	0.16	0.14	0.28	0.32	0.03	0.13	0.04	0.07	0.02	0.29	0.07	0.05	0.02	0.03	0.13
Cr_2O_3	n.d.	n.d.	0.01	0.01	n.d.	n.d.	n.d.	n.d.	n.d.	0.02	n.d.	n.d.	n.d.	n.d.	0.04
NiO	n.d.	n.d.	0.00	0.00	n.d.	n.d.	n.d.	n.d.	n.d.	0.01	n.d.	n.d.	n.d.	n.d.	0.02
LOI	2.22	0.84	2.03	2.19	1.19	2.94	1.35	1.29	0.59	2.87	1.61	0.89	1.08	1.15	2.35
Total	99.76	99.68	99.53	100.13	99.58	99.72	99.93	97.19	99.63	99.55	99.85	99.75	99.60	98.41	99.76
MALI	6.43	5.47	5.80	5.71	6.23	5.00	5.12	4.90	8.62	-5.17	6.44	6.80	3.32	1.01	-9.73
Fe*	0.68	0.76	0.82	0.80	0.60	0.57	0.55	0.72	0.78	0.49	0.75	0.76	0.83	0.63	0.58
ASI	1.37	1.05	1.05	1.18	1.26	1.51	1.47	1.32	1.07	1.26	1.64	1.25	1.77	2.25	1.03
A/CNK	1.25	0.96	0.85	0.95	1.24	1.32	1.43	1.23	1.06	0.78	1.60	1.23	1.75	1.85	0.57
A/NK	1.45	1.12	1.31	1.45	1.27	1.71	1.50	1.40	1.08	2.88	1.64	1.26	1.78	2.78	4.32
CIA	55.64	48.88	45.98	48.76	55.30	56.83	58.91	55.12	51.49	43.96	61.58	55.12	63.60	64.86	36.50
trace elements [ppm]															
Sc	4	13	17	19	6	14	4	4	5	18	4	3	3	4	36
V	59	101	220	183	20	89	18	27	2	154	15	4	27	27	299
Cr	7	66	90	86	7	92	9	17	8	184	2	5	18	23	330
Co	113	12	19	20	3	12	2	b.d.	b.d.	30	7	b.d.	2	13	41
Ni	5	17	24	21	4	23	4	5	2	109	2	b.d.	8	36	126
Cu	b.d.	12	13	8	2	13	3	4	3	30	3	3	3	10	33
Zn	60	37	93	94	50	62	27	34	80	58	42	20	14	56	93
Ga	19	9	16	18	12	19	11	11	18	15	17	13	7	6	16
Rb	117	33	87	94	78	97	102	103	131	14	130	47	92	39	5
Sr	90	57	114	633	15	55	66	23	25	121	39	49	13	34	205
Y	17	18	26	32	43	29	13	18	72	21	22	7	10	11	35
Zr	158	93	218	238	509	159	88	111	518	117	97	48	67	43	96
Nb	15	4	9	12	9	13	7	7	19	14	9	5	3	5	5
Ba	504	148	424	572	316	344	302	323	735	128	493	292	299	187	2
Pb	15	5	14	30	41	13	9	7	18	3	8	7	4	15	b.d.
Th	16	3	10	11	20	12	10	15	21	2	9	6	5	5	b.d.
U	2	b.d.	3	4	5	3	2	2	6	b.d.	2	2	b.d.	b.d.	b.d.
La	36	16	28	30	41	27	23	29	43	7	21	6	12	10	3
Ce	68	29	65	65	80	59	38	49	90	23	42	7	11	35	19
Pr	5	b.d.	4	6	5	2	5	3	7	b.d.	2	b.d.	b.d.	b.d.	b.d.
Nd	28	14	29	29	40	24	16	22	44	6	18	3	8	10	6
Sm	8	5	5	4	7	7	3	6	9	3	2	b.d.	4	b.d.	5

LOI: loss on ignition

MALI: Na_2O+K_2O-CaO

Fe*: FeO_{tot} / (FeO_{tot} + MgO)

ASI: Al/(Ca-1.67*P+Na+K)

A/CNK: molecular $Al_2O_3/(CaO+K_2O+Na_2O)$

A/NK: molecular $Al_2O_3/(K_2O+Na_2O)$

CIA: molecular $[Al_2O_3/(Al_2O_3+CaO+Na_2O+K_2O)]*100$

n.d.: not determined; b.d.: below detection limit

Appendix A-1. *(continued)*

sample	PI30	PI15	PI16	PI21	PI22	PI23	PI24	PI79	PI80	PI81	PI85	PI86	PI87	Ev4	Ev5
region	Mavrov.	Pilion	Pilion	Pilion	Pilion	Pilion	Pilion	Pilion	Pilion	Pilion	Pilion	Pilion	Pilion	Evia	Evia
age [Ma]		300	**241**	**279**	300	**546**	300	300	**309**	300	300	300	**281**	303	300
major elements [wt.%]															
SiO_2	69.50	58.55	61.49	72.01	52.32	62.26	88.78	71.28	73.62	74.41	78.12	75.57	67.03	57.49	74.73
TiO_2	0.02	0.55	0.52	0.22	1.10	1.15	0.16	0.36	0.15	0.22	0.19	0.12	0.52	0.80	0.17
Al_2O_3	0.32	17.16	17.08	14.58	17.17	16.45	4.69	14.74	14.63	12.82	12.36	13.76	15.27	17.44	13.27
$Fe_2O_{3\ tot}$	26.34	5.48	5.38	1.91	9.36	7.76	2.02	3.06	1.20	2.67	1.49	1.19	4.05	6.52	1.31
MnO	2.23	0.08	0.08	0.04	0.17	0.10	0.02	0.04	0.02	0.04	0.01	0.02	0.06	0.09	0.02
MgO	0.34	4.20	3.28	0.67	3.54	2.98	1.31	0.97	0.35	0.12	0.48	0.26	1.26	2.65	0.32
CaO	0.50	5.88	2.44	0.94	4.70	0.76	0.08	0.24	0.54	1.32	0.30	0.73	2.56	4.66	1.07
Na_2O	0.69	4.25	4.86	3.28	6.10	3.60	0.13	2.44	3.86	4.78	2.40	5.46	2.73	3.10	3.27
K_2O	0.02	1.12	2.18	4.37	0.25	1.76	1.33	4.43	4.05	2.07	2.96	1.86	3.90	3.02	5.07
P_2O_5	0.19	0.12	0.11	0.08	0.20	0.16	0.06	0.08	0.27	0.04	0.02	0.08	0.20	0.16	0.07
Cr_2O_3	n.d.	0.02	n.d.	n.d.	0.00	n.d.	n.d.	n.d.	n.d.	n.d.	n.d.	n.d.	n.d.	0.00	n.d.
NiO	n.d.	0.01	n.d.	n.d.	0.00	n.d.	n.d.	n.d.	n.d.	n.d.	n.d.	n.d.	n.d.	0.00	n.d.
LOI	0.46	2.39	2.59	1.22	5.69	2.96	1.12	1.82	1.06	0.99	1.28	0.73	1.56	3.86	1.15
Total	100.61	97.42	100.01	99.32	100.60	99.94	99.70	99.46	99.75	99.48	99.61	99.78	99.14	99.79	100.45
MALI	0.21	-0.51	4.60	6.71	1.65	4.60	1.38	6.63	7.37	5.53	5.06	6.59	4.07	1.46	7.27
Fe*	0.99	0.54	0.60	0.72	0.70	0.70	0.58	0.74	0.76	0.95	0.74	0.80	0.74	0.69	0.79
ASI	0.23	1.28	1.37	1.34	1.20	1.98	2.84	1.65	1.34	1.14	1.67	1.19	1.41	1.41	1.13
A/CNK	0.15	0.91	1.15	1.23	0.91	1.79	2.61	1.59	1.25	1.03	1.61	1.12	1.14	1.04	1.04
A/NK	0.28	2.09	1.65	1.44	1.67	2.10	2.84	1.67	1.36	1.27	1.73	1.25	1.75	2.08	1.22
CIA	13.41	47.59	53.59	55.20	47.67	64.11	72.28	61.45	55.53	50.62	61.62	52.76	53.32	50.87	50.88
trace elements [ppm]															
Sc	2	14	12	3	26	16	8	10	2	6	2	2	10	19	4
V	7	111	94	22	214	112	29	42	8	4	31	7	65	138	13
Cr	20	148	19	4	2	81	22	16	8	8	18	9	8	19	6
Co	b.d.	20	10	2	15	21	17	4	2	b.d.	2	3	2	12	3
Ni	120	65	7	3	3	35	33	2	4	3	4	b.d.	4	6	2
Cu	17	12	2	2	b.d.	b.d.	15	3	2	146	b.d.	2	4	4	2
Zn	212	65	72	41	103	97	42	45	48	106	21	23	68	83	18
Ga	4	18	18	17	18	19	5	16	20	15	13	14	19	20	11
Rb	3	15	36	168	11	56	43	164	180	52	91	73	159	114	98
Sr	113	475	256	134	246	69	7	33	50	98	60	90	225	166	136
Y	10	18	20	19	32	21	7	20	10	39	11	23	21	39	17
Zr	26	114	134	96	137	266	32	128	81	197	95	92	152	168	96
Nb	b.d.	5	7	9	9	13	4	10	14	10	4	10	12	12	5
Ba	21	134	365	567	10	263	186	484	281	528	508	337	785	443	1125
Pb	9	6	6	11	17	3	3	9	15	5	11	14	14	9	20
Th	b.d.	4	6	11	4	6	2	20	9	7	7	21	14	4	17
U	b.d.	b.d.	b.d.	2	2	b.d.	b.d.	2	2	2	1	6	4	2	b.d.
La	5	16	17	18	24	21	7	18	9	15	15	24	36	9	50
Ce	8	36	41	39	59	53	20	34	24	40	27	48	81	33	88
Pr	b.d.	b.d.	2	2	2	4	b.d.	2	b.d.	3	b.d.	6	9	2	9
Nd	2	13	19	14	22	23	3	16	10	18	14	23	34	15	43
Sm	2	7	2	3	6	3	3	3	5	5	6	5	5	5	8

LOI: loss on ignition

MALI: Na_2O+K_2O-CaO

Fe*: FeO_{tot} / (FeO_{tot} + MgO)

ASI: Al/(Ca-1.67*P+Na+K)

A/CNK: molecular $Al_2O_3/(CaO+K_2O+Na_2O)$

A/NK: molecular $Al_2O_3/(K_2O+Na_2O)$

CIA: molecular $[Al_2O_3/(Al_2O_3+CaO+Na_2O+K_2O)]*100$

n.d.: not determined; b.d.: below detection limit

Appendix A-1. *(continued)*

sample	Skia1	Skia2	Skia4	Skia6	Skia8	Skia9	Skia7	Sky1	Sky2	Pl39*	V8 *	Pl17 *	Pl52 *	Skop *	Sky4 *
region	Skiathos	Skiathos	Skiathos	Skiathos	Skiathos	Skiathos	Skiathos	Skyros	Skyros	S Veria	Varnous	Pilion	Mt. Ossa	Skopelos	Skyros
age [Ma]	**289**	300	300	300	**287**	**264**	300	**16**	16						
major elements [wt.%]															
SiO_2	70.54	73.23	75.54	72.80	76.03	71.16	59.61	63.94	62.82	54.92	56.21	84.38	72.95	83.33	76.23
TiO_2	0.35	0.23	0.12	0.26	0.11	0.16	0.39	0.43	0.52	1.61	1.16	0.29	0.67	0.15	0.30
Al_2O_3	14.86	14.22	14.34	14.66	13.28	15.32	14.77	18.16	19.03	14.85	22.74	8.79	11.56	5.29	13.28
$Fe_2O_{3\ tot}$	3.11	1.95	1.06	2.41	1.10	2.90	3.28	4.01	3.69	9.79	9.59	1.11	4.70	1.46	2.09
MnO	0.02	0.02	0.01	0.05	0.01	0.15	0.03	0.03	0.04	0.15	0.06	0.01	0.08	0.06	0.03
MgO	0.55	0.35	0.27	0.45	0.33	0.37	0.65	1.90	1.86	4.06	2.11	0.69	2.86	0.52	0.75
CaO	2.40	1.15	0.56	1.21	0.74	1.08	0.91	3.26	4.11	6.90	0.38	b.d.	0.21	3.59	0.31
Na_2O	2.96	3.87	4.42	3.88	2.77	3.59	3.63	3.44	3.62	1.69	0.96	b.d.	2.56	1.60	3.97
K_2O	2.88	3.34	1.89	2.52	4.49	3.17	3.33	2.16	2.15	3.56	2.99	1.81	1.55	0.85	1.88
P_2O_5	0.12	0.06	0.13	0.12	0.01	0.05	0.23	0.15	0.15	0.22	0.21	0.02	0.13	0.04	0.08
Cr_2O_3	n.d.	n.d.	n.d.	n.d.	n.d.	n.d.	n.d.	n.d.	n.d.	n.d.	0.02	n.d.	n.d.	n.d.	n.d.
NiO	n.d.	n.d.	n.d.	n.d.	n.d.	n.d.	n.d.	n.d.	n.d.	n.d.	0.00	n.d.	n.d.	n.d.	n.d.
LOI	1.46	1.15	1.41	1.17	0.88	1.51	1.35	2.45	2.20	1.84	3.13	2.44	2.55	3.44	1.55
Total	99.25	99.57	99.75	99.53	99.75	99.46	88.18	99.93	100.19	99.59	99.56	99.54	99.82	100.33	100.47
MALI	3.44	6.06	5.75	5.19	6.52	5.68	6.05	2.34	1.66	-1.65	3.57	1.81	3.90	-1.14	5.54
Fe*	0.84	0.83	0.78	0.83	0.75	0.88	0.82	0.66	0.64	0.68	0.80	0.59	0.60	0.72	0.71
ASI	1.48	1.30	1.48	1.46	1.32	1.49	1.46	1.68	1.61	1.17	4.63	4.54	1.95	0.78	1.52
A/CNK	1.20	1.18	1.39	1.30	1.23	1.36	1.32	1.30	1.21	0.77	4.13	4.49	1.84	0.52	1.45
A/NK	1.86	1.42	1.54	1.61	1.41	1.64	1.54	2.27	2.30	2.24	4.72	4.49	1.96	1.49	1.55
CIA	54.61	54.08	58.12	56.45	55.24	57.55	56.81	56.60	54.71	43.64	80.51	81.77	64.83	34.42	59.26
trace elements [ppm]															
Sc	7	3	b.d.	5	b.d.	8	5	18	23	25	17	5	12	5	7
V	21	13	11	22	17	6	40	89	111	250	132	34	96	23	41
Cr	9	7	13	8	11	7	8	88	82	11	124	184	617	60	30
Co	3	2	3	b.d.	b.d.	3	5	8	10	23	24	4	15	3	2
Ni	3	3	3	2	2	4	6	55	22	16	31	24	150	7	7
Cu	b.d.	2	4	b.d.	2	4	2	70	24	b.d.	30	9	20	4	5
Zn	39	29	16	39	18	33	60	49	42	110	127	19	60	18	33
Ga	17	13	12	15	11	14	17	18	19	20	28	9	11	5	14
Rb	95	79	85	85	101	100	120	59	79	142	102	55	67	34	68
Sr	292	178	128	138	172	93	117	515	672	267	159	9	15	110	61
Y	18	16	16	18	3	44	24	9	14	40	54	9	21	10	11
Zr	259	199	76	118	98	269	141	99	130	191	216	123	182	59	104
Nb	11	8	5	8	4	6	11	6	7	10	21	5	9	4	6
Ba	862	1028	690	658	1233	612	966	581	753	685	825	303	239	164	464
Pb	18	26	14	21	36	28	45	37	39	21	15	9	12	8	11
Th	28	37	7	11	b.d.	45	13	10	13	7	16	4	6	3	6
U	1	4	4	3	b.d.	7	3	4	3	2	3	1	3	b.d.	2
La	85	99	28	27	6	89	34	24	27	17	78	7	15	13	20
Ce	147	184	40	54	13	168	67	41	61	48	112	10	28	16	36
Pr	18	16	6	7	b.d.	19	7	3	6	2	9	b.d.	2	b.d.	2
Nd	57	69	20	24	6	74	28	17	26	20	53	4	13	8	14
Sm	8	10	7	3	b.d.	9	5	2	5	6	13	3	6	4	b.d.

LOI: loss on ignition

MALI: Na_2O+K_2O-CaO

Fe*: FeO_{tot} / (FeO_{tot} + MgO)

ASI: Al/(Ca-1.67*P+Na+K)

A/CNK: molecular $Al_2O_3/(CaO+K_2O+Na_2O)$

A/NK: molecular $Al_2O_3/(K_2O+Na_2O)$

CIA: molecular $[Al_2O_3/(Al_2O_3+CaO+Na_2O+K_2O)]*100$

n.d.: not determined; b.d.: below detection limit

* meta-sedimentary rocks

Appendix A-1. (*continued)*

sample	Pl75	Pl31	Pl32	Pl33	Pl34	Pl35	Pl36	PLT-1	PLT-2	P1	P2	P4	P5	P6
region	Vardar	Vardar	Vardar	Vardar	Vardar	Vardar	Vardar	Vardar	Vardar	Vardar	Vardar	Vardar	Vardar	Vardar
age [Ma]	**285**	160	155	**155**	155	158	158			**319**	**319**	160	**158**	**164**
							major elements [wt.%]							
SiO_2	73.85	71.24	73.07	74.52	77.12	75.72	77.81	74.77	76.73	72.14	73.32	48.30	75.76	71.47
TiO_2	0.08	0.28	0.22	0.23	0.08	0.13	0.10	0.06	0.59	0.38	0.28	0.24	0.15	0.30
Al_2O_3	14.93	15.17	14.11	13.04	11.68	13.06	12.26	13.78	10.92	14.88	14.13	17.73	13.22	14.60
$Fe_2O_{3\ tot}$	1.14	1.49	2.14	1.19	0.75	0.86	0.74	0.43	3.53	2.10	2.24	5.60	1.23	2.07
MnO	0.02	0.02	0.01	0.03	b.d.	0.01	0.01	0.01	0.04	0.03	0.03	0.10	0.03	0.01
MgO	0.21	0.38	1.18	1.19	0.18	0.07	0.04	0.10	1.02	0.47	0.48	10.07	0.23	0.63
CaO	1.31	0.93	0.00	0.00	0.00	0.58	0.44	0.56	0.60	0.81	1.00	16.28	0.88	1.95
Na_2O	4.34	3.74	2.63	0.55	0.17	3.40	3.59	3.11	1.35	3.68	3.01	1.18	3.39	5.41
K_2O	3.79	5.18	4.14	7.05	8.52	5.08	4.44	5.97	3.22	4.75	4.79	0.02	5.15	0.55
P_2O_5	0.03	0.16	0.01	0.01	0.02	0.01	0.01	0.17	0.04	0.22	0.19	b.d.	0.05	0.07
Cr_2O_3	n.d.	n.d.	n.d.	n.d.	n.d.	n.d.	n.d.	n.d.	n.d.	n.d.	n.d.	0.06	n.d.	n.d.
NiO	n.d.	n.d.	n.d.	n.d.	n.d.	n.d.	n.d.	n.d.	n.d.	n.d.	n.d.	0.02	n.d.	n.d.
LOI	0.69	0.67	1.76	1.47	0.69	0.32	0.21	0.34	1.16	0.95	0.69	0.77	0.33	0.81
Total	100.39	99.26	99.27	99.28	99.21	99.24	99.65	99.30	99.20	100.41	100.16	100.37	100.42	97.87
MALI	6.82	7.99	6.77	7.6	8.69	7.9	7.59	8.52	3.97	7.62	6.8	-15.08	7.66	4.01
Fe*	0.83	0.78	0.62	0.47	0.79	0.92	0.94	0.79	0.76	0.80	0.81	0.33	0.83	0.75
ASI	1.20	1.22	1.60	1.53	1.23	1.13	1.10	1.16	1.76	1.28	1.31	1.06	1.11	1.31
A/CNK	1.10	1.13	1.60	1.53	1.23	1.08	1.07	1.09	1.61	1.17	1.18	0.56	1.04	1.12
A/NK	1.33	1.29	1.60	1.53	1.23	1.18	1.14	1.19	1.91	1.33	1.39	9.03	1.19	1.54
CIA	52.29	53.00	67.58	63.18	55.14	59.04	59.14	58.84	67.87	61.69	61.62	35.97	58.39	64.86
							trace elements [ppm]							
Sc	2	6	7	8	3	3	2	b.d.	7	4	2	47	b.d.	4
V	9	21	12	16	3	10	6	4	55	30	39	133	17	29
Cr	19	7	2	3	6	5	b.d.	9	49	11	337	494	13	32
Co	2	3	b.d.	3	b.d.	b.d.	b.d.	53	58	4	2	36	b.d.	7
Ni	3	b.d.	b.d.	b.d.	4	b.d.	b.d.	4	17	2	6	128	b.d.	7
Cu	b.d.	b.d.	4	3	48	4	4	3	b.d.	2	5	98	3	20
Zn	22	32	56	39	77	8	6	3	52	54	42	30	14	13
Ga	14	17	16	14	14	14	13	12	13	21	20	13	15	12
Rb	74	128	136	160	219	232	221	177	94	155	153	3	250	24
Sr	346	161	15	31	21	168	85	91	78	183	175	91	213	312
Y	11	9	31	18	18	8	7	15	16	13	10	8	11	14
Zr	80	144	214	203	103	98	42	53	222	167	141	25	121	162
Nb	6	7	11	9	7	29	29	5	10	10	9	b.d.	32	5
Ba	1336	832	1136	1766	2070	297	103	321	878	851	754	13	387	183
Pb	23	37	4	4	235	23	18	33	22	29	27	2	31	6
Th	9	14	18	12	19	39	30	3	13	16	13	b.d.	46	14
U	b.d.	4	6	4	3	10	7	b.d.	2	4	2	b.d.	11	3
La	16	31	33	30	30	24	13	3	27	47	30	b.d.	38	15
Ce	48	62	62	51	52	35	17	12	60	102	58	4	71	21
Pr	b.d.	5	4	4	3	b.d.	b.d.	2	2	8	6	b.d.	3	b.d.
Nd	19	30	28	24	22	11	5	5	27	43	28	b.d.	19	6
Sm	2	5	5	6	4	b.d.	b.d.	4	3	9	7	2	2	4

LOI: loss on ignition

MALI: Na_2O+K_2O-CaO

Fe*: FeO_{tot} / (FeO_{tot} + MgO)

ASI: Al/(Ca-1.67*P+Na+K)

A/CNK: molecular $Al_2O_3/(CaO+K_2O+Na_2O)$

A/NK: molecular $Al_2O_3/(K_2O+Na_2O)$

CIA: molecular $[Al_2O_3/(Al_2O_3+CaO+Na_2O+K_2O)]*100$

n.d.: not determined; b.d.: below detection limit

Most samples were milled to powder in an agate mill. A tungsten-carbide mill was used for samples Pl1 - Pl10, V2, V4 - V6, PLT-1, and PLT-2. For those samples contamination of Co, Ta and Sc is possible. The high Cr concentration of sample P2 could be caused by contamination during grinding in a rotation mill.

Appendix A-2. XRF trace element replicate analyses

Appendix A-2. XRF trace element replicate analyses

	replicate analyses (n=10) on one pellet					replicate sample preparation, no. of pellets = 10				
sample Pl87	concentration					concentration				
	mean [ppm]	min. [ppm]	max. [ppm]	std. dev. [ppm]	RSD [%]	mean [ppm]	min. [ppm]	max. [ppm]	std. dev. [ppm]	RSD [%]
Sc	8.2	6.4	10.5	1.4	17.2	7.8	6.4	8.8	0.8	9.7
V	64.7	61.9	67.0	1.8	2.8	64.7	62.4	68.4	1.9	3.0
Cr	5.6	4.0	7.4	1.2	21.7	6.0	1.1	7.7	2.0	34.0
Co	4.6	2.7	7.3	1.8	39.6	4.3	2.9	5.4	0.8	19.3
Ni	4.1	2.2	6.0	1.4	32.9	4.4	2.2	6.9	1.3	29.7
Cu	3.7	3.1	5.1	0.6	15.6	3.2	2.4	3.9	0.5	14.4
Zn	69.1	67.8	70.2	0.7	1.1	69.1	68.0	70.3	0.8	1.1
Ga	19.2	18.3	20.6	0.8	4.0	19.0	18.4	19.6	0.4	2.3
Rb	158.7	157.9	159.5	0.5	0.3	158.5	157.5	160.0	0.7	0.5
Sr	223.8	221.6	225.4	1.2	0.5	220.7	219.2	221.9	0.9	0.4
Y	22.6	21.7	23.1	0.5	2.3	22.1	21.6	23.2	0.5	2.2
Zr	152.5	150.1	155.5	1.7	1.1	152.5	146.0	165.4	5.3	3.5
Nb	11.2	10.9	11.9	0.3	2.6	11.3	10.6	12.2	0.5	4.6
Ba	785.8	778.0	795.5	6.0	0.8	784.9	774.8	790.7	5.2	0.7
Pb	16.8	15.3	18.8	1.2	7.0	16.3	14.1	18.3	1.3	7.7
Th	14.1	13.3	15.4	0.7	4.9	13.2	11.6	14.9	0.9	6.9
U	4.0	3.0	5.4	0.7	17.5	4.1	2.5	4.8	0.6	15.8
La	34.7	33.0	36.1	1.1	3.2	36.0	33.8	38.9	1.4	4.0
Ce	72.7	67.2	75.9	2.8	3.9	76.2	70.1	81.1	3.5	4.6
Pr	8.2	6.7	11.2	1.6	19.7	8.7	4.4	13.2	2.5	28.2
Nd	32.5	30.1	36.1	1.6	5.0	33.5	27.8	36.5	2.3	6.8
Sm	5.7	1.8	8.9	2.4	41.7	6.5	4.7	8.1	1.0	15.8

Because the Rb and Sr concentrations obtained by XRF analyses were used to calculate initial ratios of $^{87}Sr/^{86}Sr$, the accuracy of the measurement is crucial. Therefore, a granitic sample with Rb and Sr concentrations of about 158 ppm and 224 ppm, respectively, was chosen and 10 powder pellets prepared and measured to control the effect of possible inhomogeneities due to sample preparation. One of the pellets was measured 10 times as indication for the reproducibility of measurements. It can be seen that errors are about 1ppm for the given concentrations. It has to be kept in mind that higher concentrations will result in smaller uncertainties, while the error on lower concentrations (about a few tens ppm) will increase. This is also evident by those trace elements like Cu, which have very low concentrations that are close to the detection limit and therefore subjected to much larger measurement errors. The error introduced by the sample preparation does generally not exceed the measurement error of the machine.

Appendix B-1. *Results of whole-rock laser-ablation ICP-MS analyses*

	V1	V7	V9	V10	Ka-X5	Pl40	Pl43	Pl73	Pl58	Pl61	Pl63	Pl64	Pl66	Pl70	Pl10	Pl45	Pl50	Pl51	Pl54	Pl16	Pl21	Pl23	Pl81	Pl87	Ev4	Skia1	Skia8
	Pelagonian Zone																										
[ppm]																											
La	61.01	74.77	14.22	49.00	34.48	24.25	15.60	40.49	30.92	19.09	5.89	28.35	25.05	19.39	29.53	13.29	28.80	13.04	24.31	16.27	20.10	23.06	27.44	44.71	12.94	74.46	3.32
Ce	120.52	136.10	24.56	90.70	68.38	52.12	34.03	94.36	60.87	41.19	13.29	54.93	53.94	41.32	51.49	27.88	56.36	25.60	50.09	33.87	41.35	49.05	57.63	90.28	31.99	138.31	5.02
Pr	14.11	16.52	3.50	10.59	7.11	5.61	3.92	9.86	7.81	5.53	1.55	6.57	6.02	4.78	5.70	3.33	6.82	2.51	5.49	4.11	4.80	6.11	6.89	10.45	4.98	14.88	0.60
Nd	52.13	64.03	12.57	39.25	24.99	20.00	14.59	34.93	30.18	21.74	5.61	22.22	21.32	16.93	21.42	13.51	27.07	8.45	20.10	16.19	18.05	25.08	27.20	38.51	23.63	51.80	2.12
Sm	8.88	11.61	2.56	6.37	4.28	3.43	3.27	5.84	6.05	4.14	1.15	4.08	4.28	2.97	3.86	2.76	5.67	1.31	3.62	3.38	3.60	4.78	5.88	6.94	6.70	7.92	0.40
Eu	2.08	2.72	0.18	1.61	0.97	0.68	0.26	1.09	1.06	0.96	0.02	0.40	0.32	0.41	0.92	0.66	1.04	0.22	0.51	0.77	0.67	1.05	0.88	1.03	1.26	1.40	0.65
Gd	7.12	9.39	2.58	5.08	3.28	2.49	3.52	4.40	5.52	3.47	1.04	3.64	4.04	2.50	3.34	2.65	5.30	1.08	2.98	3.10	3.15	4.16	6.12	5.31	6.87	5.82	0.32
Tb	0.95	1.30	0.46	0.69	0.41	0.31	0.66	0.55	0.80	0.50	0.16	0.59	0.71	0.39	0.46	0.38	0.83	0.15	0.43	0.48	0.45	0.59	1.03	0.76	1.12	0.68	0.05
Dy	5.33	7.38	3.17	3.95	2.16	1.58	4.54	2.89	4.66	2.90	0.95	3.67	4.66	2.55	2.70	2.37	5.04	0.84	2.59	3.01	2.60	3.54	6.84	4.30	7.12	3.34	0.31
Ho	0.98	1.37	0.67	0.75	0.37	0.28	0.94	0.49	0.88	0.54	0.18	0.74	0.96	0.53	0.51	0.48	0.99	0.16	0.50	0.61	0.49	0.69	1.42	0.78	1.40	0.55	0.06
Er	2.73	3.73	2.10	2.15	1.00	0.75	2.77	1.33	2.45	1.65	0.53	2.21	2.93	1.59	1.39	1.42	2.86	0.44	1.47	1.77	1.40	1.99	4.27	2.12	4.07	1.39	0.21
Tm	0.40	0.51	0.32	0.31	0.13	0.11	0.40	0.18	0.35	0.25	0.08	0.33	0.45	0.25	0.19	0.20	0.42	0.06	0.21	0.26	0.21	0.29	0.63	0.29	0.58	0.19	0.04
Yb	2.78	3.41	2.29	2.12	0.89	0.87	2.60	1.25	2.34	1.74	0.60	2.35	3.16	1.78	1.35	1.43	2.81	0.44	1.45	1.78	1.43	1.99	4.45	1.98	3.97	1.30	0.30
Lu	0.41	0.48	0.34	0.32	0.14	0.14	0.36	0.18	0.35	0.26	0.09	0.35	0.46	0.26	0.21	0.21	0.43	0.07	0.22	0.27	0.23	0.32	0.67	0.29	0.57	0.21	0.05
Hf	7.05	5.94	2.50	6.43	3.32	3.09	4.15	4.25	6.44	4.86	0.69	4.05	3.04	3.16	4.35	2.04	4.91	0.67	2.59	3.31	2.68	5.92	6.22	3.90	4.27	6.35	2.48
Ta	1.37	1.31	0.78	0.98	0.73	1.48	1.13	1.48	0.96	1.33	0.27	0.93	1.11	0.80	1.09	0.22	1.28	0.28	0.65	0.36	1.05	0.73	0.62	0.99	1.05	0.57	0.27
Eu/Eu*	0.80	0.80	0.22	0.86	0.80	0.71	0.23	0.66	0.56	0.77	0.04	0.32	0.23	0.46	0.78	0.75	0.58	0.55	0.47	0.72	0.61	0.72	0.45	0.52	0.57	0.63	5.58
Ce_N/Yb_N	11.21	10.33	2.78	11.05	19.89	15.51	3.39	19.46	6.73	6.12	5.77	6.05	4.42	6.00	9.87	5.06	5.19	14.98	8.94	4.91	7.45	6.36	3.35	11.82	2.09	27.61	4.36
Ce_N/Sm_N	3.28	2.83	2.32	3.44	3.86	3.67	2.52	3.90	2.43	2.40	2.78	3.25	3.04	3.36	3.22	2.44	2.40	4.72	3.34	2.42	2.77	2.48	2.37	3.14	1.15	4.22	3.05

	Pl75	Pl33	PLT-1	P2	P5	P6
	Vardar Zone					
[ppm]						
La	18.93	34.24	5.07	25.83	31.37	22.93
Ce	39.60	67.94	10.34	62.41	61.29	46.48
Pr	4.29	7.17	1.26	6.71	5.39	4.88
Nd	15.62	25.87	4.62	23.99	16.41	17.33
Sm	2.88	4.20	1.20	4.23	2.18	3.05
Eu	0.73	0.48	0.23	0.64	0.38	0.61
Gd	2.30	3.15	1.25	2.86	1.56	2.60
Tb	0.31	0.39	0.27	0.34	0.21	0.37
Dy	1.76	2.34	1.94	1.49	1.30	2.19
Ho	0.33	0.53	0.40	0.23	0.28	0.45
Er	0.93	1.79	1.23	0.55	0.97	1.40
Tm	0.13	0.31	0.20	0.07	0.17	0.22
Yb	0.94	2.40	1.48	0.43	1.34	1.68
Lu	0.15	0.40	0.22	0.06	0.22	0.27
Hf	2.04	6.17	1.23	2.96	3.09	3.82
Ta	0.22	0.86	0.77	0.55	2.07	0.40
Eu/Eu*	0.87	0.40	0.57	0.57	0.64	0.66
Ce_N/Yb_N	10.93	7.33	1.80	37.37	11.85	7.15
Ce_N/Sm_N	3.32	3.90	2.09	3.56	6.80	3.67

N: normalised to chondrite (values for chondrite from Boynton 1984)

Internal precision is *c.* 1-3% (1RSD) and the external precision is about 5% (1RSD) (Jochum *et al.* submitted)

Appendix B-2. Laser-ablation ICP-MS

Laser-ablation ICP-MS analyses of RE elements were performed on fused whole-rock samples. Powder of the samples were melted on Ir-strips and quenched in an air stream, following the procedure by Gumann *et al.* (2003). To enhance the melting properties of the granitic samples, artificial "basalt" was produced (Gumann *et al.* 2003). The Si-content of the sample was diluted with pure MgO until the SiO_2-concentration was decreased to about 51-56 wt.%. Sample powder (*c.* 100 to 180 mg) and MgO (*c.* 20 to 90 mg) were homogenized in an agate mortar with acetone. Prior to mixing, both the sample powder and the MgO were dried at 100°C for *c.* 12 hours. One sample (V7) was not mixed with MgO, because its original SiO_2-content of *c.* 54.4 wt.% is already in the aimed range. The melting procedure was performed at the Institut für Mineralogie, Johann-Wolfgang-Goethe-Universität Frankfurt, Germany. A small amount of powder was heated on an Ir-strip for about 10 to 20 sec. until solid particles were no longer visible and the degassing ceased. The droplet was then again crushed to fine powder in an agate mortar with acetone and the melting procedure was repeated. The droplets were embedded in epoxy and polished down very slightly until a plain surface was obtained.

Measurements were performed with a ThermoFinnigan Element2 ICP-MS at the Department of Geochemistry, Max-Planck-Institut für Chemie in Mainz, Germany. The instrument was equipped with a New

Table B-2.1 *Results of international geo-reference material analyses by LA-ICP-MS*

[ppm]	JG1	RSE [%]	$JG1_{dup}$	RSE [%]	ref. val. [1]	JG2	RSE [%]	ref. val. [2]	GSP2	RSE [%]	ref. val. [3]
La	15.88	0.44	16.52	1.08	22.40	18.82	2.56	19.00	159.43	1.44	186.00
Ce	36.82	0.24	36.49	1.06	45.80	46.45	1.97	45.00	373.85	2.65	445.00
Pr	4.01	0.57	4.08	1.10	4.83	5.92	2.11	6.00	47.97	2.99	50.70
Nd	15.37	0.55	15.90	1.12	19.30	24.60	1.92	24.00	183.30	2.86	207.00
Sm	3.68	1.08	3.78	1.36	4.62	7.84	1.94	7.50	23.01	3.19	26.20
Eu	0.61	0.81	0.63	1.47	0.73	0.08	0.77	0.09	1.97	2.14	2.27
Gd	3.69	1.20	4.00	0.36	4.28	9.29	1.15	9.30	12.21	2.78	12.20
Tb	0.66	0.63	0.69	1.22	0.78	1.82	1.37	1.74	1.16	1.71	-
Dy	4.28	0.89	4.61	1.05	4.14	12.81	1.87	11.70	5.09	1.92	5.74
Ho	0.87	1.42	0.93	1.66	0.81	2.80	2.43	2.52	0.83	2.32	1.00
Er	2.62	1.77	2.79	0.68	2.16	8.73	1.81	7.80	2.05	0.48	2.26
Tm	0.40	1.01	0.42	2.07	0.41	1.32	2.95	1.22	0.26	1.33	0.30
Yb	2.79	0.97	3.00	0.58	2.47	9.02	2.90	8.10	1.54	1.45	1.64
Lu	0.42	0.51	0.43	0.95	0.39	1.35	3.22	1.21	0.21	1.50	0.22
Hf	3.48	1.21	3.70	0.86	3.56	5.50	5.39	5.70	13.43	1.96	-
Ta	1.47	0.90	1.50	0.53	1.79	2.32	2.80	-	0.86	1.50	-
Sm/Nd	0.239		0.238		0.239	0.319		0.313	0.126		0.127

dupl: JG1 was analysed on two different days

[1] values for reference material JG1 from Imai *et al.* (1995)

[2] values for reference material JG2 from Dulski (2001)

[3] values for reference material GSP2 from Raczek *et al.* (2001)

Internal precision is given as 1RSE. External precision is about 5% (1RSD) (Jochum *et al.* submitted)

RSE = relative standard error = 100 * σ / (√n) / mean [%]

RSD = relative standard deviation = 100 * σ / mean [%]

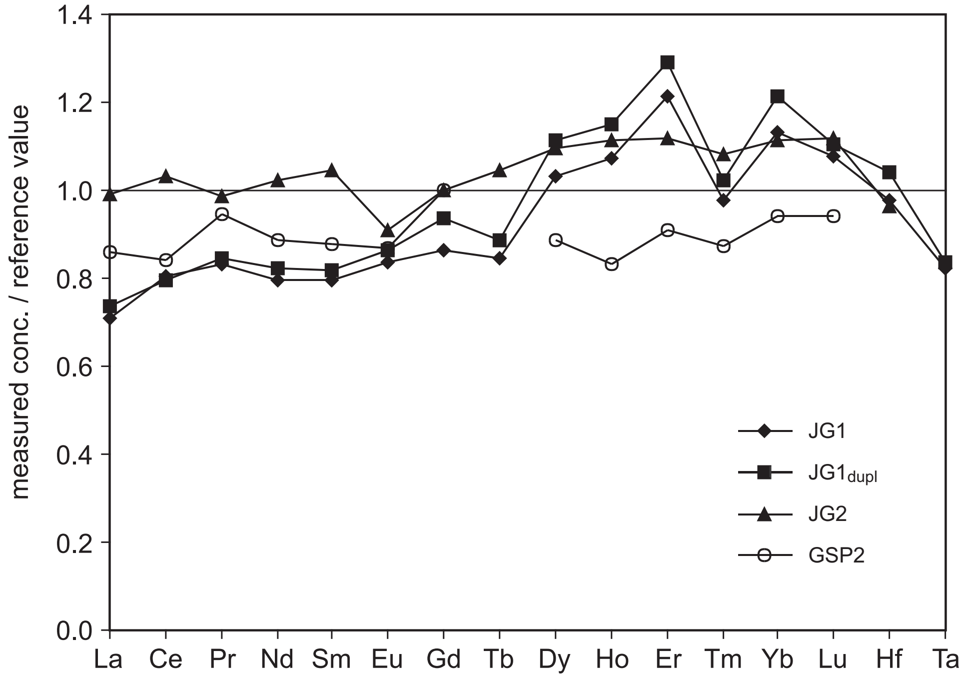

Fig. B-2.1. Ratio of the measured concentration to the reference value of some international geo-reference materials. Reference values are taken from Imai *et al.* (1995) (JG1), Dulski (2001) (JG2) and Raczek *et al.* (2001) (GSP2). The duplicate analysis of JG1, which was measured on a different day, shows a pattern identical to the results from the first measurement. This shows that the deviation is reproducible and not the result of machine settings on an individual day.

Wave UP-213 Nd:Yag laser with a wavelength of 213 nm. Laser settings for the analyses were an energy of *c.* 4.5 J/cm^2, a crater size of 120 µm and 100 sec. dwell time. To control machine drift, NIST612 or KL2G were repeatedly measured. Calcium was chosen as internal standard, because CaO concentrations can be obtained with a good precision by XRF analyses. For one sample (PI33), CaO concentrations were below the detection limit of the XRF, here a Ca content of 1250 ppm was assumed. This assumption resulted in Rb concentrations in agreement with those obtained by XRF analyses. Three spots were measured on each sample and the result is given as the average of these spots. Internal precision (1RSE) for the REE is about 1-3% while the external precision (1RSD) is about 5% (Jochum *et al.* submitted). Additionally to the samples, three international geo-reference materials (JG1, JG2, GSP2) that underwent the same sample preparation procedure were analysed (Table B-2.1). Comparison of the analyses with the reference values from the literature revealed that the measured values of the REE and Hf and Ta of JG2 and GSP2 deviate by about 2-17%. For JG1, the deviation of the concentrations from the reference values is generally larger, especially La and Er show deviations > 20%. While for GSP2 the concentrations are generally shifted to lower values (with the exception of Gd), the picture for JG1 and JG2 shows increased values for the heavy REE in both samples and a decrease in the concentration of the light REE for JG1 (Fig. B-2.1).

To rule out the possibility that droplet inhomogeneity might have caused the deviating results, investigations with the electron microprobe were undertaken for two geo-reference materials and two samples (Table B-2.2). Based on the assumption, that inhomogeneity will be reflected simultaneously both in the REE and trace elements and in the major elements, and that not one of the two groups is distributed homogeneously while the other is inhomogeneous, line analyses for major elements were

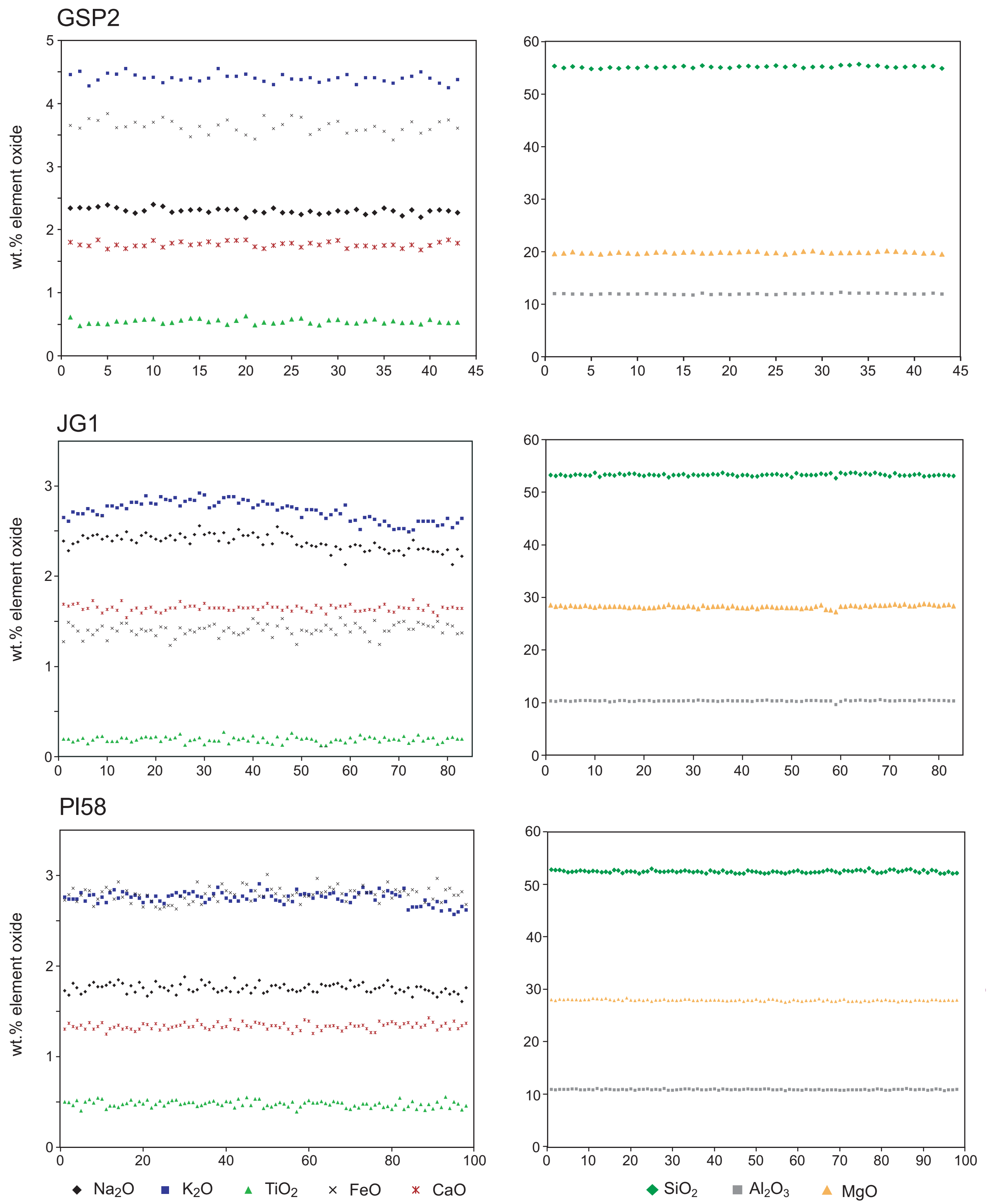

Fig. B-2.2. EMS line analyses on the fused whole-rock samples and geo-reference materials. For GSP2 spots were set 15 µm apart, resulting in a total length of 630 µm. Spot distance was 20 µm for JG1 and the resulting length was 1640 µm. For sample PI58 spot distance was 25 µm and the length of the line was 2425 µm.

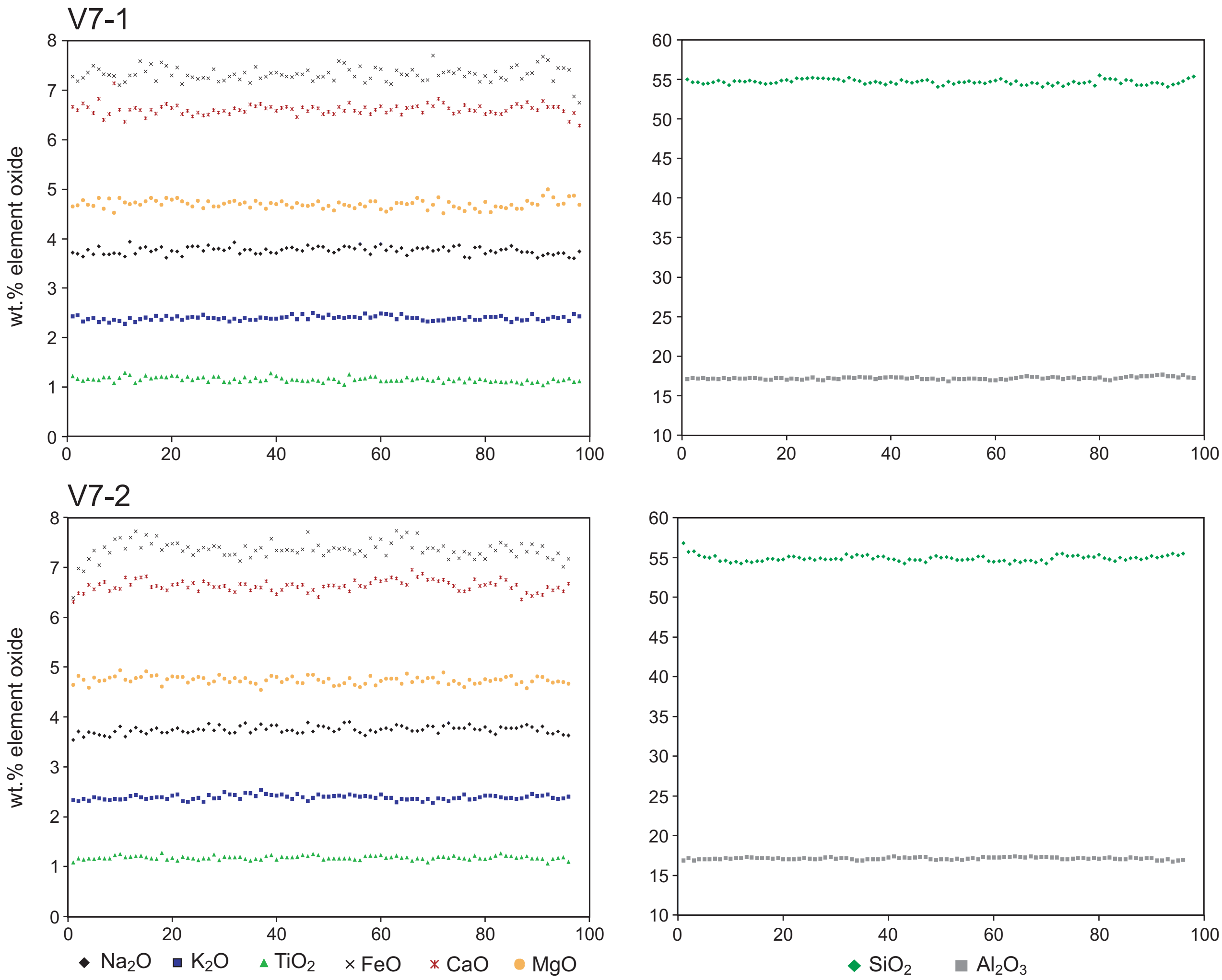

Fig. B-2.3. EMS line analyses on fused whole-rock samples, continued. Sample V7 was fused without the addition of MgO. Spot distance for V7-1 is 20 µm and total length 1940 µm, while for V7-2 a spot distance of 30 µm with a total length of 2850 µm was chosen.

performed with a JEOL JXA 8900 RL equipped with five wavelength dispersive spectrometers at the Institut für Geowissenschaften, Universität Mainz, Germany. On two of the international reference materials (JG1 and GSP2) and two samples (Pl58 with and V7 without additional MgO) analyses with a spot size of 2 µm were performed along lines with a length of about 630 to 2850 µm. Spots were 15 µm apart for the short lines and up to 30 µm for the longer lines. Measurement conditions were 15 kV acceleration voltage and 12 nA probe current. The analysed elements are SiO_2, K_2O, Na_2O, CaO, MgO, Al_2O_3, FeO_{tot}, MnO, TiO_2, and Cr_2O_3. For some elements like chromium, concentrations were close to the detection limit and therefore could not be used to draw inferences. SiO_2, Al_2O_3, MgO and the alkali-oxides, on the other hand, show a flat pattern and are homogeneously distributed, at least at the scale of the profiles (Figs. B-2.2 and B-2.3). The scatter is smaller than the negative deviation of the LA-ICP-MS analyses. This renders the assumption unlikely that the deviation of the results from XRF analyses is due to inhomogeneities caused by the melting process.

Table B-2.2 *Results of major element EMS analyses on reference materials and fused samples*

	GSP2			JG1			V7-1		V7-2		Pl58		
	EMS	EMS*	ref. val. [1]	EMS	EMS*	ref. val. [2]	EMS	RFA	EMS	RFA	EMS	EMS*	RFA
Na_2O	2.30	2.77	2.73	2.38	3.22	3.39	3.76	3.62	3.74	3.62	1.76	2.31	2.34
SiO_2	55.19	-	66.60	53.29	-	72.30	54.68	54.37	54.88	54.37	52.41	-	68.96
K_2O	4.40	5.31	5.42	2.72	3.69	3.97	2.39	2.43	2.39	2.43	2.75	3.62	3.93
TiO_2	0.54	0.65	0.69	0.19	0.26	0.26	1.15	1.14	1.17	1.14	0.48	0.63	0.63
FeO_{tot}	3.64	4.39	4.40	1.41	1.91	1.98	7.32	7.14	7.35	7.14	2.79	3.67	3.68
Al_2O_3	11.98	14.45	14.95	10.33	14.02	14.20	17.22	16.77	17.11	16.77	10.83	14.24	14.60
MgO	19.76	23.85	0.98	28.18	38.23	0.74	4.70	4.46	4.74	4.46	27.86	36.66	1.38
CaO	1.77	2.13	2.10	1.65	2.23	2.18	6.61	6.44	6.63	6.44	1.34	1.76	1.64

* normalised to the SiO_2 reference value concentration

[1] value for reference material GSP2 from Raczek *et al.* (2001)

[2] value for reference material JG1 from Govindaraju (1994)

To test the possible influence of the melting process on the results, new droplets were molten for the international reference materials JG1, JG2 and GSP2 as well as one sample. This melting was done at the Department of Geochemistry, Max-Planck-Institut für Chemie, Mainz, Germany. Droplets were melted from the same batch of material mixed with MgO that was used before. Only one melting step was performed. Approximately 30 mg of the sample were melted on an Ir-strip at 140 nA for 25 sec. For sample PI70 a second droplet was melted with a shorter time of only 15 sec. Additionally, two international reference materials with a basaltic composition (BHVO2 and BCR2) were mixed with MgO in roughly the same proportions as the granitic material (*c.* 100 mg sample and 40 mg MgO). Two droplets were melted for BCR2 and BHVO2 at 120 nA and 140 nA for 25 sec. Measurement conditions were the same as given above, only this time six spots were measured on each sample. For BHVO2 and BCR2, the results are in good agreement with the reference values (Table B-2.3 and Fig. B-2.4). It shows that for the granitic reference materials the deviation from the reference values is of the same order of magnitude as before and that also the direction of deviation for certain elements to lower or higher values corresponds (Fig. B-2.4). This underlines the assumption, that the cause for the negative deviation is most likely neither the mixing procedure with MgO nor the melting procedure. Instead it might be attributed to differences in chemical composition and matrix and a somehow different behaviour of granitic material compared with basaltic one.

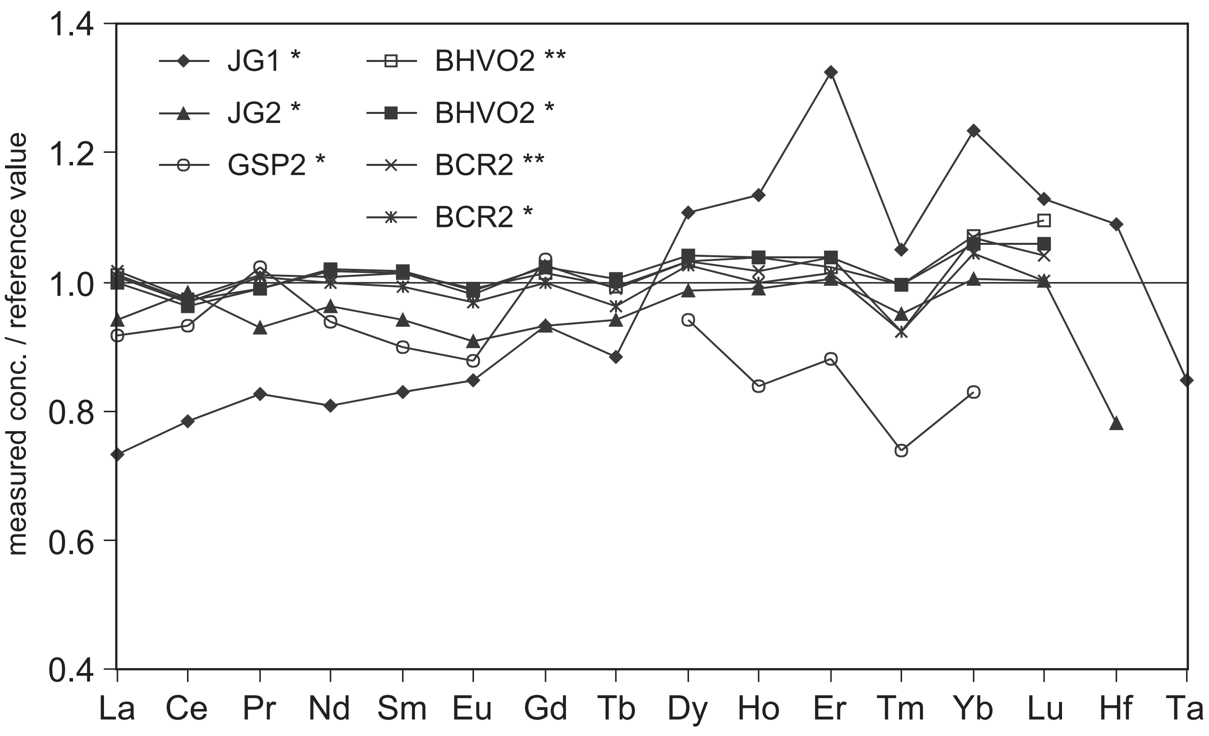

Fig. B-2.4. Ratios of measured values to reference values of geo-reference materials. Melting was performed under defined conditions (time and current, see text). Reference values are taken from Imai *et al.* (1995) (JG1), Dulski (2001) (JG2) and Raczek *et al.* (2001) (GSP2, BHVO2 and BCR2).

Table B-2.3 *Results of re-melted reference materials*

	La	Ce	Pr	Nd	Sm	Eu	Gd	Tb	Dy	Ho	Er	Tm	Yb	Lu	Hf	Ta
JG1 *	16.42	35.93	4.00	15.60	3.84	0.62	3.99	0.69	4.58	0.92	2.86	0.43	3.05	0.44	3.88	1.52
RSE [%]	1.35	1.53	1.30	1.20	1.25	1.85	1.76	1.38	1.57	1.45	1.21	1.26	1.09	1.16	1.14	1.08
JG1-ref [1]	*22.40*	*45.80*	*4.83*	*19.30*	*4.62*	*0.73*	*4.28*	*0.78*	*4.14*	*0.81*	*2.16*	*0.41*	*2.47*	*0.39*	*3.56*	*1.79*
GSP2 *	170.65	414.69	51.92	194.26	23.56	1.99	12.64	1.17	5.40	0.84	1.99	0.22	1.36	-	13.44	0.78
RSE [%]	0.57	2.24	1.96	0.58	2.45	3.12	3.11	3.54	4.57	4.67	4.82	12.15	8.38	-	1.72	5.27
GSP2-ref [2]	*186*	*445*	*50.7*	*207*	*26.2*	*2.27*	*12.2*	-	*5.74*	*1.00*	*2.26*	*0.298*	*1.64*	*0.223*	-	-
JG2 *	17.88	44.21	5.57	23.07	7.06	0.08	8.67	1.64	11.56	2.49	7.83	1.16	8.15	1.21	4.46	1.93
RSE [%]	0.83	1.00	0.91	1.10	1.71	3.66	1.04	1.05	1.17	1.05	1.04	0.99	0.94	1.31	1.81	2.01
JG2-ref [3]	*19*	*45*	*6*	*24*	*7.5*	*0.088*	*9.3*	*1.74*	*11.7*	*2.515*	*7.8*	*1.22*	*8.1*	*1.207*	*5.7*	-
BHVO2 **	15.36	36.42	5.24	24.92	6.16	2.05	6.32	0.93	5.48	1.01	2.60	0.34	2.14	0.30	4.65	1.22
RSE [%]	0.51	0.78	0.66	0.85	1.11	1.22	1.14	1.41	0.96	0.64	0.93	0.77	1.24	1.26	0.95	1.05
BHVO2 *	15.20	36.11	5.24	24.95	6.17	2.04	6.39	0.94	5.52	1.01	2.64	0.34	2.12	0.29	4.61	1.25
RSE [%]	0.31	0.32	0.44	0.55	0.55	0.54	0.68	0.63	0.52	0.61	0.66	0.67	0.39	0.69	0.17	0.40
BHVO2-ref [2]	*15.2*	*37.5*	*5.29*	*24.5*	*6.07*	*2.07*	*6.24*	*0.936*	*5.31*	*0.972*	*2.54*	*0.341*	*2.00*	*0.274*	-	-
BCR2 **	25.31	51.59	6.65	28.88	6.67	1.92	6.93	1.06	6.62	1.32	3.80	0.52	3.61	0.54	5.07	0.79
RSE [%]	0.40	0.42	0.33	0.32	0.46	0.93	0.40	0.50	0.53	0.44	0.80	0.96	0.64	0.69	0.64	0.54
BCR2 *	25.13	51.21	6.63	28.70	6.52	1.90	6.74	1.03	6.58	1.30	3.71	0.52	3.53	0.52	5.00	0.79
RSE [%]	0.53	0.47	0.50	0.66	0.34	0.67	0.54	0.71	0.84	0.55	0.62	0.87	1.20	0.90	0.53	0.60
BCR2-ref [2]	*24.9*	*52.9*	*6.57*	*28.7*	*6.57*	*1.96*	*6.75*	*1.07*	*6.41*	*1.30*	*3.66*	*0.564*	*3.38*	*0.519*	-	-
PI70 ***	20.86	43.17	4.98	17.84	3.26	0.43	2.69	0.42	2.64	0.54	1.68	0.25	1.76	0.26	2.34	0.78
RSE [%]	1.15	1.05	1.25	1.02	1.25	2.32	1.31	2.98	2.58	1.59	1.47	1.27	2.52	2.26	4.65	2.02
PI70 *	21.58	44.20	5.04	18.00	3.23	0.42	2.62	0.42	2.64	0.54	1.69	0.26	1.82	0.27	2.83	0.80
RSE [%]	0.63	0.72	0.56	0.82	0.90	2.52	0.89	1.88	1.27	1.41	1.49	0.91	1.01	1.37	2.97	1.65
PI70-RFA	*23.00*	*48.00*		*19.00*												

[1] Reference values from Imai *et al.* (1995)

[2] Reference values from Raczek *et al.* (2001)

[3] Reference values from Dulski (2001)

Internal precision is given as 1RSE. External precision is about 5% (1RSE) (Jochum *et al.* submitted)

* melted for 25 sec. at 140 nA

** melted for 25 sec. at 120 nA

*** melted for 15 sec. at 140 nA

The deviation of the measured concentrations from those obtained with XRF (for the samples) or from the reference values from the literature (for the reference materials) is a puzzling result. Contamination, either during melting or caused by mixing with potentially contaminated MgO, should result in elevated concentrations. Elevated concentrations are indeed encountered for some heavy REE in JG1 and, to a lesser extent, in JG2. Yet contamination by the melting process is doubtful because for JG1 both the glass melted in the course of the general sample preparation and the one that was melted later as a test show an identical pattern of deviation from the reference value. This reproducibility would not be expected by a fortuitous contamination. The second, and equally unlikely, possibility of addition of contaminated MgO is ruled out by the fact that the later molten glass of JG2 does show no elevated concentrations for the heavy REE (Fig. B-2.4) and that none of the basaltic reference materials, which were mixed with MgO last, shows elevated concentrations Fugacity accounts for the very high loss of Pb (not shown in Appendix B-1) but especially the REE should behave highly refractive and therefore it is improbable that the lower concentrations obtained for some elements are the effect of fugacity. The deviation observed for the REE of the reference materials might be explained by the fact that it is far more difficult to homogenise a granitic sample and to obtain a representative batch than for a basaltic one. This also leads to slightly varying concentration values for the reference material in the literature (see Fig. B-2.5) and could indicate that the batch measured in this study might be different from those used for literature values. The difference between LA-ICP-MS analyses and XRF-analyses of the samples, however, remains puzzling. A possible explanation might be that the different sample preparation procedures for each method caused the deviation, however, no obvious process is known. Another, but relatively unlikely, explanation would assume an offset of either the XRF or the ICP-MS. So far, a final solution cannot be given.

Despite the observed deviations the usability of the data is certain. First of all most deviations up to about 10% can be fairly explained by sample heterogeneity as can be seen from the differences of the individual reference values in the literature. Secondly, the ratios, e.g. Sm/Nd, are in reasonable agreement with those of the reference

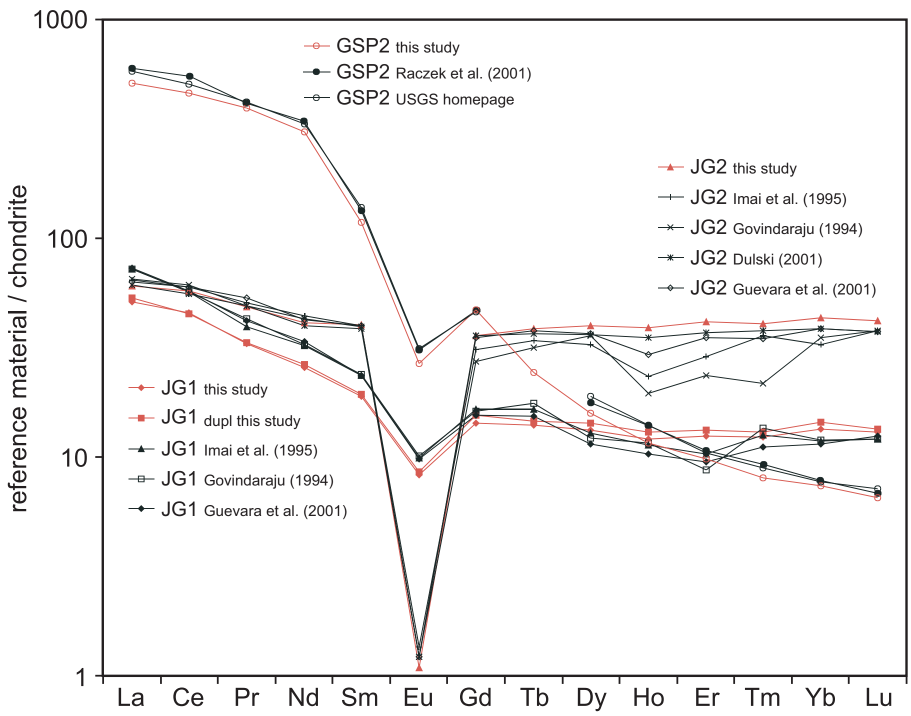

Fig. B-2.5. Chondrite-normalized REE plot for the granitic international reference materials JG1, JG2 and GSP2 (values for chondrite after Boynton 1984). The reference materials form smooth patterns. Additionally plottted are values from the literature.

values. And last, the effect in a normalized and logarithmic REE plot is negligible and will not affect the interpretation of the pattern. This can be seen in the chondrite-normalized REE plot in Fig. B-2.5. The pattern obtained from the LA-ICP-MS measurements is identical to the pattern obtained from the reference values. The variations of the individual reference values are also clearly visible. Therefore, though care has to be taken when dealing with the absolute concentrations, the REE pattern can undoubtedly be used for geochemical interpretations.

Appendix C. Results of whole-rock Sr- and Nd-isotope composition analyses

sample	age [Ma]	$^{143}Nd/^{144}Nd_{m}$	± 2σ	$^{143}Nd/^{144}Nd$ *	$^{147}Sm/^{144}Nd$ §	$^{143}Nd/^{144}Nd_{ini}$	εNd_{ini}	T_{DM} ‡ [Ga]	$^{87}Sr/^{86}Sr_{m}$	± 2σ	$^{87}Rb/^{86}Sr$	$^{87}Sr/^{86}Sr_{ini}$
V1	298	0.512328	9	0.512357	0.1032	0.512156	-1.9	1.0	0.707395	11	0.50	0.705294
V7	294	0.512348	6	0.512354	0.1098	0.512143	-2.3	1.0	0.706430	12	0.26	0.705327
V9	713	0.512189	4	0.512195	0.1233	0.511619	-2.0	1.4	0.869376	12	17.31	< 0.70000
V10	290	0.512310	7	0.512316	0.0983	0.512129	-2.6	1.0	0.707707	15	0.50	0.705658
Ka-X5	276	0.512219	10	0.512247	0.1037	0.512059	-4.4	1.1	0.713506	20	0.88	0.710043
Ka-X5 [1]	276	0.512193	14	0.512198	0.1037	0.512011	-5.3	1.2				
Pl37	300	0.512118	23	0.512123	0.1211 †	0.511885	-7.2	1.5	0.711720	19	0.65	0.708938
Pl40	300	0.512137	10	0.512142	0.1039	0.511938	-6.1	1.3	0.712923	15	1.01	0.708605
Pl40 [2]	300	0.512147	17	0.512152	0.1039	0.511948	-5.9	1.2	0.712854	18	1.01	0.708536
Pl43	137	0.512347	4	0.512352	0.1355	0.512231	-4.5	1.3	0.824348	18	44.09	0.738494
Pl73	245	0.512208	10	0.512239	0.1013	0.512077	-4.8	1.1	0.713583	16	2.66	0.704321
Pl58	710	0.512035	8	0.512041	0.1214	0.511476	-4.8	1.6	0.733084	14	2.23	0.710462
Pl61	292	0.512275	8	0.512272	0.1153	0.512052	-4.1	1.2	0.711694	6	0.81	0.708309
Pl63	244	0.512336	9	0.512341	0.1245	0.512142	-3.5	1.2	0.860183	12	46.30	< 0.70000
Pl64	710	0.512256	8	0.512285	0.1112	0.511767	0.9	1.1	0.863401	18	19.44	< 0.70000
Pl64 [2]	710	0.512302	23	0.512299	0.1112	0.511781	1.2	1.1	0.859820	19	19.45	< 0.70000
Pl66	710	0.512213	8	0.512177	0.1216	0.511611	-2.2	1.4	0.898412	19	20.88	< 0.70000
Pl70	699	0.512105	8	0.512089	0.1062	0.511602	-2.6	1.3	0.801525	16	9.87	0.703053
Pl10	283	0.512206	9	0.512212	0.1091	0.512009	-5.2	1.2	0.713717	15	1.28	0.708548
Pl45	300	0.512446	7	0.512451	0.1237	0.512208	-0.9	1.0	0.707815	13	1.68	0.700664
Pl50	266	0.512171	6	0.512167	0.1268	0.511947	-6.8	1.5	0.718029	10	5.11	< 0.70000
Pl50 [2]	266	0.512177	8	0.512182	0.1268	0.511961	-6.5	1.5	0.717689	16	5.11	< 0.70000
Pl51	300	0.512079	18	0.512085	0.0939	0.511900	-6.9	1.2	0.729619	19	4.48	0.710490
Pl54	312	0.512125	5	0.512120	0.1090	0.511898	-6.6	1.3	0.733728	9	12.99	< 0.70000
Pl13	280	0.512095	8	0.512079	0.1211 †	0.511857	-8.2	1.6	0.727150	20	9.66	< 0.70000
Pl16	241	0.512259	12	0.512265	0.1265	0.512065	-5.1	1.4	0.706569	16	0.41	0.705174
Pl21	279	0.512122	8	0.512118	0.1208	0.511898	-7.4	1.5	0.721123	11	3.63	0.706705
Pl23 [3]	300					0.512193	-1.1	1.0				0.709949
Pl23	546	0.512424	10	0.512419	0.1153	0.512007	1.4	1.0	0.719985	14	2.35	0.701687
Pl80	309	0.512141	9	0.512105	0.1211 †	0.511860	-7.4	1.5	0.751641	18	10.46	0.705642
Pl81	300	0.512310	7	0.512316	0.1309	0.512059	-3.8	1.3	0.713562	8	1.54	0.707004
Pl86	300	0.512156	10	0.512120	0.1211 †	0.511882	-7.2	1.5	0.722324	17	2.35	0.712291
Pl87	281	0.512157	8	0.512163	0.1092	0.511962	-6.1	1.3	0.717217	17	2.05	0.709035
Ev4	303	0.512294	8	0.512299	0.1717	0.511958	-5.7	2.5	0.714591	14	1.99	0.706018
Skia1	289	0.512157	10	0.512152	0.0926	0.511977	-5.6	1.1	0.712812	16	0.94	0.708939
Skia8	287	0.512050	10	0.512081	0.1136	0.511868	-7.8	1.5	0.717228	12	1.70	0.710284
Pl75	285	0.512210	6	0.512216	0.1118	0.512007	-5.1	1.2	0.710416	12	0.62	0.707906
Pl33	155	0.512311	10		0.0983	0.512211	-4.4	1.0	0.735088	16	14.97	0.702097
P2	319	0.512111	9		0.1068	0.511888	-6.6	1.3	0.718765	18	2.53	0.707268
PLT-1 [4]	160	0.512047	21		0.1573	0.511882	-10.7	2.5	0.726022	13	5.64	0.713199
P5	158	0.512412	4		0.0805	0.512329	-2.1	0.8	0.712365	12	3.40	0.704734
P5 [2]	158	0.512382	12		0.0805	0.512299	-2.7	0.8	0.712409	13	3.40	0.704778
P6	164	0.512626	17		0.1066	0.512512	1.7	0.6	0.705328	12	0.22	0.704809

* values are normalised to an average measured La Jolla $^{143}Nd/^{144}Nd$ of 0.511823; initial ratios and model ages are calculated with the normalised ratios

§ Sm and Nd concentrations of the LA-ICP-MS analyses were used to calculate the $^{147}Sm/^{144}Nd$

† a typical crustal $^{147}Sm/^{144}Nd$ of 0.1211 was assumed

‡ model ages are calculated using a $^{143}Nd/^{144}Nd_{(today)}$ of the depleted mantle reservoir of 0.513114 after Michard *et al.* (1985)

[1] duplicate measurement from the same solution

[2] replicate analysis after repeated sample preparation

[3] initial values and model age calculated for an assumed age of 300 Ma

[4] initial values and model age calculated for an assumed last homogenisation event at 160 Ma

εNd_{ini} were calculated using the values for CHUR after Wasserburg *et al.* (1981)

Over the period of measurements international standards were measured additionally. For La Jolla, the weighted average of the measured $^{143}Nd/^{144}Nd$ ratio was 0.511819 ± 9 (2σ, n=16), while for the NIST SRM 987 an $^{87}Sr/^{86}Sr$ ratio of 0.710234 ± 12 (2σ, n=16) was obtained. Despite the small error on the weighted average $^{143}Nd/^{144}Nd$ ratio for La Jolla, measurements performed on different days showed strong variations ranging from 0.511792 to 0.511859. To allow comparison of the samples that were measured on different days, the $^{143}Nd/^{144}Nd$ was normalised to the La Jolla value of the largest homogeneous group, which was 0.511823 ± 6 (95% conf, n=10). The samples from the Vardar Zone, which are described in Chapter 1, are not normalised. They were mostly analysed on days on which the La Jolla $^{143}Nd/^{144}Nd$ was close to 0.511823.

Additionally to the samples the USGS reference material GSP2 was analysed. Over the period of measurement it was measured twice and yielded $^{143}Nd/^{144}Nd$ values of 0.511290 ± 19 and 0.511334 ± 8. Published $^{143}Nd/^{144}Nd$ values for GSP2 are 0.511353 ± 5 and 0.511352 ± 7 (Raczek *et al.* 2003). Using the La Jolla $^{143}Nd/^{144}Nd$ values of Raczek *et al.* (2003), the normalised values of 0.511337 and 0.511346 are within errors to the published $^{143}Nd/^{144}Nd$ values.

Appendix D-1. Results of single-zircon Pb-Pb evaporation analyses

sample-grain	no. of ratios	$^{206}Pb/^{204}Pb_m$ [1]	$^{207}Pb^*/^{206}Pb^*$ [2]	± (2σ)	age [Ma]	± (2σ)
V1-A	131	9027	0.052156	0.000089	292	4
V1-B	124	10994	0.052246	0.000038	296	2
V1-C	87	8995	0.052130	0.000083	291	4
V1-D	170	7657	0.052034	0.000080	287	4
V1-E	113	5782	0.052384	0.000051	302	2
V1-F	131	8140	0.052466	0.000056	306	2
V1-G	59	8338	0.051115	0.000391	246	18
V2-A	58	6468	0.051361	0.000186	257	8
V2-B	151	2058	0.051928	0.000091	282	4
V2-C	129	2103	0.052060	0.000162	288	7
V2-D	190	11558	0.051773	0.000084	275	4
V2-E	76	5591	0.051322	0.000133	255	6
V2-F	153	10770	0.051983	0.000062	285	3
V2-G	95	10986	0.051573	0.000126	267	6
V2-H	124	5380	0.051521	0.000084	264	4
V4-A	97	6476	0.051720	0.000159	273	7
V4-B	113	3496	0.052607	0.000130	312	6
V4-C	191	25582	0.052243	0.000025	296	1
V4-D	93	1788	0.052005	0.000172	286	8
V4-E	38	2601	0.051952	0.000248	283	11
V4-F	57	6084	0.051199	0.000174	250	8
V4-G	58	3642	0.049935	0.000297	192	14
V4-H	37	4055	0.051882	0.000207	280	9
V5-A	131	14513	0.052172	0.000073	293	3
V5-B	133	14653	0.051722	0.000136	273	6
V5-C	38	22245	0.051905	0.000302	281	13
V5-D	75	9199	0.051009	0.000173	241	8
V5-E	188	16091	0.052246	0.000058	296	3
V5-F	210	23231	0.052029	0.000083	287	4
V5-G	156	9797	0.051727	0.000128	273	6
V5-H	37	12104	0.052028	0.000214	287	9
V5-I	76	14035	0.051632	0.000178	269	8
V7-A	171	10649	0.052006	0.000070	286	3
V7-B	152	8840	0.052144	0.000035	292	2
V7-C	132	21299	0.052141	0.000036	292	2
V7-D	110	19132	0.052259	0.000028	297	1
V7-E	152	5263	0.052176	0.000073	293	3
V7-F	129	11179	0.052249	0.000025	296	1
V7-G	152	13523	0.051780	0.000083	276	4
V7-H	152	10283	0.052187	0.000066	294	3
V7-I	152	6660	0.052375	0.000071	302	3
V9-A	134	8836	0.061591	0.000105	660	4
V9-B	109	27394	0.069183	0.000245	904	7
V9-C	76	12395	0.108649	0.000798	1777	13
V9-D	135	8949	0.061133	0.000083	644	3
V9-E	91	13407	0.062223	0.000141	682	5
V9-F	138	11636	0.062218	0.000092	682	3
V9-G	126	15070	0.063693	0.000103	731	3
V9-H	138	14144	0.062412	0.000079	688	3
V10-A	171	7214	0.051898	0.000049	281	2
V10-B	189	10051	0.052260	0.000045	297	2
V10-C	96	5998	0.051919	0.000078	282	3
V10-D	176	9110	0.052303	0.000081	299	4
V10-E	173	10288	0.052168	0.000065	293	3
V10-F	200	1772	0.052009	0.000129	286	6
V10-G	183	16970	0.052231	0.000048	296	2
V10-H	195	9365	0.051920	0.000072	282	3

Appendix D-1. *(continued)*

sample-grain	number of ratios	$^{206}Pb/^{204}Pb_m$ [1]	$^{207}Pb^*/^{206}Pb^*$ [2]	± (2σ)	age [Ma]	± (2σ)
Ka-X5-A	133	1138	0.051881	0.000170	280	8
Ka-X5-B	76	4001	0.055007	0.000313	413	13
Ka-X5-C	109	2740	0.051708	0.000072	273	3
Ka-X5-D	150	1945	0.051452	0.000096	261	4
Ka-X5-E	160	5237	0.051818	0.000091	277	4
Ka-X5-F	57	2567	0.051164	0.000175	248	8
Ka-X5-G	96	873	0.052158	0.000145	292	6
Ka-X5-H	208	1408	0.051676	0.000098	271	4
Pl61-A	151	6599	0.052081	0.000106	289	5
Pl61-B	149	3198	0.052082	0.000084	289	4
Pl61-C	172	5989	0.052047	0.000060	287	3
Pl61-D	91	14153	0.052303	0.000111	299	5
Pl61-E	113	13423	0.052256	0.000076	297	3
Pl61-F	154	1896	0.052333	0.000157	300	7
Pl5 A	117	1295	0.092091	0.000275	1469	6
Pl5 B	175	15196	0.057016	0.000074	492	3
Pl5 C	92	1966	0.051664	0.000080	271	4
Pl5 D	131	8489	0.052095	0.000068	290	3
Pl5 E	173	6288	0.052246	0.000153	296	7
Pl5 F	212	16895	0.059217	0.000179	575	7
Pl5 G	97	8364	0.060235	0.000116	612	4
Pl5 H	97	920	0.051809	0.000205	277	9
Pl5 I	133	2076	0.081120	0.000225	1224	5
Pl8-A	134	6747	0.051506	0.000110	264	5
Pl8-B	156	7020	0.056916	0.000064	488	2
Pl8-C	139	6128	0.078976	0.000567	1172	14
Pl8-D	173	11285	0.052710	0.000061	316	3
Pl8-E	152	35044	0.055095	0.000069	416	3
Pl8-F	152	10986	0.052033	0.000100	287	4
Pl8-G	94	1558	0.051877	0.000116	280	5
Pl8-H	57	7417	0.051831	0.000197	278	9
Pl8-I	114	15674	0.114665	0.000126	1875	2
Pl87-A	117	9570	0.051829	0.000126	278	6
Pl87-B	151	7453	0.051989	0.000141	285	6
Pl87-C	135	19932	0.051910	0.000133	281	6
Pl87-D	80	7184	0.051904	0.000242	281	11
Sky1-A	156	7170	0.046389	0.000052	18	3
Sky1-B	132	3180	0.046452	0.000110	21	6
Sky1-C	95	6025	0.046189	0.000099	8	5
Sky1-D	76	4448	0.046239	0.000166	10	9

[1] measured ratio

[2] ratio corrected for common Pb (using the values of Stacey & Kramers 1975)

Appendix D-2: Results of Phalaborwa (PAL) internal reference zircon analyses

Additional to the sample zircons the reference zircon PAL was analysed, applying the same measurement procedures as for the samples.

The analyses of three out of four zircon fragments, which were measured using the Pb-Pb evaporation method, resulted in a mean age of 2038 ± 18 Ma (n = 3). One grain yielded a distinctly younger age of 2008 ± 1 Ma and was therefore excluded from the age calculation (Table D-2.1, Fig. D-2.1a). This deviation could be explained either by slight inhomogeneities of the reference zircon or it might have experienced minor Pb loss that affected the $^{207}Pb/^{206}Pb$ of the zircon a bit. The possibility that the younger ages might be influenced by the Pb isotope composition of inclusions in the zircon fragments is doubtful because of the high $^{206}Pb/^{204}Pb$ ratios. Additionally, great care was taken to chose inclusion-free zircon fragments for analysis. The deviation of the obtained mean age from the age of 2060.6 Ma obtained for Baddeleyite of the same complex (Reischmann 1995) could also indicate the influence of minor Pb loss.

Table D-2.1. *Results of Pb-Pb analyses of the PAL zircon*

sample	grain	no. of ratios	$^{206}Pb/^{204}Pb_m$ [1]	$^{207}Pb^*/^{206}Pb^*$ [2]	± 2σ	age [Ma]	± 2σ
PAL	A	112	12778	0.125505	86	2036	1
PAL	B	110	9197	0.123528	55	2008	1
PAL	C	96	21211	0.126574	145	2051	2
PAL	D	132	17962	0.125410	94	2035	1

[1] measured ratio

[2] ratio corrected for common Pb (using the values of Stacey & Kramers 1975)

Analysis of the PAL reference zircon with the conventional U-Pb method resulted in an upper intercept age of 2054 ± 29 Ma (95% confidence level, n = 5, MSWD = 0.6) (Table D-2.2, Fig. D-2.1b). This age is in good agreement to the Baddeleyite-age (Reischmann 1995).

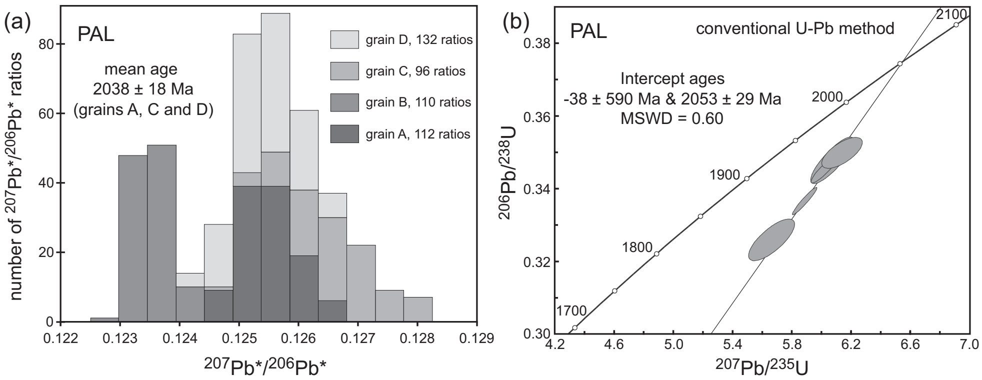

Fig. D-2.1. Diagrams showing the results of the analyses of the PAL internal reference zircon. (**a**) Pb-Pb evaporation method. (**b**) Conventional U-Pb method.

Table D-2.2. *Results of conventional U-Pb analyses of the PAL zircon*

sample.grain	$^{206}Pb/^{204}Pb_m$ [1]	U_{tot}/Pb_{rad}	$^{207}Pb/^{235}U_c$	± 2σ	$^{206}Pb/^{238}U_c$ [2]	± 2σ	$^{207}Pb/^{206}Pb_c$ [2]	± 2σ	R	$^{207}Pb/^{206}Pb$ [Ma]	± 2σ
PAL.L2	405	1.7	6.073	120	0.34759	525	0.12672	117	0.847	2053	16
PAL.L3	1144	1.5	6.023	75	0.34517	317	0.12656	53	0.908	2051	7
PAL.L4	702	1.8	6.140	112	0.34962	348	0.12737	133	0.679	2062	19
PAL.L5	1626	1.8	5.887	67	0.33629	306	0.12695	35	0.957	2056	5
PAL.L6	484	1.8	5.662	127	0.32561	473	0.12613	156	0.754	2045	22

[1] measured ratio, fractionation corrected

[2] radiogenic Pb, corrected for spike, fractionation, and common Pb (using the values of Stacey & Kramers)

Appendix E. Single-zircon conventional U-Pb analyses

		measured ratios (fract. corrected)				radiogenic ratios, corrected for spike, fractionation and common Pb								apparent ages					
		$^{206}Pb/^{204}Pb$	±	$^{207}Pb/^{206}Pb$	±	$^{207}Pb/^{235}U$	±	$^{206}Pb/^{238}U$	±	R	$^{207}Pb/^{206}Pb$	±	U_{tot}/Pb_{rad}	$^{206}Pb/^{238}U$	±	$^{207}Pb/^{235}U$	±	$^{207}Pb/^{206}Pb$	±
sample	grain		2σ		2σ		2σ		2σ			2σ		[Ma]	2σ	[Ma]	2σ	[Ma]	2σ
PLT-1	a	272	2	0.11017	10	0.4326	54	0.05530	26	0.35	0.05674	66	15.8	347	2	365	4	482	26
PLT-1	b	716	38	0.07404	65	0.3822	169	0.05145	50	0.23	0.05388	199	17.9	323	3	329	13	366	86
PLT-1	c	189	2	0.13188	19	0.2970	97	0.03919	40	0.22	0.05497	225	23.7	248	3	264	8	411	94
PLT-1	d	298	4	0.10491	11	0.3010	62	0.03843	21	0.30	0.05681	88	23.8	243	1	267	5	484	35
PLT-1	e	179	1	0.13363	19	0.2340	38	0.03272	13	0.20	0.05187	91	28.6	208	1	213	3	280	41
PLT-1	f	334	3	0.09666	15	0.2091	34	0.02861	14	0.29	0.05301	72	32.3	182	1	193	3	329	31
PLT-1	g	51	0	0.34379	44	0.2020	95	0.02597	30	0.06	0.05642	701	34.2	165	2	187	8	469	301
PLT-1	h	113	2	0.17837	33	0.1722	109	0.02568	24	0.10	0.04864	330	35.2	163	2	161	9	130	152
PLT-1	i	103	1	0.19263	27	0.1165	42	0.01691	12	0.13	0.04997	206	54.7	108	1	112	4	193	99
PLT-2	j	811	18	0.07697	40	0.7279	186	0.08881	91	0.60	0.05944	77	8.8	549	5	555	11	538	28
PLT-2	k	2465	39	0.06225	6	0.5567	52	0.07152	46	0.94	0.05645	13	12.7	445	3	449	3	470	5
PLT-2	l	1899	114	0.06385	30	0.4778	91	0.06156	30	0.31	0.05629	76	14.6	385	2	397	6	464	30
PLT-2	m	1735	76	0.06232	9	0.4106	66	0.05513	40	0.65	0.05402	44	16.1	346	2	349	5	372	18
V9	a	3961	298	0.06630	11	0.8758	115	0.10123	69	0.74	0.06275	39	8.6	622	4	639	6	700	13
V9	b	2802	87	0.06753	18	0.8675	105	0.10079	65	0.73	0.06243	37	8.4	619	4	634	6	689	13
V9	c	2077	29	0.06920	6	0.8620	73	0.10030	59	0.90	0.06233	17	8.6	616	3	631	4	686	6
V9	d	2307	43	0.06822	18	0.8475	157	0.09906	133	0.93	0.06205	33	8.4	609	8	623	9	676	11
V9	e	1772	11	0.07039	5	0.8359	60	0.09732	53	0.93	0.06230	13	8.8	599	3	617	3	684	4
V9	f	351	1	0.10221	10	0.6676	58	0.07938	34	0.53	0.06100	40	11.1	492	2	519	4	639	14
V9	g	1257	44	0.07566	16	1.0226	140	0.11520	54	0.44	0.06438	56	7.5	703	3	715	7	754	19
Pl58	h	1130	17	0.08382	19	1.4398	172	0.14632	76	0.65	0.07137	41	6.2	880	4	906	7	968	12
Pl58	i	2172	25	0.08304	13	1.4991	109	0.14194	63	0.84	0.07660	22	6.4	856	4	930	4	1111	6
Pl58	j	1010	13	0.08417	4	1.3346	155	0.13797	108	0.92	0.07016	23	6.6	833	6	861	7	933	7
Pl58	k	835	9	0.09389	8	1.4542	148	0.13713	89	0.81	0.07691	35	6.4	828	5	912	6	1119	9
Pl58	l	424	8	0.09732	11	1.0910	230	0.12386	84	0.52	0.06389	66	7.2	753	5	749	11	738	22
Pl58	m	503	7	0.09468	25	1.0916	276	0.11916	136	0.64	0.06644	86	7.5	726	8	749	14	820	27
Pl58	n	371	12	0.10860	68	1.1215	493	0.11575	139	0.28	0.07027	255	7.7	706	8	764	24	936	76
Pl58	o	300	6	0.11382	30	1.0422	320	0.11429	95	0.26	0.06614	170	7.9	698	5	725	16	811	55
Pl58	p	848	12	0.08034	14	1.0026	132	0.11423	68	0.75	0.06365	32	7.9	697	4	705	7	730	11
Pl58	q	426	3	0.09776	13	0.9931	118	0.11240	56	0.48	0.06408	54	8.1	687	3	700	6	744	18
Pl58	r	1690	15	0.07249	6	0.8987	62	0.10174	46	0.89	0.06406	14	9.0	625	3	651	3	744	5
Pl58	s	849	9	0.07892	7	0.8530	84	0.09972	48	0.70	0.06204	30	8.7	613	3	626	5	675	10
Pl58	t	633	18	0.08544	35	0.8016	347	0.09287	248	0.63	0.06260	197	9.4	572	15	598	20	695	69

Appendix E. *(continued)*

		measured ratios (fract. corrected)				radiogenic ratios, corrected for spike, fractionation and common Pb								apparent ages					
sample	grain	$^{206}Pb/^{204}Pb$	± 2σ	$^{207}Pb/^{206}Pb$	± 2σ	$^{207}Pb/^{235}U$	± 2σ	$^{206}Pb/^{238}U$	± 2σ	R	$^{207}Pb/^{206}Pb$	± 2σ	U_{tot}/Pb_{rad}	$^{206}Pb/^{238}U$ [Ma]	± 2σ	$^{207}Pb/^{235}U$ [Ma]	± 2σ	$^{207}Pb/^{206}Pb$ [Ma]	± 2σ
Pl59	u	456	1	0.11652	11	1.9157	123	0.16172	62	0.75	0.08592	28	5.2	966	3	1087	4	1336	6
Pl59	v	451	5	0.10723	14	1.6751	301	0.16007	161	0.66	0.07590	84	5.6	957	9	999	11	1092	22
Pl59	w	264	4	0.12317	37	1.1474	356	0.12058	138	0.42	0.06901	158	7.4	734	8	776	17	899	48
Pl59	x	1766	74	0.08150	6	1.0122	108	0.09995	52	0.64	0.07345	43	8.9	614	3	710	5	1027	12
Pl59	y	409	3	0.10257	6	0.8276	107	0.08898	75	0.80	0.06746	42	10.3	550	4	612	6	852	13
Pl70	z	281	3	0.11370	21	0.9207	257	0.10665	117	0.41	0.06261	140	7.5	653	7	663	14	695	48
Pl70	aa	2881	30	0.06766	11	0.9001	64	0.10412	46	0.85	0.06270	17	7.9	638	3	652	3	698	6
Pl70	bb	703	10	0.08363	11	0.9045	130	0.10378	74	0.60	0.06321	57	8.2	637	4	654	7	715	19
Pl70	cc	912	4	0.07849	4	0.8792	82	0.10173	76	0.95	0.06269	16	7.8	625	4	641	4	698	5
Pl70	dd	1768	41	0.08896	14	1.6716	169	0.14956	86	0.77	0.08106	37	5.8	899	5	998	6	1223	9
Pl70	ee	1939	15	0.08251	8	1.3082	79	0.12602	50	0.90	0.07529	14	6.4	765	3	849	3	1076	4
Pl64	ff	619	6	0.08544	26	0.8953	117	0.10454	48	0.38	0.06211	64	7.9	641	3	649	6	678	22
Pl64	gg	195	2	0.13570	15	0.8569	192	0.10132	68	0.27	0.06134	128	8.0	622	4	628	11	651	45
Pl64	hh	167	1	0.14822	33	0.7990	314	0.09392	154	0.26	0.06170	341	8.8	579	9	596	18	664	123
Pl64	ii	704	5	0.07975	8	0.5103	54	0.06256	41	0.75	0.05916	33	13.9	391	2	419	4	573	12
Pl64	jj	385	2	0.09586	26	0.4787	62	0.05965	22	0.28	0.05821	67	14.5	374	1	397	4	538	25
Pl66	kk	542	3	0.08895	9	0.8790	106	0.10226	79	0.73	0.06234	43	8.4	628	5	640	6	686	15
Pl66	ll	736	9	0.08168	20	0.8417	108	0.09827	55	0.54	0.06212	51	8.4	604	3	620	6	678	18
Pl66	mm	771	1	0.07997	3	0.7043	47	0.08335	46	0.95	0.06129	11	10.5	516	3	541	3	649	4
Pl66	nn	828	7	0.07804	13	0.6428	79	0.07686	34	0.79	0.06065	34	11.4	477	3	504	5	627	12
Pl66	oo	302	1	0.13165	11	1.7797	142	0.15166	64	0.54	0.08511	54	5.7	910	4	1038	5	1318	12
Pl66	pp	1035	10	0.08560	10	1.2963	131	0.13068	84	0.86	0.07195	27	6.7	792	5	844	6	984	8
Pl75	1	294	2	0.10171	57	0.3005	67	0.04146	34	0.60	0.05258	55	19.3	262	2	267	5	311	24
Pl75	2	1069	6	0.06595	10	0.3205	27	0.04438	21	0.78	0.05238	19	20.3	280	1	282	2	302	8
Pl75	3	786	16	0.07023	28	0.3224	75	0.04506	37	0.53	0.05189	65	19.4	284	2	284	6	281	29
Pl75	4	753	36	0.07088	42	0.3242	132	0.04550	52	0.34	0.05168	145	18.8	287	3	285	10	271	66
Pl75	5	1531	35	0.06143	16	0.3562	61	0.04961	43	0.79	0.05207	34	18.5	312	3	309	5	288	15
Ka-X5	6	427	1	0.08614	21	0.2902	43	0.04057	33	0.55	0.05189	61	21.7	256	2	259	3	280	27
Ka-X5	7	305	1	0.10018	9	0.3143	43	0.04370	34	0.63	0.05216	48	18.0	276	2	278	3	292	21
Ka-X5	8	1127	7	0.06518	2	0.3191	28	0.04434	31	0.92	0.05220	15	19.7	280	2	281	2	294	7

Appendix E. *(continued)*

		measured ratios (fract. corrected)				radiogenic ratios, corrected for spike, fractionation and common Pb								apparent ages					
		$^{206}Pb/^{204}Pb$	±	$^{207}Pb/^{206}Pb$	±	$^{207}Pb/^{235}U$	±	$^{206}Pb/^{238}U$	±	R	$^{207}Pb/^{206}Pb$	±	U_{tot}/Pb_{rad}	$^{206}Pb/^{238}U$	±	$^{207}Pb/^{235}U$	±	$^{207}Pb/^{206}Pb$	±
sample	grain		2σ		2σ		2σ		2σ			2σ		[Ma]	2σ	[Ma]	2σ	[Ma]	2σ
Ka-X5	10	359	1	0.09369	18	0.3287	83	0.04504	75	0.46	0.05294	158	19.3	284	5	289	6	326	69
Ka-X5	11	1286	9	0.06484	6	0.3375	38	0.04575	38	0.93	0.05351	18	20.3	288	2	295	3	351	7
V7	12	1171	20	0.06384	18	0.3157	51	0.04447	35	0.67	0.05149	42	17.6	281	2	279	4	263	19
V7	13	2156	166	0.05841	19	0.3184	67	0.04457	29	0.41	0.05181	70	17.8	281	2	281	5	277	31
V7	14	365	6	0.09091	21	0.3142	69	0.04467	20	0.20	0.05102	92	17.0	282	1	277	5	242	42
V7	15	2486	85	0.05750	19	0.3211	40	0.04493	20	0.51	0.05183	36	17.3	283	1	283	3	278	16
V7	16	4270	160	0.05543	10	0.3224	34	0.04488	27	0.81	0.05210	22	16.8	283	2	284	3	290	10
V7	17	1008	3	0.06607	7	0.3214	35	0.04510	36	0.90	0.05169	19	17.0	284	2	283	3	272	9
V7	18	280	3	0.10463	20	0.3246	90	0.04490	38	0.26	0.05243	147	17.3	283	2	285	7	304	65
Pl37	19	605	8	0.07606	29	0.2908	57	0.04037	25	0.44	0.05225	61	22.0	255	2	259	4	296	27
Pl37	20	600	19	0.07668	16	0.3105	78	0.04288	27	0.25	0.05251	107	20.5	271	2	275	6	308	47
Pl37	21	348	14	0.09353	25	0.3147	160	0.04407	49	0.19	0.05178	235	20.7	278	3	278	12	276	108
Pl37	22	751	6	0.07156	7	0.3255	42	0.04494	33	0.94	0.05252	13	20.0	283	2	286	3	308	6
Pl37	23	317	2	0.09904	17	0.3371	56	0.04593	31	0.51	0.05323	57	19.9	289	2	295	4	339	25
Pl37	24	206	1	0.12339	6	0.3342	35	0.04643	22	0.35	0.05220	60	18.7	293	1	293	3	294	26
Pl37	25	533	2	0.08395	3	0.3675	29	0.04697	26	0.80	0.05675	23	19.6	296	2	318	2	482	9
Pl37	26	554	34	0.07968	27	0.3728	171	0.05027	43	0.21	0.05379	187	18.0	316	3	322	13	362	80
Pl37	27	631	5	0.07936	5	0.4709	35	0.06068	20	0.49	0.05629	31	14.6	380	1	392	2	464	12
Pl37	28	1268	12	0.07018	4	0.5377	37	0.06637	29	0.80	0.05876	19	14.0	414	2	437	2	558	7
Pl40	29	276	2	0.10475	6	0.3113	43	0.04362	25	0.41	0.05176	60	21.0	275	2	275	3	275	27
Pl40	30	716	12	0.07563	34	0.4189	86	0.05492	42	0.44	0.05532	79	16.0	345	3	355	6	425	32
Pl40	31	1593	7	0.06460	2	0.4363	68	0.05702	82	0.99	0.05550	9	15.6	357	5	368	5	432	4
Pl40	32	931	36	0.07296	25	0.4931	101	0.06229	32	0.26	0.05742	93	14.2	390	2	407	7	508	36
Pl40	33	1898	63	0.06453	8	0.5233	78	0.06666	57	0.78	0.05694	37	13.1	416	3	427	5	489	15
Pl40	34	645	6	0.08638	22	0.5370	84	0.06067	50	0.71	0.06420	51	14.3	380	3	436	6	748	17
Pl44	35	403	5	0.08517	20	0.1441	38	0.02133	18	0.41	0.04898	85	43.9	136	1	137	3	147	41
Pl44	36	154	1	0.14371	60	0.1438	50	0.02145	14	0.17	0.04865	150	43.7	137	1	136	4	131	74
Pl44	37	166	1	0.13730	33	0.1462	45	0.02160	22	0.42	0.04910	99	43.7	138	1	139	4	153	48
Pl44	38	414	5	0.08421	25	0.1473	35	0.02182	15	0.37	0.04897	80	42.1	139	1	140	3	146	39
Pl44	39	435	3	0.08213	10	0.1512	23	0.02248	12	0.68	0.04878	25	40.4	143	1	143	2	137	12
Pl44	40	311	1	0.09609	26	0.1525	25	0.02248	10	0.36	0.04922	52	40.7	143	1	144	2	158	25
Pl44	41	640	7	0.07252	29	0.1566	31	0.02278	13	0.42	0.04985	57	41.3	145	1	148	3	188	27

Appendix E. *(continued)*

		measured ratios (fract. corrected)				radiogenic ratios, corrected for spike, fractionation and common Pb								apparent ages					
		$^{206}Pb/^{204}Pb$	±	$^{207}Pb/^{206}Pb$	±	$^{207}Pb/^{235}U$	±	$^{206}Pb/^{238}U$	±	R	$^{207}Pb/^{206}Pb$	±	U_{tot}/Pb_{rad}	$^{206}Pb/^{238}U$	±	$^{207}Pb/^{235}U$	±	$^{207}Pb/^{206}Pb$	±
sample	grain		2σ		2σ		2σ		2σ			2σ		[Ma]	2σ	[Ma]	2σ	[Ma]	2σ
PI63	42	104	1	0.19194	28	0.2684	81	0.03766	18	0.10	0.05169	165	21.1	238	1	241	7	272	75
PI63	43	329	2	0.09509	16	0.2695	41	0.03858	23	0.47	0.05067	50	20.8	244	1	242	3	226	23
PI63	44	123	1	0.17055	23	0.2741	89	0.03899	55	0.39	0.05099	158	20.5	247	3	246	7	241	73
PI63	45	174	1	0.13529	19	0.3083	84	0.04373	39	0.34	0.05114	116	18.6	276	2	273	7	247	53
PI73	46	383	4	0.08923	16	0.1102	18	0.01560	7	0.27	0.05123	66	55.0	100	0	106	2	251	30
PI73	47	842	3	0.06832	6	0.1535	16	0.02173	15	0.96	0.05125	10	39.5	139	1	145	1	252	4
PI73	48	664	9	0.07313	17	0.1649	33	0.02329	18	0.50	0.05136	64	36.0	148	1	155	3	257	29
PI73	49	407	5	0.08675	4	0.1866	29	0.02659	12	0.30	0.05088	64	33.1	169	1	174	2	235	29
PI73	50	247	3	0.11089	47	0.1987	92	0.02786	44	0.23	0.05172	286	30.9	177	3	184	8	273	132
PI73	51	716	29	0.07068	18	0.2444	74	0.03501	25	0.28	0.05065	108	24.4	222	2	222	6	225	50
PI73	52	1417	23	0.06046	18	0.2565	34	0.03677	20	0.65	0.05060	31	23.3	233	1	232	3	222	14
PI73	53	541	17	0.07643	7	0.2859	77	0.04144	30	0.32	0.05004	93	20.2	262	2	255	6	197	44
PI73	54	1004	25	0.06416	13	0.2997	60	0.04307	34	0.77	0.05047	32	19.4	272	2	266	5	217	15
PI73	55	1118	15	0.06361	14	0.3050	43	0.04341	29	0.73	0.05096	31	18.9	274	2	270	3	239	14
PI73	56	1043	13	0.06628	12	0.3194	51	0.04393	36	0.77	0.05273	35	19.9	277	2	281	4	317	15
PI73	57	673	16	0.07483	32	0.3654	101	0.04951	39	0.35	0.05354	102	17.2	312	2	316	8	352	44
PI5	58	254	2	0.10904	18	0.3155	59	0.04428	30	0.41	0.05167	73	19.3	279	2	278	5	271	33
PI5	59	918	19	0.06674	9	0.3134	214	0.04433	257	0.99	0.05127	49	19.7	280	16	277	17	253	22
PI5	60	231	2	0.11557	12	0.2855	54	0.03964	22	0.25	0.05223	93	21.5	251	1	255	4	296	41
PI5	61	664	25	0.07846	52	0.3366	318	0.04294	296	0.93	0.05685	146	20.5	271	18	295	24	486	58
PI5	62	130	1	0.17579	43	0.4142	134	0.04616	57	0.35	0.06508	191	18.6	291	4	352	10	777	63
PI5	63	282	1	0.10411	21	0.3299	58	0.04562	36	0.52	0.05244	65	19.0	288	2	289	4	305	29
PI5	64	159	1	0.14624	13	0.3689	98	0.04901	39	0.25	0.05459	145	17.9	308	2	319	7	395	61
PI5	65	2280	152	0.06772	18	0.5062	76	0.05968	29	0.40	0.06152	62	15.1	374	2	416	5	658	22
PI5	66	925	12	0.07795	15	0.5127	92	0.05960	72	0.87	0.06239	42	13.1	373	4	420	6	687	14
PI5	67	1983	61	0.06810	6	0.5149	50	0.06131	29	0.68	0.06090	29	14.2	384	2	422	3	636	10
PI5	68	1102	27	0.07509	31	0.5334	87	0.06220	44	0.58	0.06220	59	14.1	389	3	434	6	681	20
PI5	69	1397	28	0.07078	13	0.7348	112	0.08776	79	0.84	0.06073	35	10.3	542	5	559	7	630	12
PI5	70	2082	47	0.07216	14	0.9261	132	0.10281	99	0.89	0.06533	31	8.6	631	6	666	7	785	10
PI5	71	1235	9	0.09018	45	1.0817	95	0.09958	57	0.86	0.07878	26	8.4	612	3	744	5	1167	7
PI5	72	714	11	0.09645	116	1.2147	343	0.11487	137	0.47	0.07669	157	7.2	701	8	807	16	1113	41
PI50	73	304	4	0.09900	31	0.2658	69	0.03791	26	0.24	0.05085	119	22.4	240	2	239	6	234	55
PI50	74	594	17	0.07631	8	0.2880	60	0.04014	20	0.27	0.05203	82	22.5	254	1	257	5	286	36

Appendix E. *(continued)*

sample	grain	measured ratios (fract. corrected) $^{206}Pb/^{204}Pb$	± 2σ	$^{207}Pb/^{206}Pb$	± 2σ	radiogenic ratios, corrected for spike, fractionation and common Pb $^{207}Pb/^{235}U$	± 2σ	$^{206}Pb/^{238}U$	± 2σ	R	$^{207}Pb/^{206}Pb$	± 2σ	U_{tot}/Pb_{rad}	apparent ages $^{206}Pb/^{238}U$ [Ma]	± 2σ	$^{207}Pb/^{235}U$ [Ma]	± 2σ	$^{207}Pb/^{206}Pb$ [Ma]	± 2σ
Pl50	75	254	1	0.10806	28	0.2950	57	0.04196	33	0.47	0.05099	70	21.8	265	2	262	5	240	32
Pl50	76	471	25	0.08290	68	0.3055	179	0.04250	48	0.20	0.05213	253	19.9	268	3	271	14	291	115
Pl50	77	4202	104	0.13141	10	2.0153	196	0.11388	94	0.99	0.12835	17	7.4	695	5	1121	7	2075	2
Pl13	78	969	9	0.06627	2	0.2842	23	0.04002	17	0.92	0.05151	9	21.5	253	1	254	2	264	4
Pl13	79	231	2	0.11403	10	0.3117	60	0.04425	17	0.20	0.05108	79	19.4	279	1	275	5	244	36
Pl13	80	348	2	0.09257	13	0.3133	48	0.04430	27	0.83	0.05129	30	18.8	279	2	277	4	254	9
Pl13	81	405	4	0.08750	45	0.3208	91	0.04492	39	0.36	0.05180	105	20.3	283	2	283	7	276	47
Pl23	82	1040	26	0.07152	16	0.5346	125	0.06716	78	0.65	0.05774	75	12.0	419	5	435	8	520	29
Pl23	83	2188	36	0.06496	10	0.5918	60	0.07344	46	0.86	0.05844	21	10.6	457	3	472	4	547	8
Pl23	84	750	6	0.07776	8	0.6588	106	0.08166	94	0.91	0.05851	31	10.4	506	6	514	7	549	12
Pl23	85	633	20	0.08332	25	0.7658	246	0.09148	136	0.64	0.06072	104	9.5	564	8	577	14	629	37
Pl23	86	1302	22	0.07702	6	0.9716	96	0.10636	55	0.80	0.06626	25	8.2	652	3	689	5	814	8
Pl23	87	336	5	0.16672	16	5.2083	1134	0.29662	431	0.84	0.12735	118	2.8	1675	21	1854	19	2062	16
Pl21	88	652	3	0.07381	50	0.2935	69	0.04119	35	0.50	0.05167	73	22.8	260	2	261	5	271	33
Pl21	89	964	16	0.06681	11	0.3000	43	0.04204	29	0.66	0.05175	38	21.4	265	2	266	3	275	17
Pl21	90	673	11	0.07297	18	0.3083	63	0.04336	32	0.51	0.05156	60	20.0	274	2	273	5	266	27
Pl21	91	1244	16	0.06368	11	0.3155	38	0.04398	27	0.72	0.05204	30	20.6	277	2	278	3	287	13
Pl21	92	409	2	0.08850	18	0.3653	67	0.04973	41	0.63	0.05327	51	18.8	313	2	316	5	340	22
Pl80	93	506	2	0.08151	6	0.2580	28	0.03557	25	0.68	0.05261	37	26.0	225	2	233	2	312	16
Pl80	94	174	0	0.13653	9	0.2792	45	0.03847	33	0.27	0.05264	142	24.2	243	2	250	4	313	63
Pl80	95	540	3	0.07967	13	0.2997	33	0.04128	21	0.51	0.05265	43	22.7	261	1	266	3	314	19
Pl80	96	425	3	0.08652	15	0.3338	53	0.04637	31	0.42	0.05221	68	19.9	292	2	292	4	294	30
Pl80	97	151	1	0.14863	14	0.3746	87	0.05236	47	0.35	0.05189	110	17.7	329	3	323	6	280	49
Skia1	98	717	11	0.07226	3	0.2851	40	0.03969	25	0.59	0.05209	42	22.8	251	2	255	3	289	18
Skia1	99	1285	21	0.06338	8	0.2863	30	0.03990	21	0.63	0.05203	32	18.3	252	1	256	2	287	14
Skia1	100	722	17	0.07213	10	0.3259	88	0.04535	64	0.72	0.05212	68	19.3	286	4	286	7	291	30
Skia1	101	499	6	0.08120	8	0.3268	50	0.04544	28	0.52	0.05216	49	19.3	286	2	287	4	293	22
Skia1	102	741	7	0.07227	5	0.3365	33	0.04635	21	0.55	0.05266	34	19.5	292	1	295	3	314	15
Skia1	103	847	11	0.07117	8	0.3809	43	0.05122	27	0.58	0.05393	38	17.9	322	2	328	3	368	16
Skia8	104	398	0	0.08870	11	0.2889	27	0.04028	25	0.68	0.05203	33	23.5	255	2	258	2	287	15
Skia8	105	575	6	0.07744	9	0.2934	32	0.04093	16	0.35	0.05199	47	22.8	259	1	261	3	285	21
Skia8	106	1048	20	0.06607	11	0.3167	39	0.04406	21	0.47	0.05213	43	21.1	278	1	179	3	291	19

Appendix E. *(continued)*

		measured ratios (fract. corrected)				radiogenic ratios, corrected for spike, fractionation and common Pb								apparent ages					
		$^{206}Pb/^{204}Pb$	±	$^{207}Pb/^{206}Pb$	±	$^{207}Pb/^{235}U$	±	$^{206}Pb/^{238}U$	±	R	$^{207}Pb/^{206}Pb$	±	U_{tot}/Pb_{rad}	$^{206}Pb/^{238}U$	±	$^{207}Pb/^{235}U$	±	$^{207}Pb/^{206}Pb$	±
sample	grain		2σ		2σ		2σ		2σ			2σ		[Ma]	2σ	[Ma]	2σ	[Ma]	2σ
Skia8	107	581	9	0.07716	38	0.3235	100	0.04502	66	0.59	0.05211	98	19.8	284	4	285	8	290	43
Skia8	108	973	23	0.06740	6	0.3316	49	0.04589	30	0.55	0.05242	49	20.0	290	2	291	4	304	21
Skia8	109	1547	15	0.06215	10	0.3407	35	0.04682	28	0.76	0.05278	25	19.4	295	2	298	3	319	11
Skia9	110	474	4	0.08206	39	0.2249	41	0.03185	14	0.23	0.05121	82	29.3	202	1	206	3	250	37
Skia9	111	158	1	0.14405	14	0.2474	49	0.03491	23	0.25	0.05139	113	25.8	221	1	224	4	259	51
Skia9	112	508	13	0.07760	22	0.2478	75	0.03633	32	0.35	0.04948	104	25.2	230	2	225	6	170	50
Skia9	113	991	13	0.06642	11	0.2893	35	0.04056	24	0.63	0.05173	36	23.0	256	1	258	3	274	16
Skia9	114	761	6	0.07059	12	0.2901	32	0.04095	24	0.66	0.05138	33	22.8	259	1	259	3	258	15
Skia9	115	163	4	0.13776	95	0.2959	258	0.04427	46	0.09	0.04847	395	20.3	279	3	263	20	122	182
Skia9	116	538	6	0.07708	6	0.3095	44	0.04444	26	0.74	0.05051	25	19.9	280	2	274	3	219	12
Skia9	117	676	45	0.06949	29	0.3019	162	0.04519	65	0.31	0.04845	188	20.5	285	4	268	13	121	94
Skia9	118	404	6	0.08688	19	0.3212	72	0.04551	25	0.31	0.05119	79	19.4	287	2	283	6	249	36
Skia9	119	2243	57	0.05931	5	0.3461	33	0.04747	25	0.79	0.05288	21	18.8	299	2	302	2	324	9
Skia9	120	583	77	0.07615	116	0.3420	352	0.04829	49	0.06	0.05137	477	18.0	304	3	299	27	257	229
Skia9	121	957	13	0.10866	21	0.8453	69	0.06486	25	0.63	0.09451	42	13.5	405	1	622	4	1518	8

Appendix F. Results of zircon SIMS analyses

								radiogenic ratios, SQUID corrected					apparent ages				
sample	grain.spot	U [ppm]	Th [ppm]	Th/U	$^{206}Pb_{rad.}$ [ppm]	$^{204}Pb/^{206}Pb$	f_{206} ‡ [%]	$^{207}Pb/^{235}U$	± [%]*	$^{206}Pb/^{238}U$	± [%]*	R	$^{206}Pb/^{238}U$ [Ma]	± [Ma]	$^{207}Pb/^{206}Pb$ [Ma]	± [Ma]	discordance
PI58	1.1	286	43	0.15	28.2	- [2]	-	1.029	1.4	0.1147	0.67	0.464	700	5	777	27	11
PI58	2.1	369	76	0.20	36.5	0.00012	0.21	0.994	1.7	0.1150	0.61	0.356	702	4	698	34	-1
PI58	3.1	242	54	0.22	24.3	0.00016	0.27	1.022	2.3	0.1167	0.71	0.308	711	5	726	47	2
PI58	3.2	186	264	1.42	42.1	0.00011	0.18	3.390	1.2	0.2620	0.68	0.551	1500	9	1505	20	0
PI58	4.1	178	47	0.26	16.3	0.00030	0.53	0.894	3.5	0.1063	0.83	0.233	651	5	637	74	-2
PI58	5.1	223	52	0.23	22.5	0.00006	0.10	1.029	2.1	0.1175	0.72	0.345	716	5	725	42	1
PI58	1.2	202	48	0.24	20.4	0.00015	0.26	1.025	2.7	0.1178	0.75	0.275	718	5	712	56	-1
PI58	6.1	682	124	0.18	71.6	0.00003	0.04	1.062	1.0	0.1220	0.50	0.506	741	4	711	18	-4
PI58	7.1	792	72	0.09	75.9	0.00006	0.10	0.949	1.1	0.1114	0.49	0.442	681	3	666	21	-2
PI58	8.1	249	66	0.26	24.7	0.00006	0.11	1.018	2.2	0.1151	0.70	0.321	702	5	746	44	6
PI58	9.1	167	71	0.43	16.8	0.00028	0.48	0.995	3.0	0.1170	0.84	0.282	713	6	662	61	-7
PI58	9.2	338	49	0.15	34.1	0.00016	0.28	1.028	1.8	0.1172	0.64	0.354	714	4	729	36	2
PI58	10.1	465	44	0.10	46.4	0.00007	0.12	1.000	1.5	0.1161	0.57	0.374	708	4	689	30	-3
PI33	1.1	686	294	0.43	13.8	0.00010	0.19	0.154	2.5	0.0233	1.30	0.510	149	2	97	52	-35
PI33	2.1	761	298	0.39	15.8	0.00012	0.23	0.160	2.5	0.0241	1.30	0.500	153	2	113	52	-26
PI33	3.1	555	230	0.41	11.6	0.00014	0.26	0.165	3.0	0.0243	1.30	0.440	155	2	155	63	0
PI33	4.1	516	179	0.35	10.9	0.00024	0.44	0.161	3.8	0.0245	1.30	0.360	156	2	78	83	-50
PI33	5.1	647	116	0.18	13.7	0.00022	0.41	0.158	4.1	0.0246	1.30	0.320	157	2	24	93	-85
PI33	5.2	692	139	0.2	15	0.00046	0.85	0.177	6.0	0.0250	1.40	0.240	159	2	252	134	58
P5	x	2533	1497	0.59	52.8	0.00110	2.02	0.154	11.4	0.0238	0.80	0.070	151	1	54	272	-65
P5	6.1	1005	805	0.8	21.4	0.00029	0.53	0.166	3.5	0.0246	0.70	0.200	157	1	148	80	-5
P5	7.1	1173	855	0.73	25	-	-	0.173	1.9	0.0248	0.60	0.350	158	1	226	41	43
P5	6.2	754	427	0.57	16.1	0.00003	0.05	0.169	8.0	0.0248	1.00	0.120	158	2	170	187	7
P5	8.1	1328	1047	0.79	29.7	0.00201	3.71	0.182	7.0	0.0251	0.80	0.110	160	1	318	159	99
P5	9.1	1652	1153	0.7	36.4	0.00104	1.91	0.169	5.1	0.0252	0.70	0.140	160	1	125	120	-22
P5	xx	1571	1069	0.68	34.6	0.00003	0.06	0.175	3.2	0.0257	0.60	0.190	163	1	177	73	8
P5	6.x	2427	3924	1.62	54.5	0.00013	0.24	0.178	2.5	0.0261	0.50	0.220	166	1	178	56	7
P2	11.1	236	182	0.77	9.8	0.00022	0.41	0.336	3.3	0.0482	1.30	0.410	304	4	218	69	-28
P2	10.1	1026	29	0.03	40.1	0.00010	0.18	0.327	1.7	0.0454	1.20	0.720	286	3	296	27	3
P2	12.1	1429	23	0.02	60.3	0.00003	0.06	0.348	1.7	0.0491	1.20	0.710	309	4	258	28	-17
P2	13.1	1060	5	0.0	45.7	- [2]	-	0.368	1.7	0.0501	1.30	0.740	315	4	337	26	7
P2	10.2	2005	59	0.03	88.2	0.00070	1.28	0.377	3.1	0.0506	1.20	0.400	318	4	376	63	18

Appendix F. *(continued)*

								radiogenic ratios, SQUID corrected					apparent ages				
sample	grain.spot	U [ppm]	Th [ppm]	Th/U	$^{206}Pb_{rad.}$ [ppm]	$^{204}Pb/^{206}Pb$	f_{206} ‡ [%]	$^{207}Pb/^{235}U$	± [%]*	$^{206}Pb/^{238}U$	± [%]*	R	$^{206}Pb/^{238}U$ [Ma]	± [Ma]	$^{207}Pb/^{206}Pb$ [Ma]	± [Ma]	discordance
P2	14.1	533	144	0.27	23.3	0.00014	0.25	0.357	2.1	0.0508	1.30	0.590	319	4	241	40	-25
P2	11.2	2007	38	0.02	88	0.00002	0.04	0.369	1.3	0.0510	1.20	0.900	321	4	303	13	-5
P2	14.2	1168	204	0.17	51.7	- [2]	0.00	0.379	1.4	0.0516	1.20	0.870	324	4	340	16	5
P2	12.2	361	104	0.29	27.2	0.00006	0.11	0.717	1.8	0.0875	1.40	0.800	541	7	583	24	8
P2	13.2	121	90	0.74	10.4	0.00022	0.39	0.795	2.9	0.0993	1.40	0.480	611	8	530	55	-13
P2	10.3	83	181	2.17	12.2	0.00010	0.17	1.686	2.1	0.1702	1.40	0.670	1013	13	981	32	-3
P6	15.1	518	268	0.52	11.3	0.00018	0.33	0.175	3.0	0.0253	1.30	0.430	161	2	206	64	28
P6	16.1	552	387	0.7	12.1	0.00015	0.27	0.167	2.9	0.0255	1.30	0.440	162	2	70	63	-57
P6	17.1	478	205	0.43	10.6	0.00007	0.13	0.178	2.3	0.0257	1.30	0.570	163	2	206	43	26
P6	18.1	642	551	0.86	14.3	0.00019	0.36	0.173	3.3	0.0258	1.30	0.390	164	2	134	72	-19
P6	19.1	615	332	0.54	13.7	0.00006	0.11	0.181	2.9	0.0258	1.30	0.450	165	2	233	59	41
P6	20.1	569	324	0.57	12.7	0.00002	0.04	0.183	2.4	0.0260	1.30	0.540	165	2	247	47	50
P6	21.1	275	148	0.54	6.3	0.00013	0.24	0.198	4.6	0.0267	1.40	0.300	170	2	369	99	118
PLT-1	22.1	2455	64	0.03	55.2	0.00199	3.66	0.172	8.1	0.0252	1.30	0.160	161	2	176	186	9
PLT-1	23.1	646	206	0.32	25.2	0.00030	0.54	0.323	2.5	0.0451	1.20	0.490	284	3	281	51	-1
PLT-1	24.1	558	48	0.09	26.1	0.00076	1.37	0.419	3.5	0.0537	1.30	0.360	337	4	475	73	41
PLT-1	25.1	855	26	0.03	45.4	0.00094	1.71	0.460	4.1	0.0608	1.20	0.300	381	5	405	87	6
PLT-1	22.2	849	440	0.52	50.9	0.00069	1.24	0.522	2.7	0.0689	1.20	0.460	430	5	410	53	-4
PLT-1	26.1	1053	97	0.09	67.4	0.00003	0.05	0.565	1.4	0.0745	1.20	0.870	463	5	411	16	-11
PLT-1	27.1	263	228	0.87	19	-	-	0.681	1.7	0.0841	1.30	0.750	521	6	555	25	7
Pl40	7.1	149.36	138.30	0.93	6.05	0.00032	0.58	0.338	9.5	0.0469	1.31	0.14	295	4	295	214	0
Pl40	3.2	230.49	69.18	0.30	9.37	0.00018	0.33	0.336	6.2	0.0472	1.04	0.17	297	3	272	141	-9
Pl40	6.1	306.24	152.39	0.50	12.59	0.00004	0.07	0.340	2.9	0.0478	0.87	0.31	301	3	263	62	-13
Pl40	6.2	705.01	64.23	0.09	28.88	0.00011	0.20	0.346	2.0	0.0476	0.65	0.32	300	2	321	43	7
Pl40	2.1	492.97	235.55	0.48	20.30	- [2]	0.00	0.352	2.0	0.0479	0.73	0.37	302	2	339	42	12
Pl40	3.1	572.79	197.82	0.35	23.63	0.00002	0.04	0.355	2.6	0.0480	0.70	0.28	302	2	354	55	17
Pl40	5.2	849.37	39.61	0.05	42.29	-	-	0.448	1.4	0.0580	0.59	0.43	363	2	454	28	25
Pl40	1.1	110.76	31.11	0.28	8.16	- [2]	0.00	0.726	3.0	0.0858	1.16	0.38	531	6	653	60	23
Pl40	4.1	246.94	143.87	0.58	24.43	0.00011	0.20	0.990	2.4	0.1149	0.79	0.34	701	5	691	47	-1
Pl40	8.1	323.68	10.02	0.03	34.90	- [2]	0.00	1.124	1.5	0.1255	0.77	0.52	762	6	772	27	1
Pl40	5.1	366.39	176.21	0.48	63.90	0.00001	0.02	2.294	1.1	0.2030	0.63	0.57	1191	7	1245	18	5

Appendix F. *(continued)*

sample	grain.spot	U [ppm]	Th [ppm]	Th/U	$^{206}Pb_{rad.}$ [ppm]	$^{204}Pb/^{206}Pb$	f_{206} ‡ [%]	radiogenic ratios, SQUID corrected: $^{207}Pb/^{235}U$	± [%]*	$^{206}Pb/^{238}U$	± [%]*	R	apparent ages: $^{206}Pb/^{238}U$ [Ma]	± [Ma]	$^{207}Pb/^{206}Pb$ [Ma]	± [Ma]	discordance
Pl37	6.2	95.20	110.80	1.16	3.86	0.00086	1.56	0.330	12.1	0.0464	1.47	0.12	292	4	267	276	-9
Pl37	6.1	143.82	197.23	1.37	5.88	0.00047	0.86	0.327	9.2	0.0472	1.19	0.13	297	3	205	212	-31
Pl37	10.2	505.96	126.13	0.25	21.11	0.00017	0.32	0.341	2.9	0.0484	0.65	0.23	305	2	243	65	-20
Pl37	8.1	995.17	95.53	0.10	41.98	0.00014	0.26	0.347	2.1	0.0490	0.53	0.25	308	2	258	47	-16
Pl37	9.1	1532.95	118.54	0.08	65.07	0.00003	0.06	0.358	1.1	0.0494	0.47	0.41	311	1	312	24	1
Pl37	1.1	973.84	340.79	0.35	41.69	0.00013	0.24	0.354	2.0	0.0497	0.53	0.27	313	2	269	44	-14
Pl37	1.2	752.80	309.00	0.41	32.69	0.00019	0.34	0.356	2.1	0.0504	0.57	0.26	317	2	253	48	-20
Pl37	11.1	1751.60	26.75	0.02	76.67	0.00009	0.16	0.359	1.3	0.0509	0.45	0.35	320	1	249	28	-22
Pl37	3.1	1640.76	485.41	0.30	72.16	0.00033	0.59	0.363	2.1	0.0509	0.47	0.22	320	1	272	48	-15
Pl37	10.1	1247.56	415.67	0.33	54.67	0.00005	0.09	0.366	1.5	0.0510	0.48	0.32	320	2	288	32	-10
Pl37	4.1	2695.64	265.10	0.10	122.19	0.00004	0.08	0.380	0.9	0.0527	0.41	0.46	331	1	299	18	-10
Pl37	8.2	1700.35	122.42	0.07	79.07	0.00014	0.25	0.395	1.5	0.0540	0.45	0.31	339	1	332	31	-2
Pl37	5.1	327.00	136.97	0.42	26.91	- [2]	-	0.835	1.4	0.0958	0.64	0.45	590	4	715	27	21
Pl37	7.1	583.22	543.37	0.93	50.18	0.00007	0.12	0.822	1.2	0.1000	0.53	0.43	615	3	589	24	-4
Pl37	2.1	324.38	145.89	0.45	32.88	0.00002	0.04	1.030	1.4	0.1180	0.63	0.44	719	4	719	27	0
Pl54	3.1	85.10	46.60	0.55	3.47	0.00062	1.13	0.321	7.8	0.0469	1.21	0.16	295	3	177	179	-40
Pl54	14.1	448.61	115.43	0.26	18.97	0.00010	0.19	0.359	2.1	0.0491	0.71	0.33	309	2	331	46	7
Pl54	12.1	269.50	91.14	0.34	11.47	0.00018	0.32	0.356	2.7	0.0494	0.79	0.30	311	2	298	58	-4
Pl54	17.1	328.20	143.28	0.44	14.03	0.00018	0.33	0.348	2.8	0.0496	0.92	0.33	312	3	236	61	-25
Pl54	13.1	469.86	161.83	0.34	20.30	0.00012	0.23	0.362	2.3	0.0502	0.70	0.30	316	2	302	50	-4
Pl54	15.1	193.67	65.71	0.34	12.35	0.00007	0.12	0.572	2.1	0.0741	0.81	0.38	461	4	450	44	-2
Pl54	10.1	367.61	264.69	0.72	32.51	0.00007	0.13	0.866	1.2	0.1028	0.68	0.55	631	4	642	22	2
Pl16	21.2	94.475	44.388	0.470	3.067	0.00075	1.36	0.223	10.7	0.0373	1.69	0.157	236	4	-149	262	-163
Pl16	26.2	109.625	68.732	0.627	3.595	0.00091	1.66	0.221	12.9	0.0375	1.68	0.130	238	4	-190	320	-180
Pl16	37.1	115.062	55.862	0.485	3.827	0.00098	1.80	0.215	12.3	0.0380	1.63	0.132	241	4	-290	311	-221
Pl16	3.1	105.327	47.302	0.449	3.544	0.00076	1.39	0.241	9.3	0.0386	1.62	0.175	244	4	-45	222	-119
Pl16	13.2	110.364	82.838	0.751	3.774	0.00097	1.78	0.233	12.1	0.0391	1.66	0.137	247	4	-152	298	-161
Pl16	10.2	205.590	103.370	0.503	9.761	0.00021	0.38	0.394	3.7	0.0551	1.40	0.376	345	5	281	79	-19
Pl16	10.1	268.035	151.061	0.564	12.966	0.00020	0.35	0.410	2.8	0.0561	1.34	0.485	352	5	331	55	-6
Pl16	29.1	287.252	131.366	0.457	23.364	0.00006	0.11	0.790	2.1	0.0946	1.28	0.613	583	7	626	36	7
Ev4	28.1	575.75	159.95	0.28	23.58	0.00015	0.28	0.341	1.8	0.0475	0.68	0.38	299	2	287	37	-4
Ev4	32.2	806.92	384.60	0.48	33.41	0.00009	0.16	0.344	1.4	0.0481	0.65	0.48	303	2	280	27	-8
Ev4	29.2	221.96	72.71	0.33	9.25	0.00026	0.46	0.331	4.5	0.0483	0.84	0.19	304	3	183	103	-40

Appendix F. *(continued)*

								radiogenic ratios, SQUID corrected					apparent ages				
		U	Th	Th/U	$^{206}Pb_{rad.}$	$^{204}Pb/^{206}Pb$	f_{206} ‡	$^{207}Pb/^{235}U$	±	$^{206}Pb/^{238}/U$	±	R	$^{206}Pb/^{238}U$	±	$^{207}Pb/^{206}Pb$	±	discordance
sample	grain.spot	[ppm]	[ppm]		[ppm]		[%]		[%]*		[%]*		[Ma]	[Ma]	[Ma]	[Ma]	
Ev4	16.1	793.90	249.67	0.31	33.09	0.00009	0.15	0.351	1.3	0.0484	0.64	0.48	305	2	311	27	2
Ev4	10.1	593.03	264.03	0.45	25.72	- [2]	-	0.371	1.2	0.0505	0.66	0.57	317	2	341	22	8
Ev4	32.1	740.56	280.83	0.38	32.63	0.00008	0.15	0.371	1.5	0.0512	0.84	0.57	322	3	312	28	-3
Ev4	22.1	81.98	41.52	0.51	3.86	0.00032	0.57	0.437	4.5	0.0545	1.81	0.40	342	6	536	90	57
Ev4	29.1	238.65	364.37	1.53	64.45	0.00002	0.03	5.343	0.8	0.3142	0.70	0.84	1761	11	2005	8	14

Samples Pl40, Pl37, Pl58 and P5 were analysed with SHRIMP II at the Center of Isotopic Research, St. Petersburg, Russia

Samples P2, P6, Pl33, PLT-1, Pl54, Pl16 and Ev4 were analysed with SHRIMP II at the ANU, Canberra, Australia

f_{206} [%] denotes the percentage of ^{206}Pb that is common Pb

Errors in reference calibration are not included in the above errors. Error in referenc zircon calibration Temora was 0.33% for Pl40 and P5 and 0.25% for Pl37 and Pl58

Error in reference zircon calibration FC1 was 0.22% for Pl54 and Ev4 and 0.31% for Pl16, Pl33, P2, P6 and PLT-1

Pb_c correction by SQUID was performed using the measured ^{204}Pb and assuming that the common Pb isotopic composition is accordance with the model of Stacey & Kramers (1975) for the age of each spot

* Uncertainties are given at 1 σ level

[2] for some spots counts on ^{204}Pb were below background level, a $^{204}Pb/^{206}Pb$ of 0.00001 was then assumed to perform the common Pb correction

Appendix G. Results of electron microprobe monazite analyses

	age	±	Th	U	Pb	Si	Ca	Nd	Er	Al	P	Ce	Dy	Y	La	Gd	Eu	Sm	Pr	O	Total:
	[Ma]	2σ	wt.%	wt.%	wt.%	wt.%	wt.%	wt.%	wt.%	wt.%	wt.%	wt.%	wt.%	wt.%	wt.%	wt.%	wt.%	wt.%	wt.%		
detection limit wt%			0.0055	0.0088	0.0037	0.0019	0.0038	0.0184	0.0121	0.0015	0.0076	0.0277	0.0136	0.0060	0.0180	0.0323	0.0218	0.0343	0.0343		
sample-grain.spot																					
P2-1.1	143	33	3.83	0.67	0.0380	0.054	0.791	10.06	0.099	-	14.20	23.72	0.457	1.86	11.51	1.24	0.105	1.73	2.56	28.57	101.49
P2-2.1	154	32	3.78	0.77	0.0426	0.047	0.810	10.45	0.070	-	14.15	23.96	0.440	1.47	11.06	1.16	0.123	1.81	2.44	28.41	100.98
P2-3.1	180	36	4.18	0.44	0.0447	0.059	0.796	10.18	0.122	-	14.37	24.62	0.399	1.62	11.73	1.11	0.000	1.57	2.64	28.91	102.79
P2-3.2	169	34	3.77	0.64	0.0437	0.110	0.711	10.32	0.085	-	14.23	24.37	0.449	1.70	11.51	1.22	0.086	1.76	2.59	28.74	102.34
P2-3.3	156	45	3.59	0.27	0.0309	0.217	0.486	10.39	0.018	-	13.86	25.51	0.226	0.74	12.43	0.91	0.037	1.61	2.62	28.20	101.14
P2-4.1	166	43	3.04	0.51	0.0344	0.200	0.475	10.66	0.034	-	13.86	25.33	0.270	0.88	12.46	0.96	0.000	1.56	2.78	28.22	101.26
P2-4.2	180	31	4.06	0.79	0.0526	0.291	0.598	10.21	0.024	-	13.80	25.01	0.279	0.87	12.30	0.99	0.000	1.54	2.64	28.30	101.75
P2-5.1	167	31	4.48	0.62	0.0478	0.349	0.699	9.67	0.045	-	13.74	24.83	0.270	0.85	12.67	0.88	0.037	1.54	2.50	28.26	101.48
P2-5.2	168	36	4.97	0.18	0.0415	0.542	0.296	10.92	0.000	-	13.45	25.21	0.230	0.52	11.92	1.10	0.000	1.72	2.75	28.10	101.96
P2-7.1	148	35	4.46	0.42	0.0380	0.262	0.624	10.35	0.051	-	13.82	24.59	0.299	1.00	12.23	1.00	0.000	1.64	2.54	28.29	101.60
P2-7.2	157	38	4.11	0.40	0.0377	0.068	0.775	10.35	0.070	-	14.37	24.81	0.355	1.42	11.60	1.05	0.000	1.67	2.61	28.87	102.57
P2-8.1	172	45	3.78	0.19	0.0337	0.224	0.494	10.37	0.024	-	13.84	25.70	0.221	0.71	12.72	0.92	0.000	1.38	2.56	28.23	101.41
P2-8.2	163	39	4.10	0.32	0.0371	0.260	0.537	10.07	0.040	-	13.77	25.09	0.283	0.83	12.23	1.01	0.019	1.51	2.61	28.10	100.80
P2-10.1	171	36	3.46	0.65	0.0422	0.073	0.690	10.52	0.062	-	13.97	24.93	0.357	1.33	11.75	1.18	0.000	1.69	2.63	28.34	101.67
P2-10.2	207	45	2.92	0.45	0.0401	0.194	0.598	9.57	0.021	-	13.88	26.36	0.185	0.70	13.75	0.82	0.000	1.33	2.61	28.34	101.77
P2-10.3	145	37	4.02	0.43	0.0348	0.248	0.528	10.41	0.031	-	13.84	25.64	0.278	0.83	12.19	1.01	0.000	1.62	2.72	28.37	102.21
P2-10.4	144	32	3.76	0.77	0.0398	0.061	0.749	10.19	0.096	-	14.20	24.26	0.518	1.85	11.47	1.29	0.000	1.82	2.63	28.69	102.38
P2-11.1	184	32	3.84	0.77	0.0516	0.035	0.801	10.24	0.132	-	14.09	23.37	0.607	2.21	10.81	1.32	0.000	1.73	2.54	28.38	100.91
P2-11.2	128	24	6.59	0.57	0.0477	0.480	0.699	9.62	0.015	-	13.43	23.61	0.250	0.74	11.94	0.92	0.000	1.38	2.45	27.89	100.62
P2-12.1	176	32	3.93	0.75	0.0496	0.054	0.795	10.22	0.118	-	14.09	23.39	0.549	2.18	10.94	1.33	0.000	1.80	2.46	28.42	101.08
P2-12.2	163	35	4.15	0.49	0.0414	0.060	0.889	10.30	0.051	-	14.11	24.11	0.288	0.98	11.31	0.97	0.000	1.62	2.60	28.25	100.20
P2-14.1	148	26	5.94	0.54	0.0506	0.331	0.825	10.06	0.042	-	13.72	24.33	0.294	0.93	11.83	0.91	0.087	1.62	2.62	28.37	102.50
P2-15.1	105	34	3.80	0.69	0.0280	0.049	0.811	10.45	0.054	-	14.01	24.19	0.369	1.21	11.46	1.07	0.091	1.73	2.66	28.26	100.95

Appendix G. *(continued)*

	age	±	Th	U	Pb	Si	Ca	Nd	Er	Al	P	Ce	Dy	Y	La	Gd	Eu	Sm	Pr	O	Total:
	[Ma]	2σ	wt.%	wt.%	wt.%	wt.%	wt.%	wt.%	wt.%	wt.%	wt.%	wt.%	wt.%	wt.%	wt.%	wt.%	wt.%	wt.%	wt.%		
P2-16.1	143	32	3.72	0.77	0.0392	0.068	0.800	10.56	0.057	-	14.12	23.79	0.374	1.28	11.15	1.18	0.141	1.71	2.56	28.33	100.64
P2-17.1	160	32	4.38	0.58	0.0444	0.066	0.844	10.16	0.087	-	14.24	23.85	0.447	1.74	11.27	1.13	0.106	1.61	2.51	28.63	101.71
P2-17.2	127	20	8.23	0.71	0.0591	0.674	0.777	9.37	0.000	-	13.32	22.72	0.303	0.94	11.14	0.97	0.080	1.50	2.50	28.02	101.32
P2-17.3	141	24	6.50	0.56	0.0520	0.420	0.786	9.51	0.061	-	13.56	23.32	0.299	1.20	11.25	0.96	0.074	1.54	2.41	27.99	100.48
P2-17.4	148	35	4.08	0.53	0.0378	0.049	0.799	10.16	0.118	-	14.20	23.80	0.483	1.95	11.20	1.12	0.077	1.63	2.53	28.55	101.32
P2-17.5	159	31	4.31	0.70	0.0461	0.063	0.849	10.25	0.078	-	14.10	23.65	0.411	1.58	11.00	1.07	0.028	1.66	2.61	28.35	100.76
P2-17.6	132	36	4.11	0.46	0.0327	0.053	0.797	10.14	0.109	-	14.14	23.48	0.424	1.65	11.56	1.11	0.056	1.54	2.59	28.37	100.63
P2-17.7	168	35	4.38	0.41	0.0426	0.069	0.809	10.27	0.054	-	14.17	23.70	0.346	1.48	11.22	1.13	0.095	1.65	2.58	28.42	100.84
P2-18.1	151	19	8.20	0.82	0.0724	0.600	0.863	9.64	0.027	-	13.45	22.71	0.333	1.06	10.95	1.07	0.110	1.62	2.42	28.23	102.17
P2-18.2	146	24	6.22	0.67	0.0544	0.427	0.786	9.90	0.067	-	13.67	22.92	0.342	1.23	11.62	1.16	0.115	1.59	2.46	28.25	101.48
P2-18.3	161	20	7.51	0.79	0.0719	0.531	0.819	9.51	0.047	-	13.32	22.18	0.327	1.01	10.99	1.11	0.065	1.66	2.33	27.74	100.01
P2-18.4	177	32	4.27	0.61	0.0489	0.066	0.843	9.99	0.062	-	14.08	23.77	0.400	1.43	11.17	1.07	0.045	1.61	2.51	28.25	100.22
P2-18.5	171	26	5.59	0.63	0.0577	0.061	1.080	9.52	0.115	-	14.09	22.30	0.565	2.05	10.63	1.31	0.068	1.70	2.44	28.36	100.58
P2-18.6	164	33	4.50	0.46	0.0434	0.062	0.856	10.05	0.098	-	14.04	23.62	0.368	1.49	11.45	1.04	0.043	1.57	2.52	28.24	100.45
P2-19.1	142	28	4.87	0.70	0.0449	0.307	0.671	9.99	0.034	-	13.72	23.63	0.357	1.10	11.46	1.11	0.103	1.64	2.55	28.03	100.32
P2-21.1	172	29	4.50	0.78	0.0533	0.144	0.900	9.94	0.045	-	13.92	24.04	0.293	1.03	11.37	1.01	0.000	1.58	2.62	28.15	100.37
P2-21.2	149	28	4.67	0.81	0.0480	0.078	1.040	10.23	0.047	-	14.09	24.13	0.299	1.07	11.46	1.04	0.000	1.58	2.66	28.47	101.70
P2-24.1	170	27	4.88	0.83	0.0571	0.318	0.663	9.96	0.032	-	13.66	24.14	0.343	1.08	11.68	1.01	0.117	1.57	2.53	28.07	100.92
P2-24.2	176	29	4.79	0.66	0.0541	0.323	0.610	10.26	0.037	-	13.59	24.31	0.297	0.98	12.04	1.02	0.049	1.58	2.54	28.03	101.16
P2-24.3	181	35	3.55	0.65	0.0453	0.212	0.596	10.42	0.040	-	13.77	24.59	0.353	1.19	12.00	1.04	0.087	1.62	2.72	28.13	101.00
P2-24.4	170	35	3.63	0.63	0.0427	0.218	0.605	10.35	0.048	-	13.72	24.09	0.291	1.12	11.88	1.04	0.114	1.66	2.57	27.94	99.96
P2-24.5	197	36	3.86	0.52	0.0482	0.245	0.532	9.97	0.036	-	13.61	25.14	0.245	0.85	12.36	0.97	0.015	1.48	2.54	27.87	100.30
P2-24.6	166	30	4.38	0.69	0.0485	0.294	0.577	10.14	0.013	-	13.52	24.33	0.294	0.98	12.06	0.90	0.118	1.57	2.62	27.83	100.37
P2-30.1	140	48	3.14	0.33	0.0262	0.207	0.454	10.35	0.016	-	13.84	25.76	0.203	0.70	13.18	0.85	0.000	1.51	2.68	28.24	101.49
P2-32.1	140	74	1.77	0.29	0.0168	0.061	0.363	11.22	0.066	-	14.15	26.10	0.280	1.04	12.18	1.02	0.000	1.52	2.71	28.41	101.21
P2-33.1	126	36	4.08	0.43	0.0307	0.070	0.792	9.98	0.088	-	14.15	24.08	0.400	1.58	11.53	1.01	0.000	1.51	2.59	28.40	100.73

Appendix G. *(continued)*

	age	±	Th	U	Pb	Si	Ca	Nd	Er	Al	P	Ce	Dy	Y	La	Gd	Eu	Sm	Pr	O	Total:
	[Ma]	2σ	wt.%	wt.%	wt.%	wt.%	wt.%	wt.%	wt.%	wt.%	wt.%	wt.%	wt.%	wt.%	wt.%	wt.%	wt.%	wt.%	wt.%		
P2-33.2	177	42	3.22	0.45	0.0368	0.211	0.476	10.19	0.033	-	13.84	25.65	0.283	0.92	12.47	0.92	0.085	1.53	2.62	28.19	101.12
P2-36.1	128	31	4.00	0.78	0.0370	0.066	0.855	9.99	0.041	-	14.18	23.86	0.290	1.02	11.79	1.02	0.000	1.68	2.57	28.36	100.52
P2-37.1	163	41	3.43	0.47	0.0357	0.172	0.559	10.07	0.038	-	14.06	24.93	0.317	1.15	12.15	1.01	0.098	1.53	2.60	28.38	101.02
P2-38.1	141	30	4.72	0.59	0.0413	0.307	0.528	9.79	0.018	-	13.77	24.97	0.195	0.74	12.63	0.82	0.105	1.43	2.55	28.20	101.41
P2-39.1	172	28	4.71	0.77	0.0550	0.302	0.659	10.26	0.063	-	13.75	24.37	0.340	1.05	11.79	1.08	0.036	1.56	2.53	28.24	101.57
P2-42.1	165	36	4.03	0.48	0.0408	0.060	0.794	9.97	0.116	-	14.21	24.71	0.452	1.79	11.60	1.08	0.114	1.64	2.47	28.69	102.25
P2-42.2	161	32	3.77	0.81	0.0454	0.052	0.835	10.40	0.082	-	14.15	23.73	0.507	1.74	11.12	1.17	0.110	1.80	2.61	28.50	101.43
P2-42.3	144	37	3.78	0.53	0.0350	0.255	0.527	10.24	0.023	-	13.80	25.39	0.287	0.87	12.32	0.94	0.088	1.53	2.53	28.22	101.38
P2-42.4	159	34	4.12	0.57	0.0420	0.277	0.561	10.16	0.020	-	13.81	25.22	0.263	0.85	12.31	0.97	0.099	1.49	2.63	28.29	101.68
P2-42.5	163	34	4.12	0.56	0.0430	0.271	0.565	10.02	0.018	-	13.80	25.43	0.247	0.85	12.28	0.94	0.100	1.54	2.70	28.28	101.74
P2-42.6	114	34	3.79	0.67	0.0300	0.053	0.793	10.19	0.133	-	14.13	23.55	0.573	2.22	11.24	1.33	0.086	1.72	2.59	28.55	101.65
F5-2.1	324	16	5.75	2.29	0.1899	0.194	1.220	8.21	0.097	-	13.97	23.79	0.569	1.90	10.58	1.05	0.091	1.30	2.40	28.54	102.15
F5-2.2	328	16	5.61	1.84	0.1695	0.183	1.140	7.96	0.068	-	13.89	24.42	0.411	1.39	11.54	0.95	0.085	1.15	2.37	28.33	101.50
F5-2.3	368	50	2.89	0.32	0.0648	0.064	0.552	10.21	0.111	-	14.09	23.71	0.960	2.98	9.83	1.76	0.119	2.16	2.68	28.45	100.96
F5-2.4	361	36	4.35	0.34	0.0879	0.101	0.765	9.18	0.087	-	13.99	23.43	0.820	2.49	10.72	1.54	0.094	1.77	2.56	28.31	100.63
F5-2.5	324	16	6.73	1.94	0.1880	0.221	1.310	7.84	0.076	-	13.81	23.77	0.422	1.45	10.94	0.95	0.057	1.18	2.32	28.29	101.49
F5-3.1	333	14	7.17	2.49	0.2260	0.243	1.440	8.49	0.067	-	13.84	21.61	0.685	2.01	9.47	1.41	0.088	1.62	2.37	28.36	101.58
F5-3.2	341	14	6.28	2.39	0.2132	0.214	1.280	8.20	0.087	-	14.00	23.12	0.625	2.04	10.17	1.14	0.062	1.38	2.41	28.59	102.20
F5-3.3	336	17	6.23	2.27	0.2038	0.215	1.270	8.20	0.116	-	13.93	22.72	0.585	1.94	10.28	1.13	0.061	1.34	2.31	28.37	101.17
F5-3.4	343	17	6.03	2.22	0.2026	0.189	1.300	8.21	0.111	-	14.01	23.22	0.546	1.82	10.66	1.06	0.048	1.39	2.42	28.55	101.97
F5-3.5	321	14	6.52	2.61	0.2141	0.243	1.340	8.06	0.115	-	13.93	22.86	0.587	1.96	10.17	1.06	0.092	1.36	2.39	28.52	102.04
F5-8.1	315	28	3.78	1.01	0.0991	0.126	0.738	8.90	0.099	-	13.94	24.20	0.643	2.15	11.46	1.37	0.148	1.58	2.48	28.32	101.04
F5-8.2	339	25	4.28	1.14	0.1208	0.141	0.818	8.89	0.112	-	13.88	23.87	0.665	2.19	11.25	1.33	0.123	1.60	2.32	28.25	100.99
F5-8.3	296	25	4.26	1.15	0.1054	0.147	0.825	8.89	0.128	-	13.96	23.69	0.631	2.17	11.25	1.36	0.112	1.58	2.38	28.34	100.99
F5-8.4	300	27	4.25	1.00	0.1000	0.138	0.823	9.23	0.111	-	13.89	23.82	0.662	2.14	11.13	1.45	0.089	1.60	2.47	28.30	101.22
F5-8.5	340	27	3.94	1.06	0.1119	0.130	0.781	9.19	0.113	-	13.92	23.80	0.681	2.18	11.02	1.47	0.131	1.60	2.39	28.26	100.78
F5-8.6	360	27	3.90	1.06	0.1181	0.129	0.767	9.00	0.120	-	13.93	24.16	0.632	2.17	11.44	1.38	0.071	1.47	2.49	28.33	101.16

Appendix G. *(continued)*

	age	±	Th	U	Pb	Si	Ca	Nd	Er	Al	P	Ce	Dy	Y	La	Gd	Eu	Sm	Pr	O	Total:
	[Ma]	2σ	wt.%	wt.%	wt.%	wt.%	wt.%	wt.%	wt.%	wt.%	wt.%	wt.%	wt.%	wt.%	wt.%	wt.%	wt.%	wt.%	wt.%		
F5-8.7	323	27	3.98	1.10	0.1086	0.129	0.780	9.08	0.107	-	13.84	23.93	0.647	2.17	11.19	1.42	0.079	1.70	2.52	28.20	100.98
F5-8.8	334	26	4.19	1.10	0.1157	0.137	0.827	9.24	0.091	-	14.00	23.84	0.705	2.23	10.89	1.38	0.104	1.65	2.43	28.43	101.36
F5-8.9	344	25	5.10	0.94	0.1251	0.187	0.906	9.19	0.023	-	13.96	24.80	0.362	1.28	11.65	1.09	0.061	1.41	2.49	28.47	102.04
F5-8.10	336	26	4.31	1.04	0.1151	0.149	0.830	8.95	0.143	-	13.86	23.83	0.645	2.08	11.13	1.26	0.042	1.49	2.41	28.16	100.45
F5-8.11	349	26	4.42	1.04	0.1214	0.148	0.850	9.01	0.114	-	13.85	23.74	0.605	2.05	11.32	1.28	0.101	1.55	2.33	28.19	100.71
F5-8.12	333	26	4.68	0.98	0.1165	0.159	0.873	9.05	0.093	-	13.91	23.76	0.599	1.94	11.13	1.25	0.076	1.50	2.50	28.27	100.87
F5-8.13	352	26	4.32	1.02	0.1198	0.150	0.819	8.84	0.127	-	13.82	23.92	0.619	1.95	11.40	1.29	0.149	1.52	2.35	28.13	100.54
F5-8.14	329	28	4.03	0.95	0.1044	0.122	0.789	8.92	0.085	-	14.03	24.03	0.733	2.29	11.38	1.39	0.103	1.56	2.34	28.44	101.29
F5-8.15	342	28	4.32	0.91	0.1107	0.152	0.799	9.36	0.083	-	13.90	24.44	0.557	1.73	11.29	1.21	0.079	1.57	2.51	28.30	101.31

Appendix H. Sample localities (GPS coordinates)

		N	E
Pelagonian Zone			
Varnous Mts.			
V1	tonalitic granite	40° 47.35'	21° 19.52'
V2	monzogabbro	40° 47.35'	21° 19.52'
V3	monzogabbro	40° 47.17'	21° 18.05'
V4	monzogabbro	40° 47.17'	21° 18.05'
V5	granodiorite	40° 49..98'	21° 20.17'
V6	granite	40° 49..98'	21° 20.17'
V7	dioritic granitoid	40° 47.17'	21° 18.05'
V8	mylonitic paragneiss	40° 46..88'	21° 19.35'
V9	alkali granitic gneiss	40° 47.03'	21° 21.90'
V10	tonalitic granite	40° 49..98'	21° 20.17'
W Voras Mts.			
Ka-X1		sampled along the road leading northeast from the locality of Ka-X5 into the mountains; Ka-X1 is the NEernmost sample	
Ka-X2	alkali granite		
Ka-X3			
Ka-X4	granitic augengneis	40° 52.79'	21° 48.30'
Ka-X5	granodioritic granite	40° 52.29'	21° 47.06'
Ka-X6	granodioritic granite	40° 51.31'	21° 46.32'
S of Veria			
Pl 37	granodiorite	40° 23.67'	22° 06.60'
Pl 38	granodiorite	40° 23.67'	22° 06.60'
Pl 39	dioritic	40° 23.67'	22° 06.60'
Pl 40	granodiorite	*c.* 500m N along road from Pl39 loc.	
Pl 41	granite	N exit of Kastania village	
Pl 43	alkali granite	40° 25.95'	22° 08.68'
Pl 44		40° 25.95'	22° 08.68'

Appendix H. (*continued*)

		N	E
NE Mt. Olympos			
Pl 73	granitic mylonite	40° 10.12'	22° 23.03'
Pl 74	granitic mylonite	40° 09.95'	22° 23.54'
NW PZ			
Pl 58	granodioritic augengneiss	40° 34.33'	21° 29.82'
Pl 59	granitic augengneiss	40° 34.33'	21° 29.82'
Pl 61	deformed granite	40° 35.02'	21° 22.51'
Pl 62	deformed granite	40° 35.02'	21° 22.51'
Pl 63	alkali rhyolite	40° 22.00'	21° 26.48'
Pl 64	alkali granite augengneiss	39° 50.17'	21° 48.24'
Pl 65	alkali granite	sampled in Fotino village	
Pl 66	alkali granite	39° 50.42'	21° 47.45'
Pl 67	alkali granite	39° 50.74'	21° 47.17'
Pl 68	gneiss	39° 51.00'	21° 46.99'
Pl 69	alkali granite augengneiss	39° 58.04'	21° 48.29'
Pl 70	coarse-grained granitic gneiss	39° 55.40'	21° 49.39'
Pl 71	granitic augengneiss	39° 56.72'	21° 53.05'
Pl 72	monzonitic gneiss	39° 52.41'	22° 07.19'
Verdikoussa area			
Pl1	granodiorite	samples Pl1 – Pl8 were sampled along the road from Verdikoussa to Elassona town, Pl9 was sampled NE of Elassona town	
Pl3	granite		
Pl4	granodiorite		
Pl5	granodiorite		
Pl6	granodiorite		
Pl7	granodiorite		
Pl8	granodiorite		
Pl9	granodiorite		
Pl10	tonalitic strongly deformed gneiss	39° 59.38'	22° 17.17'

Appendix H. (*continued*)

		N	E
Pl11	granitic mylonite	39° 59.62'	22° 18.3'
<u>Mt. Ossa</u>			
Pl 45	granitic blueschist	39° 51.29'	22° 32.46'
Pl 46	greenish syenitic gneiss	39° 51.29'	22° 32.46'
Pl 48	qtz-monzonitic gneiss medium	39° 51.29'	22° 32.46'
Pl 49	gneiss	39° 51.02'	22° 44.37'
Pl 50	granodioritc gneiss	39° 50.81'	22° 43.01'
Pl 51	highly sheared gneiss	39° 50.46'	22° 42.82'
Pl 52	phyllite	39° 4765'	22° 38.59'
Pl 54	gneiss	39° 47.09'	22° 37.33'
Pl 55	alkali granitic gneiss, coarse	39° 46.10'	22° 35.87'
<u>Mt. Mavrovouni</u>			
Pl12	gabbro	near locality of Pl 29	
Pl13	granite	same locality as Pl 25	
Pl 25	alkali granitic orthogneiss	39° 35.73'	22° 46.08'
Pl 26	leucocratic orthogneiss	39° 35.30'	22° 46.76'
Pl 27	leucocratic orthogneiss	39° 34.45'	22° 46.60'
Pl 29	gabbronorite	39° 34.38'	22° 46.55'
Pl 30		39° 33.98'	22° 45.98'
<u>Pilion peninsular</u>			
Pl 15	dioritic mylonite	39° 19.5'	23° 09.60'
Pl 16	tonalitic mylonite	39° 19.67'	23° 09.60'
Pl 17	quartzite	39° 19.57'	23° 11.73'
Pl 21	granitic gneiss	39° 20.58'	23° 12.23'
Pl 22	monzonitic gneiss	39° 24.00'	23° 07.92'
Pl 23	granodioritic gneiss	39° 24.50'	23° 04.50'
Pl 24	gneiss	39° 23.72'	23° 03.40'
Pl 79	granitic mylonitic gneiss	39° 12.25'	23° 13.90'

Appendix H. (*continued*)

		N	E
Pl 80	granitic mylonitic gneiss	39° 11.53'	23° 13.85'
Pl 81	granitic mylonitic gneiss	39° 09.07'	23° 16.50'
Pl 85	augengneis	39° 06.70'	23° 07.83'
Pl 86	granitic augengneiss	sampled on the S coast of the	
Pl 87	granodi. augengneiss	Pilion Peninsula	
<u>Evia Island</u>			
Ev - 4	tonalitic gneiss	38° 51.11'	23° 14.19'
Ev - 5	granite	38° 52.91'	23° 00.24'
<u>Skiathos</u>			
Skia 1	fine-grained granodioritic gneiss	39° 08.75'	23° 24.68'
Skia 2	coarse-grained granitic gneiss	39° 08.75'	23° 24.68'
Skia 4	granitic leukosome of a migmatite	39° 09.28'	23° 23.37
Skia 6	fine-grained granitic gneiss	39° 09.90'	23° 26.75'
Skia 7	coarse-grained granitic augengneiss	39° 09.90'	23° 26.75'
Skia 8	granitic leucocratic gneiss	39° 09.62'	23° 26.57'
Skia 9	granitic gneiss	39° 10.37'	23° 26.17'
<u>Skyros Island</u>			
Sky 1	severley weathered granodiorite	38° 49.49'	24° 34.09'
Sky 2	sev. weathered tonalitic granite	38° 49.49'	24° 34.09'
Sky 4	road cut a bit N of Sky 1 locality	38° 49.49'	24° 34.09'

Vardar Zone

Pl 75	granitic two-mica gneiss	41° 00.96'	21° 58.80'
Pl 31	granitic dyke near Pinis	41° 01.20'	22° 29.72'
Pl 32	granitic mylonite	41° 05.35'	22° 22.03'
Pl 33	mylonite	41° 04.92'	22° 22.58'
Pl 34	mylonite	41° 04.72'	22° 22.85'
Pl 35	alkali granite	41° 05.03'	22° 27.88'

Appendix H. (*continued*)

		N	E
Pl 36	alkali granite	41° 05.03'	22° 27.88'
P1	granitic bt-ksp-gneiss	41° 00.85'	22° 29.30'
P2	granitic bt-ksp-gneiss	41° 00.91'	22° 29.22'
P4	diorite?	41° 05.67'	22° 25.32'
P5	granite	41° 04.85'	22° 29.23'
P6	rhyodacite	41° 04.29'	22° 33.74'

rock classification using the R1-R2 classification after De la Roche *et al.* (1980)

Kommt man auch zu keinem Ende, kommt man
doch immer zu einem Schluß

Elazar Benyoëtz